REACTION ACCOMPANIED MASS TRANSFER BETWEEN LIQUID PHASES - AN EXPERIMENTAL STUDY

by

P. SETO

A Thesis

Submitted to the Faculty of Graduate Studies

in Partial Fulfilment of the Requirements

for the Degree

Doctor of Philosophy

McMaster University

January 1969

DOCTOR OF PHILOSOPHY (1969)
(Chemical Engineering)

McMaster University
Hamilton, Ontario.

TITLE : Reaction Accompanied Mass Transfer Between Liquid Phases - an Experimental Study

AUTHOR : P. Seto, B.A.Sc. (University of Toronto)
M. Eng. (McMaster University)

SUPERVISORS : Professors A. I. Johnson and A. E. Hamielec

NUMBER OF PAGES : xxiii, 440

SCOPE AND CONTENTS:

This dissertation describes an experimental study of the simultaneous mass transfer and chemical reaction at a plane liquid-liquid interface involving the saponification of simple esters transferring into aqueous caustic solutions. The transfer experiments were carried out with both liquid phases stirred and unstirred respectively.

Special emphasis was placed on the stagnant-phase systems. Turbulent reaction layer propagation rates were measured for ester phases (pre-saturated with water) in contact with aqueous caustic solutions (at various concentration levels). The distortion of the moiré pattern was used to indicate the position of the propagating layer front. The cause and nature of the turbulent layer were elucidated. An apparatus, capable of withdrawing small samples of the liquid with probes precisely located in the aqueous phase, was constructed. Experimental techniques were developed to measure

the abnormal concentration profiles of the reactants and the products within the turbulent layer. From the component concentration distribution data, the turbulent layer thicknesses, the reaction zone (within the turbulent layer) thicknesses, the mass transfer rates, and the enhancement factors were deduced. The effects of turbulence in the aqueous phase were estimated in terms of the derived eddy diffusivities and of the differences between the experimentally measured and the theoretically predicted (by molecular diffusion with reaction equation) enhancement factors.

In the steady state transfer study using stirring in both phases, transfer rate data and enhancement factor data were obtained for three formate-sodium hydroxide systems.

In addition to the mass transfer studies, a preliminary investigation on the diffusion coefficient measurement in binary and ternary liquid systems employing the moiré pattern method was carried out. A diffusion cell was designed and built to enable the quick acquisition of the experimental data with reasonable accuracy.

ACKNOWLEDGEMENTS

The author is grateful to Dr. A. I. Johnson and Dr. A. E. Hamielec for their guidance and supervision throughout the course of this work and the preparation of this thesis.

He is also indebted to Dr. C. Calvo for his many helpful discussions and advice.

He wishes to thank Dr. W. F. Furter for his guidance and encouragement on various aspects of this study during the author's two-year lecturership at the Royal Military College of Canada.

The assistance of Mr. M. Li in drawing the figures and Mrs. P. Rogerson in typing the thesis is greatly appreciated.

Partial financial support in the construction of the apparatus was obtained from the Royal Military College of Canada.

He wishes to thank his wife, Mavis, for her encouragement, understanding and valuable support throughout the course of this study and for proof-reading the thesis.

TABLE OF CONTENTS

Page

LIST OF TABLES

LIST OF FIGURES

CHAPTER 1

INTRODUCTION

Ever since the development of chemical engineering, interphase mass transfer has been one of the vital operations in the field. Important practical examples are numerous; such as the gas absorption of sulphur trioxide and nitrogen dioxide in the manufacture of acids. There are many industrial operations involving the application of liquid-liquid extraction, for example, the sulphur removal from petroleum fractions, the nitration and sulfonation of organic compounds and the saponification of esters. A considerable number of these mass transfer processes are accompanied by simultaneous chemical reaction. Interphase mass transfer is frequently complicated by interfacial phenomena, for example, interfacial turbulence, interfacial resistance, spontaneous emulsification and the change in physical equilibria between phases. These interfacial phenomena are more pronounced in reacting systems, because the products formed and the heat evolved by the reaction continually change the physio-chemical nature of the interfacial region. It is evidently desirable to be able to predict and to know how the reactions and the associated interfacial phenomena affect the transfer rates which are the key data for designing the equipment for the operations.

Gas absorption with simultaneous chemical reaction has

been an active area of research for some years, both theoretically and experimentally. On the other hand, relatively little work has been done in the field of liquid-liquid mass transfer, especially with chemical reaction. Theories for gas-liquid reaction systems may sometimes be applicable to certain types of two-phase liquid systems. However, the analogy in theories between the two types of system does not always hold. As an example, transfer-and-reaction theory for gas-liquid systems is clearly not valid in liquid systems where the reactants and the products can transfer across the interface in both directions. Moreover, the experimental evidence from the literature indicates that the mass transfer across the liquid-liquid interface tends to be affected to a larger extent by the interfacial phenomenon than the mass transfer across the gas-liquid interface. Thus liquid-liquid reacting systems have more complex features than the gas-liquid systems and they require more careful study.

Previous investigations of the interphase mass transfer in some ester-aqueous caustic systems[S9] indicated that, in the case where two phases were stagnant, a turbulent reaction layer was observed at the interface. When both phases of an ester-caustic system were stirred, the turbulent layer disappeared and the reaction transfer rates obtained were smaller than the corresponding physical transfer rate in the same ester-aqueous caustic system.

The object of the present study is to obtain further

experimental information on the reaction mass transfer in the ester-aqueous caustic systems with both liquid phases unstirred and stirred respectively. Special emphasis is placed on the stagnant-phase systems. The study is directed towards the acquisition of information on the cause and nature of the turbulent reaction layers and on the effects of a large scale turbulence on mass transfer rates. In particular, the structure and the propagation of the turbulent reaction layers, the abnormal concentration profiles within the layers, the reaction zone thicknesses and the transfer rates are investigated. In the stirred-phase systems, mass transfer rates and enhancement factor data are collected for several ester-aqueous caustic systems. These data may be useful in probing the various factors governing the rates of interphase transfer. In addition, a preliminary study on the diffusion coefficient measurement in binary and ternary liquid systems employing the moiré pattern method is carried out.

In Chapter 2 of this dissertation, pertinent literature on the subject is reviewed and discussed. Relevant theories on interphase mass transfer and on diffusion are given in Chapter 3. In Chapter 4, the experimental work is presented. The experiments are grouped into four parts. Each part is divided into three main areas: experimental details, results, and the discussion of results. 4.1 - PART A and 4.2 - PART B are concerned with the studies in stagnant-phase systems. 4.3 - PART C deals with the investigations in

two-phase stirred systems. 4.4 - PART D describes the measurement of diffusion coefficientsin binary systems using the moiré pattern method. In Chapters 5, 6 and 7, the conclusions, recommendations and summary of contributions to knowledge are presented respectively.

Although the results are still preliminary in nature, it is hoped that the present investigations will lay the groundwork for further studies towards the understanding of the effects of interfacial phenomena on interphase mass transfer.

CHAPTER 2

LITERATURE REVIEW

Literature on interface mass transfer has been extensive and has been reviewed periodically by many workers. General discussions on mass transfer and interfacial phenomena were presented by Sherwood and Pigford (S12), Davies (D9), Astarita (A4) and Bird et al. (B8). Discussions on drops and bubbles phenomena were presented by Kintner (K4). Comprehensive annual surveys on mass transfer are published in Industrial and Engineering Chemistry.

In this Chapter, only the pertinent literature will be reviewed. The literature information is grouped under the following three categories: interfacial turbulence, interphase mass transfer, and diffusion coefficient measurement. Special emphasis is placed on the interfacial turbulence section.

2.1 Interfacial Turbulence

2.1.1 Previous Experimental Observations in Physical Mass Transfer Systems

2.1.1.1 Two-Phase Liquid-Liquid Systems

2.1.1.1.1 Plane Interface, Static Systems

Literature reports on the occurrence of interfacial turbulence are numerous in the three-component systems, and, to a much lesser extent, in the binary systems. Ward and Brooks[W1] were among the first to observe the existence of the spontaneous, highly localized interfacial agitation accompanying mass transfer. Kroepelin and Neumann[K12] photographed the flat, turbulent interface of the system ethyl acetate-acetic acid-water using the Schlieren apparatus. The active interface of the system amyl alcohol-acetic acid-water was photographed by Brückner[B20]. Davies[D12] contacted a solution of 4% acetone dissolved in toluene with water. The rapid, jerky movements of the interface were revealed by talc particles sprinkled onto the interface. Davies[D9] summarized the results of a number of diffusion experiments in ternary systems with and without surface active agents such as sodium lauryl sulfate[W3] or sorbitan mono-oleate[H1]. He concluded that, in general, interfacial turbulence would increase the rate of mass transfer in the otherwise unstirred systems. Monolayers would reduce or prevent the interfacial turbulence in the diffusion systems, and theory and experiment were then in good agreement.

Recently, Hoshino and Sato[H15] employed the moiré pattern method to observe the weak interfacial turbulence occurring in the diffusion of acetic acid and then of propionic acid across the stationary interface in the water-acid-toluene system with and without a surface active agent. They found that the rates of interface mass transfer were not influenced by the existence of a surface active agent.

All the above-mentioned experimental observations at the interface indicated that the phenomenon of interfacial turbulence is a chaotic and disorganized process. Some semblance of ordered flow could however be achieved for short durations by directing a thin jet of solute towards a flat interface between two pure immiscible liquids[K10][S18]. Linde[L9][L10][L11] succeeded in producing a non-chaotic interfacial cellular convection during the diffusion of a surface active agent across a stationary interface in many alcohol-water systems. Orell and Westwater[05] used the Schlieren technique to study in detail the spontaneous interfacial cellular convection accompanying mass transfer in the ethylene glycol-acetic acid-ethyl acetate system. They found that the interface exhibited a dominant pattern of stationary and propagating polygonal cells, accompanied by stripes and ripples. The average wave length, frequency and speed of propagation of the cells, stripes and ripples were measured. Gore[G10] studied optically the cellular pattern in benzene-acetic acid-glycol systems. Bakker et al.[B1]

studied the development of convective cells in a number of ternary systems. They measured the size of the convection cells and found them to be in the order of the magnitude of the penetration depth.

2.1.1.1.2 Dynamic Systems

Maroudas and Sawistowski[M3] conducted experiments on the separate and simultaneous transfer of propionic acid and phenol between carbon tetrachloride and water, using vertical and horizontal laminar co-current liquid-liquid contactors with moving interfaces. In all the runs the existence of interfacial turbulence was confirmed by visual or Schlieren observations. They concluded that, under conditions of spontaneous interfacial turbulence, the rate of mass transfer depended to a large extent on the induced rate of interface renewal and was directly proportional to the square root of the molecular diffusivity. More recently, Bakker et al.[B2] studied the mass transfer in ternary systems under well-defined hydrodynamic flow conditions. By changing the direction of mass transfer of the solute, experiments could be performed with and without interfacial turbulence. The ratio of the mass transfer rates with and without interfacial movement was found to be a function of the concentration driving force only. At high solute concentrations, the ratio approached an asymptotic value between 2 to 3 for different systems used. Merson and Quinn[M5] studied the diffusion in a number of binary liquid systems using a newly developed contacting device

in which a thin layer of one liquid (immersed in another liquid) flowed horizontally and radially outward from a central source. They detected a highly structured interfacial turbulence in several of the binary systems studied. However, the scale of motion (in isobutanol-water systems), though clearly visible, was sufficiently small. Therefore, it had very little effect on the rate of mass transfer.

With the phases stirred, the interfacial turbulence was not as pronounced as that observed in the static systems. Nevertheless, such effects were observed by Lewis(L4) and Blokker(B10) for some of their stirred systems. The effects of interfacial turbulence on the mass transfer rates were studied later by Topp(T9) and Olander(O3). In these studies, the mass transfer coefficients in ternary systems were found to depend on the direction of the transfer and the solute concentration levels. The enhancement of transfer coefficients over the theoretically predicted values without interfacial turbulence was in the order of 2 - 3.

2.1.1.1.3 Drops

Pendent drops or free-falling drops with rippling, pulsation, kicking and eruptions were studied extensively. Lewis and Pratt(L5) noticed that when drops of oil were either pendent or free in water, and a solute, e.g. acetone, was present initially in one phase, the drops underwent violent and erratic pulsations. The frequency of kicking for any one drop decreased as the time from the formation of

the drop increased. They were also able to demonstrate that during kicking of the drop, a violent circulation of the liquid took place at the interface. They also showed that for a wide variety of systems, addition of detergents or proteins inhibited the kicking. Haydon[H9] contacted a solution of acetone in toluene with water and observed the vigorous kicking of the drop. However, if the water phase was replaced with either sodium chloride solution or with dodecyl trimethylammonium bromide, the kicking was inhibited. Based on the experiments, he concluded that during diffusion across an interface, the non-uniform solute concentration at the interface gave rise to local interfacial tension variations which in turn caused instability in drops. Other work on the elucidation of the mechanism of interfacial turbulence was reported by Kroepelin and Neumann[K11], Goltz[G9], Haydon[H8] and Garner et al.[G3]. Sigwart and Nassenstein[S19] made an extensive photographic study of eruptions in pendent drops using a colour Schlieren microscope. More recently, Bakker et al.[B1] studied the interfacial behaviour during the growing of a drop in a number of three-component systems with mass transfer being directed out of as well as into the droplet and with phases being alternatively dispersed and continuous. They found that interfacial turbulence occurred when mass transfer was in one direction but did not necessarily occur when transfer was in the opposite direction.

Several investigators found that rising or falling drops

behaved in the same manner as the pendent drops[L3][S18].

Interfacial turbulence was also observed in binary liquid systems as reported by Austin et al.[A5] in their pendent drop experiments.

2.1.1.1.4 Spontaneous Emulsification

Interfacial turbulence was also observed in many ternary systems which exhibited spontaneous emulsification. McBain and Woo[M4] and, later, Haydon[H8] studied the phenomenon of emulsion with interfacial turbulence in solutions of methyl and ethyl alcohol in toluene placed in contact with water. They found that when protein or detergent was adsorbed at the interface, the interfacial turbulence was inhibited, but the emulsification was not appreciably affected. Kaminski and McBain[K1] examined the emulsion with turbulence formed when benzene, toluene or xylene was placed gently on strong solutions of dodecylamine hydrochloride. They found that either the dilution of the hydrochloride (to less than 0.1 N) or the presence of a detergent would inhibit the emulsion formation. Indeed, interfacial turbulence has been advanced as one of the three probable mechanisms of spontaneous emulsification.

An excellent review on the subject of spontaneous emulsification was given by Davies and Haydon[D10].

2.1.1.2 Two-Phase Gas-Liquid Systems

Surface instability also occurred in the gas-liquid systems. A classic example was furnished by Langmuir's

experiments[L1] on the evaporation of ether from a saturated solution in water. Talc sprinkled on the surface showed abrupt local movements, caused by the differences in surface tension in the different regions of the surface. A monolayer of oleic acid on the surface was observed to reduce the turbulence considerably. A similar effect was found by Groothuis and Kramers[G12] for the absorption of sulphur dioxide in n-heptane. The surface of the liquid became violently agitated. Using Schlieren and interferometric techniques, Kroepelin and Prott[K13] showed that the transfer of methanol vapor to water was an example of eruptive transfer. Ramshaw and Thornton[R3] showed that when either acetone or methanol vapor was absorbed into water, considerable interfacial turbulence occurred with ripple formation and surface oscillations. Using a capacitance probe and photographic techniques, Ellis and Biddulph[E1] measured the amplitude of the waves induced during the absorption of acetone or methanol into water. One of the common examples of surface-tension-driven flows is the ripples and tears at the surface in a glass of strong wine.

2.1.2 Previous Experimental Observations in Reaction Mass Transfer Systems

2.1.2.1 Two-Phase Liquid-Liquid Systems

2.1.2.1.1 Plane Interface, Static Systems

Interfacial turbulence phenomenon is more pronounced in systems with chemical reaction. Gad[G2] and Brücke[B19]

noticed that when solutions of a fatty acid (e.g. lauric) in oil were placed very gently upon the sodium hydroxide solution, an emulsion with interfacial turbulence was formed in the aqueous phase. Sherwood and Wei[S15] studied a number of ternary and quaternary reaction systems and concluded that the interfacial turbulence was pronounced in the case of exothermic neutralizations. Seto et al.[S9], while studying the reaction mass transfer in ester-caustic systems, observed the formation of a turbulent reaction layer with turbulent liquid motion at and near the interface. They also found that the addition of a trace of surface active agent would reduce the layer turbulence as well as the layer propagation rates. Cho and Ranz[C1] used the Schlieren method to follow the diffusion-controlled reaction zones resulting from the contact of two reactive liquid phases. They reported that the abnormally high rates of reaction zone propagation and transfer in some systems were due to the interfacial turbulence.

2.1.2.1.2 Dynamic Systems

Searle and Gordon[S6], Sherwood and Wei[S15], and Osborne[O6] performed transfer experiments on systems with instantaneous reaction in stirred vessels. They reported mass transfer rates several times as great as those predicted from Hatta's theory[H7]. Bakker et al.[B2] used a wetted-wall apparatus to study the reaction transfer of the acetic acid in the iso-butanol-aqueous sodium hydroxide system. The hydrodynamic

flow conditions of the two phases were well-defined. They confirmed the abnormally high transfer results of Sherwood and Wei.

Gaven[G4] and Sherwood et al.[S15] reported the "miniature explosion" of a drop of benzene containing acetic acid as it rose through an aqueous solution of ammonia.

2.1.2.2 Two-Phase Gas-Liquid Systems

Interfacial turbulence also occurred during the gas absorption with reaction. Using a highly sensitive interferometer, the optical study of interfacial turbulence occurring during the absorption of carbon dioxide into monoethanolamine solution was carried out by Thomas and McKNicholl[T4] in order to determine the conditions under which interfacial turbulence occurred. They also obtained the relationship of the time lapse (after the phase contact and before the onset of interfacial turbulence) versus the MEA concentration. Danckwerts and Da Silva[D5] observed the surface instability during the absorption of carbon dioxide by a drop of 1 N monoethanolamine solution.

Other literature data on the absorption of carbon dioxide into monoethanolamine under well-defined hydrodynamic conditions were obtained by many investigators using different kinds of experimental apparatus including Clarke[C2] and Astarita[A3] using laminar jets; Emmert et al.[E2] and Brian et al.[B18] using wetted-wall columns. Most of the absorption data by these investigators fell above the theoretically

predicted values due to the occurrence of interfacial turbulence.

2.1.3 Interfacial Turbulence Produced by Temperature Gradient at the Interface

Interfacial turbulence can also be induced by the local variation of temperature alone at the interface. Early in 1900, Bénard[B6] described his observations of a cellular deformation produced on the free surface of a liquid film (0.5 to 1.0 mm. thick), the bottom of which was uniformly heated and hotter than the top surface. He also observed a cellular flow associated with the deformation. Experiments have shown[P4] that drying paint films often display a steady cellular circulatory flow of the same type as that observed in the case of fluid layers heated from below. Block[B9] demonstrated experimentally that the Bénard cells observed were caused by surface-tension-driven flows which, in turn, were induced by the temperature gradients at the surface. He also observed that the addition of a monolayer at the free surface of the film would inhibit the formation of the flow cells. Mitchell and Quinn[M9] investigated the convective flow in a thin liquid layer heated from below and confirmed the findings of Block. Furthermore, they observed oscillating temperature and velocity fields in thin horizontal films.

2.1.4 Interfacial Turbulence Produced by Density Variation

Interfacial turbulence can also be induced by the action of buoyancy forces as a result of the density variation. Experimental investigations by Zierep[Z1] and Schmidt et al.[S3]

revealed a cellular motion in a liquid layer bounded by horizontal plates (to eliminate the surface-tension-driven flows), when the bottom plate was hotter than the top plate.

A small disturbance analysis was carried out by Rayleigh[R5] and others for the case of free-surface instability due to density gradients. They obtained a critical film thickness (2 mm.) below which there was stability.

Block[B9] performed experiments with a thin film heated from the bottom whereby the Bénard cells (due to surface tension variation) were first produced and then removed by covering with a monolayer. Then the thickness of the liquid film (covered by a monolayer) was increased until cellular surface deformation and circulation could again be seen. The thickness of the film at the reappearance of the cellular motion was 2 mm., which was about the predicted critical depth for the onset of convective instability due to density variation.

2.1.5 Theoretical Treatment of Interfacial Turbulence

It is well known that local variations of interfacial tension not only cause movement in a liquid surface but also bring forces to bear on the underlying liquid, setting it in motion. This has been called the Marangoni effect[B7]. The surface tension variation can be brought about by the local variations of component concentration at the interface as the result of mass transfer. Alternatively, a temperature variation at the interface, produced by uneven distribution of heat of solution or heat of reaction, will also cause the

local variation of interfacial tension. The development of detailed theory relating the Marangoni effect to the interfacial turbulence proceeded at a slow rate owing to the inherent complexity of a reasonable mathematical description.

Haydon[H9] proposed a kicking mechanism to explain the drop oscillation during mass transfer. Later Davies and Haydon[D11] derived the equations of motion for the pendent drop oscillation, thus enabling the prediction of oscillation frequencies and energy dissipated against viscous forces during the damping of the oscillations.

Recent available analyses usually dealt with the stability of the transfer systems towards small disturbances. The onset of a steady, cellular convection driven by surface tension gradients (which, in turn, were caused by surface temperature gradients) on a thin layer of liquid was examined by Pearson[P4]. His results indicated the existence of a critical "Marangoni number" for the onset of instability. Sternling and Scriven[S22] formulated a theoretical model describing surface-tension-driven interfacial activity (which in turn was caused by surface concentration gradients) at plane liquid-liquid interfaces. They mathematically analyzed the simplified, two-dimensional model (roll cells) by means of the theory of linearized stability coupled with the traditional hydrodynamic and diffusion principles. They developed criteria for the onset of instability and determined the nature of the dominant disturbance, predicting its wave

length, amplification factor, speed of propagation, and temporal period. The Sternling and Scriven theory has been partially confirmed by many workers(O5)(L12)(L13). The Pearson's analysis was later modified by Scriven and Sternling(S5) to include the effects of surface viscosity and by Smith(S21) to include the effects of surface viscosity and gravity waves. Recently, Vidal and Acrivos(V3) extended Pearson's analysis to include the effect of nonlinear conductive temperature profiles on the stability of liquid layers subject to surface tension gradients.

Ruckenstein and Berbente(R12) extended the Sternling and Scriven's analysis(S22) to the case where diffusion was accompanied by a first-order chemical reaction in one of the two phases. They established conditions under which the Marangoni effect produced interfacial turbulence in reacting systems and concluded that even a slow first-order reaction might cause instabilities in an otherwise stable system. Ruckenstein(R10) also examined the influence of the Marangoni effect on the mass transfer in the continuous phase from a spherical drop or bubble when $Re < 1$. He concluded that the Marangoni effect should be a factor only in transfer from small drops or bubbles.

Surface instability due to buoyancy effects is probably, in most cases, considered of secondary importance and has, accordingly, received much less attention. Rayleigh(R5) analyzed the stability with respect to buoyancy-driven

convection of a fluid layer heated from underneath. His analysis was subsequently extended by Jeffreys(J1), Low(L15) and Pellew et al.(P5). Conditions for instability were established. Recently, Sani(S1) analyzed the convective instability of a system undergoing heat and mass transfer, to buoyancy-driven finite amplitude roll cell disturbances. The distortion of the mean temperature and concentration fields by the disturbance and the transport of heat and mass at a finite amplitude roll cell equilibrium state were investigated.

2.1.6 Recent Trends of Interfacial Turbulence Study

Apart from the continuing interest in theoretical stability analysis, recent developments are also concerned with the enhancement of physical mass transfer under controlled mechanical interfacial turbulence. Boyd and Marchello(B12) studied the influence of small surface waves on the absorption of carbon dioxide into water. Small amplitude, progressive, two-dimensional waves were mechanically generated in a sealed ripple tank. Goren et al.(G11) investigated the effect of standing waves of controlled amplitude and frequency on the steady state rate of mass transfer through thin horizontal liquid layers. Both groups of investigators reported a transfer increase due to the agitations.

At the same time, attention is directed to the study of physical mass transfer under falling wavy film conditions. Thus Banerjee et al.(B4) developed a physical model describing a small eddy structure near the interface. They showed that

the mass transfer process was likely to be controlled by small eddies for which viscous dissipation was important. An expression for the mass transfer coefficient in terms of the viscous dissipation near the surface has been obtained. Another model was proposed by Banerjee et al.(B3), using a partial surface renewal concept, to predict mass transfer rates under falling wavy liquid films. The model was based on the action of large single eddies associated with the wave motion. Comparison of the computed values of mass transfer coefficient from the large-eddies-model with data from the literature gave good agreement at low Reynolds numbers (100 to 800). Howard and Lightfoot(H17) applied the surface-stretch model to predict rates of gas absorption into laminar rippling films in terms of surface velocities. Oliver and Atherinos(O4) measured the enhancement of physical mass transfer to liquid films on an inclined plane. The enhancement was due to rippling.

All the above-mentioned studies may be a step in the direction towards the understanding of the effects of turbulence (at or near the interface) on the mass transfer rates.

2.2 Interphase Mass Transfer

2.2.1 Theoretical Considerations

2.2.1.1 Physical Mass Transfer

Ever since the advent of Nernst's diffusion layer theory (N3)(N2), a considerable number of models have been proposed to describe the mechanism (and thus to predict the rates) of physical mass transfer across an interface. The over-simplified two-film theory of Lewis and Whitman(L6) has been superseded by the more elegant concepts such as the penetration theory of Higbie(H11) and the surface renewal theory of Danckwerts(D3). Both the Whitman and Higbie-Danckwerts models have been elaborated on (Hanratty(H2), Perlmutter(P6)) or combined and elaborated on (Toor and Marchello(T8)(M2), Harriott(H6), Dobbins(D16), Ruckenstein(R9)), but progressively improved agreement with observation has only been achieved at the expense of increasing the complexity. Alternatively, a steady state phenomenological approach has been advanced by Kishinevskii(K6)(K7), in which the turbulent convective effects give rise to an eddy diffusivity which is obtained from experiments. Derivations of mass transfer rates have been developed(L8)(S13) based on the boundary layer theories first proposed by Prandtl et al.(P10)(V6). More recently developed models tend to be more realistic in describing the actual experimental interphase transfer conditions with particular attention to the flow very near the surface (e.g. the quasi-steady large scale model(F1) and the small eddy structure

model[B4]). A generalized penetration theory for unsteady convective mass transfer taking into account the convective motions along the interface and along the normal at the interface was proposed by Ruckenstein[R11]. Szekely et al.[29] obtained an analogue computer solution for transient diffusion in two-phase systems with the bulk flow and concentration dependent diffusion coefficient.

Multicomponent diffusion problems are important in many chemical and physical processes. Exact treatment of such problems is seldom feasible, since the governing differential equations are complicated and nonlinear. For small concentration differences, however, a linearized treatment of the multicomponent mass transfer equations leads to a set of equivalent binary equations. Solutions of the linearized equations of multicomponent mass transfer were obtained by Toor[T6] and Stewart and Prober[S24].

Theoretical studies on multicomponent mass transfer have been developed by Toor et al.[T5], and by Roper et al.[R8] on gas absorption. The mass transfer equations obtained differed in form from the usual binary component equations and they predicted qualitative as well as large quantitative differences between binary and ternary transfer.

2.2.1.2 Mass Transfer with Chemical Reaction

All of the above models concerning the mechanism of interphase mass transfer combined with chemical kinetics of a reaction can lead toward the predictions of the effect of a

simultaneous chemical reaction upon the rate of mass transfer. Several cases have been treated (B16)(V1)(P7)(D2)(D6)(D1)(H7)(H19)(D4)(P2)(F3)(S13).

The effect of ions diffusing in mixed electrolytes has been discussed(S14)(V4) and, in several cases, it has been combined with existing theories(S14)(V4)(M1)(V2)(B14). In general (except under certain conditions as specified in Reference (B14), e.g. equal ionic self-diffusion coefficients of the ionic species)it was found that mass transfer rates calculated taking into account ion diffusion effects departed significantly from those which would be obtained with molecular diffusion(B14). The effect of heat of reaction on mass transfer with chemical reaction has been investigated by Kobayashi and Saito(K8). The effect of bulk flow on mass transfer accompanied by homogeneous chemical reaction was discussed by Szekely(S28) in terms of the "film model". Some problems of analyzing processes of mass transfer with chemical reaction were discussed by Mutriskov and Maminov(M10). Brian et al.(B15) presented theoretical solutions for gas absorption accompanied by a two-step chemical reaction involving a transient intermediate species.

The type of chemical system which has received the most attention is that in which a gaseous species dissolves and then reacts irreversibly with a non-volatile solute already present in the liquid phase. In the case of a second-order chemical reaction between the dissolving species and the

non-volatile solute, an approximate solution to the film theory was presented by Van Krevelen and Hoftijzer[V1], and the accuracy of this approximated solution was demonstrated by Peaceman[P3]. The penetration-theory solution for this case was obtained numerically by Perry and Pigford[P7] for a limited range of variables and later by Brian et al.[B16] for a much wider range of variables.

Generalized penetration theory solutions with respect to the order of the chemical kinetic equation were presented by Brian[B13] and Hikita et al.[H12].

Location and thickness of the reaction zone in liquid-liquid systems with reaction were derived by Scriven[S4] for unsteady state transfer. On the other hand, reaction zone thickness was derived by Friedlander et al.[F2] for steady state transfer.

Although most of the theories are proposed specifically for gas absorption, their extension to certain types of liquid-liquid system does not involve assumptions differing significantly from those postulated for gas-liquid systems.

2.2.2 Experimental Studies

Various experimental investigations have been conducted, aimed mostly at testing the various transfer models. Probably the type of apparatus used (i.e. the flow pattern) is clearly related to the theory chosen. For example, the film theory would be expected to work better for a gently stirred vessel, where steady state mass transfer across an unbroken interface

occurs, than for a packed tower, where the liquid flows over a piece of packing for a very short period of time before being mixed and then flows to the next piece.

2.2.2.1 Physical Mass Transfer

A comprehensive summary of the reported experimental work up to 1963 was given previously in Seto's Master s Thesis[S8]. Recent developments include the study of turbulent and convective transfer in apparatus such as turbulent jets[D13] and agitated vessels[K3]. Physical interphase mass transfer rates were measured for mechanically-controlled wavy films[B12][G11], vibrating spheres[N5] and cylinders[S27]. Thus the enhancement of transfer due to imposed mechanical motion was obtained. Other advances include mass transfer from a rotating disk into power-law-liquids[H4] and the detection of interphase mass transfer by measuring electrochemiluminescence in a electrolytic cell[C3].

2.2.2.2 Reaction Mass Transfer

Many experimental investigations are concerned with gas absorption involving a chemical reaction. Thus Nijsing et al.[N4] carried out studies on the absorption of carbon dioxide into laminar jets and laminar falling films of aqueous solutions of sodium, potassium and lithium hydroxides. Danckwerts and co-workers have carried out a series of studies on the absorption of carbon dioxide into alkaline solutions with a variety of interfacial geometrics, such as rotating drum[D7], wetted-wall column[R7] and laminar jet[S11]. The carbon

dioxide-monoethanolamine system has been the subject of many investigators(C2)(A3)(E2)(B18). Many studies of gas absorption with chemical reaction in stirred vessels have been reported(A1)(P1)(V2)(K9). A bubble of carbon dioxide absorbed by the monoethanolamine solution was studied by Houghton (H16).

Reaction mass transfer studies in liquid-liquid systems have been performed mostly by using stirred vessels. Thus Osborne(O6), Searle and Gordon(S6), Sherwood and Wei(S15) extracted acetic acid from isobutanol using aqueous sodium hydroxide solution. The extraction of acetic acid from water by a solution of cyclohexylamine in isobutanol and the extraction of n-butyric acid from benzene by aqueous sodium hydroxide were also performed by Sherwood and Wei(S15). Abnormally high transfer rates were obtained due to interfacial turbulence. On the other hand, Fujinawa et al. (F4)(F6) carried out a large number of experiments in liquid-liquid extraction with chemical reaction. In each of the systems under study, chemical extraction rates were found to be constant in the range above a certain critical value of the initial sodium hydroxide concentration. Their conclusion was in support of the film theory. Raal and Johnson(R2) derived a non-linear differential equation on liquid extraction where the solute, on transferring across the interface, reacted to form a dimer through a rapid second-order reversible reaction with the solvent. However, experimental results

deviated from the predicted ones(R1). Seto et al.(S8) studied the reaction transfer of esters into caustic solutions. Abnormally low transfer rates (as compared to theory) were obtained.

Reaction transfer across a liquid-liquid interface in stagnant two-phase systems was studied by Cho and Ranz(C1) and by Seto et al.(S9). They reported that the abnormal enhancement of transfer rates and reaction layer propagation rates were due to interfacial turbulence.

Very little information concerning mass transfer with reaction in drops is available. Nevertheless, extraction of acetic acid and butyric acid from various solvent drops by aqueous potassium hydroxide was carried out by Fujinawa and Nakaike(F5). They found that in the case of acetic acid transfer from solvent drops, the transfer rates, in general, decreased with increasing potassium hydroxide concentration; while in the case of butyric acid transfer from solvent drops, the transfer rates, in general, slightly increased with increasing caustic concentration. Drop study with reaction was also carried out by Watada(W2) of this Department.

Comparisons between experimental results and theoretical predictions have not only been used to check the applicability of the theory but they have also been used to infer the kinetics and the mechanisms of very fast gas-liquid reactions(B17)(D6)(G7)(R7)(J2)(J3)(G5) and of the liquid-liquid reaction(N1).

Recent advances included mass transfer with reaction in gas-fused salt systems[R14][O2][O1][G1][R13][G8] and the measurement of concentration distribution of gases in a reacting trickling film by a fluorescence method[H10a].

2.3 Diffusion Coefficient Measurement

The experimental and theoretical investigation on binary gaseous diffusion has been fairly adequate for moderately low temperatures and pressures. A number of semi-empirical equations were proposed to predict the diffusion coefficient of low density gases, such as the Gilliland's[G6], the Hirschfelder, Bird and Spotzs'[H14], the Slattery and Bird's[S20]. Equations predicting diffusion coefficients for a gas diffusing into a multicomponent gas solution based on the binary diffusion coefficients have also been developed. For a three-component system, Curtiss and Hirschfelder derived[C7] an expression relating the multicomponent diffusion coefficient to the binary diffusion coefficients. Methods of evaluating multicomponent diffusion coefficients for special cases have been developed by Wilke[W5], Stewart[S23], Hsu and Bird[H18]. These methods simplify the calculations somewhat. The most well-known of all is the Stefan-Maxwell equations[B8] which are usually the starting point for the calculation of ordinary diffusion in multicomponent gas mixtures.

On the contrary, the advent of liquid diffusion is not as extensive, notwithstanding the fact that experimental liquid diffusion data are actually more essential. One of the possible explanations is that the diffusivities for most liquids vary quite markedly with concentration as well as viscosity even if the temperature and pressure are constant. Furthermore, there is considerable difference in the diffusion

process between ionic liquids and non-electrolytes. Nevertheless, a few correlations determining the diffusivities at dilute solutions have been proposed. For the non-electrolytes, these are the Arnold equation(A2), the Wilke correlation(W4), the Wilke and Chang equation(W6). Recently, a note by Shrier(S16) reinforced the continued use of the Wilke-Chang correlation. An expression was also developed to account for the effect of concentration on diffusion of non-electrolytes (P9). Among the recent developments are the analysis of Pynn and Fixman(L7) which allows the extension of the hydrodynamic model to concentrated systems, the analyses of Olander and of Gainer and Metzner(L7) which extend the Eyring theory to dilute solutions of very high viscosity. Cullinan(C6) proposed a modification of the absolute rate theory of Eyring which resulted in an expression to predict the concentration dependence of binary diffusion coefficients for non-ideal solutions, in terms of two coefficients at infinite dilution and a thermodynamic factor. The proposed relation works well except for associated mixtures (those exhibit maxima). Hansen(H3) presented simple correlation factors for the rapid calculation of the true diffusion coefficients obtained by absorption and desorption methods based on an exponential dependence on concentration. He pointed out that very serious errors were made when concentration dependence was neglected.

Very little work has been done on the prediction of

multicomponent diffusion in liquids. More recently, the technique developed by Pynn and Fixman has been applied by Lightfoot and Cussler[L7] to obtain a first approximation of multicomponent diffusion. This development is in semi-quantitative agreement with data of the polystyrene –toluene system. Both Toor[T7] and Kass and O'Keefee[K2] discussed methods for predicting the concentration distribution and hence evaluating diffusivities that depended on concentration. Mijnlieff and Vreedenberg[M7] solved the mass balance for isothermal, isopiestic diffusion in a three-component electrolytic system with concentration dependent diffusivities. Included was a method of evaluating the diffusion coefficients as a function of concentration. Hays and Curd[H10] described a variational technique for concentration dependent diffusion.

The diffusion coefficient in very dilute solution of completely ionized simple univalent electrolytes was given by the Nernst equation. The case of diffusion in mixed electrolytes was treated by Vinograd and McBain[V4] and Sherwood and Wei[S14].

Since no adequate theory for the prediction of diffusion coefficients of liquids exists, experimental measurements are generally required. Much effort has been spent to improve the design of apparatus for diffusion measurements. A number of diffusion cells have been developed. The most common one is the use of pseudo-steady state diffusion through a diaphragm cell[S25][M8][T3]. Although the apparatus is simple to

construct, the diffusion process through the diaphragm is slow and often requires a considerable amount of experimental time. Generally, the component allowed to diffuse is limited to a small amount; thus, rendering the analysis of concentration inaccurate. In the extreme case, e.g. polymer diffusion, such cells may not be suitable because of the difficulties encountered by the molecules passing through the pores. The diffusion coefficient measured with the diaphragm cell is the integral value over the concentration increment and at the particular experimental concentration level. Several theories which include the effect of concentration dependence of diffusion coefficient have been developed for the diaphragm cell[S26], but they are difficult to use.

For higher accuracy measurements, either free or restricted diffusion method is used. In order to get accurate diffusivities using such methods, two difficulties must be overcome while performing the experiment. They are (a) to form a sharp initial boundary of contact, (b) to probe the concentration profiles without disturbing the system. There are a number of diffusion cells designed to give good contact between two solutions. The Fürth cell[F7] is an example of the earlier development. A thin draw slide is used to separate the two solutions initially inside the Fürth cell. It is more popular to provide the initial contact between the two solutions by a shearing mechanism such as the Claesson cell[C1b]. An excellent design for very viscous solution is the flow-junction

diffusion cell[P7a]. On the other hand, a simple cell for free diffusion measurements has been recommended by Lamm[L1a]. Damper type cells as well as invertible type cells were recommended by Inoue et al.[I1]. Some other methods have been developed to sharpen the boundary between solutions such as that of Polson and Kahn [P7b]. A few methods have been proposed to trace the concentration profiles without actual sampling. Radioactive tracers were used[E3] although the diffusion coefficients so obtained may not be the binary ones[M7a]. Less accurate but well executed measurements have been made with electrical conductivity[M7a]. However, the most accurate methods so far yet devised are the optical methods. These are the light absorption method[K3a], Guoy's diffusiometer[G11a] and Rayleigh interferometer[C4b], and Schlieren knife-edge method by Takamatsu et al.[T1]. More recently, Sato[S2] proposed a method to calculate the concentration profiles making use of the moiré pattern. This method has also been extended to cover two-phase, three-component systems[H15]. Similar method has been applied by Secor[S7] for polymer diffusion measurements. Of all the methods discussed so far, Sato's method is the easiest to use experimentally.

Even with so many experimental techniques available, diffusion coefficient data are quite scarce. Only a few systems have been studied at various concentrations[T2][S2][J4].

Further detailed literature review can be obtained in Reference (L2).

CHAPTER 3

THEORETICAL PRINCIPLES

3.1 Mass Transfer with Chemical Reaction

The following discussion deals with a two-phase liquid system whereby reactant A is the solvent of phase I and is partially soluble in phase II; while reactant B is the solute in phase II but practically insoluble in phase I. In addition, the mass transfer situation will be further simplified if the solvent of phase I is pre-saturated with the solvent of phase II, so that upon the contact of the two phases, only reactant A from phase I will transfer across the interface and react with B in phase II as described by the following equation:

$$A + B \longrightarrow C + D \qquad (1)$$

The transfer phenomenon in phase II can be described by the following general equation:

$$\frac{\partial C_i}{\partial t} + \bar{v}\cdot\nabla C_i = \nabla\cdot D_i\nabla C_i + G_i \qquad (2)$$

where,

C_i = concentrations of species i, moles/cm^3

t = time, seconds

$\bar{v}$ = velocity of convective current, cm/sec.

D_i = diffusion coefficient of species i in phase II, cm^2/sec.

G_i = rate of formation of species i, moles/cm^3/sec.

If the experiments are carried out with two stagnant phases, one resting on top of the other in a cell of constant cross-sectional area with respect to the cell length, the transfer situation as described by equation (2) can be reduced to:

$$\frac{\partial C_i}{\partial t} = \frac{\partial}{\partial x}\left(D_i \frac{\partial C_i}{\partial x}\right) + G_i \qquad (3)$$

Further restrictions of constant diffusion coefficients and an irreversible second-order reaction reduce equation (3) to the following set of equations:

$$\frac{\partial C_A}{\partial t} = D_A \frac{\partial^2 C_A}{\partial x^2} - kC_AC_B \qquad (4a)$$

$$\frac{\partial C_B}{\partial t} = D_B \frac{\partial^2 C_B}{\partial x^2} - kC_AC_B \qquad (4b)$$

$$\frac{\partial C_C}{\partial t} = D_C \frac{\partial^2 C_C}{\partial x^2} + kC_AC_B \qquad (4c)$$

$$\frac{\partial C_D}{\partial t} = D_D \frac{\partial^2 C_D}{\partial x^2} + kC_AC_B \qquad (4d)$$

where the subscripts A and B represent the reacting species, the subscripts C and D represent the reaction products, k is the second order reaction rate coefficient, cm^3/mole-sec. and x is the distance, cm.

If the reaction rate is infinitely fast, the zone of reaction is of negligible thickness as illustrated in Figure 1a. The transfer process becomes diffusion controlled and independent of the chemical reaction (A4)(S12). On the other hand, if the reaction rate is slow, the reaction zone tends to spread throughout the solution as shown in Figure 1c.

The reaction becomes pseudo-first order with respect to $A^{(S12)}$. Finally, if the reaction rate is finite, then the reaction zone thickness (the region in which non-negligible concentrations of both reacting species exist simultaneously) will also be finite as shown in Figure 1b. Such is the case for the reaction systems in the present study.

FIGURE 1

CONCENTRATION PROFILES FOR TWO CHEMICAL SPECIES REACTING NEAR AN INTERFACE

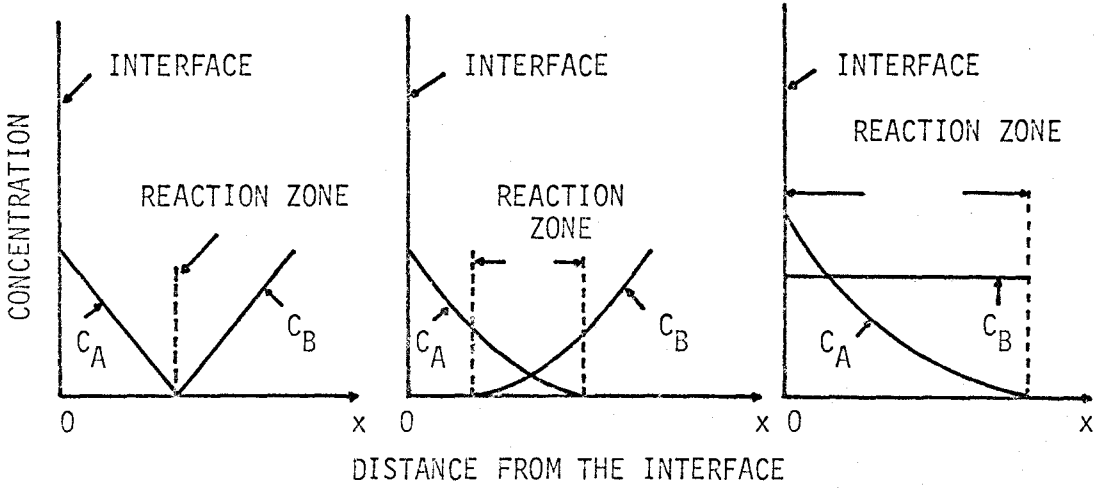

1a. Diffusion Controlled infinite reaction rate

1b. Finite reaction rate

1c. Pseudo-first order; slow reaction rate - high diffusivity of B

3.1.1 Estimation of the Reaction Zone Thickness

(Refer to 4.2 - PART B)

If the transfer process is a steady state one, equations (4a) and (4b) will be reduced to

$$D_A \frac{d^2C_A}{dx^2} - kC_AC_B = 0 \qquad (5a)$$

$$D_B \frac{d^2C_B}{dx^2} - kC_AC_B = 0 \qquad (5b)$$

With the assumptions of constant k and negligible thermal effects, equation (5a) is subtracted from (5b) and the resulting equation is integrated twice with the following boundary conditions:(F2)

$$\text{at } x = +\infty; \quad C_A = 0, \ \frac{dC_A}{dx} = 0, \ \frac{dC_B}{dx} = -\frac{J_B}{D_B}$$

$$x = -\infty; \quad C_B = 0, \ \frac{dC_B}{dx} = 0, \ \frac{dC_A}{dx} = -\frac{J_A}{D_A}$$

$J_A = J_B = J$; (steady state molal fluxes; moles/cm^2-sec.)

The relationship between the concentrations of the reacting species is:

$$C_B = \frac{1}{D_B}(D_AC_B + JX) \qquad (6)$$

where,

$X = x - x_o$ and x_o is an arbitrary constant of integration.

Substitution of (6) into (5a) yields;

$$\frac{d^2C_A}{dX^2} = \frac{k}{D_B}(C_A^2 + \frac{J}{D_A}C_AX) \qquad (7)$$

With the aid of equation (7), the dimensional analysis gives:

$$C_A = \left(\frac{J}{D_A}\right)^{2/3} \left(\frac{D_B}{k}\right)^{1/3} \psi_A(\eta) \qquad (8)$$

where,

$\eta = X/l$

$l = (D_A D_B / Jk)^{1/3}$

Substitution of equation (8) back to (7) gives

$$\frac{d^2\psi_A}{d\eta^2} = \psi_A^2 + \psi_A \eta \qquad (9)$$

By the transformation $\psi_A = \phi_A - \frac{1}{2}\eta$, equation (9) becomes

$$\frac{d^2\phi_A}{d\eta^2} = \phi^2{}_A - \frac{\eta^2}{4} \qquad (10)$$

With the following boundary conditions:

at $\eta = -\infty$, $\frac{d\phi_A}{d\eta} = -\frac{1}{2}$

$\eta = +\infty$, $\frac{d\phi_A}{d\eta} = +\frac{1}{2}$

Equation (10) was solved by Friedlander et al.[F2] With the reaction zone defined as the region in which the flux of species A was reduced from 95% of its initial value to 5% of its initial value, they found that the thickness of the reaction zone was 4.4 l.

The above theory should also apply to transient diffusion where the stationary-state assumption is valid.

3.1.2 Estimation of the Enhancement Factor

3.1.2.1 Penetration Theory (unsteady state)

(Refer to 4.2 - PART B)

Normalizing equations (4a) and (4b) by changing the variables into dimensionless ones[B16].

$$\frac{C_A}{C_{Ai}} \longrightarrow a$$

$$\frac{C_B}{C_{Bo}} \longrightarrow b$$

$$kC_{Bo}t \rightarrow \theta$$

$$D_B/D_A \rightarrow r$$

$$C_{Bo}/C_{Ai} \rightarrow q$$

$$(kC_{Bo}/D_A)^{\frac{1}{2}}x \rightarrow z$$

results in:

$$\frac{\partial^2 a}{\partial z^2} - \frac{\partial a}{\partial \theta} = ab \qquad (11a)$$

$$rq\frac{\partial^2 b}{\partial z^2} - q\frac{\partial b}{\partial \theta} = ab \qquad (11b)$$

with the following boundary conditions:

at $\theta = 0$, any $z > 0$: $a = 0$, $b = 1$

$z = 0$, any $\theta > 0$: $a = 1$, $\frac{\partial b}{\partial z} = 0$

$z \rightarrow \infty$, any θ : $a = 0$, $b = 1$

By defining $\phi = k_L/k_L^*$

where

k_L = mass transfer coefficient with chemical reaction based on the average transfer rate over the contact time interval, cm./sec.

k_L^* = average physical mass transfer coefficient for transfer without reaction, cm./sec.

ϕ_a = enhancement factor of mass transfer involving an infinitely rapid chemical reaction

$$\phi_a = 1/\text{erf}\ (\sigma) \qquad (12a)$$

$$q\sqrt{r} = (1 - \text{erf}\ (\sigma/\sqrt{r}))/\left[\text{erf}(\sigma)\ \exp(\sigma^2(1-1/r))\right] \qquad (12b)^{\dagger}$$

Also, by defining

$$M = (\pi/4)\theta = kD_A C_{B_o}/(k_L^*)^2$$

Brian et al. speculated that:

$$\phi = \frac{\left[(M)\ (1 - ((\phi-1)/(\phi_a-1)))\right]^{\frac{1}{2}}}{\tanh\left[((M)(1 - ((\phi-1)/(\phi_a-1))))^{\frac{1}{2}}\right]} \qquad (13)$$

They then proceeded to solve equations (11a) and (11b) numerically using the linearized time-centred, implicit finite difference methods of Crank and Nicholson(C4a). The ϕ values so obtained from the numerical solutions were compared with those approximated by equation (13) by Brian et al. Calibration curves were made to adjust the ϕ values obtained by equation (13) to within 3% of the ϕ values by the true penetration solution. (For details of the calibration curves, Reference (B16) should be consulted.)

† σ is defined implicitly by equation (12b).

3.1.2.2 Film Theory (steady state)

(Refer to 4.3 - PART C)

By assuming the concentration of the reactant B from the lower phase (phase II) is constant throughout the proper reaction zone in the liquid film, Van Krevelen and Hoftijzer[V1] presented an approximate solution to the film theory.

$$\phi = \frac{\left[(M)(1 - (\phi-1)/rq)\right]^{\frac{1}{2}}}{\tanh\left[((M)(1 - (\phi-1)/rq))^{\frac{1}{2}}\right]} \qquad (14)$$

A more detailed discussion of the film theory solution is available [S8].

3.2 Molecular Diffusion in Homogeneous Binary Liquid Systems

(Refer to 4.4 - PART D)

3.2.1 Diffusion Coefficient

Consider the diffusion process between two solutions, A and B. For this process, Fick's law can be written as follows: (for one dimensional transfer)

$$N_A = - D_{AB} \frac{\partial C_A}{\partial x} + x_A(N_A + N_B) \qquad (15)$$

where

N_A is the molar flux of the substance A

N_B is the molar flux of the substance B

x_A is the molar fraction of the substance A

x distance in the diffusion direction from the boundary

D_{AB} diffusion coefficient between A and B at the concentration C_A.

For a constant volume diffusion cell, the net flow of volume through any plane perpendicular to the x direction must be equal to zero. Hence, we have:

$$N_A\overline{V}_A + N_B\overline{V}_B = 0 \qquad (16)$$

where

$$\overline{V}_A = \frac{\partial V}{\partial n_A}$$

and

$$\overline{V}_B = \frac{\partial V}{\partial n_B}$$

$\overline{V}_A$, $\overline{V}_B$; partial molar volumes of A and B.

From (16) we have:

$$N_B = - \frac{\bar{V}_A}{\bar{V}_B} N_A$$

1) If there is no volume change on mixing, we have:

$$\bar{V}_A = V_A^{\circ}$$

$$\bar{V}_B = V_B^{\circ}$$

If $V_A^{\circ} = V_B^{\circ}$; $N_A = - N_B$ and (15) can be written

$$N_A = - D_{AB} \frac{\partial C_A}{\partial x}$$

or

$$\frac{\partial C_A}{\partial t} = \frac{\partial}{\partial x} \left(D_{AB} \frac{\partial C_A}{\partial x} \right)$$

2) If $V_A^{\circ} \neq V_B^{\circ}$ and there is volume change on mixing,

$$N_A = - D_{AB} \frac{\partial C_A}{\partial x} + x_A \left(N_A - \frac{\bar{V}_A}{\bar{V}_B} N_A \right)$$

$$N_A = - \frac{D_{AB}}{1 - x_A \left(1 - \frac{\bar{V}_A}{\bar{V}_B} \right)} \frac{\partial C_A}{\partial x}$$

Duda et al.(D17) have treated this case in detail. However, if $x_A \ll 1$, we can write:

$$N_A = - D_{AB} \frac{\partial C_A}{\partial x}$$

or

$$\frac{\partial C_A}{\partial t} = \frac{\partial}{\partial x} \left(D_{AB} \frac{\partial C_A}{\partial x} \right)$$

Summarily, if there is no volume change on mixing or if the concentrations involved are low, the diffusion process in a solution of A and B can be represented by the following differential equation.

$$\frac{\partial C_A}{\partial t} = \frac{\partial}{\partial x} \left(D_{AB} \frac{\partial C_A}{\partial x} \right)$$

Boltzmann[B11] has treated this equation by using a similarity transformation:

$y = \frac{x}{\sqrt{t}}$ for the following conditions:

$C_A = C_{A_o}$ for $x < 0$ and $t = 0$

$C_A = 0$ for $x > 0$ and $t = 0$

$C_A = C_{A_o}$ for $x = -\infty$ and $t \geq 0$

$C_A = 0$ for $x = +\infty$ and $t \geq 0$

Free diffusion situation is assumed with this transformation. Upon substitution one obtains:

$$-\tfrac{1}{2} y \frac{dC_A}{dy} = \frac{d}{dy}\left(D_{AB}\frac{dC_A}{dy}\right)$$

Integrating

$$-\tfrac{1}{2}\int_{C_{A_o}}^{C_A} y\, dC_A = \left(D_{AB}\frac{dC_A}{dy}\right)_{C_A} - \left(D_{AB}\frac{dC_A}{dy}\right)_{C_{A_o}}$$

Noting that $\frac{dC_A}{dy} = 0$ at $C_A = C_{A_o}$

$$\therefore D_{AB} = -\tfrac{1}{2}\left(\frac{dy}{dC_A}\right)_{C_A} \int_{C_{A_o}}^{C_A} y\, dC_A$$

If y is replaced back by $\frac{x}{\sqrt{t}}$

$$D_{AB} = -\frac{1}{2t}\left(\frac{dx}{dC_A}\right)_{C_A} \int_{C_{A_o}}^{C_A} x\, dC_A \qquad (17)$$

or

$$D_{AB} = -\frac{1}{2t}\left(\frac{dx}{dC_A}\right)_{x} \int_{-\infty}^{x} x\frac{dC_A}{dx}\, dx \qquad (18)$$

where x is the distance, in the diffusion direction, from the

boundary of the two solutions. This boundary must be defined by the condition(J5):

$$\int_0^{C_{A_o}} x \, dC_A = 0$$

according to the law of conservation of mass. All the material of A found in the region $x > 0$ must come from the region $x < 0$.

It can be seen by the expression of D, that if the concentration profile (i.e. the curve of C_A vs. x) is available, D can easily be found.

CHAPTER 4

EXPERIMENTATION

In this Chapter, the experimental work is presented. Due to the nature of this project, the experiments can best be grouped into four parts; each part is self-contained.

In 4.1 - PART A, descriptions are made of experiments concerning the qualitative and quantitative investigation of the cause and nature of the turbulent layer in various ester-aqueous caustic systems.

Experiments in 4.2 - PART B deal with the measurement of the concentration distribution inside the turbulent layer in two ester-aqueous caustic systems with slow chemical reaction.

Associated with the stagnant phase systems, mass transfer experiments were carried out with both phases stirred, as described in 4.3 - PART C.

In each experiment in PARTS A, B and C, with the exceptions otherwise stated, the upper phase was presaturated with water at 24 ± 1°C.

In 4.4 - PART D, an improved design of a diffusion cell is described. The cell enables the quick measurement of the diffusion coefficient as a function of concentration in binary liquid systems.

It should be realized that the following experimental apparatus and the procedure sections contain only the information necessary to give the reader a basic understanding of the design and function of the experimental equipment and how the experiments were done. Further details may be found in the appropriate appendices.

4.1 - PART A

QUALITATIVE AND QUANTITATIVE INVESTIGATIONS ON THE CAUSE AND NATURE OF THE TURBULENT LAYER IN ESTER-AQUEOUS CAUSTIC SYSTEMS

4.1.1 Qualitative Investigations of the Turbulent Layer by Means of Colour Indicators

Indicators change colour in a particular pH range. By initially adding a small amount of a suitable indicator to the ester-caustic system, the turbulent layer and the diffusion of components, particularly that of the sodium hydroxide, can be traced.

4.1.1.1 Experimental Details

4.1.1.1.1 Apparatus

The experimental apparatus used is shown in Figure 2. The dimensions of the cubical optical cell (1) are 4.8 X 4.9 X 5.5 cm. Caustic solution was run under the ester phase through a sintered glass disc (pyrex coarse grade) forming the end of the caustic delivery tube (2). The capacity of the delivery tube was 100 ml. The phenomena observed in the test cell were recorded with a Pentax camera (8). A detailed description of the caustic delivery tube is given in Appendix III: Section III.1.1

4.1.1.1.2 Procedure

(Numbers in the following description refer to Figure 2)

To start an experiment, 25 ml. of re-distilled ester pre-saturated with water were first introduced into the optical cell (1), then the caustic delivery tube (2) containing approximately 95 ml. of sodium hydroxide solution at the desired concentration level was lowered into the optical cell until the fritted glass disc just touched the bottom of the cell. The top of the cell was covered with a pair of glass plates (5) in order to reduce any liquid motion induced by evaporation. The sodium hydroxide solution, premixed with a small amount of colour indicator, was allowed to run out slowly through the sintered glass disc into the cell under the ester phase. Zero time was taken as soon as the first drop of the caustic solution was in contact with

FIGURE 2

EXPERIMENTAL SET-UP FOR THE COLOUR INDICATOR RUNS

1 CUBICAL CELL
LENGTH - 4.8 CM
WIDTH - 4.9 CM
HEIGHT - 5.5 CM

2 CAUSTIC DELIVERY TUBE

3 CAPILLARY TUBE

4 CONNECTED TO a PIPETTE FILLER WHEN LOADING THE CAUSTIC SOLUTION

5 GLASS PLATES

6 GROUND GLASS PLATE

7 LAMP

8 CAMERA

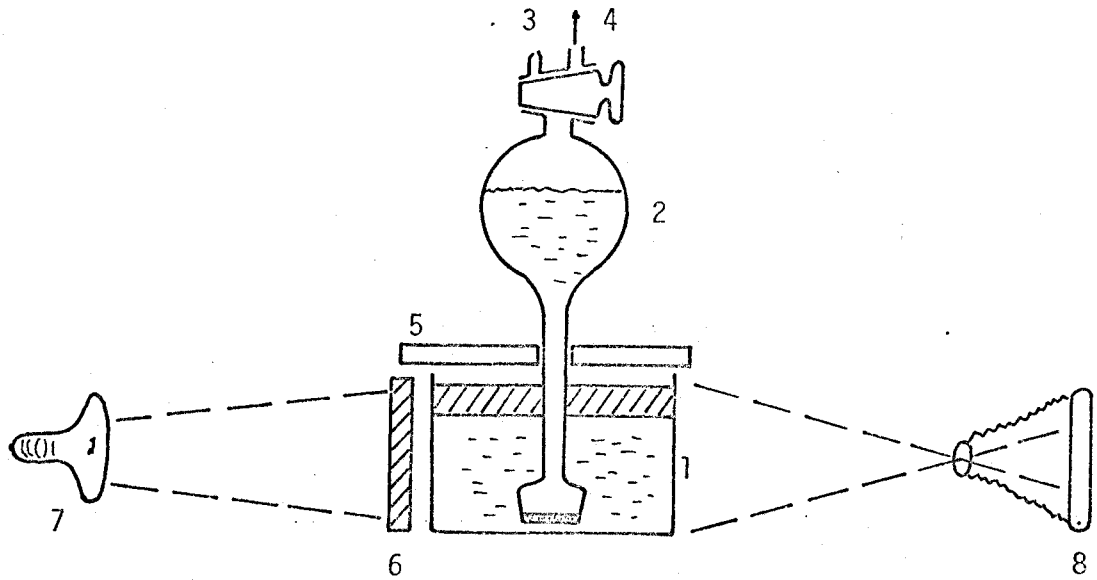

the ester phase. The filling rate of the caustic phase was controlled at 25 ml./minute by the intake of air through the capillary device (3). At such a rate, a smooth and apparently undisturbed interface was obtained between the ester and the aqueous phase during filling. The same rate of introduction of the caustic phase was used for every experiment, so that the degree of disturbance on the initial contacting of the phases would be reproduced for each experiment. As more of the sodium hydroxide solution was introduced into the cell, the ester-air interface moved up gradually to a pre-determined level which was 1 cm. below the top of the cell.

The duration of the experiment was 100 minutes. During each run, colour photographs of the turbulent layer were made at regular intervals. The caustic delivery tube was left inside the cell throughout the run.

Before the start of each experiment, the cell, the delivery tube, and the cover plates were carefully washed with concentrated sodium hydroxide-ethanol solution, rinsed with water, washed with concentrated chromic acid, and finally rinsed with a large amount of distilled water.

4.1.1.1.3 Number of Ester-Caustic Systems Investigated

Experiments were conducted at 24 ± 1°C with the following ester-caustic systems:

I Ethyl formate-sodium hydroxide with B.D.H. Universal indicator.

II Ethyl acetate-sodium hydroxide with alizarin yellow as indicator.

III Ethyl acetate - sodium hydroxide with thymolphthalein as indicator.

IV Methyl acetate - sodium hydroxide with alizarin yellow as indicator.

4.1.1.2 Results of the Colour Indicator Experiments

4.1.1.2.1 Ethyl formate - sodium hydroxide system

When the B.D.H. Universal indicator was added to the ethyl formate-sodium hydroxide system, the turbulent layer revealed itself as a green colour band against the yellow upper phase and the dark blue bulk sodium hydroxide. Also, sodium hydroxide movement in the layer could be observed as circulating blue streaks.

At the later stage of each run, an additional thin zone was observed within the turbulent layer immediately below the interface. The colour of this zone was also yellow inside which no blue caustic streaks were noted. A typical photograph of the turbulent layer of this system is shown in Figure 3.

4.1.1.2.2. Ethyl acetate - sodium hydroxide system

The pH of the turbulent layer in the ethyl acetate-sodium hydroxide system was previously measured to be approximately 10.2[S8]. Under this pH value, the B.D.H. Universal indicator was already dark blue in colour. Consequently, the B.D.H. Universal indicator was not suitable for this particular reaction system.

When alizarin yellow was added to the ethyl acetate-caustic system, the turbulent layer was yellow against the almost colourless ester phase and the red bulk sodium hydroxide phase. The sodium hydroxide inside the layer revealed itself as red patches.

FIGURE 3

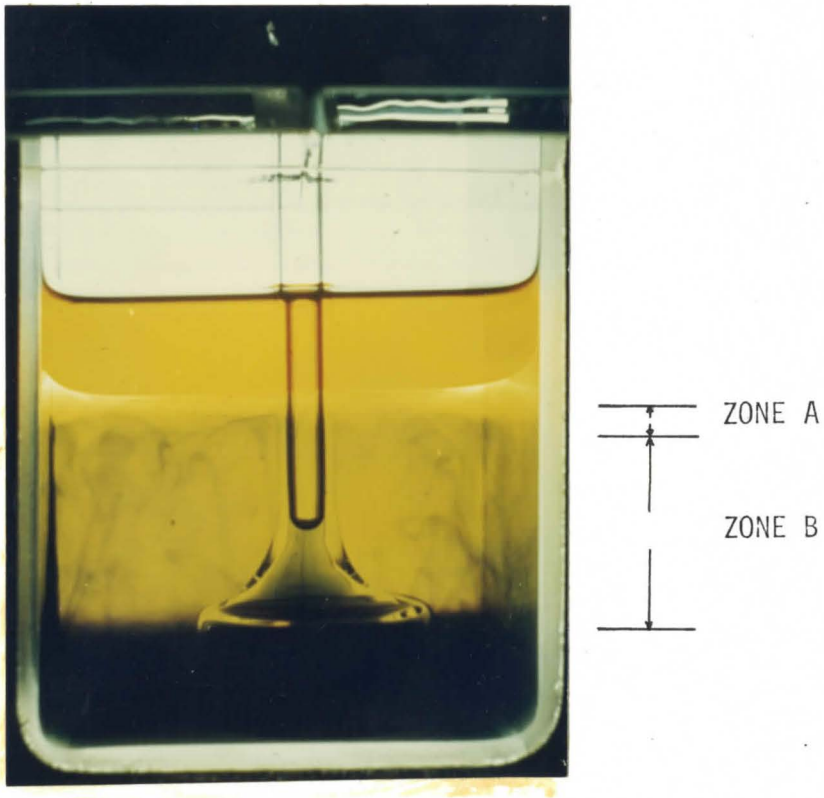

ETHYL FORMATE - 1.0 N NaOH SYSTEM WITH
B.D.H. UNIVERSAL INDICATOR : 106 MINUTES
AFTER THE INITIAL PHASE CONTACT

On the other hand, when thymolphthalein was added to the system, the turbulent layer was colourless against the light blue bulk sodium hydroxide phase. The sodium hydroxide inside the layer revealed itself as light blue patches.

In both cases, the caustic patches were quite uniformly distributed cross-sectionally and concentrated at the front of the turbulent layer.

4.1.1.2.3. Methyl acetate - sodium hydroxide system

When alizarin yellow was added to methyl acetate-sodium hydroxide system, the turbulent layer was mainly yellow, and red streaks were seen wherever sodium hydroxide was present within the reaction layer. The layer was wider than the one in the ethyl acetate-sodium hydroxide system but narrower as compared to that in the ethyl formate-sodium hydroxide system.

At the later stage of the run, an additional zone was again observed within the turbulent layer and located just below the liquid-liquid interface. This zone was yellow in colour and was similar in nature to that observed in the ethyl formate-sodium hydroxide system.

4.1.1.3 Discussion of the Colour Indicator Studies of the Turbulent Layer

The mainly green colour of the turbulent zone in the ethyl formate-sodium hydroxide system indicates that the pH of the liquid inside the layer is approximately 7. The saponification rate of the ester-caustic system is fairly rapid (Table 1). The concentration of sodium hydroxide inside the layer is low and the transfer of ethyl formate across the interface is fast. Consequently, the speed of turbulent layer growth is high.

Results of the thymolphthalein and alizarin yellow indicator in the ethyl acetate-sodium hydroxide experiments and alizarin yellow in the methyl acetate-sodium hydroxide systems (together with experiments using B.D.H. Universal indicator in both liquid systems) show that the average pH value of the liquid in these turbulent layers is higher than that in the ethyl formate-sodium hydroxide system. The turbulent layer growth rate is slower and the turbulence inside the layer is less. These qualitative results are as expected since the reaction velocities of the two systems are much lower as compared to that of the ethyl formate-sodium hydroxide system (Table 1).

Examination of the colour pictures of the turbulent layer in ethyl formate-sodium hydroxide and methyl acetate-sodium hydroxide systems taken at higher caustic concentration runs (e.g. 1 N) and at longer contact times indicate that the

TABLE 1

COMPARISON OF THE PROPERTIES OF VARIOUS ESTERS

	Methyl Formate	Methyl Acetate	Methyl Propionate	Ethyl Formate	Ethyl Acetate	Ethyl Propionate	Propyl Formate
Chemical Formula	$HCOOCH_3$	CH_3COOCH_3	$CH_3CH_2COOCH_3$	$HCOOC_2H_5$	$CH_3COOC_2H_5$	$CH_3CH_2COOC_2H_5$	$HCOOC_3H_7$
Molecular Weight	60.05	74.08	88.10	74.08	88.10	102.13	88.10
Boiling point, °C	31.50	57.1	79.9	54.3	77.15	99.10	81.3
Melting point, °C	-99.0	-98.1	-87.5	-80.5	-83.6	-73.9	-92.9
Density, gm/cc	$0.975^{(\frac{20}{4})}$	$0.9274^{(\frac{25}{4})}$	$0.9148^{(\frac{20}{4})}$	$0.9236^{(\frac{25}{4})}$	$0.901^{(\frac{20}{4})}$	$0.89574^{(15)}$	$0.9006^{(\frac{20}{4})}$
Solubility, gm/100 ml water	$30.4^{(20)}$	$31.9^{(20)}$	$6.5^{(20)}$	$11.8^{(25)}$	$8.6^{(20)}$	$2.4^{(20)}$	$2.79^{(20)}$
Diffusivity in water at infinite dilution, cm^2/sec	-	-	-	$1.1X10^{-5}$ ++	$0.98X10^{-5}$ *	-	-
Reaction constant at 25°C (with NaOH), litre/(Mole-min)	2400	~10	5.9 +	1240	6.3 **	5.3	-
Refractive index at 20°C	1.344	1.35935	1.3779	1.35975	1.3701	1.38385	1.3771

Note: Data are obtained from the "Handbook of Chemistry and Physics" and from the "International Critical Tables" unless otherwise stated.

* Experimentally measured diffusion coefficient (4.4 - PART D)
+ Experimentally determined; conductivity method (Reference R6)
** Refer to Figure VIII.1.
++ Estimated by Othmer and Thaker method.

turbulent layer actually consists of two separate zones "A" and "B" (Figure 3). Zone "A" is a zone of turbulent inter-diffusion of the ester from the upper phase and the alcohol from the lower phase. The colour indicator study reveals that the caustic concentration in this zone is extremely small and is essentially equal to zero. Although no circulating colour streaks were observed in this zone, interfacial turbulence as a result of the uneven alcohol distribution at the interface does exist. Zone "B" is a zone of reaction where the concentration of caustic is substantial. A similar structure of the turbulent layer is expected in the ethyl acetate-sodium hydroxide system. The two-zone phenomenon may be observed at lower caustic concentration runs and at shorter contact times as compared to the ethyl formate-sodium hydroxide system. However, the turbulent layer developed in ethyl acetate-sodium hydroxide system is quite small, and the presence of the two zones inside the layer is not conspicuous.

The observation of the two zones in the turbulent layer is in agreement with most of the proposed models(F2)(S4) for transient systems with fairly rapid to moderately slow reactions. The models state that the reaction zone proper moves away from the interface with increasing contact time.

According to available literature discussion (Refer to Chapter 3), for systems with similar physical properties, the thickness of the reaction zone ("B") decreases with

increasing reaction velocity of the system. Such a statement is not valid for the systems studied here. The reaction zone, where the saponification occurs, appears to be the widest in the ethyl formate-sodium hydroxide system which has the largest reaction rate constant of the three systems. Actually, the reaction zone of the ethyl formate-sodium hydroxide system is even wider than the whole turbulent layer of the ethyl acetate-sodium hydroxide system. This abnormal behaviour of the reaction zone can be attributed to the turbulent nature of the system. The convective liquid current, rising from the lower zone front with high velocity, helps to carry more sodium hydroxide further up the turbulent layer before the caustic is completely consumed. The result is a rather dilute caustic concentration existing throughout the entire reaction zone as is evident in Figure 3.

The change of interfacial tension caused by the addition of the indicators was not studied. It was observed that with the ethyl acetate-sodium hydroxide system, the rate of layer propagation was very much reduced by the indicators. With ethyl formate-sodium hydroxide and methyl acetate-sodium hydroxide systems, the rate was affected to a lesser degree. As a result, these experiments served only as a qualitative study of the reaction zone.

4.1.2 Measurement of the Turbulent Layer Propagation

It was found previously[S9] that the use of a moiré pattern was very effective in observing the mixing patterns inside the turbulent layer. Furthermore, the distortion of the pattern could serve as a method to indicate the position of the propagating layer front. The object of this investigation was to measure the turbulent layer propagation rate in various ester-caustic systems by means of a changing moiré pattern.

4.1.2.1 Experimental Details

4.1.2.1.1 Apparatus

Figure 4 shows the experimental set-up. The cubical test cell (1) and the caustic delivery tube (2) were the same as those used previously (4.1.1). Light beams from the point source (9) (Sylvania concentrated arc lamp, K25) became parallel after passing through the convex lens (8). The moiré pattern image on the ground glass (7) was photographed, using a Pentax camera (10) equipped with close-up extension tubes Nos. 1 and 2.

4.1.2.1.2 Procedure

The method employed to bring the two liquid phases into contact was the same as that used previously in the colour indicator experiments (4.1.1.1.2).

The duration of the experiment was, again, arbitrarily set at 100 minutes. During the run, 10 to 30 photographs of the turbulent layer were taken.

Before the start of the experiment, the cell and the delivery tube were carefully washed in the way described in Section 4.1.1.1.2.

4.1.2.1.3 Temperature Control

All the experiments were performed at room temperature of 24 ± 1°C. Temperature variation within each experimental run was less than 1°C.

4.1.2.1.4 Measurement of the Turbulent Layer Propagation

Photograph negatives were made into slides which were

FIGURE 4

1 Cubical cell
Length - 4.8 CM
Width - 4.9 CM
Height - 5.5 CM

2 Caustic Delivery Tube

3 Capillary Tube

4 Connected to a Pipette Filler when Loading the Caustic Solution

5 Glass Cover Plates

6 Moiré Plates

7 Ground Glass Plate

8 Convex Lens

9 Light Source

10 Camera

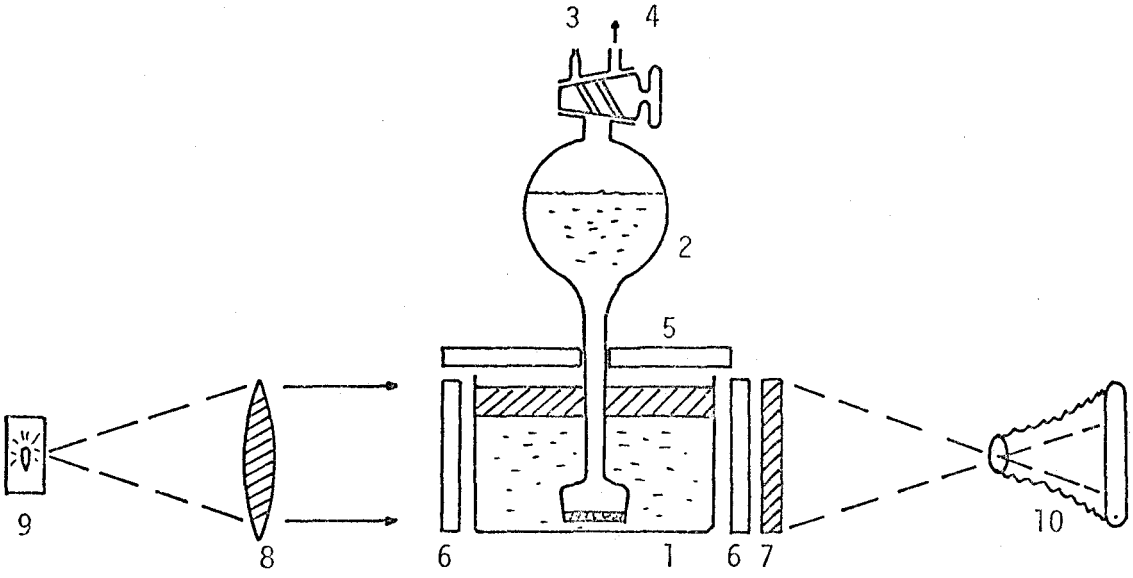

subsequently projected and enlarged onto a wall. Dimensions of the turbulent layer for each slide were recorded. These projected measurements were converted back to the actual layer thicknesses, which were then related to the corresponding times when the pictures were taken to give the rate of layer propagation. Detailed descriptions of the turbulent layer measurement are presented in Appendix II.

4.1.2.1.5 Number of Experiments Performed

4.1.2.1.5.1 Methyl ester-aqueous caustic solution systems:

Experiments on the measurement of propagation of the turbulent layer were performed using methyl formate, methyl acetate and methyl propionate respectively as the upper phase. For each kind of ester, runs were performed at various concentration levels of sodium hydroxide and potassium hydroxide solutions respectively. The esters used were purified by fractional distillation (Appendix I).

4.1.2.1.5.2 Ethyl ester-aqueous caustic solution systems:

Layer propagation measurements were performed using ethyl formate, ethyl acetate and ethyl propionate, respectively as the upper phase. For the ethyl formate-sodium hydroxide system, a large number of runs were performed with sodium hydroxide concentrations centred around 0.1 N. The results of these runs, together with the results of the same system previously obtained[S8] were plotted out to define whether or not a maximum did occur in the curve of the speed of layer propagation versus initial sodium hydroxide solution concentrations (Figure 7).

Only two runs were performed with the ethyl acetate-sodium hydroxide system at two different sodium hydroxide concentration levels and the results were compared with the data previously obtained in order to check the reproducibility of the experiments. More runs were performed with the ethyl acetate-potassium hydroxide, ethyl propionate-sodium hydroxide and ethyl propionate-potassium hydroxide systems respectively at various caustic concentration levels.

In addition, a few trial runs were performed on the ethyl formate-sodium hydroxide and the ethyl acetate-sodium hydroxide systems using the "sliding diffusion cell" described in Part D of the dissertation.

4.1.2.1.5.3 Propyl ester-aqueous caustic solution system:

Layer propagation experiments were performed on the propyl formate-sodium hydroxide system at various caustic concentration levels. The other propyl ester systems were not investigated because of their low solubilities in aqueous solutions.

4.1.2.2 Results of the Measurement of Turbulent Layer Propagation

4.1.2.2.1 Methyl Ester-Aqueous Caustic Solution Systems

4.1.2.2.1.1 Methyl formate-sodium hydroxide system:

A few runs were performed on the methyl formate-sodium hydroxide system; no meaningful turbulent layer thickness measurements could be made. Reaction was observed to be vigorous. In runs with more dilute caustic concentrations, most of the sodium hydroxide in the aqueous phase was consumed during the filling period. Turbulence was observed throughout the entire lower phase. In runs with higher caustic concentrations, the turbulent layer propagated almost to the bottom of the cell at the end of the filling period (approximately three minutes of contact time). The layer thickness was very uneven.

It was evident that the method of contacting the two reacting phases was not suitable for this particular system.

4.1.2.2.1.2 Methyl acetate-caustic systems:

Nine runs were performed with the methyl acetate-sodium hydroxide system with sodium hydroxide concentration levels ranging from 0.1 N to 1.5 N; 8 runs were performed with the methyl acetate-potassium hydroxide system at similar caustic concentration levels. In addition, 5 runs were performed on the methyl acetate-0.1 N sodium hydroxide system with the density and viscosity of the lower phase changed by adding glycerol, sodium chloride, sodium acetate and a

combined mixture of glycerol and sodium acetate respectively. The purpose in adding these materials to the 0.1 N caustic solution was to simulate either the viscosity or the density or both of the 1.0 N sodium hydroxide solution.

At the beginning of the run, straight moiré lines were observed extending from the bottom of the cell up to very near the lower front of the turbulent layer. Inside the layer, turbulent liquid motion was noted. Just below the lower layer front in the bulk caustic, curved moiré lines were observed. With low initial caustic concentration runs, the strip where the lines curved themselves was quite narrow. On the other hand, with more concentrated caustic solution runs, the curved line portion was perhaps wider.

In the runs with low initial caustic concentration, the turbulent layer was found to extend down to the bottom of the cell within a short period of time. Motion of the liquid within the layer was observed to be vigorous and a cycling convective current was set up. With higher sodium hydroxide or potassium hydroxide concentration runs, the turbulent layer also propagated quite fast at the beginning. In time, liquid motion inside the layer became less turbulent and the speed of the layer front propagation reduced. The thin zone, whose liquid refractive index was different from the rest of the system, gradually took shape within the turbulent layer immediately below the liquid-liquid interface as illustrated in Figure 5. Such observations were in

FIGURE 5

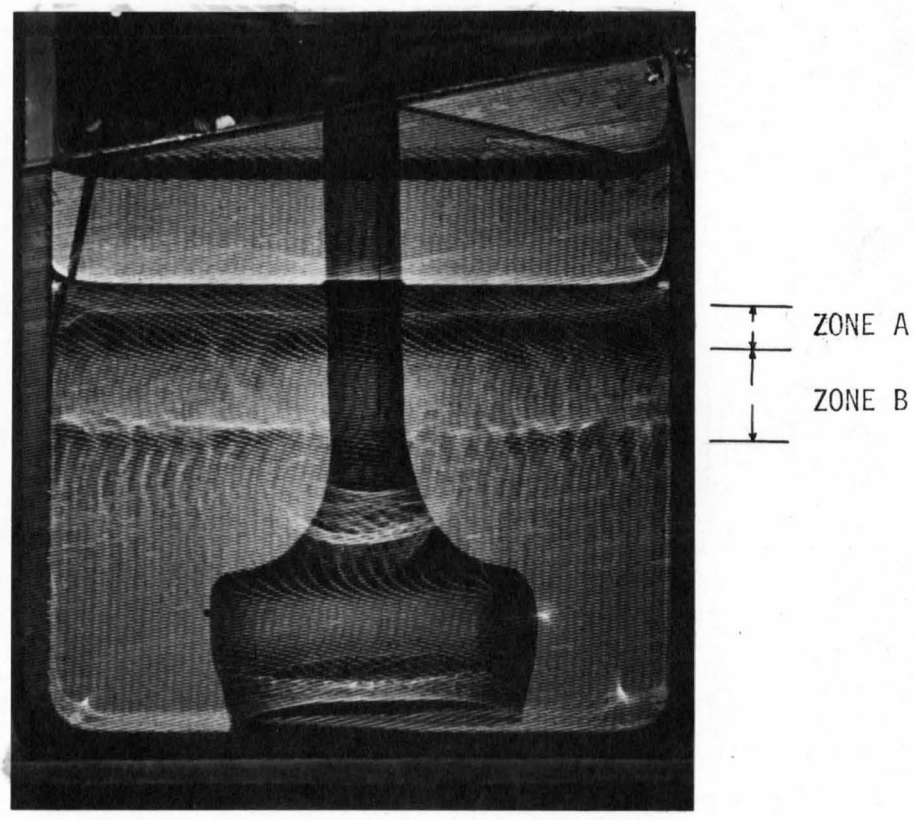

METHYL ACETATE - 0.4 N KOH SYSTEM :
100 MINUTES AFTER INITIAL PHASE CONTACT

agreement with the earlier colour indicator experiments (4.1.1.3).

Measurements of layer thickness from photographs for each run were made. An example of the measurement data from Run #6 (methyl acetate-0.407 N sodium hydroxide), after being converted back to the actual layer thicknesses, is shown in Appendix II. For each experiment, $(\text{layer thickness})^2$ was plotted against contact time. Thus for the methyl acetate-sodium hydroxide system, a set of straight lines was obtained, each representing a particular sodium hydroxide concentration level, as shown in Figure 6. Then, the slope of each line in Figure 6 was plotted against the initial sodium hydroxide concentration of the experiment from which the line was obtained. The resulting graph is shown in Figure 7. Similar sets of straight lines were obtained for the methyl acetate-potassium hydroxide system (Figure XVIII.1: Appendix XVIII) and methyl acetate-0.1 N sodium hydroxide system with the density and viscosity of the lower phase solution adjusted (Figure XVIII.2: Appendix XVIII). The slope of each straight line for the methyl acetate-caustic system was plotted against the initial caustic concentration accordingly.

4.1.2.2.1.3 Methyl propionate-caustic systems:

Ten runs were performed with the methyl propionate-sodium hydroxide system and 7 runs were performed with the methyl propionate-potassium hydroxide system at various

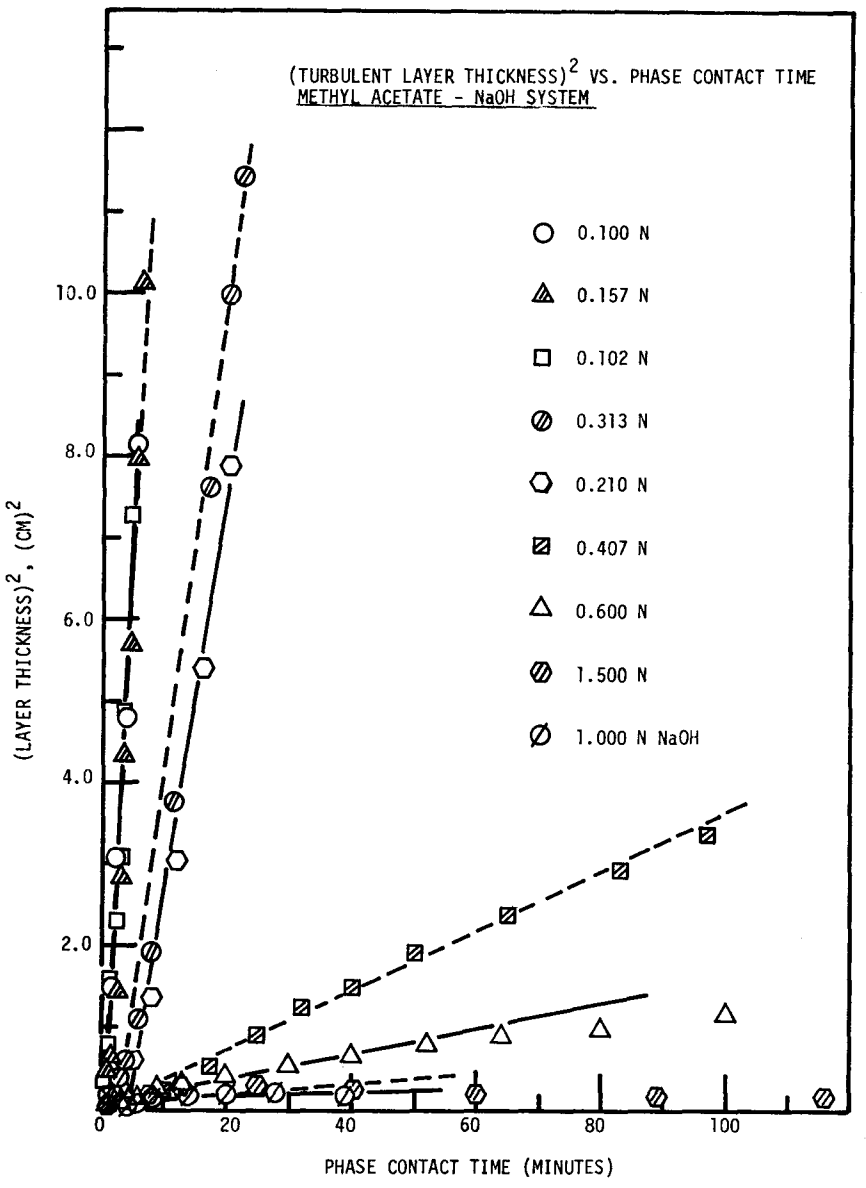
(TURBULENT LAYER THICKNESS)^2 VS. PHASE CONTACT TIME
METHYL ACETATE - NaOH SYSTEM
0.100 N
0.157 N
0.102 N
0.313 N
0.210 N
0.407 N
0.600 N
1.500 N
1.000 N NaOH
(LAYER THICKNESS)^2, (CM)^2
PHASE CONTACT TIME (MINUTES)

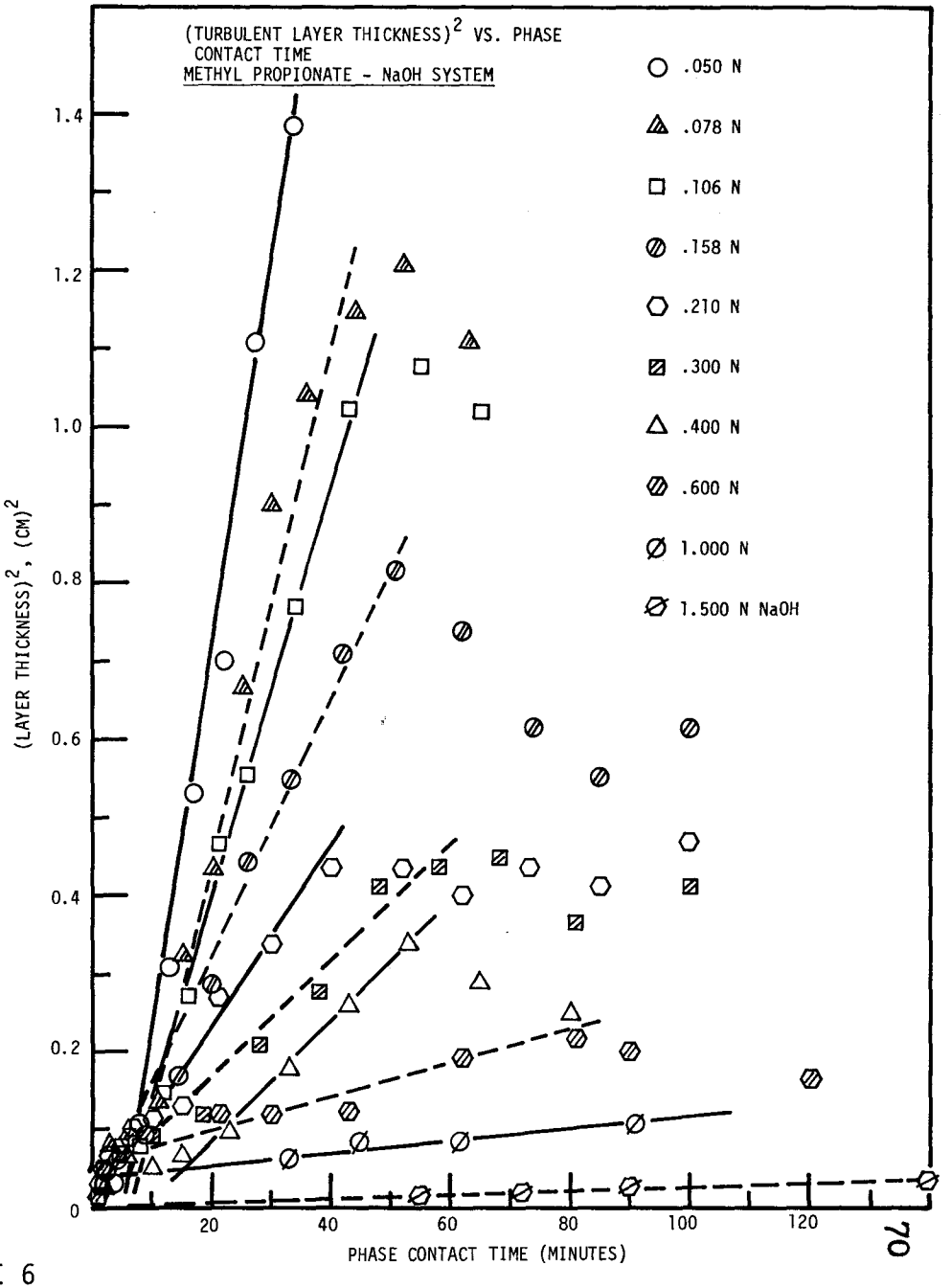
(TURBULENT LAYER THICKNESS)^2 VS. PHASE CONTACT TIME
METHYL PROPIONATE - NaOH SYSTEM
.050 N
.078 N
.106 N
.158 N
.210 N
.300 N
.400 N
.600 N
1.000 N
1.500 N NaOH
(LAYER THICKNESS)^2, (CM)^2
PHASE CONTACT TIME (MINUTES)

FIGURE 6

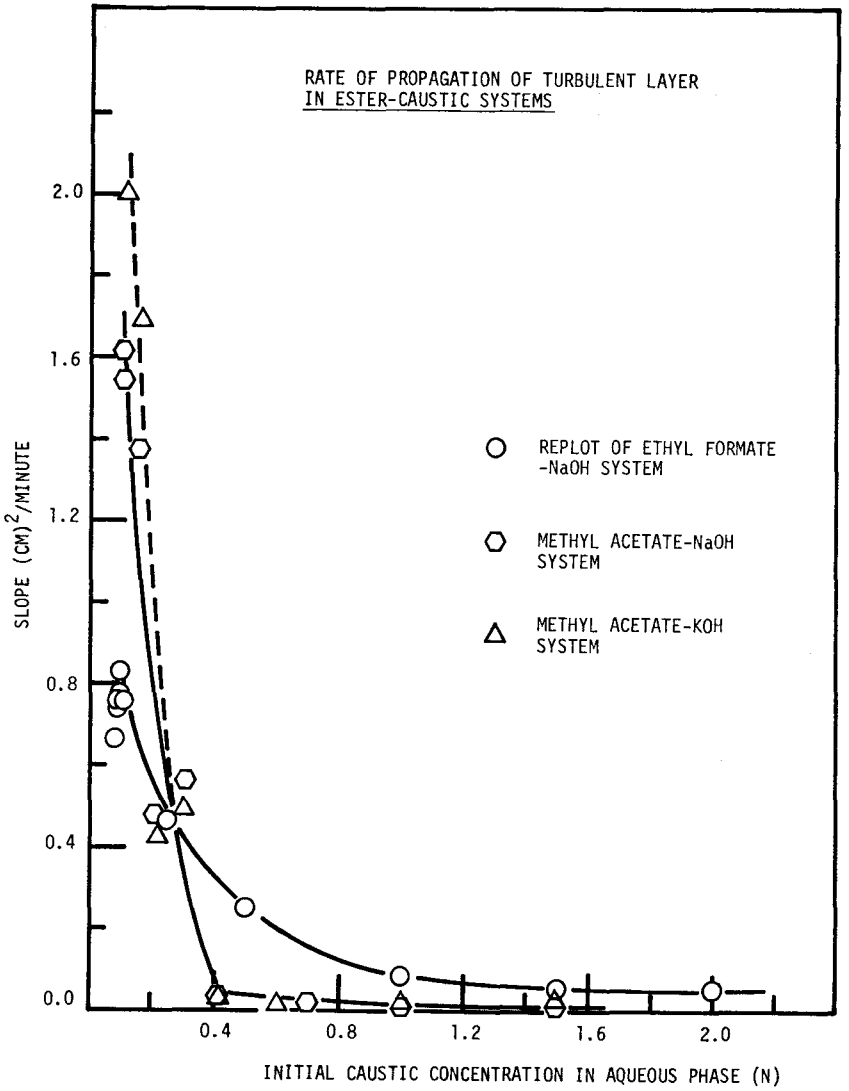
RATE OF PROPAGATION OF TURBULENT LAYER
IN ESTER-CAUSTIC SYSTEMS
REPLOT OF ETHYL FORMATE -NaOH SYSTEM
METHYL ACETATE-NaOH SYSTEM
METHYL ACETATE-KOH SYSTEM
SLOPE (CM)^2/MINUTE
INITIAL CAUSTIC CONCENTRATION IN AQUEOUS PHASE (N)
0.0
0.4
0.8
1.2
1.6
2.0

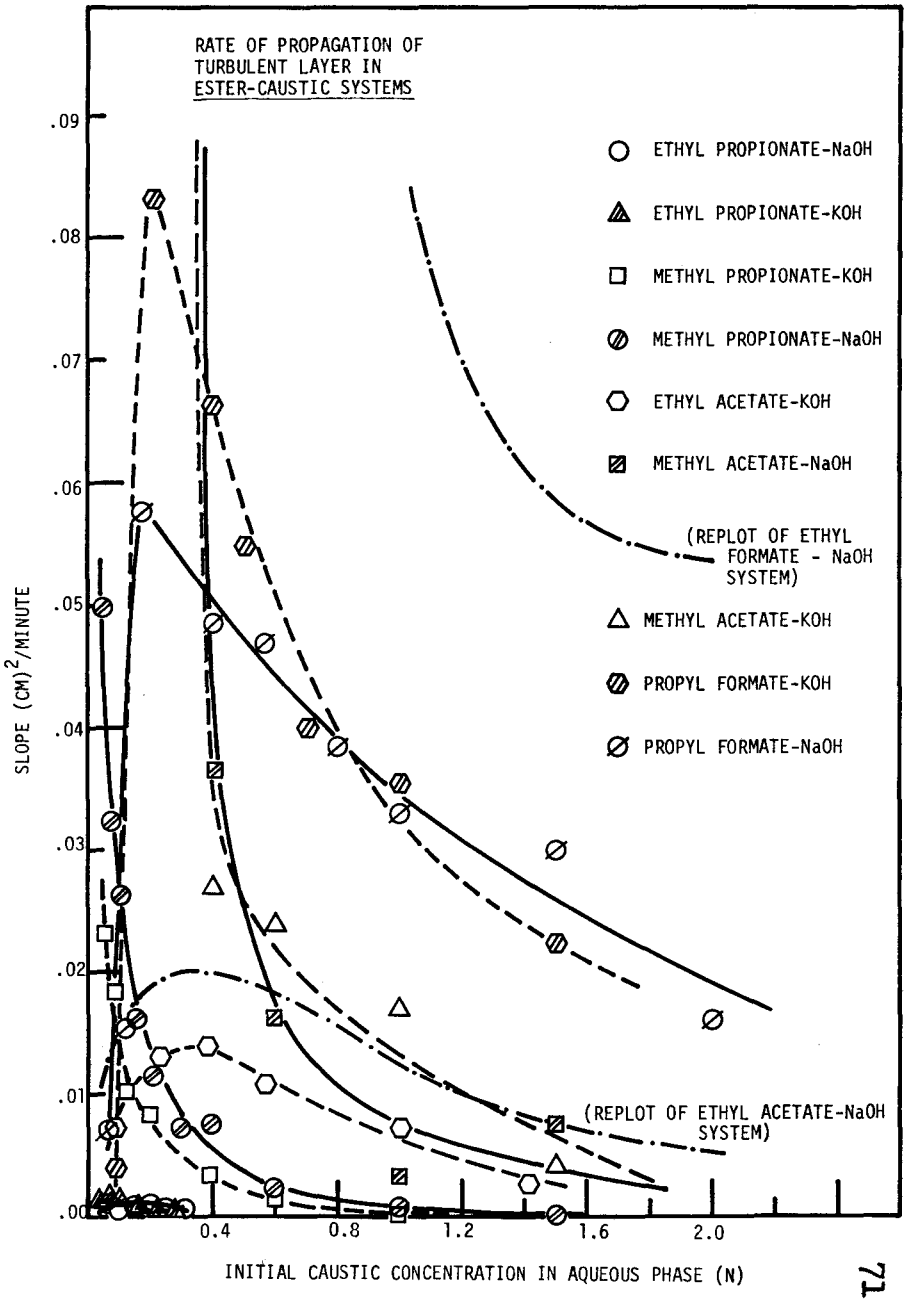
RATE OF PROPAGATION OF
TURBULENT LAYER IN
ESTER-CAUSTIC SYSTEMS
ETHYL PROPIONATE-NaOH
ETHYL PROPIONATE-KOH
METHYL PROPIONATE-KOH
METHYL PROPIONATE-NaOH
ETHYL ACETATE-KOH
METHYL ACETATE-NaOH
(REPLOT OF ETHYL FORMATE - NaOH SYSTEM)
METHYL ACETATE-KOH
PROPYL FORMATE-KOH
PROPYL FORMATE-NaOH
(REPLOT OF ETHYL ACETATE-NaOH SYSTEM)
SLOPE (CM)^2/MINUTE
INITIAL CAUSTIC CONCENTRATION IN AQUEOUS PHASE (N)
.00
.01
.02
.03
.04
.05
.06
.07
.08
.09
0.4
0.8
1.2
1.6
2.0

FIGURE 7

caustic concentration levels.

The speed of the layer propagation for these systems was much slower than the previous methyl ester-caustic systems. At the beginning of a run, the observations of the turbulent layer were generally similar to those of the methyl acetate-sodium hydroxide system. In the course of time, the liquid motion inside the turbulent layer became less turbulent and the speed of layer propagation again slowed down. The layer stayed at a certain thickness for some time, and shrank subsequently at a very, very slow rate. At the same time, the lower layer front became diffused. In experiments with higher initial caustic concentrations, streaks of the salt product were seen diffusing out of the layer and blurring the moiré pattern below the layer front, thus rendering both the observation and measurement of the layer difficult.

Data obtained for these runs were treated in the same way as with the other methyl acetate-caustic systems. Layer propagation data were plotted on graphs as shown in Figure 6 and Figure XVIII.3: Appendix XVIII, respectively.

4.1.2.2.2 Ethyl Ester-Aqueous Caustic Solution Systems

4.1.2.2.2.1 Ethyl formate-caustic systems:

Five runs were performed on the ethyl formate-sodium hydroxide system with the caustic concentration levels centred around 0.1 N.

The observations of the turbulent layer were generally in agreement with those described previously [S8]. Previous

data for the same system[S8] were also incorporated. The curve of [(layer thickness)^2/time] versus initial caustic solution concentration is shown in Figure 7.

4.1.2.2.2.2 Ethyl acetate-caustic systems:

Two runs were performed on the ethyl acetate-sodium hydroxide system in order to check the reproducibility of previous data [S9]. Eight runs were performed on the ethyl acetate-potassium hydroxide system with lower phase concentrations ranging from 0.08 N to 1.4 N.

The observations of the turbulent layer structure were similar to those described previously (Section 4.1.2.2.1). Data obtained were treated in the same way as that described in the methyl acetate-caustic systems. Results are shown in Figure XVIII.4 and Figure XVIII.5 respectively in Appendix XVIII.

4.1.2.2.2.3 Ethyl propionate-caustic systems:

Six runs were performed with the ethyl propionate-sodium hydroxide system. An additional six runs were performed with the ethyl propionate-potassium hydroxide system.

The observations of the turbulent layer were, in general, similar to those of the ethyl acetate-caustic systems. The speed of the layer propagation was very slow and the turbulent liquid motion inside the zone was less vigorous. Furthermore, the final layer thickness for each run was quite small, thus rendering the propagation measurements rather inaccurate. Nevertheless, data obtained were treated in the same way as

with the other systems and the results are shown in Figures XVIII.6 and XVIII.7 in Appendix XVIII.

4.1.2.2.3 Propyl Ester-Caustic Systems

4.1.2.2.3.1 Propyl formate-caustic systems:

Nine runs were performed with the propyl formate-sodium hydroxide system. The sodium hydroxide concentrations used ranged from 0.1 N to 1.98 N. In addition, 7 runs were performed on the propyl formate-potassium hydroxide system with the lower phase concentrations ranging from 0.087 N to 1.5 N.

The observations of the turbulent layer were generally similar to those of the ethyl acetate-caustic runs with a few exceptions as described in the following. The speed of layer propagation was faster than that of the ethyl acetate-caustic system. The turbulence inside the layer was apparently greater.

In the runs with low initial caustic concentrations, e.g. below 0.2 N, the turbulent layer was not clearly defined. The lower layer front became diffused at the early stage of the run, thus rendering the layer propagation measurements for these runs rather approximate. With initial caustic concentrations higher than 0.2 N, the usual moiré pattern of the turbulent layer was observed. Also, some material, probably propanol, transferred from the lower into the upper phase. The final steady state layer thickness was found to extend almost down to the bottom of the cell. A typical

moiré pattern for this system is shown in Figure XVIII.10 (Appendix XVIII). With still higher initial caustic concentrations, for example, 1.5 N and 1.98 N, the propagation of the lower layer front was much slower and only to a comparatively small thickness.

Data obtained were treated in a similar way as with the other systems. The graphical results are presented in Figures XVIII.8 and XVIII.9 in Appendix XVIII.

4.1.2.3 Discussion of the Measurement of the Turbulent Layer Propagation

4.1.2.3.1 Reaction Runs

Using the moiré pattern, the turbulent liquid motion inside the layer is quite well revealed. The pattern is particularly useful in observing the interfacial turbulence which is not clearly observed in the colour indicator experiments. Yet on the other hand, the two separate zones within the turbulent layer, which are so nicely shown in the colour indicator experiments, are not well defined by the moiré pattern.

Since no contaminants are added to the liquid systems in this set of runs, quantitative measurements of the layer growth in pure liquid systems are possible. Photographs taken in each run are analysed for turbulent layer thickness.

4.1.2.3.1.1 Errors involved in the analysis of turbulent layer thickness:

Probably due to the angle of the incident light source (Figure 4), the moiré pattern of the lower zone front in an ester-caustic system usually appears as a thick dark band as illustrated in Figure 5. The exact location of the plane of the lower zone front within the dark band is not certain. In this study, it is assumed to always coincide with the lower edge of the dark band in the moiré picture. In this way, even if an error is made in judging the exact location of the lower zone front, the error would behave as an added constant throughout the analysis. Such an error is not expected to

be serious in systems with a high speed of layer growth (such as ethyl formate-caustic and propyl formate-caustic systems). In those systems, the layer thickness is much larger than the band, except for the first two pictures taken at very short contact times. However, in systems with a very slow speed of layer propagation, errors arising from misjudging the location of the zone front may be significant (e.g. ethyl propionate-caustic systems).

The lower edge of the dark band representing the zone front is not always sharply defined in the moiré pattern picture. This is particularly so with pictures taken at high caustic concentration runs and at longer contact time when the boundary of the zone front is blurred by the downward diffusion of the salt. Thus, when the moiré picture is projected and magnified on the screen, errors are inevitably induced from such measurements of thickness between the interface and the lower edge of the zone front.

Scattering of data is probably caused by the slightly uneven turbulent layer thickness in each run. For each photograph, three layer thickness measurements were taken at three equally spaced locations. The layer thickness was recorded as the average of the three measurements. As an example, a complete calculation of the layer thickness data is shown in Appendix II.

4.1.2.3.1.2 Straight line relationship:

For all the systems under study, the plot of (layer thickness)^2

versus contact time for each experiment yielded a straight line for a reasonable period of time. In general, with the exception of the propyl formate-caustic system, the higher the initial caustic concentration, the longer the straight line relationship holds. With the propyl formate-caustic system, the reverse appears to be true.

In some systems, particularly in those with slow layer growth (e.g. ethyl propionate-caustic systems), extrapolations of the straight lines to zero contact time do not pass through the origin. This can be explained by the inaccuracy in locating the plane of the lower zone front as described in the preceding section (4.1.2.3.1.1). In addition, the phase contact turbulence may help to sweep down some of the ester into the aqueous phase during the filling period, thus creating an initial turbulent layer thicker than it should be if without the mechanical mixing of the liquids. It should be realized, however, that the error in shifting the origin does not affect the slope $\left[(\text{layer thickness})^2/\text{time}\right]$ of the line, which gives some indication of the speed of layer growth. Furthermore, the phase contact turbulence is approximately the same for each run by virtue of using the same filling rate of the lower phase.

With the uncertainties in judging the location of the zero point of the straight line and the portion of (layer thickness)^2 data which fit the straight line relationship, it is felt that all the straight lines drawn by eye would be

sufficiently accurate.

4.1.2.3.1.3 Speed of the turbulent layer propagation:

On examining the plot of (layer thickness)^2/time versus the initial caustic concentration for each system in Figure 7, it becomes clear that in each of the systems, ethyl acetate-caustic solution and ethyl propionate-caustic solution, the speed of zone front propagation passes through a maximum as initial caustic concentration increases. All the regions of maximum layer growth lie below 0.4 N of the caustic concentration. With the systems of methyl acetate-caustic and methyl propionate-caustic solutions, no maxima are observed. As for the ethyl formate-sodium hydroxide system, it appears to have a maximum layer propagation speed located at approximately 0.1 N area. However, the reproducibility of the experiment in this dilute caustic concentration region is particularly poor as is evident in Figure 7. Consequently the maximum region may not be considered significant. In each run with the propyl formate-caustic system, the straight line relationship of the (layer thickness)^2 versus contact time plot only holds for a short period of time. Particularly in runs with caustic concentration less than 0.2 N, the layer formed becomes very diffused after 20 minutes. The turbulence inside the layer is very weak. Precise measurements of the layer thickness become difficult. Straight lines drawn, based on data obtained in 15 to 20 minutes of contact time, become inaccurate. For these reasons, the speed of layer

propagation for runs below 0.2 N caustic concentration should be discarded.

Closer studies of the speed of layer propagation versus caustic concentration plots in Figure 7 suggest that in a dilute caustic concentration (e.g. 0 to 0.3 N), the speed of layer propagation in different systems depends on a combination of several factors. Some of the more important ones are solubility and density of the aqueous ester solution. As an example, the high speed of layer propagation of the methyl acetate-caustic systems in dilute caustic concentration range is probably due to its high solubility as well as its ability to form an aqueous solution having a density slightly higher than that of water (Table 2). Similarly, a higher speed of layer growth in the methyl propionate-caustic systems as compared to ethyl acetate-caustic systems in dilute caustic concentration range (0 to 0.1 N) is probably due to its ability to form an aqueous ester solution which is comparable to that of water (Table 2). On the other hand, at a high caustic concentration level, the more important controlling factors of the speed of layer growth in different systems are probably the salt effects and the rate constant of the system which, in turn, governs the amount of alcohol produced. The speed of layer growth follows the order of the rate constant of the system. Furthermore, for systems having similar reaction velocities, the layer growth speed decreases with the production of the higher member of the homologous series

TABLE 2

DENSITIES OF VARIOUS ESTER SOLUTIONS EXPERIMENTALLY DETERMINED AT 22°C

Degree of saturation of ester solution / aqueous ester solution		Aqueous solution saturated with ester	Aqueous solution half saturated with ester
Water	Density (gm/c.c.)	.996948 .996902 .996786 .996750 .996748 average= .996827	
Ethyl acetate	Density (gm/c.c.) Specific gravity	.996486 .999658	.996414 .999586
Methyl propionate	Density (gm/c.c.) Specific gravity	.996948 1.000121	.996814 .999987
Methyl acetate	Density (gm/c.c.) Specific gravity	.999748 1.002930	1.000036 1.003219
Ethyl formate	Density (gm/c.c.) Specific gravity	.999332 1.002513	.998086 1.001263

of the salt (e.g. formate, acetate and propionate). Comparing the systems of methyl ester-caustic and ethyl ester-caustic at high caustic concentration levels, the effects of methanol and ethanol on the layer growth appear to be the same. This is, again, probably due to the fact that the turbulent layer is predominately influenced by the salt effects. In each ester-caustic system, a similar shape of the curves of (layer thickness)^2/time versus caustic concentration are obtained for sodium hydroxide and potassium hydroxide as shown in Figure 7, although the potassium hydroxide curve is not always below the sodium hydroxide curve.

The speed of layer propagation in ethyl ester-sodium hydroxide system is much slower in the sliding diffusion cell as compared to that obtained in the optical cell experiments. In the ethyl acetate-sodium hydroxide system, the turbulent layer is so diffused that layer propagation can hardly be measured. These observations suggest that in a small cell, the wall effect is important to layer turbulence.

4.1.3 Qualitative Study of the Interfacial Phenomena in Various Two Component Ester-Water Systems and in the Three Component Ester-Solute-Water Systems

Parallel to the reaction runs (Section 4.1.2), experiments in physical mass transfer were also performed with various ester-water systems. A moiré pattern was again used to observe the turbulent phenomena at and near the liquid interface.

4.1.3.1 Experimental Details

4.1.3.1.1 Apparatus and Procedure

The apparatus and the operational procedure were identical with those described in Sections 4.1.2.1 and 4.1.2.2.

4.1.3.1.2 Number of Experiments Performed

4.1.3.1.2.1 Two component ester-water systems:

Moiré patterns of various ester-water systems were obtained.

4.1.3.1.2.2 Three component ester-solute-water systems:

Physical mass transfer in three component systems was studied qualitatively. The transfer of ethanol from the ester phase into the water phase and vice versa were investigated in the ethyl acetate-ethanol-water and ethyl propionate-ethanol-water systems. In addition, the transfer of the acetic acid from the ester phase into water in the ethyl acetate-acetic acid-water system was also studied.

4.1.3.2 Results of the Physical Transfer Runs

4.1.3.2.1 Ester-Water Systems

Physical diffusion of ester into water was studied for all the esters employed in the previous reaction runs. The basic transfer behaviour of different systems can be classified roughly into the following two groups:

4.1.3.2.1.1 Systems with insignificant interfacial turbulence accompanying mass transfer:

The ethyl acetate-water and ethyl propionate-water systems fall into this category. The moiré pattern of the ethyl acetate-water system has been described in detail previously(S8) and will not be repeated here.

During the run, extremely slow liquid motion was observed at and near the interface. However, the amount of visible interfacial turbulence was so small that the basic moiré pattern of molecular diffusion was practically undisturbed, except for a thin region which was observed in the water phase just below the liquid-liquid interface. This region of liquid had a refractive index different from that of the lower bulk phase, probably because of the presence of more concentrated ester solution. The demarcation line between this region and the rest of the lower bulk phase was not distinct. The region became diffused at long contact time.

4.1.3.2.1.2 Systems with turbulence accompanying mass transfer:

All three methyl ester-water systems showed turbulent

phenomena when the ester was transferring into the water phase. A turbulent liquid motion was observed at or near the liquid-liquid interface apart from the "liquid streaks" protruding slowly into the lower bulk phase. The degree of turbulence was dependent on the systems under study. Generally, the degree of apparent turbulence (and the number of liquid streaks) decreased in runs using higher members of the homologous series of the ester.

A similar type of turbulent liquid motion was observed in ethyl formate-water. With the propyl formate-water system, turbulent liquid motion was so slow, both at the interface and inside the aqueous phase, that it was almost not observable. Occasionally, a liquid streak or two slowly extended into the lower phase.

From visual observations, the degree of turbulence decreased qualitatively with systems using increasing order of methyl, ethyl and propyl formate consecutively as the upper phase.

4.1.3.2.2 Three-Component Systems

The physical transfer situations of the three-component systems can best be summarized by the following Table 3:

TABLE 3

SUMMARY OF PHYSICAL MASS TRANSFER IN THREE COMPONENT SYSTEMS

System	Remarks (in aqueous phase)
1. Ethyl propionate-water; ethanol (0.86 N) transferring from the ester phase into the water phase.	Considerable interfacial turbulence both during the filling period and at the beginning of the run. Turbulence spread out into a thin region next to the interface. Decreasing turbulence with increasing contact time; occasionally stronger turbulence at the corners of the cell. At the later stage of the experiment, turbulent liquid motion diminished, and a thin zone, having different refractive index, existed between the two liquid phases.
2. Ethyl propionate-water; ethanol (0.172 N)transferring from the ester phase into the water phase.	Similar observation as in (1.), except in smaller scale of turbulence.
3. Ethyl propionate-water; ethanol (0.172 N)transferring from the water phase into the ester phase.	Similar kind of turbulence. More turbulent than (2.) Also, the "zone of different refractive index" was wider than that observed in (2.), but less well defined.
4. Ethyl acetate-water; ethanol (0.172 N) transferring from water phase into the ester phase.	Stronger interfacial turbulence than with the ethyl propionate-water systems. In addition, a number of liquid streaks extended all the way down to the bottom of the cell. Turbulence phenomenon lasted longer. The "zone of different refractive index" was quite well defined.
5. Ethyl acetate-water; ethanol (0.172 N) transferring from the ester phase into the water phase.	Degree of turbulence in this system was very much similar to that in (2.)
6. Ethyl acetate-water; equal concentrations of ethanol in both phases (0.172 N)	Despite the equal normality of the ethanol in both phases, there was mass transfer across the interface accompanied by vigorous interfacial turbulence at the early stage of the run. Such phenomenon was as expected since the alcohol distribution coefficient between the two phases probably differed from the ratio of 1. Visual turbulent phenomenon was similar to that in (5.) No liquid streaks were observed.
7. Ethyl acetate-water; acetic acid (0.26 N) transferring from the ester phase into the water phase.	The turbulence, both interfacial and inside the aqueous phase, was very vigorous. Turbulent phenomenon existed at long contact times. No "additional zone" was observed below the liquid-liquid interface.

4.1.3.3 Discussion of the Physical Transfer Runs

With esters such as ethyl acetate and ethyl propionate transferring into the water phase, the moiré patterns observed are normal. The minute amount of interfacial turbulence, which creates a thin region of more concentrated ester solution next to the interface, is probably the result of uneven distribution of ethanol and acid produced at a very slow rate by the hydrolysis reaction of the ester.

On the other hand, the eruptive transfer of ester into the water phase as observed with the methyl acetate-water as well as the ethyl formate-water systems is rather unusual. Similar observations of the turbulent nature of the two systems were also reported by other investigators[A5]. It is speculated that the eruptive transfer is due to the effect of so-called "density flow" phenomenon. The ester, transferring from the upper phase into the lower phase, dissolves in water to form a solution whose density is either slightly heavier or very nearly equal to that of water at the same temperature (Table 2). Under such a condition, if there is any turbulent motion of the liquid at the interface, generated perhaps by the uneven concentration distribution of the alcohol and the acid from the hydrolysis reaction, this disturbance motion, in the form of liquid streaks, can travel a long way down the aqueous phase because of the similar densities between the streaks and the surrounding aqueous medium. The streaks phenomenon may be more

intensified in:

I Systems having higher rates of hydrolysis reaction with water;

II Systems having the products of hydrolysis reaction (i.e. alcohol and acid) strongly affecting the liquid-liquid interfacial tension;

III Systems whose aqueous ester solutions are heavier than water.

Streaking phenomena do not occur in reaction runs at high caustic concentration levels simply because the densities of sodium hydroxide solutions are higher than aqueous ester solutions.

With the propyl formate-water system, a small number of very weak streaks with negligible interfacial turbulence are observed. Perhaps the effects of propanol on the interfacial turbulence are small in this system.

As a matter of coincidence, all the systems exhibiting significant turbulent liquid streaks during physical mass transfer do not show a maximum in the speed of layer growth versus caustic concentration plots (Figure 7).

4.1.4 Investigation of the Factors Affecting the Turbulent Layer Propagation

The following section describes the experiments performed to determine the various factors contributing to the formation of the turbulent layer and to the control of the rate of layer propagation. The apparatus used to produce the moiré pattern of the liquid systems for these experiments is basically the same as described in the previous section (4.1.2). In some cases, minor modifications of the apparatus were necessary and are described accordingly.

4.1.4.1 Factors for the Formation of the Turbulent Layer

4.1.4.1.1 Alcohol

In the ethyl acetate-water system, a small amount of aqueous ethanol solution was injected very slowly, from a syringe through a long hypodermic needle, under the interface of the two-phase system. Several similar runs were performed with various concentrations of the aqueous ethanol solution. Other components comprising the reaction system were also injected in separate experiments but in a similar way.

The same procedure of injections was repeated for the methyl acetate-water system.

4.1.4.1.2 Surface Tension

In one run, a surface active agent was added to the lower phase of the ethyl formate-sodium hydroxide system. The turbulent layer propagation phenomenon was studied.

4.1.4.1.3 The Interface

In one experiment, water, pre-saturated with ethyl acetate, was stored in the caustic delivery tube. The solution was allowed to run out of the sintered glass disc very slowly and carefully and was put in contact with and floated on top of 0.5 N aqueous sodium hydroxide solution originally in the optical cell. Under such conditions, mass transfer occurred in only one homogeneous phase. This experiment was also repeated in the "sliding diffusion cell" (described in PART D of the dissertation).

4.1.4.2 Factors Affecting the Turbulent Layer Propagation

4.1.4.2.1 Density and Viscosity

In order to investigate the possible effects of viscosity and density of the lower phase on the rate of layer propagation, experiments were performed with the following systems: The upper phase was ethyl formate pre-saturated with water at room temperature; while the lower phase was, in consecutive order, (a) 1 N aqueous sodium hydroxide solution; (b) 0.1 N sodium hydroxide; (c) 0.1 N sodium hydroxide solution with added glycerol so that the viscosity of the solution was equivalent to that of the 1 N sodium hydroxide solution. The density of the solution, on the other hand, was below that of the 1 N sodium hydroxide; (d) and (e) sodium chloride and sodium acetate were added to separate 0.1 N sodium hydroxide solutions to simulate the density of the 1 N sodium hydroxide, with the viscosity of the solution below and above that of the 1 N sodium hydroxide respectively; (f) glycerol and sodium chloride were added together in appropriate amounts to the 0.1 N sodium hydroxide to simulate both the density and the viscosity of the 1 N sodium hydroxide solution.

Photographs were taken for each run and analysed subsequently.

Similar runs with the glycerol, sodium chloride and sodium acetate as additives to the lower phase were performed with the ethyl acetate-sodium hydroxide and the methyl acetate-sodium hydroxide systems.

4.1.4.2.2 Viscosity

A few quantitative runs were performed on the ethyl formate-carboxy methyl cellulose (CMC)-sodium hydroxide system. The aqueous sodium hydroxide used for these runs was pre-mixed with a controlled amount of sodium carboxy methyl cellulose which could greatly change the viscosity of the solution without significantly altering its density.

4.1.4.3 Results of the Investigation of the Factors Affecting the Turbulent Layer Propagation

4.1.4.3.1 Factors for the Formation of the Turbulent Layer

4.1.4.3.1.1 Alcohol:

When the aqueous ethanol solution was injected slowly under the interface of the ethyl acetate-water system, the ethanol was observed to ascend to the interface due to its lower density, and to induce turbulent motion as shown in Figure 8. The turbulence gradually disappeared as the ethanol diffused into both phases. Thus a turbulent mixing layer rather similar to the type observed with the saponification runs could be created. Concentrations of aqueous ethanol solution ranging from 8 N to 0.25 N were used for the injection. In all cases, turbulence of various degrees according to the normality of the ethanol solution was produced with the injection of a small amount of the solution (0.05 ml. to 0.2 ml.). Other components comprising the reactants and the products of the system, such as sodium acetate and water saturated with the ester, were also injected in separate experiments. No layer of turbulence was observed.

Similar observations were obtained with the injection of dilute methanol solution into the methyl acetate-water system.

4.1.4.3.1.2 Surface Tension:

When a drop of liquid surface active agent was added to the ethyl formate-0.1 N sodium hydroxide system, the speed

FIGURE 8

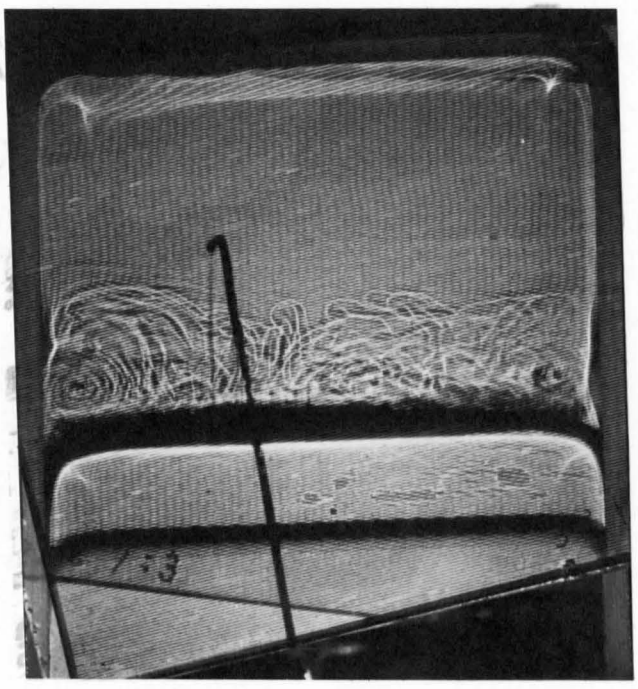

ETHYL ACETATE - WATER SYSTEM :
IMMEDIATELY AFTER THE INJECTION
OF 0.05 ML. OF 8.16 N AQUEOUS
ETHANOL SOLUTION

of the layer propagation was reduced. Also, the circulatory movement of the liquid in the turbulent layer was checked, and random turbulent liquid streaks instead were observed. The surface active agent used was a mixture of "9 moles of ethylene oxide concentrate/mole of nonyl phenol, 100% active."

4.1.4.3.1.3 The Interface:

When water, saturated with ethyl acetate, was carefully floated on top of the aqueous sodium hydroxide solution (0.5 N), no layer of turbulence was observed; instead, a shaded band appeared as shown in Figure 9. Such a phenomenon was observed in experiments performed in both the cubic optical cell and the sliding diffusion cell.

4.1.4.3.2 Factors Affecting the Turbulent Layer Propagation

4.1.4.3.2.1 Viscosity and Density:

Photographic results of the experiments performed on the ethyl formate-sodium hydroxide system with the 0.1 N sodium hydroxide solution added with glycerol, sodium acetate and sodium chloride respectively to simulate the density and viscosity of the 1 N sodium hydroxide solution were analysed for layer thickness. Data were treated in a similar way as with the other reaction systems. Lines of (layer thickness)^2 versus contact time were plotted and these are shown in Figures XVIII.11 and XVIII.12 in Appendix XVIII.

Two runs were performed on the ethyl acetate-glycerol-sodium hydroxide system; one with 0.1 N sodium hydroxide

FIGURE 9

WATER SATURATED WITH ETHYL ACETATE
IN CONTACT WITH 0.5 N AQUEOUS NaOH
SOLUTION (ONE PHASE) :
6.5 MINUTES AFTER INITIAL PHASE CONTACT

solution, and the other with 0.5 N sodium hydroxide solution. The viscosities of both the lower phase solutions were adjusted to that of the 1 N sodium hydroxide solution with glycerol. Results on the layer propagation were shown in Figure XVIII.13. Five runs were also performed on the methyl acetate-sodium hydroxide system with glycerol, sodium chloride and sodium acetate added in various amounts to the lower phase. The results of the layer propagation are shown in Figure XVIII.2.

4.1.4.3.2.2 Viscosity:

Two experiments were carried out on the ethyl formate-CMC-sodium hydroxide system. The sodium hydroxide solutions, being at 0.115 N and 0.341 N respectively, were added with the appropriate amounts of sodium carboxy methyl cellulose so that their viscosities were adjusted to that of the 1 N sodium hydroxide solution. Data of the layer propagation for these two runs are presented in Figure XVIII.14, Appendix XVIII.

4.1.4.4 Discussion of the Investigation of the Factors Affecting the Turbulent Layer Propagation

4.1.4.4.1 Factors Affecting the Zone Formation

The generally accepted cause of interfacial turbulence of the type observed in this study is the existence of local interfacial tension changes across a liquid-liquid interface. As indicated qualitatively in Figure 10, if there is a local decrease in interfacial tension caused by the presence of alcohol produced by the saponification reaction and indicated by the dots in the figure, then the liquid interface will pull away from the region of decreased tension. This interface movement will cause a fluid motion of the type indicated, bringing more concentrated or less concentrated

FIGURE 10

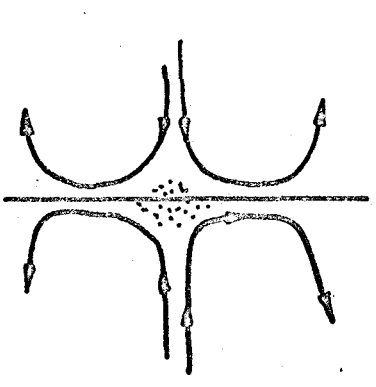

INTERFACIAL TURBULENCE IN ESTER SAPONIFICATION

alcohol solution to the interface. This process of non-uniform concentration of the aqueous alcohol solution flowing to the interface can sustain or even amplify the effect. Such explanations of the interfacial turbulence are consolidated by the results obtained from both the alcohol injection experiments and the physical transfer experiments involving a third component moving across the liquid-liquid interface. If all these are interfacial phenomena, then the turbulent layer will not form without an interface. Such an induction seems to be confirmed by experiments (Figure 9: Section 4.1.4.3).

4.1.4.4.2 Factors Affecting the Speed of Layer Propagation

On examining the layer growth results of the ester-sodium hydroxide systems with the viscosities and densities of their sodium hydroxide phases adjusted to that of the 1 N sodium hydroxide solution by additives such as glycerol, sodium acetate and sodium chloride, it became evident that both the increase of viscosity and density in a solution have retarding effects on the speed of layer propagation. The density effect seems to be the more predominant factor of the two.

Unfortunately, in these tests, the effects of viscosity and density cannot be isolated, since the additives increase both the viscosity and density of the solutions at the same time. Furthermore, in some additives, the salt effect is ever present - thus complicating the systems to a greater

extent. Nevertheless, experiments performed on the ethyl formate-sodium hydroxide system with sodium carboxyl methyl cellulose appear to support the statement that viscosity effect on layer propagation for an ester-caustic system is minor as compared to the salt and density effects.

Again in these experiments, the effects of the additives on the rest of the properties of a system, such as interfacial tension and diffusivities, are not yet fully known. Hence the conclusions derived so far from these experiments can only be treated as tentative and qualitative.

4.2 - PART B

MEASUREMENT OF THE CONCENTRATION DISTRIBUTION WITHIN THE TURBULENT LAYER IN THE ESTER-AQUEOUS CAUSTIC SYSTEMS WITH SLOW CHEMICAL REACTION

In this part, descriptions are given of the experimental work performed in order to obtain information on the concentration distribution of both the reactants and the products within the turbulent layer in the ester-caustic systems with slow saponification rates. The two systems studied were ethyl acetate-sodium hydroxide and methyl propionate-sodium hydroxide. Concentration profiles of the components in the systems were measured by withdrawing small samples of the liquid with probes precisely located in the aqueous phase.

The apparatus as well as the experimental techniques developed for the sampling are described in Section 4.2.1 and in Appendices III and IV. The concentration profiles obtained are presented (Section 4.2.2. and Appendix XVII) and discussed (Section 4.2.3).

Based on these concentration data, the structure of the turbulent layer was explained. Diffusivity values of various components in the aqueous phase were calculated from an eddy diffusion model. Enhancement factors as well as the reaction zone thicknesses were estimated and compared with those calculated from the existing theoretical models which were formulated on the basis of the reaction transfer without the effects of turbulence. All these results are presented and discussed in Section 4.2.3.

4.2.1 Experimental Details

4.2.1.1 The Apparatus

Figure 11 shows the experimental apparatus for probing the concentration in the reaction layer by withdrawing small samples. The pyrex circular test cell (6) was 21.2 cm. in diameter and 7 cm. high. The mid bottom of the cell contained a fritted glass disc (pyrex coarse grade) through which the lower aqueous phase could be introduced into the cell. The sintered glass disc was 9 cm. in diameter. During the experiment the cell was covered tightly with a 0.51 cm. thick circular brass plate (3) equipped with an adjustable point gauge, for the location of the liquid-liquid interface, and 15 long (type 316) stainless steel needles (.071 cm. O.D.) of various lengths for the sampling of the lower phase at various depths (4).

Figure 12 shows a typical needle sampling arrangement. The top end of each stainless steel needle (14) was connected with, and silver soldered to, a No. 18 B-D (Becton-Dickinson and Co.) hypodermic needle, on top of which a pre-cleaned B-D #MS09 spring loaded stopcock was fitted (5). The height of each needle above the plate was made the same. The bottom end of each needle was bent 90°, so that liquid sample could be drawn in horizontally. The heights and directions of individual needles were adjustable through the gland (13). The needle inlets were so orientated that the maximum distance could be obtained between any two sampling inlets. The

1. B-D Cornwall syringe (5 ml. capacity)
2. Cathetometer (for general checking purpose)
3. 15 Needles brass plate plus point gauge
4. 28/1000 O.D. stainless steel needles fitted with Luer-Lok adapters
5. B-D Spring loaded stopcock (MS09)
6. Pyrex glass cell (21.2 cm diameter) with a sintered glass disc (pyrex coarse grade) at bottom.
7. Tripod iron frame bolted to the floor
8. NaOH reservoir
9. Wooden plate
10. Teflon stopcock
11. Clamps

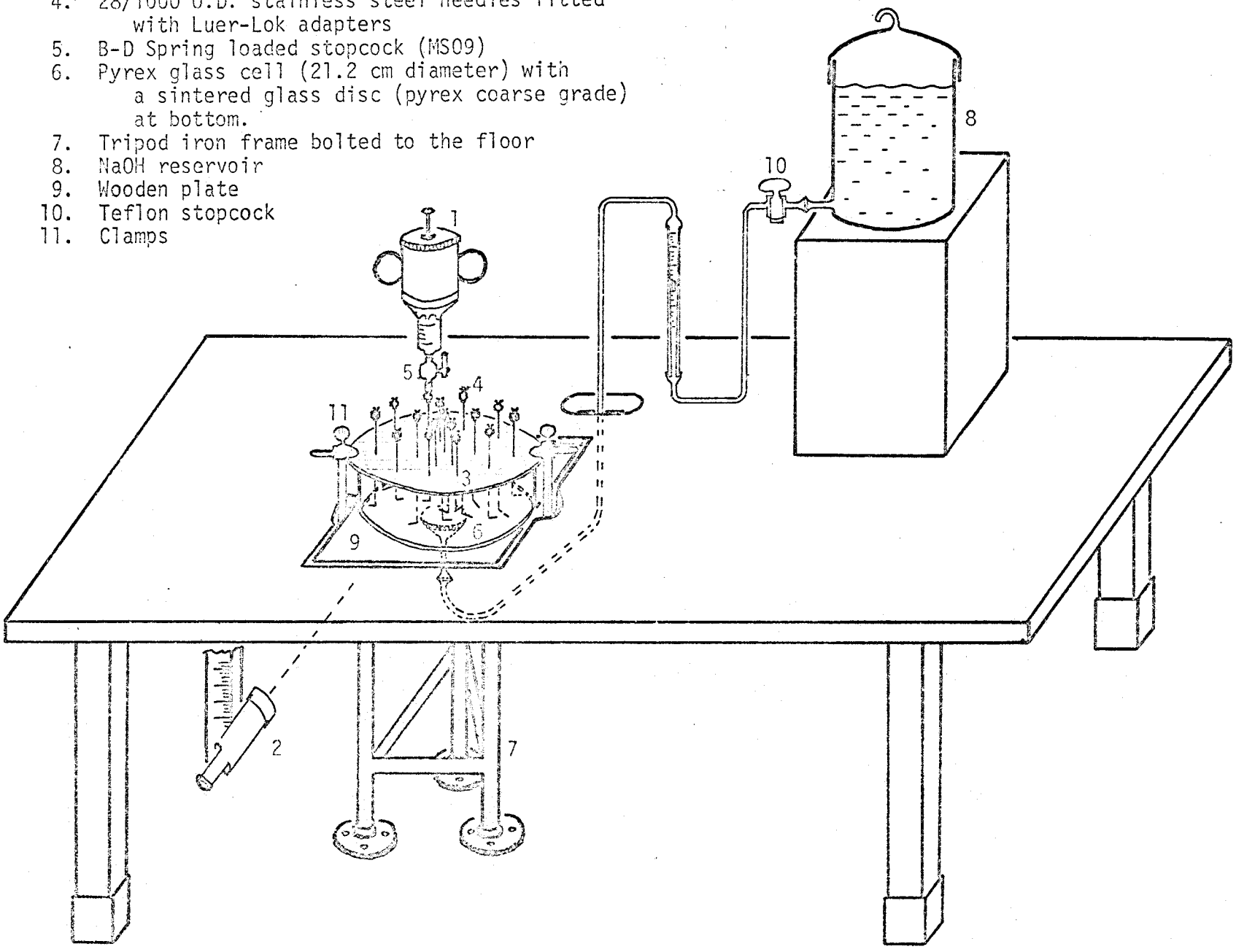

FIGURE 11 THE EXPERIMENTAL SET-UP

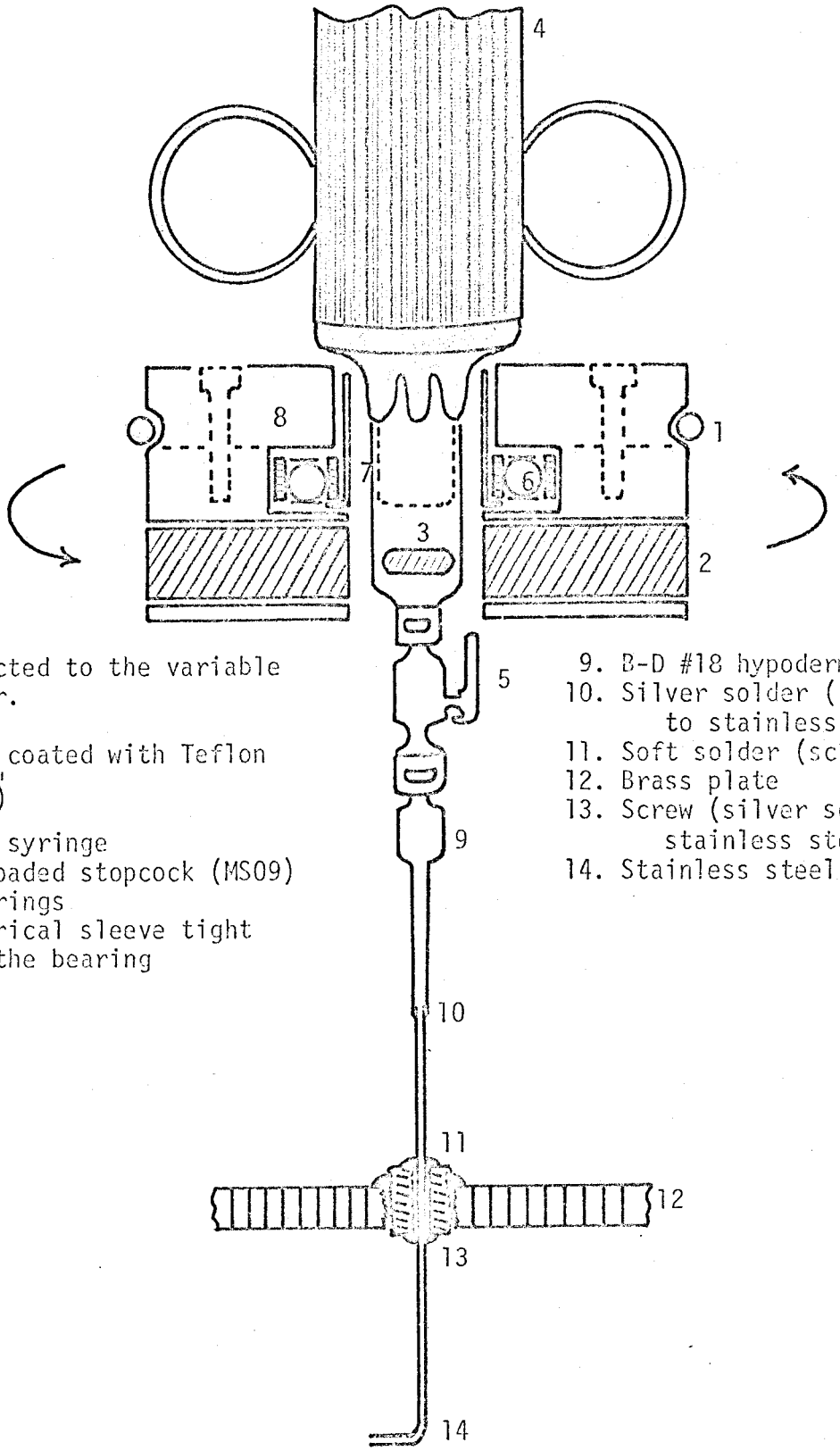

1. O ring connected to the variable speed motor.
2. Magnet
3. Small magnet coated with Teflon ($\frac{1}{8}$" x $\frac{1}{8}$" x $\frac{3}{8}$")
4. B-D Cornwall syringe
5. B-D Spring loaded stopcock (MS09)
6. SKF ball bearings
7. Brass cylindrical sleeve tight fitted to the bearing
8. Lucite block
9. B-D #18 hypodermic needle
10. Silver solder (hypodermic needle to stainless steel needle)
11. Soft solder (screw to plate)
12. Brass plate
13. Screw (silver soldered to the stainless steel needle)
14. Stainless steel sampling needle.

FIGURE 12 APPARATUS FOR SAMPLING

relative vertical heights of all needle inlets with respect to the tip of the point gauge were precisely measured before the start of each experiment.

A special sampling device (Figure 12) was used to create mixing between a liquid sample and a known amount of hydrochloric acid in the sampling syringe so that any residual sodium hydroxide in the sample was immediately neutralized and the saponification reaction was thus halted. Mixing was produced by a small stirring magnet bar coated with Teflon (3). Motion of the stirrer was induced by another two large rotating magnets (2) housed in a donut-shaped Lucite block (8) and in the direction opposite to each other. The revolving Lucite block with magnets was tightly fitted to a stationary cylindrical brass sleeve (7) by means of an SKF ball bearing (6).

During sampling, the B-D Cornwall syringe, pre-loaded with a known volume of hydrochloric acid, was inserted through the stationary brass sleeve and connected to the spring loaded stopcock attached on top of the sampling needle. The Lucite block with its magnets was revolved around the sleeve by means of an O ring (1) connecting the block to a variable speed motor. In this way, the Teflon coated stirrer inside the syringe was made to revolve and provide vigorous mixing of liquids. The whole sampling device was mounted on a frame which could be moved horizontally on the working table with ease as to facilitate the sampling from needle to needle.

The legs of the frame were cushioned with soft rubber to absorb most of the mechanical vibration from the electric motor.

Detailed description of the individual pieces of the equipment may be found in Appendix III.

4.2.1.2 Experimental Procedure

4.2.1.2.1 Reaction Runs (with reference to Figure 11)

A clean test cell was placed in a preset position and supported by the wooden plate (9). The flow system was connected. Small amounts of sodium hydroxide solutions from the reservoir (8) were repeatedly allowed to run into the cell and withdrawn in order to flush out the trapped air and water inside the pores of the sintered glass disc.

Five hundred ml. of water-saturated redistilled ester was gently poured into the cell. The brass plate holding the needles was then put into the set, horizontal position by means of adjusting clamps (11). The caustic solution, at the desired concentration level, was fed through the sintered glass disc and contacted the ester phase at a carefully controlled flowrate in order to minimize the phase contact mixing. A flowrate of 0.042 litres/minute was used for the first four minutes, 0.166 litres/minute for the next five minutes and finally 0.187 litres/minute until the liquid-liquid interface just touched the tip of the point gauge.

Small liquid samples were withdrawn (one at a time) from different needles precisely located inside the turbulent layer at a slow, controlled rate using Cornwall syringes pre-loaded with a known amount of hydrochloric acid. Reaction inside the syringe was stopped by neutralization.

Reactant and product concentrations in a sample were

analysed. Sodium hydroxide was analysed by acid-base titration. Ester and alcohol were analysed by gas chromatography and finally, the salt was analysed by conductometric titration.

A detailed account of the entire experimental procedure may be found in Appendix IV.

4.2.1.2.2 Physical Runs

A similar procedure to the reaction runs was followed to contact the two phases.

The sampling procedure, however, was much simpler as compared to that adopted for the reaction runs. Since the hydrolysis reaction of ester in the neutral medium liquid phase was known to be rather slow,[I2] the samples (not more than 0.5 ml. for each sample) were simply drawn into the Cornwall syringes and subsequently transferred into the small sample tubes (2 ml. in capacity). The procedure for the pre-filling of the syringes with standard hydrochloric acid solutions and the pre-filling of the water for dilution in the sample tubes (Appendix IV: IV.1.3) was not used here.

Concentrations of the upper phase in the samples were analysed by the refractive index method as described in detail in Appendix IV: IV.4.

4.2.1.3 Number of Concentration Probing Experiments Performed

4.2.1.3.1 Physical Runs

4.2.1.3.1.1 n-Butanol-water system:

Five runs were performed at room temperature. In the first four runs, the flowrates of the water phase into the cell were varied in order to study the effects of phase contact turbulence on the concentration profiles. The filling rate data for various runs are given in Table 4. After the best set of the lower phase filling rates was determined from these runs, one additional run was carried out using the determined best set of filling rates to check the reproducibility of the sampling experiments.

TABLE 4

FILLING RATES OF THE AQUEOUS PHASE FOR THE FIVE RUNS IN THE n-BUTANOL-WATER SYSTEM

Run	Filling Rate (litres/minute)
1	0.500
2	0.322
3	0.166 0.187
4	0.042 0.166 0.187
5	0.042 0.166 0.187

The sets of experiments in this liquid system also served to establish the validity of the methods used to obtain the concentration profiles of all subsequent experiments. The diffusion coefficient of n-butanol in water is well known[J4]. The theoretical concentration profiles for the system could easily be evaluated and compared with the experimental profiles.

4.2.1.3.1.2 Ester-water systems:

Physical diffusion of ethyl acetate in water and methyl propionate in water at room temperature were studied separately. Concentration distributions of ester in the aqueous phase at various contact times were measured.

4.2.1.3.2 Reaction Runs

4.2.1.3.2.1 Ethyl acetate-aqueous sodium hydroxide system:

A total of eleven runs were performed at 24 ± 1°C and at five sodium hydroxide concentration levels (0.2, 0.4, 0.6, 1.0 and 1.4 N). Two runs were performed at each concentration level with the exception of 0.2 N sodium hydroxide; at which level, three runs were performed. In the first run of a particular caustic concentration level, samples were drawn from a set of four needle inlets at various depths below the interface. In the second run, samples were withdrawn from a succeeding set of four needles which were so chosen that each needle inlet was situated slightly lower from the interface than the corresponding needle of the first set. As an example, in Run No. 4-1, samples were withdrawn

from needles Nos. 2, 4, 6 and 8; which were .094, .361, .620 and 1.016 cm. away from the interface. In Run No. 4-2, the set of needles used were Nos. 3, 12, 7 and 9, which were .262, .524, 0.793 and 1.270 cm. below the interface respectively. Results from the two related runs at the same sodium hydroxide concentration level were combined to form one experiment for subsequent data analysis. In this way, the consistency of the experimental results in the paired runs could be checked.

4.2.1.3.2.2 Methyl propionate-aqueous sodium hydroxide system:

Six runs were carried out at the controlled room temperature of 24 ± 1°C and at three sodium hydroxide concentration levels (0.4, 0.6, and 1.0 N). The general proceedings were similar to that of the ethyl acetate-sodium hydroxide system.

4.2.1.4 Method of Calculation

4.2.1.4.1 Reaction Runs

4.2.1.4.1.1 Concentrations of reactants and products in a sample:

Concentrations of the reactants and products in each sample obtained from analyses (Appendix IV: IV.3) were individually multiplied by the ratio of the final volume of the sample after successive steps of dilution to the volume of the initial sample. These would convert the analysed concentrations into the original component concentrations in the location inside the cell where the sample was taken.

4.2.1.4.1.2 Original concentration versus contact time curves for each component:

For each needle, original concentrations for a particular component were plotted against the contact times at which the samples were taken. Thus, for an experiment, a family of such curves was obtained, each curve representing the concentration variation of a component as a function of time at the position where the needle inlet was located (for example, see Figure 17 in Section 4.2.2).

Altogether, a total of four families of such curves were plotted for each experiment. Each set represented one component.

4.2.1.4.1.3 Concentration profiles for individual components:

From a family of plots of original concentration versus contact time for a particular component in the ester-caustic

system (see Figure 17 for example), the concentrations at various needle inlet positions (corresponding to various depths from the liquid-liquid interface) at any fixed contact time may be read out simultaneously. Data so obtained for the component were used to plot original concentration versus distance from the interface curves at 25, 50 and 75 minutes after the start of the run. Concentration profiles of the other components of the system were also drawn for the same time intervals in a similar way (see Figure 18 for example).

4.2.1.4.1.4 Mass transfer rates determination:

An area under a concentration profile could be integrated by means of a planimeter. If the area so obtained was multiplied by the cross-sectional area of the cell, the total amount of that component, which the profile represented in the lower phase at that particular time, was calculated. Thus in this way, the total amount of individual components (except for the caustic amount) in the lower phase at 25, 50 and 75 minutes for each ester-sodium hydroxide experiment was evaluated.

In contrast to the rest of the components in the reacting system, it was the amount of lower phase sodium hydroxide which disappeared, rather than the amount of accumulation that was of immediate interest. In a particular experiment, the total amount of sodium hydroxide reacted at a particular time was obtained by subtracting the residual amount of sodium hydroxide from the original total amount of sodium

hydroxide. In the concentration profiles graph, the amount of sodium hydroxide which reacted would be represented by the area bounded by the liquid-liquid interface, the initial sodium hydroxide concentration line and the sodium hydroxide concentration profile (with reference to Figure 18).

If the total amount of the ester and the disappearance of sodium hydroxide in the lower phase were added, the resulting amount would be equivalent to the total transfer of the ester across the liquid-liquid interface up to that particular contact time. Similarly, total mass transfer of the ester was also calculated for the same ester-sodium hydroxide experiment but at other time intervals. In this way, the total amount of ester transferred could be plotted against the time after the start of the experiment. From this plot, the average mass transfer rate up to any contact time of the run could be calculated. In addition, the mass transfer data could be fitted by a polynomial equation using the orthogonal polynomial method(H13). By differentiating the resulting fitted equation, instantaneous mass transfer rates could be estimated roughly at any time interval of that particular experiment. Mass transfer rates for other experiments were determined in a similar way.

4.2.1.4.2 Physical Runs

The general methods of calculation for the data of physical runs were much the same as for those of the reaction runs. The amount of calculation involved was less because

only one component (either the ester or the n-butanol) was present in the water phase. Since the samples drawn from the cell were directly analysed without dilution, the back conversion of the analysed sample concentrations to the original concentrations as described in the reaction runs (Section 4.2.1.4.1.1) was not required.

4.2.2 Results

4.2.2.1 Physical Mass Transfer Runs

4.2.2.1.1 n-Butanol-water System

The various filling rate data of the water phase into the cell for the five runs are tabulated in Table 4. In the runs with higher rates of introduction of water into the cell, phase contact turbulence was perceived; the higher the filling rate, the more pronounced the turbulence. In the first run, the flowrate of the lower phase was so high that a slow, circular liquid movement in the cell was evident during filling.

Samples withdrawn from the lower phase of each run were analysed for n-butanol concentrations. Results were tabulated. These data were plotted with concentration of n-butanol versus contact time for each needle inlet position for each run. (See Figure 14: ethyl acetate-water system for example.) From all these plots, concentration profiles of the five n-butanol-water runs at 60 minutes, 273 minutes and 546 minutes after the start of the runs were derived as shown in Figure 13.

4.2.2.1.2 Ester-water Systems

The best set of experimental lower phase filling rates as determined from the n-butanol-water runs was used in both the ethyl acetate-water and methyl propionate-water systems.

In the ethyl acetate-water system, visual observations during experiments indicated that a thin region of liquid

FIGURE 13 CONCENTRATION PROFILES
(N BUTANOL-WATER SYSTEM)

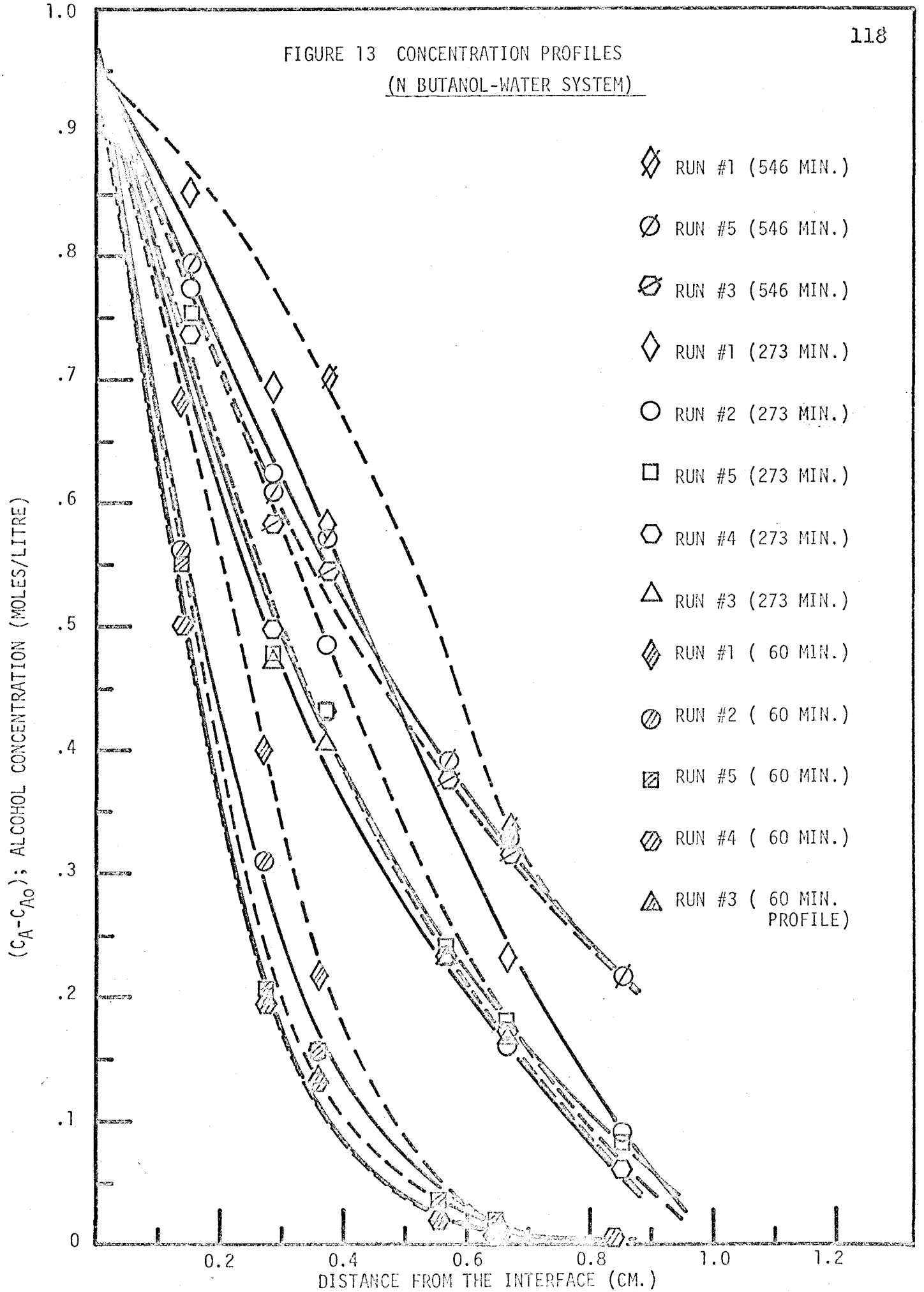

having different refractive index from the rest of the bulk lower phase again existed just below the interface. Such observations were in agreement with previous optical cell experimental results (Section 4.1.3.2.1.1). Samples obtained were analysed and sets of concentration profiles at various contact times were derived in the way similar to those derived in the n-butanol-water system. As an example, concentration data of the ethyl acetate-water system are presented in Table XV.1 in Appendix XV. These data were plotted as shown in Figure 14. The ethyl acetate concentration profiles are shown in Figure 15.

On the other hand, when methyl propionate was in contact with water, liquid streaks were observed protruding slowly but randomly into the lower bulk phase. This observation was, again, in agreement with the phenomenon observed in earlier optical cell experiments (Section 4.1.3.2.1 2). Samples were obtained during the run, and the concentration data acquired were analysed in the same way as with the other physical transfer systems. Concentration profiles at various contact times were plotted as shown in Figure 16.

FIGURE 14 VARIATION OF ESTER CONCENTRATIONS WITH PHASE CONTACT TIME
(ETHYL ACETATE - WATER SYSTEM)

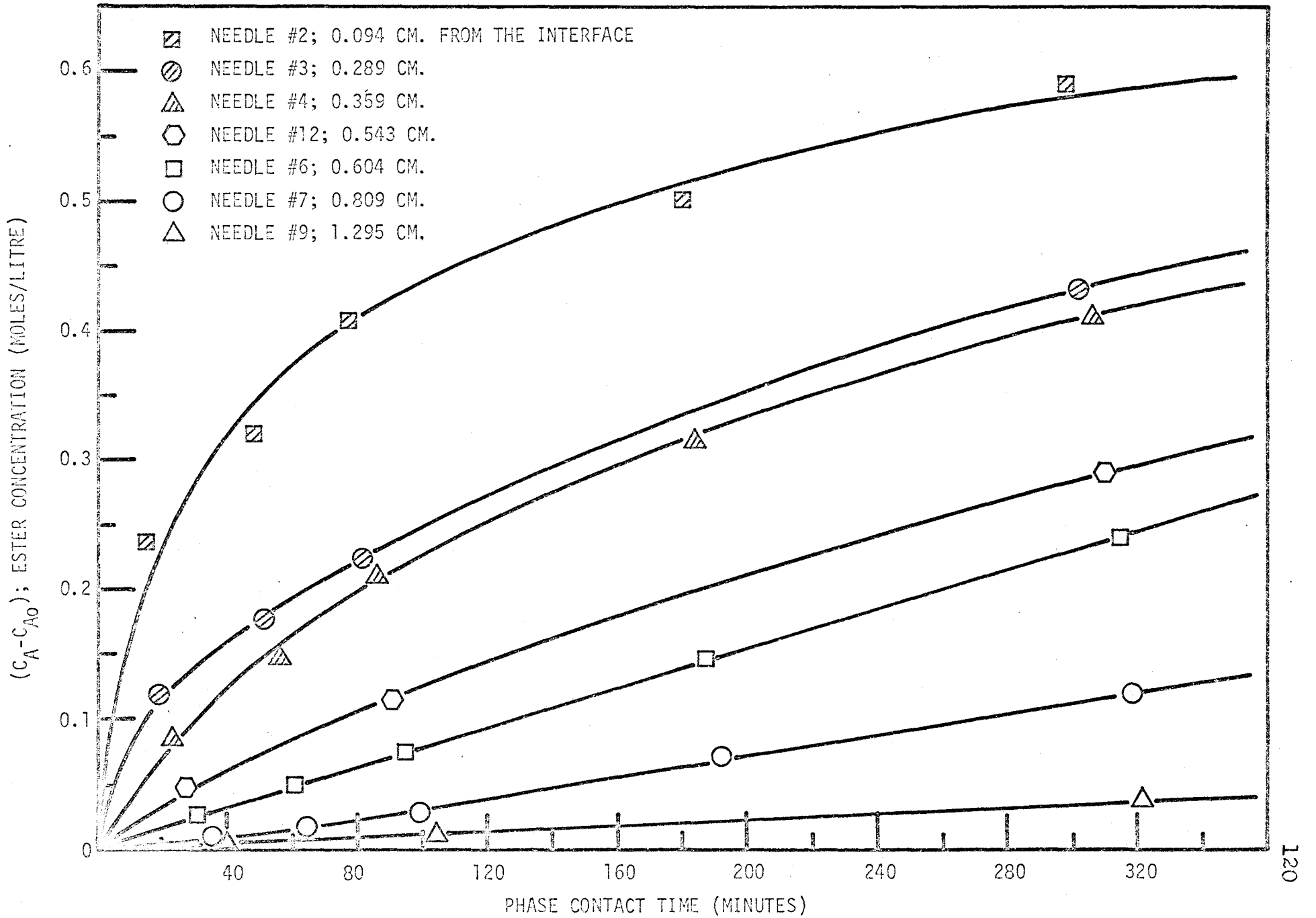

FIGURE 15

CONCENTRATION PROFILES
(ETHYL ACETATE-WATER SYSTEM)

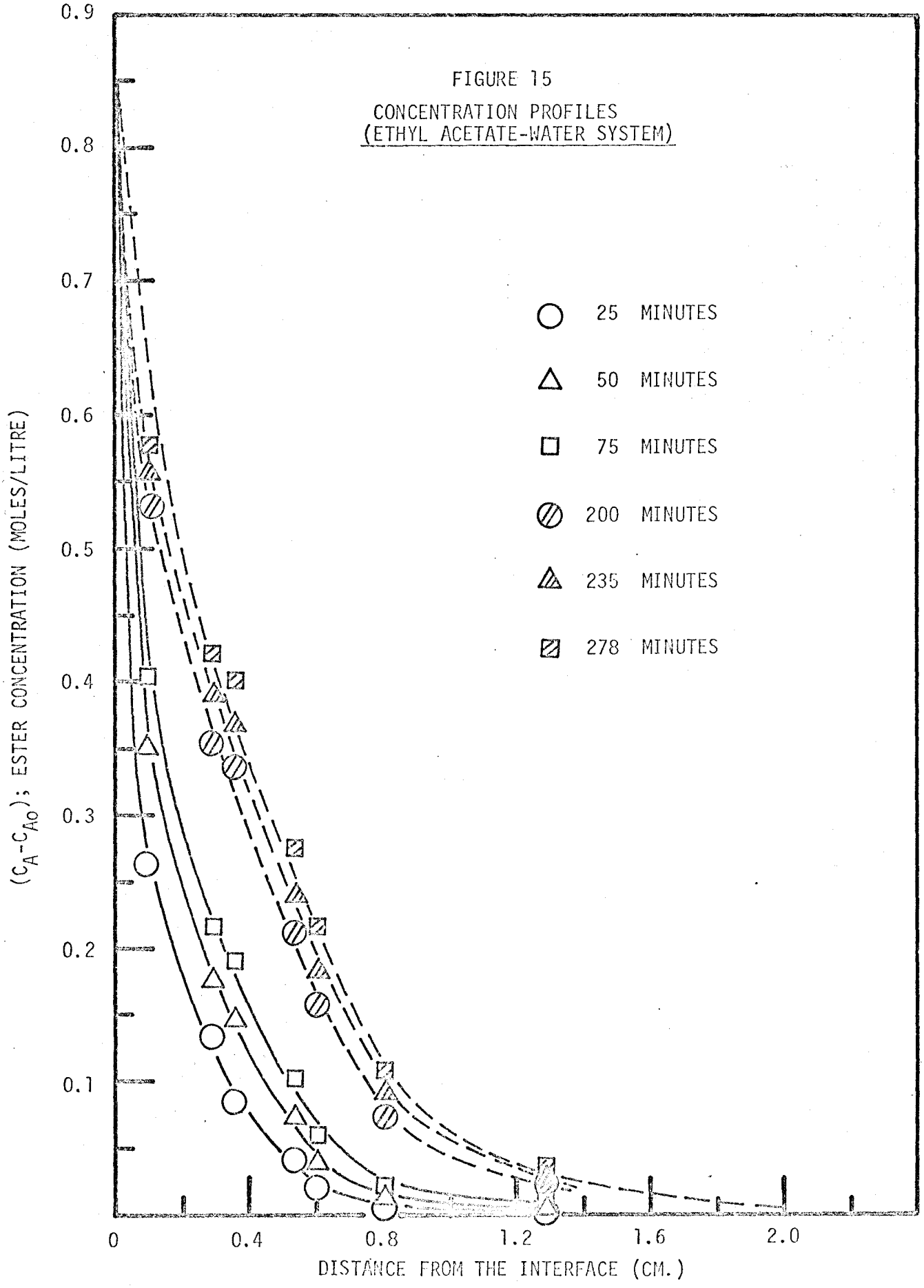

FIGURE 16

CONCENTRATION PROFILES OF
METHYL PROPIONATE - WATER SYSTEM

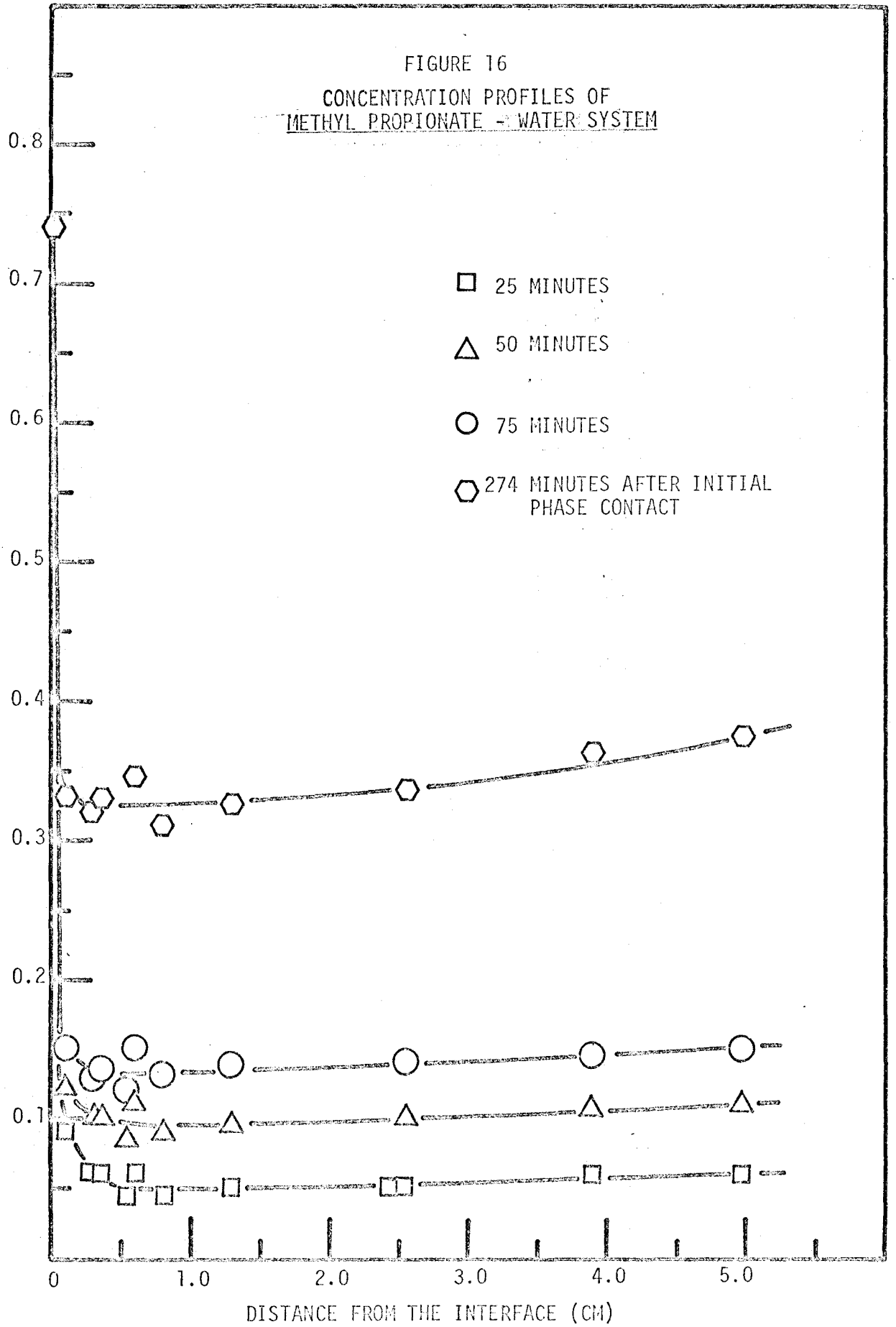

4.2.2.2 Reaction Mass Transfer Runs

4.2.2.2.1 Ethyl Acetate-Aqueous Sodium Hydroxide System

In general, the turbulent layer thus formed among these runs behaved, by visual observations, very much the same way as those in the layer propagation measurement runs performed in the 5 cm. cubic optical cell(S8). Despite the large cross-sectional area of the present round test cell, the turbulent layer extended quite uniformly downward; although the plane of the lower front was slightly undulating. Occasionally during a run and usually in the later stage of the run, a very slow surge of liquid upward was observed in small, rather isolated and restricted regions near the lower layer front. These upsurges extended about one-third of the way into the layer and then diffused out. Existence of the upsurges of the liquid was transient. The upsurges could possibly start to form anywhere across the plane of the lower front. The number of upsurge occurrences increased with increasing initial sodium hydroxide concentration. The upsurge of the liquid was probably due to localized hot spots being developed as a result of the uneven distribution of the heat of the reaction. Small pockets of the liquid were heated up and they ascended due to buoyancy force. The upsurge motion of the liquid could also be induced or intensified by the rising alcohol being released as a product of the reaction. Viewing from the top of the cell, the liquid-liquid interface was by no means smooth. Ripples and

flow cells of different sizes were observed as a result of the mixed solution of alcohol and possibly other components hitting the interface and causing the interfacial turbulence.

Samples taken from the runs were analysed for both the reactants and the products. The corresponding final concentrations were calculated accordingly and were tabulated. As an example, concentration data for ethyl acetate-1.0 N sodium hydroxide runs are presented (Tables XV.2 and XV.3 in Appendix XV). These data were plotted with the original concentrations of individual components versus contact time for each needle position. The resulting graphs are shown in Figure 17. From these graphs, concentrations of both reactants and products as a function of distance from the interface could be obtained at 25, 50 and 75 minutes respectively as shown in Figure 18. Similar concentration profiles of the individual components for the other nine runs are also presented in Appendix XVII.

4.2.2.2.2 Methyl Propionate-Sodium Hydroxide System

Turbulent layers in these runs were comparatively thinner than those with the ethyl acetate-sodium hydroxide system. Such observations were again in agreement with the earlier findings in the optical cell experiments (Section 4.1.2.2.1.3). The layer, in a typical run, also propagated quite uniformly as with the ethyl acetate-sodium hydroxide system. Probably due to its smaller thickness, the upsurge of pockets of the liquid inside the layer was not as obvious.

VARIATION OF THE REACTANTS AND PRODUCTS CONCENTRATIONS WITH PHASE CONTACT TIME
(ETHYL ACETATE - 1.0 N NaOH SYSTEM; 24 ± 1°C)

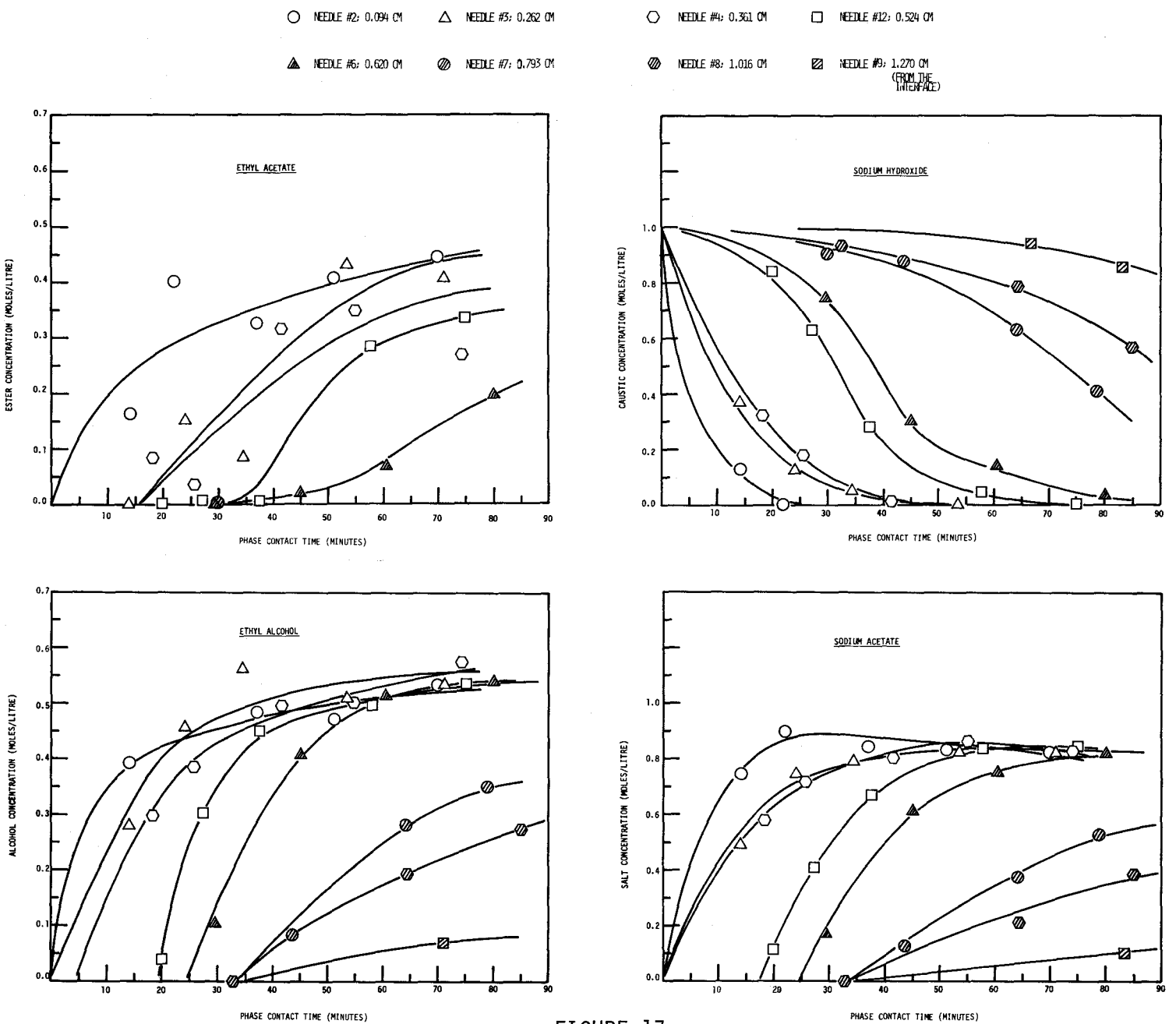

FIGURE 17

FIGURE 18

CONCENTRATION PROFILES OF REACTANTS AND PRODUCTS IN THE AQUEOUS PHASE (ETHYL ACETATE - 1.0 N NaOH; 24 ± 1°C)

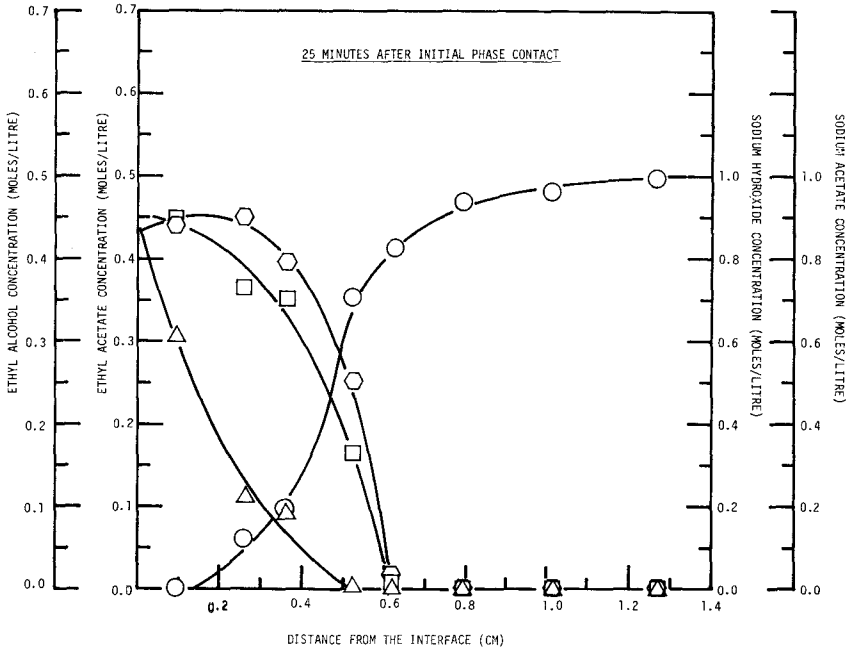

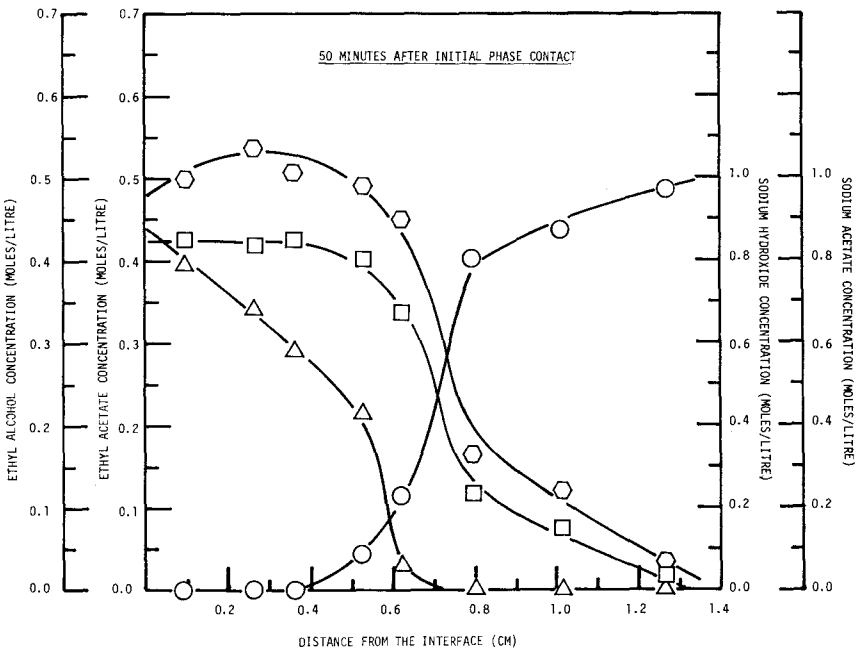

△ △ ETHYL ACETATE

○ ○ SODIUM HYDROXIDE

⬡ ⬡ ETHYL ALCOHOL

□ □ SODIUM ACETATE

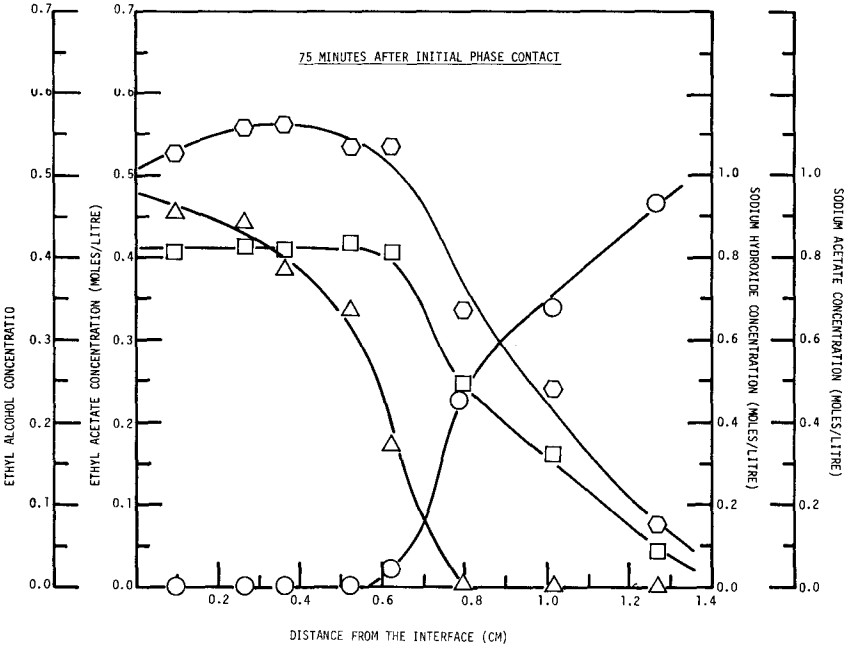

Nevertheless, the interfacial turbulence, in the form of ripples and waves, and turbulent liquid motion inside the layer was quite evident.

Liquid samples were analysed in the same way as with the ethyl acetate-sodium hydroxide system. Concentration profiles of the individual components for the six runs at three initial sodium hydroxide concentration levels were prepared. For each caustic concentration level, three sets of concentration profiles, coinciding with 25, 50 and 75 minutes after starting the runs, were constructed. Typical concentration profiles for methyl propionate-0.4 N sodium hydroxide system are shown in Figure 19. Similar concentration profiles for the other runs of the system are shown in Appendix XVII.

FIGURE 19

CONCENTRATION PROFILES OF REACTANTS AND PRODUCTS
IN THE AQUEOUS PHASE
(METHYL PROPIONATE - 0.4 N NaOH; 24 ± 1°C)

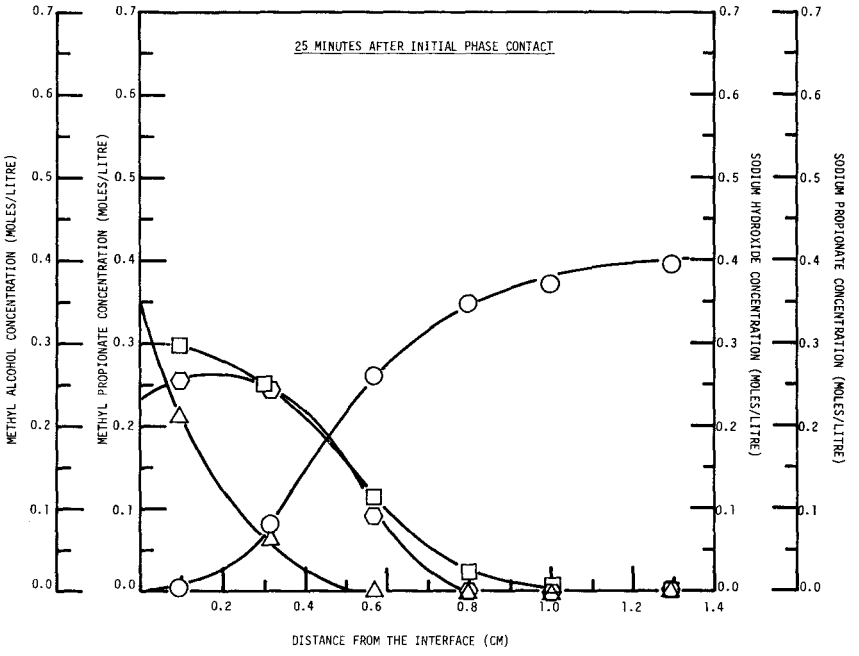

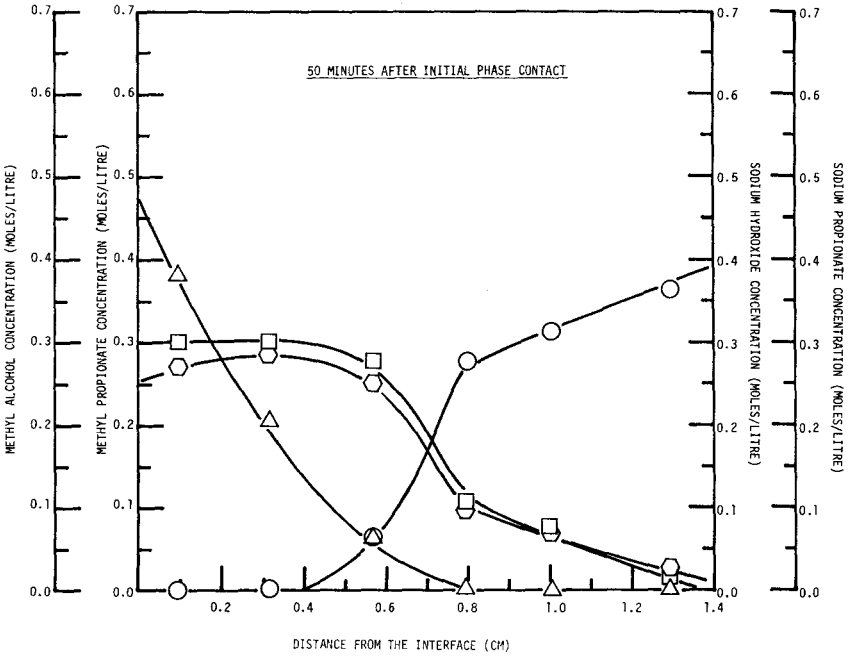

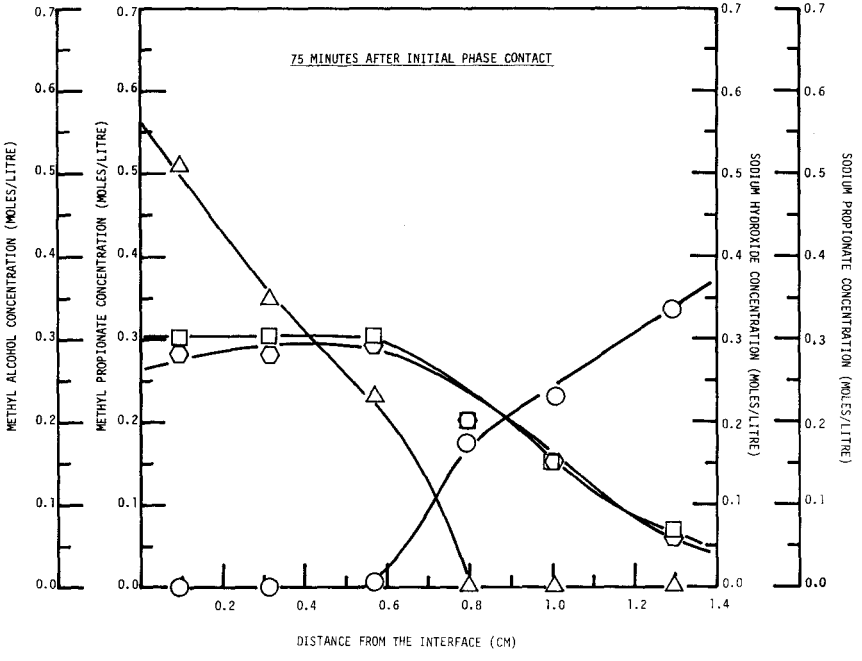

△ △ METHYL PROPIONATE
○ ○ SODIUM HYDROXIDE
⬡ ⬡ METHYL ALCOHOL
□ □ SODIUM PROPIONATE

4.2.2.3 Mass Transfer of the Ester Across the Liquid-Liquid Interface

Except for the n-butanol-water system, all the areas under the concentration profiles for the rest of the experimental runs were integrated. From these data, total mass transfer of the ester across the liquid-liquid interface at different contact times was evaluated for each run. The method of evaluation was described earlier in Section 4.2.1.4.1.4.

These transfer data were also plotted. Thus a family of curves of total ester transfer versus contact time was obtained for each system, and each curve represented a particular initial sodium hydroxide concentration level. The sets of curves for the ethyl acetate-caustic system and for the methyl propionate-sodium hydroxide system are shown in Figure 20.

All these mass transfer curves were fitted with polynomial equations using the orthogonal polynomial method(H13). A C.G.E.-265 (Canadian General Electric Co.) digital computer was used for the curve fitting calculations. Standard computer programs for such calculations were readily available from the C.G.E. Time Sharing Program Library. The polynomial equations obtained were tabulated as shown in Table 5.

FIGURE 20

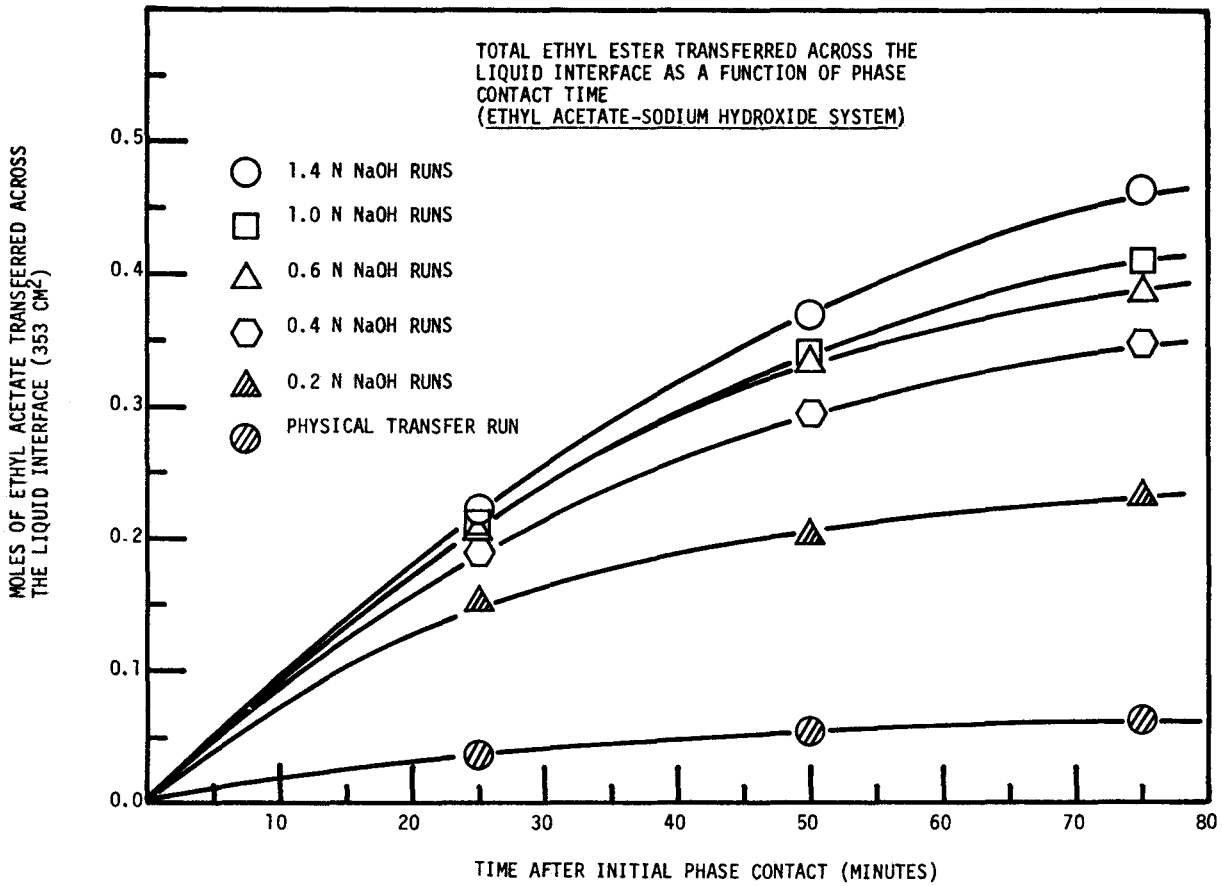
TOTAL ETHYL ESTER TRANSFERRED ACROSS THE LIQUID INTERFACE AS A FUNCTION OF PHASE CONTACT TIME
(ETHYL ACETATE-SODIUM HYDROXIDE SYSTEM)
1.4 N NaOH RUNS
1.0 N NaOH RUNS
0.6 N NaOH RUNS
0.4 N NaOH RUNS
0.2 N NaOH RUNS
PHYSICAL TRANSFER RUN
MOLES OF ETHYL ACETATE TRANSFERRED ACROSS THE LIQUID INTERFACE (353 CM2)
0.0
0.1
0.2
0.3
0.4
0.5
10
20
30
40
50
60
70
80
TIME AFTER INITIAL PHASE CONTACT (MINUTES)

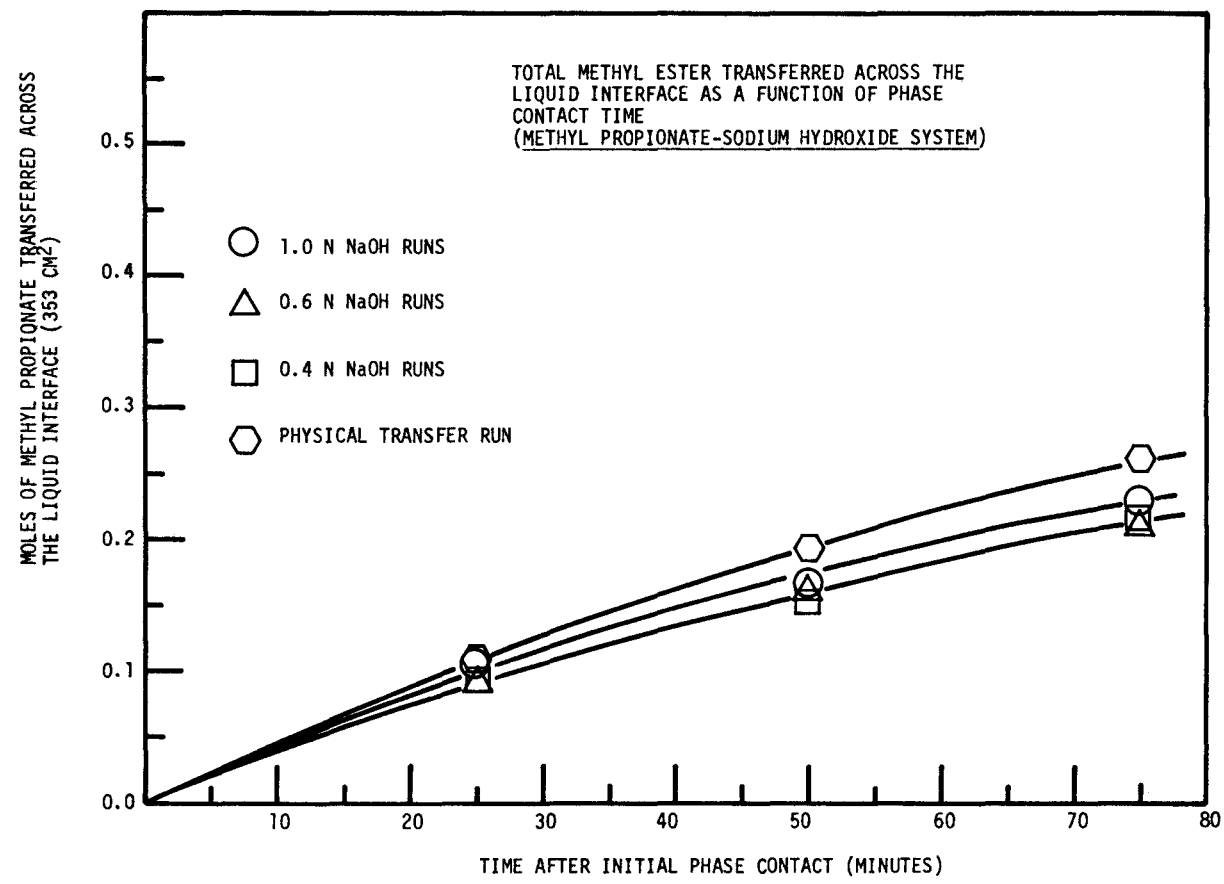
TOTAL METHYL ESTER TRANSFERRED ACROSS THE LIQUID INTERFACE AS A FUNCTION OF PHASE CONTACT TIME
(METHYL PROPIONATE-SODIUM HYDROXIDE SYSTEM)
1.0 N NaOH RUNS
0.6 N NaOH RUNS
0.4 N NaOH RUNS
PHYSICAL TRANSFER RUN
MOLES OF METHYL PROPIONATE TRANSFERRED ACROSS THE LIQUID INTERFACE (353 CM2)
0.0
0.1
0.2
0.3
0.4
0.5
10
20
30
40
50
60
70
80
TIME AFTER INITIAL PHASE CONTACT (MINUTES)

TABLE 5

REGRESSION DATA OF TOTAL ESTER TRANSFERRED ACROSS THE LIQUID INTERFACE AS A FUNCTION OF PHASE CONTACT TIME

Lower phase concentration	A X 10^3	B X 10^5	C X 10^8
EtAc - NaOH system			
Water	2.00_{083}	-2.46_{916}	12.3_{070}
0.2 N	8.53_{625}	-11.9_{548}	62.6_{741}
0.4 N	9.37_{035}	-8.25_{884}	25.5_{396}
0.6 N	10.2_{243}	-7.84_{199}	15.0_{106}
1.0 N	10.0_{589}	-7.11_{946}	13.6_{246}
1.4 N	10.2_{117}	-5.79_{432}	4.79_{571}
MePr - NaOH system			
Water	4.86_{741}	-2.30_{492}	5.92_{941}
0.4 N, 0.6 N	4.27_{033}	-2.84_{129}	13.1_{618}
1.0 N	4.73_{207}	-2.96_{525}	9.94_{199}

Regressions equation:

$$N = AT + BT^2 + CT^3$$

where N = total ester transferred across the liquid interface, moles

T = Phase contact time, minutes

4.2.3 Discussion

4.2.3.1 General Assumptions

The ester is pre-saturated with water so that only the ester can transfer across the interface and react with the sodium hydroxide in the lower phase. This assumption is probably a valid one. In separate experiments, the ester phase was placed in contact with the aqueous sodium hydroxide phase for several hours and subsequently part of the ester was evaporated to dryness. No traces of the sodium hydroxide or the salt were found. Furthermore, once the turbulent layer was developed, the interfacial concentration of the sodium hydroxide dropped either to zero or almost to zero depending on the initial concentration levels of the caustic and on the systems under study (Figures 18-19 and also Appendix XVII). The alcohol, on the other hand, would diffuse in both directions. The upward diffusion of the alcohol probably would not significantly interfere with the downward transfer of the ester.

The second assumption involved is that the layer propagation must be uniform. In other words, the concentrations at different locations in a cross-sectional plane, parallel to the interface, are the same. In this way, three-dimensional profiles will be reduced to one-dimensional. Such an assumption seems to be substantiated by:

I Uniform turbulent layer thickness was observed in the optical cell experiments.

II Agreement of the experimental and theoretical concentration profiles was obtained in the n-butanol-water system.

III Concentration variation of samples obtained from different needle inlets in two consecutive runs always behaved accordingly and as normally expected. The two consecutive runs formed one experiment (with reference to Section 4.2.1.3.2).

4.2.3.2 Experimental Errors

4.2.3.2.1 Temperature

In general, the room temperature was kept fairly constant by means of an air cooler. Although the temperature range from day to day could be as high as 24 ± 1°C, the variation of temperature in a run usually lay within ½°C and in no case exceeded 1°C. The room temperature for all the runs was therefore considered to be constant. However, inside the system, the situation is entirely different. Heat of reaction, though quite small (-13.08 kcals./mole for the ethyl acetate-sodium hydroxide system[B5]), becomes increasingly significant with the runs of higher sodium hydroxide concentration or at the later stage of a run. Under such conditions, a substantial amount of the ester and the caustic is consumed by the reaction with the corresponding quantity of heat being released. Most of the heat is used to heat the liquid near and inside the reaction zone. Convective currents are set up inside the turbulent layer with the warmer liquid as well as with the alcohol-rich liquid pockets rising towards the interface. Turbulent heat transfer takes place both inside the layer and at the interface. As a result, a temperature gradient as much as 1½°C across the liquid system is possible. (Refer to Appendix VI: Temperature Profile Measurement in the Turbulent Layer.) For the same reasons of incomplete mixing inside the two-still-liquid-phase system, it would appear to have

little added advantage to thermostat the test cell in addition to the present existing room temperature control.

4.2.3.2.2 Sampling

Each liquid sample drawn out from the aqueous phase for analysis is from a certain volume at the needle inlet rather than from the point. Consequently, the analysis represents the average concentration of a certain volume of liquid in the lower phase. Moreover, due to the presence of the convective flow and the interfacial turbulence, sampling has to be done carefully so that representative samples may be obtained. Nevertheless, the sampling rate is quite slow (~0.75 ml./minute). Visual observations during sampling indicate that a rather small, restricted volume of the liquid immediately in the vicinity of the needle inlet is affected. Also, the variation of concentration at a particular needle inlet due to the irregular convective flow of the liquid pockets may be averaged out over a period of two minutes' sampling time.

After a sample has been taken, the spring-loaded stopcock is closed. The liquid inside the sampling needle is trapped until the next round of sampling. In this way, part of the sample taken is actually the liquid left behind from the previous sample in which the concentration is different from the present sample. Since the volume of the liquid trapped in the needle is quite small (less than 1% of the sample volume), the effect of "liquid trapping" is assumed to

be negligible.

Errors due to the measurement of the sampling needle inlet positions are also estimated. The error involved in reading the cathetometer is relatively insignificant (± 0.001 cm.). The error range in the measurement of the sampling needle inlet positions is assumed to be equal to the internal diameter of the needle inlet (i.e. ± 0.02 cm.). Such an assumption is based on the comparison of experimental and theoretical concentration profiles of the n-butanol-water system (Section 4.2.3.3.1.3: Figure 21).

4.2.3.2.3 Mechanical Vibrations

Care has been exercised during sampling in order to keep mechanical vibrations to a minimum. The vibrations are mainly caused by the electric motor used to drive the rotating magnets in the sampling device. (Refer to Appendix III: III.2.4.) Since the test cell and the sampling needles are mounted on a tripod frame bolted to the floor and detached from the working table, mechanical disturbances to the system during sampling can probably be assumed negligible.

4.2.3.2.4 Analysis of Samples

Errors are accumulated in the determination of concentrations due to the uncertainties involved in the measurement of sample volumes, titration volumes and chromatograms. A sample error analysis on the concentrations of reactants and products is presented. (Refer to Appendix VII: Error

Analysis.) As a result of the analysis, it was found that the so-called probable errors for both the ester and the salt concentrations were below ±5%. Probable errors for the sodium hydroxide were slightly higher (~4-10%, depending on the concentration level). Probable errors for ethanol in the ethyl acetate-sodium hydroxide system ranged mostly below 10%. However, it could be as high as 17% in the extreme cases of dilute caustic concentration runs. On the other hand, probable errors for methanol in the methyl propionate-sodium hydroxide system were below 5%. The higher level of error in the ethanol determination is due to an additional calibration step in the calculation (with reference to Appendix VII).

Another source of error is involved when a sample is being taken. The liquid travels along the tube and reacts before it reaches the syringe and is neutralized. As a result, analysed reactant concentrations are lower than they should be inside the test cell. Back calculations showed that the differences were so small that they would not influence the concentration profiles (with reference to Appendix VIII). The concentration profiles, if corrected for reaction in the sampling tubes, would be higher in reactants and lower in products. The averaged mass transfer rates derived from the profiles would probably remain roughly the same; while the derived eddy diffusivities for the reactants would be slightly higher because of the less curved

concentration profiles. However, the increase in diffusivity would probably be insignificant.

4.2.3.2.5 Concentration Profiles

The final concentration profiles for individual components are derived from the original concentrations versus time curves for each needle inlet position and for each component. (Refer to Section 4.2.1.4: Method of Calculation.) Whenever possible, the concentration versus time curves are drawn closely through the data points. In some instances, a portion of the ethyl acetate concentration data are somewhat scattered due to the turbulent nature of the layer. Under such circumstances, average curves are drawn by eye instead. (Refer to Figure 17 and Figure XV.1 in Appendix XV.) Sometimes, particularly with the sampling needles whose inlet positions are situated below the reaction zone front, a limited number of samples are taken at the earlier stage of the experiment. Consequently, when drawing each of the sodium hydroxide concentration versus time curves for needle inlets beyond the reaction zone front, interpolation has to be employed between the origin and the first data point; thus bias may be introduced (refer to Figure 17).

The bias from the concentration versus time curves is directly transferred when drawing the concentration profiles. Finally, for runs with a higher speed of layer propagation and at longer contact times (refer to Figure XVII.2: Ethyl Acetate-0.4 N Sodium Hydroxide System, 75 minutes after

contact), a substantial amount of the products diffuses out of the reaction zone and far into the lower phase. Due to the limited amount of experimental data available, concentration profiles extending approximately 1.3 cm. beyond the interface have to be extrapolated. However, the bias incurred as a result of the extrapolation will not affect the overall picture of the profiles within the turbulent layer.

It must be realized that in each run, a certain volume of the liquid in the turbulent layer is drawn out for the purpose of sample analyses. The total amount of the liquid taken plus the volume of alcohol transferring back into the upper phase are roughly equal to the volume of ester transferred into the lower phase. Therefore the level of the interface stays virtually stationary. However, the concentration profiles thus determined are shrunk somewhat due to the slight decrease in the volume of the turbulent layer. Approximate estimations indicate that about 5 percent of the liquid in the turbulent layer is taken out as samples for each run in the ethyl acetate-sodium hydroxide system. A slightly smaller volume of the sample liquid (averaged about 3 percent) is taken out for each run in the methyl propionate-sodium hydroxide system. If the profiles were corrected for the sampling volume loss, the averaged mass transfer rates derived from the modified profiles would probably be slightly higher due to the slight displacement

of the reactant profiles towards the lower phase. (Refer to Section 4.2.1.4: Methods of Calculations.) For the same reason, the eddy diffusivities of the components are slightly varied. On the other hand, since the amount of the liquid sampled for each run is kept roughly the same, the corresponding experimental concentration profiles will be affected to a similar extent. Although the absolute values of the transfer rates and the eddy diffusivities may be slightly affected by the sample volume loss, yet the relative ratios of the values will likely remain roughly constant.

4.2.3.2.6 Initial Mixing During the Phase Contact

A small amount of the ester (although reproducible for each run) will be transferred into the aqueous phase during the contact of the two phases (refer to Section 4.2.3.3). The ester transferred in such a way will distribute quite uniformly in the lower phase and react with the caustic to form salt and alcohol. As a result, part of the salt and the alcohol measured by sampling in a run is contributed by the initial phase mixing. However, the correction to the product concentration profiles would be small (of the order of .001 N to .002 N). On the other hand, the concentration profiles of the reactants remain unaffected by the initial mixing.

4.2.3.3 Results of Physical Transfer Runs

4.2.3.3.1 n-Butanol-Water System

The interdiffusion of the n-butanol-water system has been studied carefully by many researchers(J4)(B8). The system was found to exhibit a normal diffusion pattern with no interfacial turbulence. This is the main reason for the choice of such a liquid system as a standard in order to evaluate the experimental techniques adopted for subsequent transfer runs.

4.2.3.3.1.1 Effect of the lower phase filling rates:

On examining Figure 13 as well as Table 4, it becomes evident that the initial filling rate of the water phase has a substantial effect on the concentration profiles developed later. As the filling rate decreases, the effect of the phase contact turbulence diminishes gradually and becomes constant when the flowrate is below 0.166 litres/minute. The best set of experimental filling rates was determined to be 0.042 litres/minute for the first four minutes, 0.166 litres/minute for the next five minutes and finally 0.187 litres/minute until the liquid-liquid interface just touched the tip of the point gauge.

Individual sets of concentration profiles of the five runs drawn at different time intervals (e.g. 60 minutes, 273 minutes, etc.) merge gradually at a distance further away from the interface. Profiles within the same set become quite close to each other at the region approximately 0.6-0.7 cm.

below the interface with the exception of the Run #1, 273 minutes-profile which eventually merges with the others of the same set at the region of 0.85 cm. below the interface. These findings lead to the beliefs that if the initial filling rates are below 0.32 litres/minute and 0.50 litres/minute respectively, regions which are 0.6 cm. and 0.85 cm. below the interface will not likely be affected by the initial phase contact turbulence.

4.2.3.3.1.2 Reproducibility between runs:

A comparison of the profiles from Runs #3, 4 and 5 in Figure 13 indicates that the experiments are quite reproducible. The areas under individual concentration profiles for Runs #3, 4 and 5 at 60 and 273 minutes respectively were integrated numerically using the 5-point Simpson's Rule. The results are shown in Table 6.

TABLE 6

INTEGRATED AREAS UNDER THE CONCENTRATION PROFILES IN FIGURE 13 IN THE n-BUTANOL-WATER SYSTEM

Run # / Contact Time	3	4	5
area under the conc. profile drawn at 60 mins. of contact time (mole-cm./litre)	.1757	.1752	.1907
area under the conc. profile drawn at 273 mins. of contact time (mole-cm./litre)	.3450	.3596	.3659

4.2.3.3.1.3 Comparison with theoretical concentration profiles:

The 273 minute and 546 minute profiles of Runs #3, 4 and 5 in Figure 13 were replotted in the form of dimensionless concentration profiles as shown in Figure 21. These plots are compared with the theoretical profiles calculated based on an averaged constant binary diffusion coefficient obtained from the literature[C4]. Deviations of the experimental concentration profiles from the theoretical ones are small. In general, the experimental profiles compare favourably with the theoretical profiles as is evidenced from the profiles of Run #4 and #5; while the profiles obtained from Run #3 are slightly lower than the theoretical profiles. The maximum deviation between the experimental and the theoretical profiles, (within the range of comparison) measured in terms of the actual distance in the cell, x, is .046 cm. (Refer to the profiles of Run #3: Figure 21) Furthermore, since the theoretical profiles were calculated with the concentration averaged, constant diffusion coefficient, the experimental concentration profiles should cross the theoretical ones as observed in the profiles of Run #5 as well as in the 546 minute profile in Run #3. Based on the above comparisons, it is felt that the sampling techniques employed for these experiments are reliable.

Alternatively, theoretical dimensionless concentration profiles were calculated numerically using a digital computer

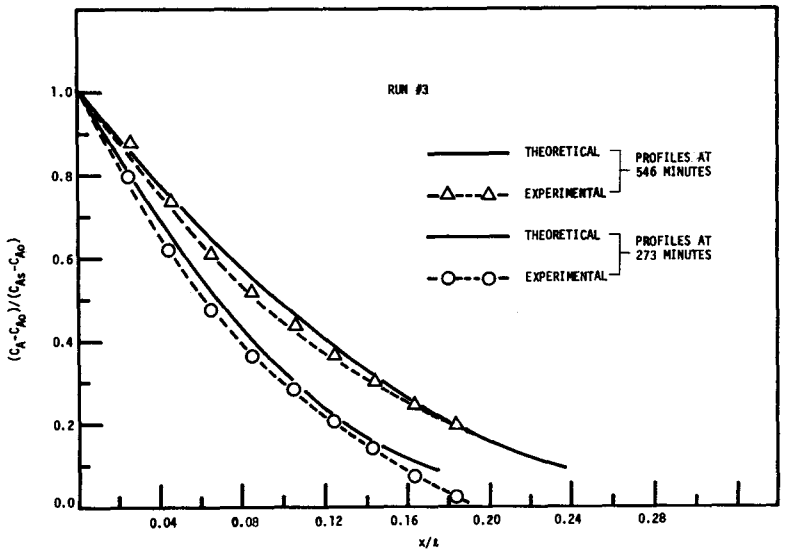

FIGURE 21
COMPARISON OF THEORETICAL AND EXPERIMENTAL
DIMENSIONLESS CONCENTRATION PROFILES
IN THE n-BUTANOL - WATER SYSTEM

C_A = CONCENTRATION OF THE UPPER PHASE IN THE AQUEOUS PHASE
C_{As} = CONCENTRATION OF THE UPPER PHASE AT THE INTERFACE
C_{Ao} = ORIGINAL UNIFORM CONCENTRATION OF THE UPPER PHASE IN THE AQUEOUS PHASE
x = DISTANCE FROM THE INTERFACE
ℓ = LENGTH OF THE TEST CELL

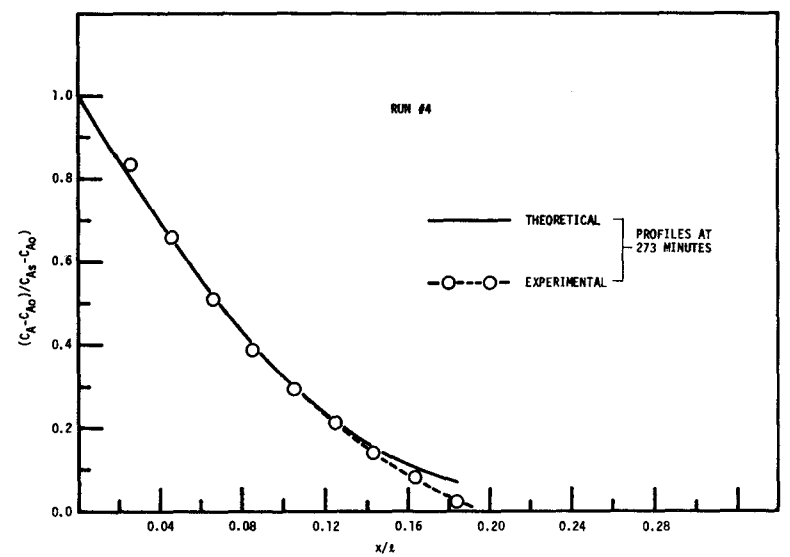

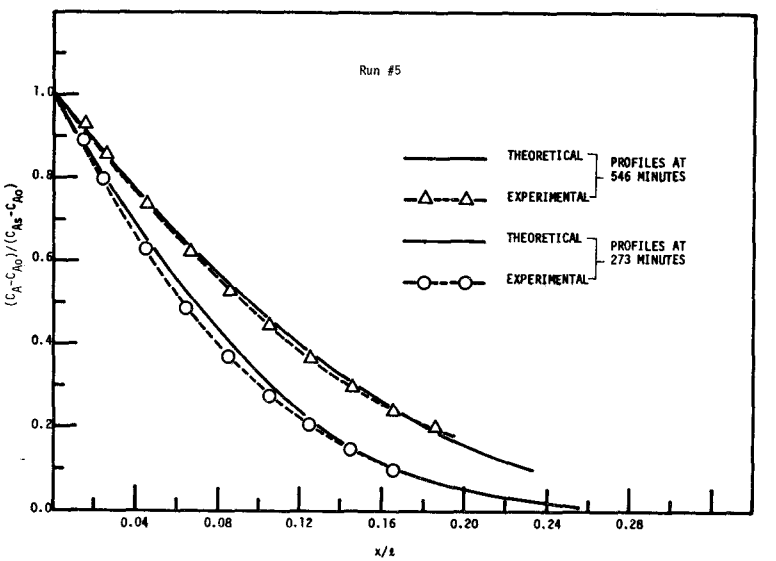

with an experimentally determined variable diffusion coefficient and also separately, with the averaged constant diffusion coefficient. These profiles were, again, compared with the experimental concentration profiles. Detailed descriptions of the calculations and the comparison of the profiles are shown in Appendix XIV.

In addition to some of the experimental errors mentioned previously (i.e. Section 4.2.3.2), there are two more types of error involved in calculating the dimensionless concentration profiles. Firstly, the bottom of the cell is not perfectly flat. Furthermore, the middle portion of the cell, where the sintered glass disc is situated, is about one to two mm. deeper than the rest of the cell. The cell length was determined from the average of six measurements from the locations traversed across the bottom of the cell. Secondly, the solubility of the n-butanol in water was taken directly from available literature data[J4]. These data were recorded with the system at equilibrium conditions. The experimental measurement of the solubility of the n-butanol in water obtained in this laboratory always yielded lower values.

4.2.3.3.2 Ethyl Acetate-Water System

4.2.3.3.2.1 Comparison of the experimental and the theoretical concentration profiles:

Since the best determined set of the lower phase filling rates from the n-butanol-water runs was used for this system,

a very small amount of ester was expected to transfer initially into the aqueous phase as a result of the phase contact turbulence. The concentration profile at 278 minutes of the ethyl acetate-water system (Figure 15) was replotted in the form of a dimensionless concentration profile as shown in Figure 22. This plot was compared with the corresponding theoretical one which was calculated from an averaged constant diffusion coefficient, experimentally determined (Figure 39: 4.4 - Part D). The experimental plot was found to cross the theoretical curve rather than to match it. However, the areas under the curves were roughly the same.

The flattening of the concentration profile is not unexpected. Part of the discrepancy is due to the assumption of constant averaged diffusion coefficient in calculating the theoretical profile. The rest of the discrepancy probably may be attributed to the minute amount of interfacial turbulence, though visibly insignificant, as a result of the presence (at or near the interface) of the alcohol and the acid which are released as products of the very slow hydrolysis reaction. The theoretical dimensionless concentration profile at 278 minutes was again calculated numerically with an experimentally determined variable diffusion coefficient (Figure 39). The calculated and the experimental profiles were compared as shown in Figure XIV.6, Appendix XIV.

FIGURE 22

COMPARISON OF THEORETICAL AND EXPERIMENTAL DIMENSIONLESS CONCENTRATION PROFILES (ETHYL ACETATE - WATER SYSTEM)

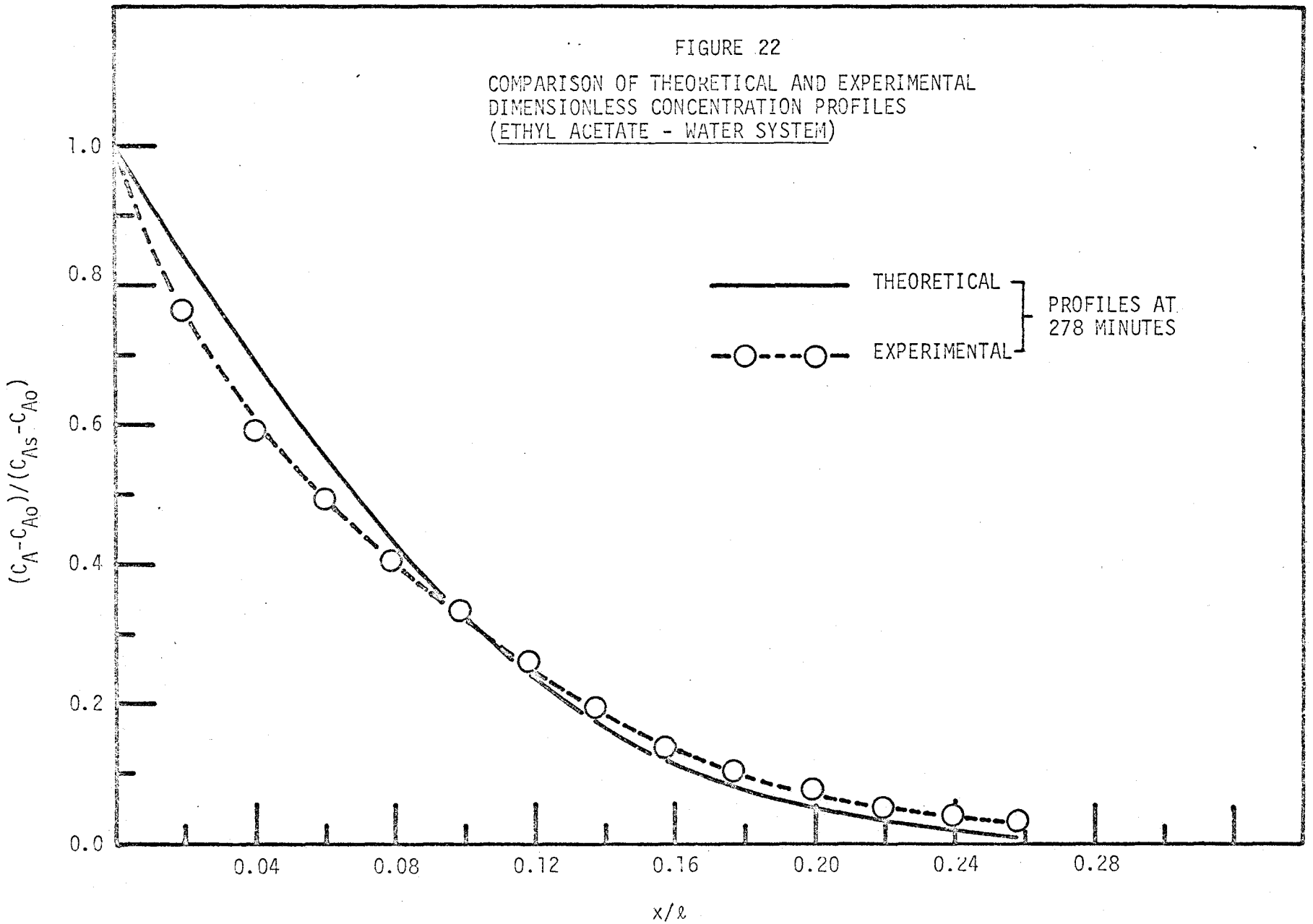

4.2.3.3.2.2 Comparison of the experimental and theoretical physical mass transfer coefficients:

Higbie's penetration model[Hll] predicts the rate of the molecular diffusion of a component into an infinite medium with the boundary conditions of the uniform concentration at t = 0 and a constant surface concentration for t > 0;

$$\frac{N}{A} = \text{instantaneous flux} = \sqrt{\frac{D}{\pi t}}\,(C_{A_i} - C_{A_\infty}) = k^*_{L(\text{inst.})}\, C_{A_i} \qquad (19)$$

The time averaged mass transfer coefficient is,

$$k^*_{L(\text{avg.})} = \left(\int_0^t \sqrt{\frac{D}{\pi t}}\, dt\right)/t = 2\sqrt{\frac{D}{\pi t}} \qquad (20)$$

The total amount of mass transfer up to time "t" will be,

$$\int_0^t \frac{N}{A}\, dt \quad \text{or} \quad 2\sqrt{\frac{D}{\pi t}}\,(t)(C_{A_i}) = 2\sqrt{\frac{Dt}{\pi}}\, C_{A_i} \qquad (21)$$

Assuming the constant diffusion coefficient of the ethyl acetate in water (the value of "D" is averaged over the solubility range of the ester; Figure 39) to be 0.8×10^{-5} $cm^2/sec.$, the theoretical instantaneous mass transfer rates, the averaged mass transfer rates and the total ester transferred at different contact times were calculated. The theoretical calculated values compared favourably with the experimental data as shown in Table 7.

TABLE 7

COMPARISON OF EXPERIMENTAL AND THEORETICAL MASS TRANSFER RATES
(ETHYL ACETATE - WATER SYSTEM)

Contact time (min)	Instantaneous mass transfer rates (moles/cm^2-sec) X 10^8		Average mass transfer rates (moles/cm^2-sec) X 10^8		Total amount of ester transferred across the interface 353 cm^2 (moles)	
	Experimental	Theoretical	Experimental	Theoretical	Experimental	Theoretical
25	4.71	3.50	6.90	7.00	.036	.037
50	2.15	2.48	5.07	4.95	.054	.052
75	1.77	2.02	3.97	4.04	.064	.064

4.2.3.3.3 Methyl Propionate-Water System

The experimental concentration profiles obtained for this system were rather unusual. At the beginning stage of the run, e.g. 25 minutes after the initial phase contact, the ester concentration was uniform throughout the lower phase with the exception of a narrow region at the interface where a slightly higher ester concentration was observed. On the contrary, at the later stage of the run, e.g. at 274 minutes, the ester concentration was found to be slightly higher at the bottom of the cell instead. Such a phenomenon may be explained by the fact that the propionate ester, transferred from the upper phase, dissolved in the water forming a solution whose density is comparable to that of water (Table 2). The turbulent liquid motion at the interface, generated perhaps by the methyl alcohol and the propionic acid from the hydrolysis reaction, is strong enough to cause streaks of the solution to sink far down towards the bottom of the cell because of the similar densities between the streaks and the surrounding aqueous medium.

4.2.3.4. Results of Reaction Transfer Runs

4.2.3.4.1 Ethyl Acetate-Sodium Hydroxide System (with reference to Figure 18, Appendix XVII and Appendix XII)

Two separate sets of experiments were performed on the ethyl acetate-sodium hydroxide system - the present set and the preliminary set (Appendix XII).

The two sets of experiments cannot be compared directly since their respective sodium hydroxide filling rates are different. The filling rate used for the preliminary set of runs is higher than that used for the current runs. Consequently, the ester transfer for the preliminary runs is, in general, relatively higher. Nevertheless, the shape of the corresponding concentration profiles obtained from the two sets of experiments are similar. They are, therefore, discussed together.

4.2.3.4.1.1 Concentration profiles of ethyl acetate:

In general, a rather normal diffusion concentration profile of the ethyl acetate was observed at the beginning of a run. At the later stage, the profile changed gradually. The overall ester concentration inside the turbulent layer increased with time, but particularly more so somewhere in the middle of the layer. As a result, a rather unusual kind of "hump shaped" profile was obtained as was evident from some of the profiles drawn at 50 minutes and 75 minutes respectively.

With experiments having a lower initial sodium hydroxide

concentration in the aqueous phase, the "hump shaped" profile appeared at the earlier stage of the run. On the contrary, with runs of a higher caustic concentration, the "hump shaped" profile appeared progressively later. For the 1.4 N sodium hydroxide run, the "hump shaped" profile did not occur even at 50 minutes after the phase contact.

When comparing the sets of three ester profiles drawn at different contact times for each run, it becomes obvious that for lower sodium hydroxide concentration runs, there is a drastic change in shape between the 25 minute and the 50 minute profiles. After 50 minutes, the profile has almost developed to its final form (i.e. hump shaped), and there is little change in shape observed in the next 25 minutes. While for the higher sodium hydroxide concentration runs, the change in shape is rather gradual, although there is still a bigger change between the 25 minute and 50 minute profiles than between the 50 minute to 75 minute profiles.

The phase contact time at which the "hump shaped" profile appears is generally related to the initial caustic concentration of the run in the opposite way to the speed of the turbulent layer propagation (i.e. the "hump shaped" profile appears at shorter contact time with the run having a higher speed of turbulent layer propagation).

4.2.3.4.1.2 Concentration profiles of sodium hydroxide:

A close examination of the sodium hydroxide concentration profiles reveals that the region immediately below the interface

is depleted of the sodium hydroxide at a rather early stage of the run, with the exception of the 1.4 N sodium hydroxide runs, in which the caustic concentration is appreciable near the interface even at 25 minutes after the initial phase contact.

The region of the caustic depletion expands towards the bottom of the test cell during the course of the run. The speed of the extension of the zero caustic concentration region is again related to the input caustic concentration levels in the same way as the speed of turbulent layer propagation is related to the caustic concentrations. In the meantime, the shape of the caustic profile also changes. A point of inflection on the profile is developed in the vicinity of the lower zone front.

4.2.3.4.1.3 Concentration profiles of ethanol:

The amount of the ethanol retained in the lower phase is relatively low as compared to the total amount of the alcohol produced by the reaction. The alcohol is soluble in the ethyl acetate phase. The combined effects of the diffusivity and the buoyancy flow of the ethanol coupled with the ever present interfacial turbulence result in a sizable transfer of the alcohol to the upper phase. Such a transfer situation results in the negative slope of the ethanol profile at the interface.

A visual comparison of the profiles indicates that within each experiment, both the overall concentration as well as the

total amount of the ethanol in the lower phase increases with time. Among the experiments, the "time averaged" ethanol concentration (which is the average of the ethanol concentration derived from the three profiles at 25, 50 and 75 minutes drawn for each experiment) increases with increasing initial sodium hydroxide concentration.

Moreover, the areas under the individual ethanol profiles were integrated and the total amount of the ethanol in the lower phase was separately calculated for each profile. It was found that about 38% to 77% of the ethanol formed, remained in the lower phase. Within each experiment, the percentage of the alcohol retention also increased with time, which means that a higher percentage of the alcohol formed was transferred to the upper phase at the early stage of the run. This is rather expected, since, at the beginning of the run, the turbulent layer is thin and the influence of interfacial turbulence is strong. In the course of time, the layer becomes thicker and the alcohol released as a reaction product has to travel a longer path before it reaches the interface. The longer travelling path enhances the possibility of the alcohol mixing with the liquid inside the turbulent layer and is thus diluted before reaching the interface.

It should be noted that the set of ethanol concentration profiles in Experiment No. 1 (viz. Ethyl acetate-0.2 N sodium hydroxide) is not included in the above discussion. Being

the first in the set of experiments as well as the lack of experience, the measurement of the alcohol concentration in this particular run is not as reliable as with the other runs. The general shape of the set of the alcohol profiles, however, is probably representative.

4.2.3.4.1.4 Concentration profiles of sodium acetate:

The sodium acetate cannot diffuse upward because of its extremely low solubility in the ester phase. Therefore, all the salt produced remains in the aqueous phase. This is illustrated by the relatively higher overall concentration of the salt than the ethanol as well as the horizontal salt profile at the interface.

A visual comparison of the profiles indicates that, among the experiments, the "time averaged" sodium acetate concentration increases with increasing initial sodium hydroxide concentration. Within each experiment and for runs with low initial sodium hydroxide concentrations, the salt concentration remains at a more or less constant level despite the propagation of the turbulent layer with time. This is probably because of the fact that with low sodium hydroxide concentration runs, the turbulent layer itself propagates at a speed faster than the salt can diffuse out of the layer and down into the lower bulk phase. Consequently, most of the salt thus produced by the reaction remains within the layer. On the other hand, with the high initial sodium hydroxide concentration runs, the speed of layer propagation

is lower. Coupled with the fact that a higher salt concentration is produced, the tendency of salt diffusing out of the layer and further down into the lower bulk phase is accentuated. The outward diffusion of salt causes a slight decrease in the salt concentration inside the layer with time. This is quite clearly demonstrated in the salt profiles of 1.0 N sodium hydroxide and 1.4 N sodium hydroxide runs. (Figure 18 and Figure XVII.4.)

The "time averaged" constant salt concentration inside the layer ranged from 80% to 86% of the initial sodium hydroxide concentration used. In general, it is logical to think that the curve of the ratio of salt to caustic concentration within the layer vs. the initial sodium hydroxide concentration should follow the same trend as the curve of the speed of the turbulent layer propagation vs. the initial sodium hydroxide concentration (viz. a higher speed of layer propagation should have a higher salt to caustic ratio). Such a case is actually observed with the salt profiles of Runs Nos. 1 to 5 at 75 minutes (85% at 0.4 N sodium hydroxide to 82% at 1.4 N sodium hydroxide as well as 80% at the 0.2 N sodium hydroxide run).

4.2.3.4.2 Methyl Propionate-Sodium Hydroxide System

One of the main reasons for choosing the methyl propionate-sodium hydroxide as the second system to the ethyl acetate-sodium hydroxide is because of their close similarity in physical properties; some of which are tabulated in Table 1.

Since the molecular weight as well as the chemical formula* of the two esters are exactly the same, their molecular sizes and the chemical properties may, generally, be expected to be similar.

Visual observations showed that the turbulent layer developed in this system was thinner and less turbulent. The streaks observed with the methyl propionate-water system were absent, at least visually, from the present reaction system. In general, the shape of all the concentration profiles of this system are similar to the corresponding profiles with the ethyl acetate-sodium hydroxide system and will not be repeatedly discussed. Nevertheless, there are some excpetions and extra points which are discussed in the following section.

4.2.3.4.2.1 Concentration profiles of methyl propionate:

The concentration of the methyl propionate in the aqueous phase is comparatively much lower than the corresponding ethyl acetate concentration in the ethyl acetate-sodium hydroxide system. The "hump shaped" profile does not develop until much later (longer than 50 minutes after phase contact). In Run No. 7 (1.0 N sodium hydroxide), the "hump shaped" profile does not appear even at 75 minutes after the initial phase contact.

4.2.3.4.2.2 Concentration profiles of sodium hydroxide:

The region of complete caustic depletion expands more slowly towards the bottom of the cell in this system as compared to the ethyl acetate-sodium hydroxide system.

*Same chemical formula means same number of C, H and O atoms per molecule between the two esters.

With the 1.0 N sodium hydroxide run, a substantial amount of sodium hydroxide is still detected in the region near the interface even at 75 minutes after phase contact.

4.2.3.4.2.3 Concentration profiles of methanol:

Like the ethyl acetate-sodium hydroxide system, the methanol is also miscible in the ester phase. Ranging from 58.2% to 79.6% of the methanol produced remained in the turbulent layer of these runs. A higher methanol retention percentage was found for runs with lower initial sodium hydroxide concentrations. This is probably mainly because of the fact that the turbulent layer propagates faster in the lower sodium hydroxide concentration runs.

Also, a higher percentage of methanol retention in the aqueous phase and higher methanol concentration in the turbulent layer than the corresponding ethanol in the ethyl acetate-sodium hydroxide system was observed. The same conclusion could also be deduced qualitatively by observing the less distinguishable negative slopes of the methanol profiles at the interface.

There are many possible explanations for the relatively higher methanol retention in the turbulent layer. The degree of the layer turbulence as well as the layer thickness in the methyl propionate-caustic system were observed to be comparatively smaller than that in the ethyl acetate-caustic system. Moreover, the effect of methanol on the interfacial tension changes may be less. The distribution

coefficient of methanol in the methyl propionate-aqueous sodium hydroxide system under reaction conditions may be less than that of ethanol in the ethyl acetate-aqueous sodium hydroxide systems. The salt effects of sodium propionate (apart from the decrease in ester solubility in the aqueous phase) may be more pronounced than the corresponding sodium acetate. All these speculative factors are inter-dependent and should be investigated by further experimental work.

4.2.3.4.2.4 Concentration profiles of sodium propionate:

A slightly lower salt concentration to initial sodium hydroxide concentration was obtained with the 0.4 N and 0.6 N sodium hydroxide runs (75% and 79% respectively) as compared to the corresponding runs in the ethyl acetate-sodium hydroxide system (86% and 84% respectively). The reason is because of the slower speed of the turbulent layer propagation. More salt can diffuse out of the layer and further down into the lower bulk phase. With the 1.0 N sodium hydroxide run, the caustic concentration within the region adjacent to the interface did not drop down to zero even at 75 minutes after the phase contact. Consequently, no portion of the constant salt profile was obtained within the layer for this run.

4.2.3.4.3 Induction Based on the Experimental Concentration Profiles

Summing up the aforementioned discussions on the experimental profiles of both the ethyl acetate and the methyl propionate-caustic systems, the actual interface mass

transfer situation for a run, in general, is speculated as the following:

At the beginning of the run, molecular diffusion of ester into the aqueous phase occurs. Both the salt and alcohol are produced as the ester is saponified by the caustic. The alcohol concentration at the interface is probably not uniformly distributed. As a result, Marangoni type roll cells are created due to the local interfacial tension gradients, and interfacial turbulence is thus induced. The mass transfer rate, at this point, is relatively rapid for both the ester downward and the alcohol upward. The reaction zone front propagates downward at a moderate speed.

As time goes on, the reaction zone front moves further downward and the turbulent layer gradually takes shape. The region of complete caustic depletion also starts to be established. The reaction zone proper starts to move away from the interface. At this time, the shape of the profiles is still normal and as expected.

In course of time, the reaction zone propagates more slowly while the mass transfer from the upper phase becomes less. The reaction inside the zone may be uniform macroscopically but not microscopically across a horizontal cross-section of the zone. In other words, as an example, pockets of reaction product (rather than well mixed) may be uniformly distributed across the horizontal cross-section of the reaction

zone front. Pockets of alcohol ascend to the interface due to buoyancy force and cause turbulence. At the same time, a certain quantity of heat is released by the reaction. While most of the heat released remains within the reaction zone and causes a rise in temperature, some of the heat is transferred to the interface by turbulence and especially by pockets of rising alcohol. The uneven temperature gradient at the interface caused by the heat transfer may also help to intensify the interfacial turbulence.

The interfacial turbulence helps to sweep down the ester from the interface. This sweeping motion, though continuous, is probably slow. The abnormal "hump shaped" ester profile gradually takes shape. At this stage, two distinct regions are established between the liquid interface and the lower reaction zone front as sketched in Figure 23. In zone "A" the ester is essentially transferred across the interface downwards in substantial amounts as a result of the combined effects of molecular diffusion and interfacial turbulence. Concentration of sodium hydroxide in this zone is very low (in the order of 10^{-3} N or less) as observed previously in the colour indicator experiments. (Refer to Section 4.1.1.) The salt concentration profile in zone "A" is flat and rather constant because of the turbulent mixing and there is negligible salt transfer into the ester phase. On the other hand, the shape of the alcohol concentration profile in zone "A" is somewhat dependent on the zone

FIGURE 23

REPLOT OF THE CONCENTRATION PROFILES
(ETHYL ACETATE - 0.6 N NaOH; 50 MINUTES
AFTER INITIAL PHASE CONTACT)

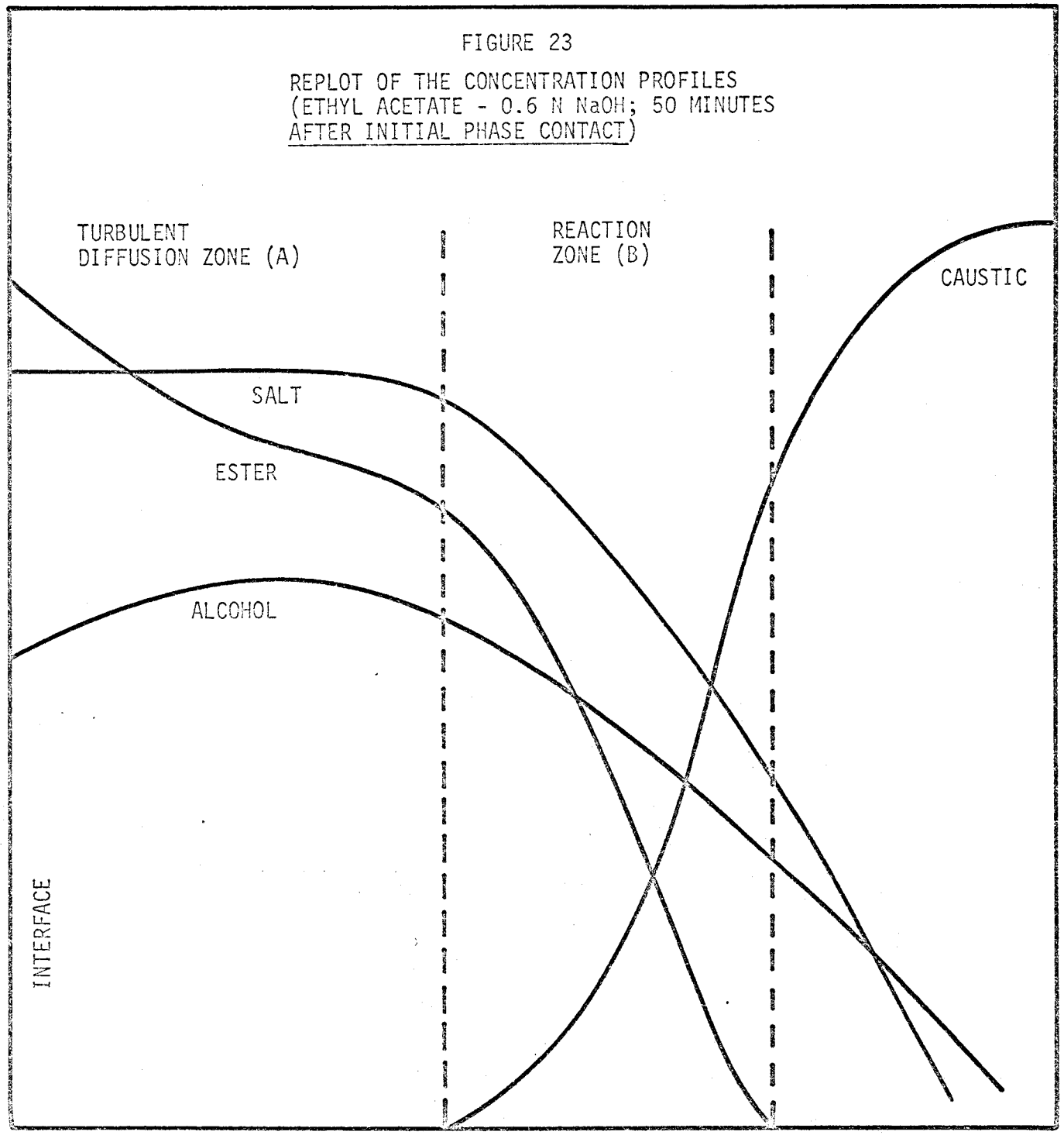

turbulence as well as the concentration level. In any case, a negative slope is observed on the profile indicating part of the alcohol has transferred into the upper phase.

Zone "B" is the reaction zone in which the effect of interfacial turbulence is presumably less significant. A normal pattern of mass transfer with chemical reaction prevails. Diffusion of ester into this zone from zone "A" is comparatively slower than the ester transferred from the interface to zone "A". Consequently, there is a build-up of ester in zone "A", causing the ester concentration profile to be abnormal. Sodium hydroxide starts from negligible concentration near the boundary to zone "A" and rises across the zone to a substantial percentage of the original bulk concentration. It is believed that at the lower reaction zone front, the sodium hydroxide concentration profile may exhibit a point of inflection. At this point, the transfer of caustic into zone "B" is higher than the transfer of sodium hydroxide to the zone front from the bulk lower phase. Therefore, the reaction zone moves downwards. The point of inflection on caustic profile at the zone front can actually be observed in some of the runs. While with the others, the existence of the inflection point is uncertain because of insufficient amount of experimental data. (Refer to Figures 18 and 19 and also Appendix XVII.) Both the alcohol and the salt profiles decrease across zone "B". The salt profile starts to decrease in the region at the

boundary to zone "A", while the alcohol profile usually passes through a maximum in the region in zone "A" slightly preceding the boundary between zones "A" and "B". No distinct discontinuity of alcohol profile is detected when crossing the boundary between the two zones. On the lower side of zone "B", both the salt and the alcohol profiles extend beyond the reaction zone front as a result of the diffusion of products into the bulk aqueous phase.

As time goes on, higher concentrations of the alcohol and the salt accumulate near the interface. Additional alcohol reaching the interface has a decreasing effect on the promotion of interfacial turbulence. At this time, the reaction zone front is moving quite slowly. Ester transfer into zone "B", although also quite slow, is still comparatively higher than the diffusion of sodium hydroxide into the reaction zone. Therefore, the thickness of the turbulent layer seems to be apparently stationary with respect to time, the concentration profiles inside are changing particularly inside the reaction zone proper, zone "B", where the ester concentration profile increases and the caustic profile decreases. The result is a reduction in the thickness of the reaction zone "B".

All the concentration profiles show abrupt gradient changes within the narrow region in the vicinity of the reaction zone front. It is therefore understandable that the edge of the turbulent layer can be so conspicuously

visible.

Eventually, the turbulent layer becomes thick enough so that localized, highly concentrated pockets of alcohol or hot fluid formed inside the reaction zone can usually disperse and mix with the rest of the liquid in the layer and seldom directly ascend to the interface. Thus the interfacial tension gradients begin to ease off. The ester transfer across the interface decreases accordingly, partly because of the diminishing interfacial turbulence and partly because of increasing ester concentration in zone "A". Normal diffusion gradually takes place. The spectacular turbulent layer phenomenon slowly ceases to exist and the lower zone front becomes diffused.

Moiré pattern photographs of the turbulent layer also indicated clearly the existence of the two zones for some ester-caustic systems. A typical example is shown in Figure 5.

4.2.3.4.4 Further Information Derived from the Experimental Concentration Profiles

It should be realized that since the experimental concentration profiles are subjected to the types of error discussed previously (Sections 4.2.3.1 and 4.2.3.2), the derived information will also inherit the same errors plus whatever is produced in the process of derivation. It is suggested that the derived data in the following be considered as semi-quantitative.

4.2.3.4.4.1 Comparison of experimental equilibrium interfacial concentrations of the ester with those derived from the concentration profile:

As discussed in the previous sections (Sections 4.2.3.4.1, 4.2.3.4.2.1 and 4.2.3.4.3), the ester profiles (except for the methyl propionate-1.0 N sodium hydroxide run) have almost developed to their final forms after 50 minutes of contact time. Therefore, extrapolation of the ester profiles at longer contact times (e.g. 75 minutes) back to the interface may possibly give their respective experimental ester interfacial concentrations under the influence of the salt and the alcohol effects.

It should be realized, of course, that such extrapolations are not accurate. For some runs, the profiles at 75 minutes are, although approaching, still not yet at steady state. Furthermore, the portions of ester profiles adjacent to the interface may be steep and extrapolations of the profiles in this region with insufficient data may be highly inaccurate. Examination of the ester profiles in the ethyl acetate-water system (Figure 15) suggests that profiles drawn after 60 minutes of contact time may be "flat" enough for reasonable extrapolations.

Ester interfacial concentrations derived from 75 minute profiles are shown in Table 8. These values (ethyl acetate-sodium hydroxide system) are compared with the ester solubilities in the sodium chloride solutions as well as in the sodium acetate solutions at concentration levels

TABLE 8

COMPARISON OF EXPERIMENTAL AND EQUILIBRIUM INTERFACIAL CONCENTRATION OF ESTER

Ethyl Acetate-NaOH system	Extrapolated from 75 min. profiles	Literature data NaCl solution	Estimated data NaAc solution
0.2 N	0.700 moles/l.	0.76 moles/l.	0.757 moles/l.
0.4 N	0.690 moles/l.	0.69 moles/l.	0.687 moles/l.
0.6 N	0.580 moles/l.	0.63 moles/l.	0.626 moles/l.
1.0 N	0.485 moles/l.	0.53 moles/l.	0.530 moles/l.
1.4 N	0.425 moles/l.	0.45 moles/l.	0.451 moles/l.
Methyl Prop.-NaOH system			Estimated data NaPr solution
0.4 N	0.565 moles/l.		0.620 moles/l.
0.6 N	0.290 moles/l.		0.568 moles/l.
1.0 N	0.240 moles/l.		0.485 moles/l.

corresponding to that of the sodium hydroxide solutions. The ester solubility data in sodium chloride solutions are obtained from literature[S17] while the solubility data in sodium acetate solutions are obtained from the present (Figure XIII.1: Appendix XIII) and from the previous experiments[S8]. Study of the concentration profiles at 75 minutes indicates that the experimental values should tend to agree more with the ethyl acetate solubilities in sodium acetate solutions.

Available literature information[S17] indicates that the presence of alcohol at the interface should enhance the solubility of ester in the aqueous phase (approximately 10% increase in 1 N ethanol solution). Such an effect is perhaps small in the present systems so that it is not readily observed. Since the interfacial concentration of the ester is of secondary importance in this study, the effect of the alcohol on the enhancement of the ester solubility is not pursued further.

The interfacial turbulence, on the other hand, will also play a role in the distortion of the concentration profiles, causing the extrapolation of the profiles to be less accurate.

In the methyl propionate-sodium hydroxide system, with the exception of 0.4 N sodium hydroxide run, ester solubilities estimated by extrapolation of the profiles yield lower values than the equilibrium solubility data. This is probably

because of insufficient data for extrapolation in the runs of the higher caustic concentration.

4.2.3.4.4.2 Mass balance:

Similar to the treatment of the alcohol concentration data, the areas under individual salt profiles were integrated and thus the total amount of salt in the lower phase up to the distance covered by the profile was separately calculated. Thus, for each run, a mass balance can be set up on the sodium hydroxide consumed and the salt produced (provided all the salt stays in the lower phase).

The mass balances so calculated from the concentration profiles for the two ester-caustic systems are shown in Table 9.

In addition to the experiments testing the solubilities of the salt and the caustic in the ester phase as described in Section 4.2.3.1, one experiment was also performed at room temperature by mixing vigorously (shaking for 3 minutes) 400 ml. of ethyl acetate saturated with water and 400 ml. of 1 N sodium hydroxide solution in a separatory funnel. After settling, 225 ml. of the ester phase were evaporated to dryness. The amount of the residue was negligible. Similar results were obtained with the methyl propionate-sodium hydroxide system.

The discrepancy in mass balance (Table 9) therefore, cannot be attributed to the transfer of the salt or the caustic to the ester phase. It is mainly due to the inaccuracy in

TABLE 9

MASS BALANCE IN THE ESTER-CAUSTIC SYSTEMS
(AMOUNT OF THE SALT IN THE AQUEOUS PHASE/AMOUNT OF THE CAUSTIC REACTED)

Systems \ Time (minutes) — mass balance (%)	25	50	75
Ethyl acetate - 0.2 N NaOH	86.4	82.1	82.7
Ethyl acetate - 0.4 N NaOH	88.3	85.5	84.0
Ethyl acetate - 0.6 N NaOH	86.3	86.3	84.3
Ethyl acetate - 1.0 N NaOH	80.6	87.5	85.1
Ethyl acetate - 1.4 N NaOH	79.5	79.6	82.3
Methyl propionate - 0.4 N NaOH	75.0	78.2	83.5
Methyl propionate - 0.6 N NaOH	73.1	82.0	84.6
Methyl propionate - 1.0 N NaOH	79.5	82.7	81.3

the drawing of the caustic and the salt concentration profiles. In some higher sodium hydroxide concentration runs and particularly at longer contact times (e.g. Figure XVII.2), the salt concentration spreads out beyond the region of sampling (about 1.3 to 1.4 cm. from the interface). The portion of salt below the region of sampling, although usually quite small, can only be estimated roughly for the purpose of mass balance.

4.2.3.4.4.3 Derivation of eddy diffusion coefficients:

A careful study of the families of curves of turbulent layer thickness versus sodium hydroxide concentration in both the ethyl acetate-sodium hydroxide and the methyl propionate-sodium hydroxide systems (refer to Figure 6 and Reference (S8)) reveals that the reaction zone front propagation starts to slow down sharply after 25 minutes of initial contact of phases for some runs at lower caustic concentrations. For some higher caustic concentration runs, zone front propagation does not slow down until 50 minutes after phase contact. Furthermore, an examination of the families of curves of the ester presence in the turbulent layer versus contact time (Figure 28) as well as the pertinent concentration profile curves indicates that for some runs with low caustic concentration, the amount of ester present in the turbulent layer stays approximately constant at and after 50 minutes of phase contact. Also, for the same runs, the ester concentration profile for each run changes very little with time. While

for the other runs, the changes in both the ester concentration profile and the amount of ester present inside the layer are so slow that they may be considered to be practically constant. Under such conditions, a quasi-steady state mass transfer situation may be assumed to prevail within the turbulent layer. Equations (4a), (4b), (4c) and (4d) (Chapter 3: Theoretical Principles) may be then reduced to the following equations:

$$D_A \frac{d^2 C_A}{dx^2} = k C_A C_B \qquad (5a)$$

$$D_B \frac{d^2 C_B}{dx^2} = k C_A C_B \qquad (5b)$$

$$D_C \frac{d^2 C_C}{dx^2} = -k C_A C_B \qquad (5c)$$

$$D_D \frac{d^2 C_D}{dx^2} = -k C_A C_B \qquad (5d)$$

where, as before, C_A = ester

C_B = sodium hydroxide

C_C = alcohol

C_D = salt

Instead of solving the set of non-linear equations (5a), (5b), (5c) and (5d) by providing enough initial and boundary conditions to obtain the concentration profiles of the reactants and the products across the entire layer, the available experimental concentration profiles of all the components can conversely be simulated by means of an analog

computer employing the same mathematical model which involves the following assumptions:

I Turbulent layer is considered as a single zone whereby diffusion with chemical reaction prevails in the entire layer.

II Quasi-steady state mass transfer occurs inside the layer.

III The effect of interfacial turbulence on a concentration profile is expressed by combining the corresponding molecular diffusivity and the so-called eddy diffusivity. Alternatively speaking, it means that the enhancement in mass transfer (which, originally, is due to the interfacial turbulence) may be expressed in terms of an increase in diffusivity of the component in the aqueous phase.

IV The back diffusion of alcohol into the upper phase has no effects on the mass transfer of ester. The increase of the ester solubility in the aqueous phase due to the presence of alcohol is assumed negligible.

V Salt effects, other than that of decreasing the ester solubility in the aqueous phase, are neglected.

If the turbulent layer observed is mainly due to the mechanical mixing of the liquids, then the effective diffusion coefficients (which characterize the degree of the layer turbulence) for all the components involved should be quite high and roughly the same. Furthermore, the molecular diffusivities for the components are comparatively small in magnitude and range from 1.0 to 2.14 X 10^{-5} cm^2/second.

Therefore the eddy diffusivities, which are the sums of the corresponding effective and molecular diffusivities for the components in the layer should be, in general, insensitive to the small variation in molecular diffusivities and remain roughly the same.

With this pre-conceived idea in mind, the analog simulation is carried out. In the simulation, the initial conditions as well as the constants of equations (5a), (5b), (5c), and (5d) (i.e. ratios of reaction velocity to eddy diffusivity in this case) are individually adjusted to the values which will enable the simulated concentration profiles for each component to fit the experimental points as closely as possible. Simulation of the profiles is carried out from the liquid-liquid interface to as far as the reaction zone front. Any portion of the profiles below the front of the ester profile is beyond the scope of the present study. A detailed description of the procedure for the analog simulation study with a worked example is given in Appendix IX. Other sets of profiles were simulated in the same way.

Both a PACE TR-10 analog computer and an IBM 7040 digital computer with "MIMIC PROGRAMMING" were tested for their suitability in the simulation of profiles. It was found that both computers would serve the purpose well (Appendix XII). The digital computer simulation has the advantage of giving out more accurate results. This is particularly useful in evaluating the small initial values

such as the interfacial concentration of the sodium hydroxide which is usually of the order of 10^{-3} N or less. Moreover, with the master programs stored in the computer library, the "MIMIC PROGRAMMING" is straight-forward and easy to apply. With the large storage area, the digital computer can handle a more complicated mathematical problem. However, it suffers from the disadvantage of giving out results in a discrete form rather than in continuous curves; although with extra programming, results can be plotted out by the computer as well. One of the serious disadvantages in using the digital computer is its inaccessibility. About two to three batches are processed per normal working day in the McMaster Computing Centre. The exploratory nature of the simulation study calls for numerous trials of initial conditions and the adjustment of constants before a set of concentration profiles can be satisfactorily simulated. On the other hand, the TR-10 analog computer is readily available in the Department. Once the required input is fed in, the computer is capable of giving out immediate results in the form of continuous curves, although the results may be less accurate as compared to those given out by the digital computer. Because of the size of the computer, large problems are restricted. Almost every problem of simulation will have to be scaled due to the small overload limits of the electrical components inside the computer. In simulating a couple of odd profiles, the potentiometer units

in one computer were all tied up. Extra potentiometer units had to be hooked in (though without any difficulty) from another TR-10. Despite all the disadvantages mentioned, the TR-10 analog computer is preferred over the digital computer for the present study.

The output from the analog computer can be connected to a double-channelled oscilloscope with a change of integrator units modified for repetitive operations. The use of the double-channelled oscilloscope is valuable for the present simulation work since the two reactant profiles are visible simultaneously on the scope and their response to the continuous varying input can be evaluated immediately. This will greatly facilitate the operations and at the same time, minimize the time required for simulation. Unfortunately, due to the limited surface area available on the scope, the profiles on the scope cannot be accurately measured. As a result, the oscilloscope is used only for preliminary, qualitative simulation work. For quantitative evaluation runs, the output of the computer is connected to a Variplotter which, in turn, can draw the simulated profiles one at a time.

4.2.3.4.4.3.1 Simulation criteria:

Abnormal concentration profiles, particularly those of the esters', are developed at the later stage of a reaction run. These abnormalities have not been accounted for during the formulation of the mathematical model. Under such

circumstances, average concentration profiles have to be drawn through the experimental points.

Special attention should be given to the drawing of the ester profile. As discussed previously (Section 4.2.3.4.3 and also Figure 23), the turbulent layer observed at some time after the initial phase contact can be subdivided into two regions; the turbulent diffusion in zone "A" with little or no chemical reaction, and the reaction zone "B" with a relatively small influence of turbulence effects. Since the overall eddy diffusivity of each component is the prime interest in this simulation study, it is decided to be better, for each component, to simulate one average profile across the two sub-zones rather than simulating the two sections of the profile in separate sub-zones and then averaging the results. The concentration of the sodium hydroxide in zone "A" is so small that the amount of reaction is, generally, negligible. Therefore the slight variation in shape and magnitude of the ester profile in zone "A" has insignificant influence on the profiles of other components in the same zone.

Three criteria are to be followed whenever possible in simulating an average concentration profile of the ester. (Refer to Figure 24 and Figures IX.2 - IX.4 for example.)

I The interfacial concentration of the ester should not be higher than 0.85 moles/litre which is the solubility of the ester in water, and not lower than the experimentally

FIGURE 24

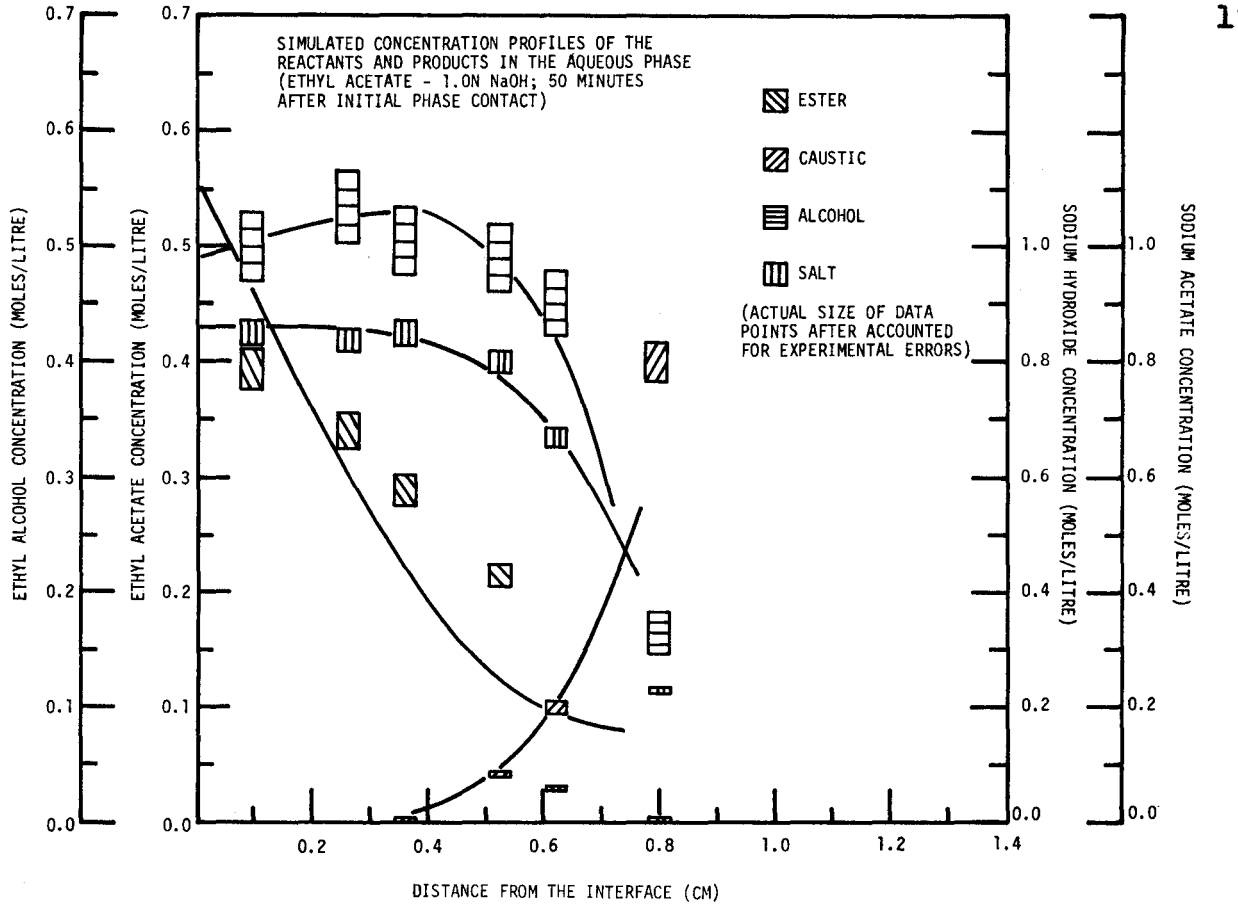
SIMULATED CONCENTRATION PROFILES OF THE REACTANTS AND PRODUCTS IN THE AQUEOUS PHASE (ETHYL ACETATE - 1.0N NaOH; 50 MINUTES AFTER INITIAL PHASE CONTACT)
ESTER
CAUSTIC
ALCOHOL
SALT
(ACTUAL SIZE OF DATA POINTS AFTER ACCOUNTED FOR EXPERIMENTAL ERRORS)
ETHYL ALCOHOL CONCENTRATION (MOLES/LITRE)
ETHYL ACETATE CONCENTRATION (MOLES/LITRE)
SODIUM HYDROXIDE CONCENTRATION (MOLES/LITRE)
SODIUM ACETATE CONCENTRATION (MOLES/LITRE)
DISTANCE FROM THE INTERFACE (CM)

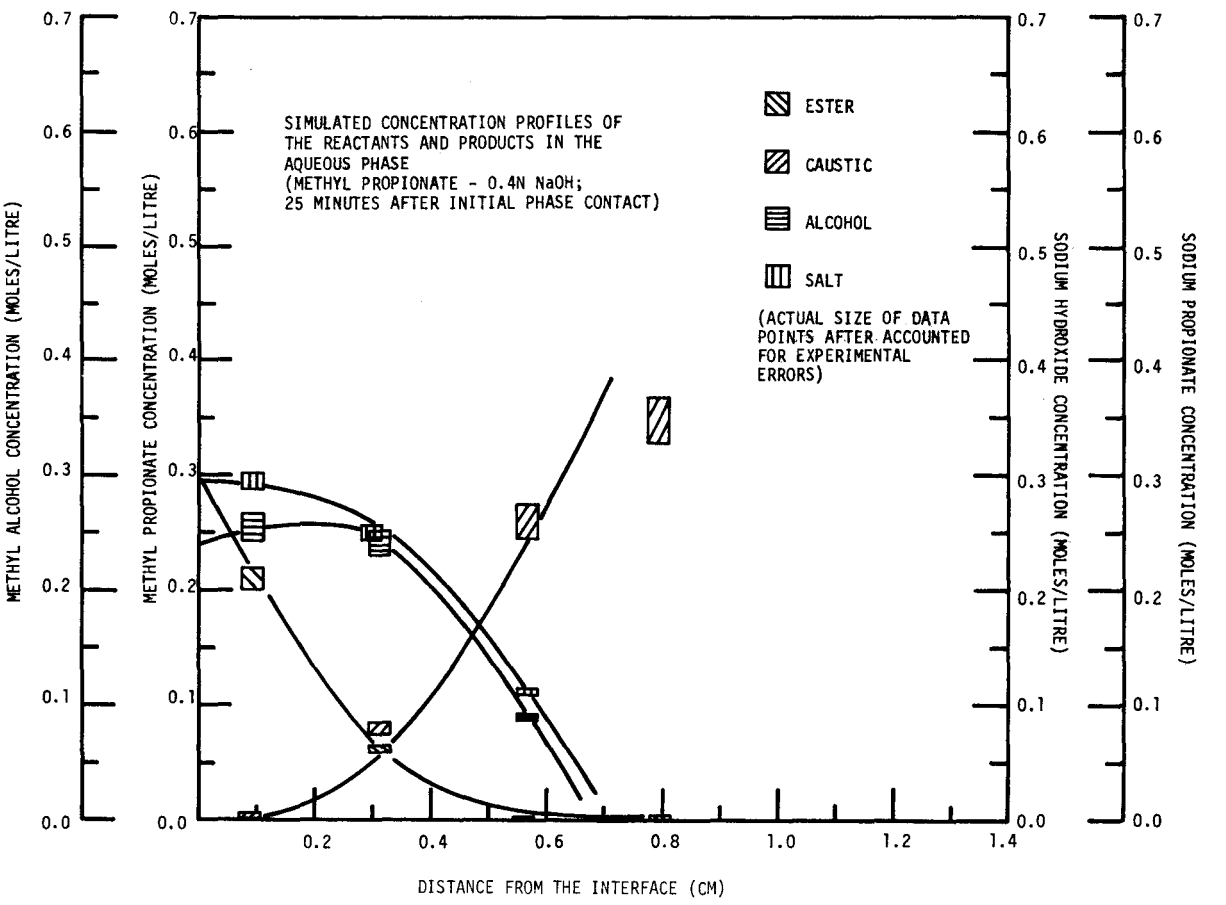
SIMULATED CONCENTRATION PROFILES OF THE REACTANTS AND PRODUCTS IN THE AQUEOUS PHASE (METHYL PROPIONATE - 0.4N NaOH; 25 MINUTES AFTER INITIAL PHASE CONTACT)
ESTER
CAUSTIC
ALCOHOL
SALT
(ACTUAL SIZE OF DATA POINTS AFTER ACCOUNTED FOR EXPERIMENTAL ERRORS)
METHYL ALCOHOL CONCENTRATION (MOLES/LITRE)
METHYL PROPIONATE CONCENTRATION (MOLES/LITRE)
SODIUM HYDROXIDE CONCENTRATION (MOLES/LITRE)
SODIUM PROPIONATE CONCENTRATION (MOLES/LITRE)
DISTANCE FROM THE INTERFACE (CM)

measured value. Successively lower interfacial concentrations should be used for higher initial sodium hydroxide concentration runs because of the salt effects.

II The total amount of the ester derived from the actual profile (by integration of the area under the profile) should be equal to that derived from the simulated average profile.

III The simulated (normal shape) profile should fit the experimental points as closely as possible.

On the other hand, the experimental sodium hydroxide concentration profile usually exhibits a point of inflection at or near the reaction zone front. Unfortunately, due to insufficient data points, a clear-cut inflection point cannot be accurately located; instead, a rather wide region of inflection is observed. The criterion for the simulation of the caustic profile in the region of inflection is to draw an average curve through this region as closely to the experimental points as possible. (Refer to Figure 24 and Figures IX.2 - IX.4.)

Since the differential equations describing the reactant concentration distribution are coupled with each other, the simulation of C_A and C_B must be carried out simultaneously. There are five variables which can be adjusted in simulating the reactant profiles. The variables are C_{A_o}, C_{B_o}, k/D_{EA}, k/D_{EB}, and $\left.\frac{dC_A}{dx}\right|_{x=0}$. C_{B_o} is usually very sensitive. A little change in value of C_{B_o} would affect

both the shape and the magnitude of the profile to a great extent. In order to be realistic, C_{B_o} is kept as low as possible except for simulating those profiles with significant experimentally measured C_{B_o} (e.g. methyl propionate-1.0 N sodium hydroxide: 25 minutes after phase contact). $^{k}/D_{EA}$ and $^{k}/D_{EB}$ would affect mainly the shape of the profiles respectively. However, all the variables must be adjusted simultaneously in the simulation. Most of the profiles tend to yield low C_{B_o} values and the values of $^{k}/D_{EA}$ and $^{k}/D_{EB}$ derived usually agree closely with each other for the same run.

Not much difficulty is encountered in simulating the product concentration profiles, once the reactant profiles are determined. In some higher sodium hydroxide concentration runs and at longer phase contact times, the product concentration profiles also exhibit similar regions of inflection near the reaction zone front. Under these situations, average curves, again, have to be drawn through those regions.

4.2.3.4.4.3.2 Results of the simulation studies:

Typical simulated concentration profiles are shown in Figure 24 and also in Figures IX.2 - IX.4 in Appendix IX. The eddy diffusion coefficients derived from the analog simulation are tabulated in Tables XVI.1 - XVI.8 (Appendix XVI). Over half of these diffusivity results have been cross-checked by MIMIC simulation on the digital computer.

On examining the results, it is found that except for a few sets of profiles (such as that of 0.2 N sodium hydroxide, 75 minutes after phase contact; 0.6 N sodium hydroxide run, 25 minutes after phase contact and 1.4 N sodium hydroxide, 75 minutes after phase contact) the values of eddy diffusion coefficients for the four components of the reaction system derived from the same set of profiles are fairly close to each other as intuitively expected. For this reason, the eddy diffusivities of the four components involved in a run and at a particular contact time are considered to be the same. The "mean eddy diffusivity" is taken as the averaged values of the four.

In general, although the data are somewhat scattered, some useful information can still be derived. For the ethyl acetate-sodium hydroxide system, the "mean eddy diffusivities" for various caustic concentration levels generally increase slightly with phase contact time (Figure 25). Alternatively, the "mean eddy diffusivities" at various phase contact times increase initially with caustic concentration, pass through a maximum at approximately 0.4 N, then decrease with further increasing caustic concentration (Figure 25). The "mean eddy diffusivities" range between 6 to 39 times higher than the molecular diffusivity of ethyl acetate in water. If, for each run at the particular caustic concentration level, the "mean eddy diffusivities" over the three contact times are averaged, then a curve may

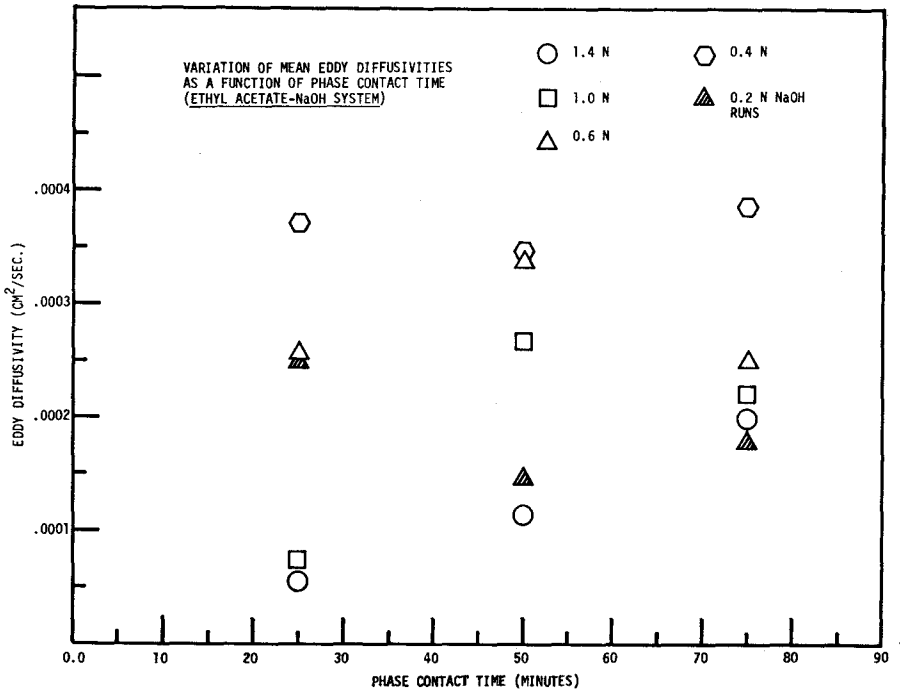
VARIATION OF MEAN EDDY DIFFUSIVITIES
AS A FUNCTION OF PHASE CONTACT TIME
(ETHYL ACETATE-NaOH SYSTEM)
1.4 N
1.0 N
0.6 N
0.4 N
0.2 N NaOH
RUNS
EDDY DIFFUSIVITY (CM²/SEC.)
.0004
.0003
.0002
.0001
0.0
10
20
30
40
50
60
70
80
90
PHASE CONTACT TIME (MINUTES)

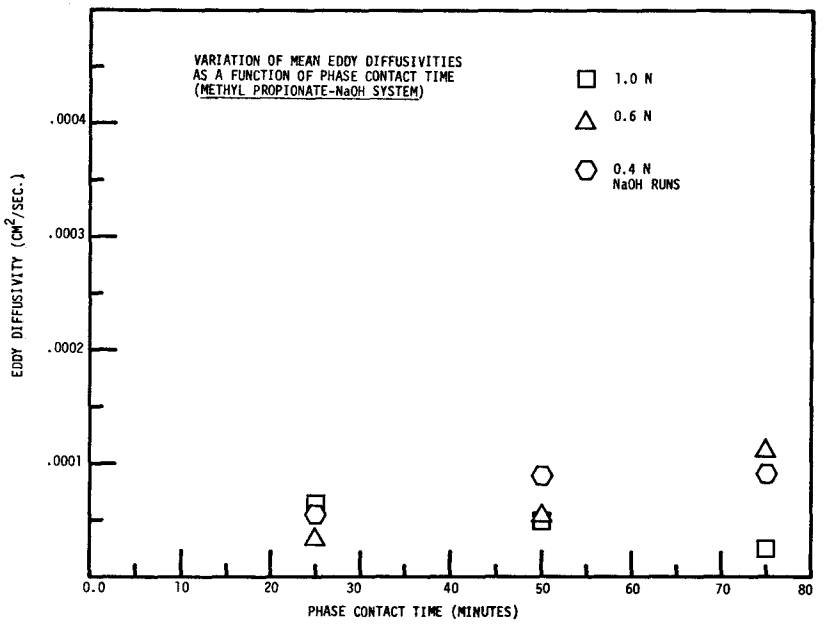
VARIATION OF MEAN EDDY DIFFUSIVITIES
AS A FUNCTION OF PHASE CONTACT TIME
(METHYL PROPIONATE-NaOH SYSTEM)
1.0 N
0.6 N
0.4 N
NaOH RUNS
EDDY DIFFUSIVITY (CM²/SEC.)
.0004
.0003
.0002
.0001
0.0
10
20
30
40
50
60
70
80
PHASE CONTACT TIME (MINUTES)

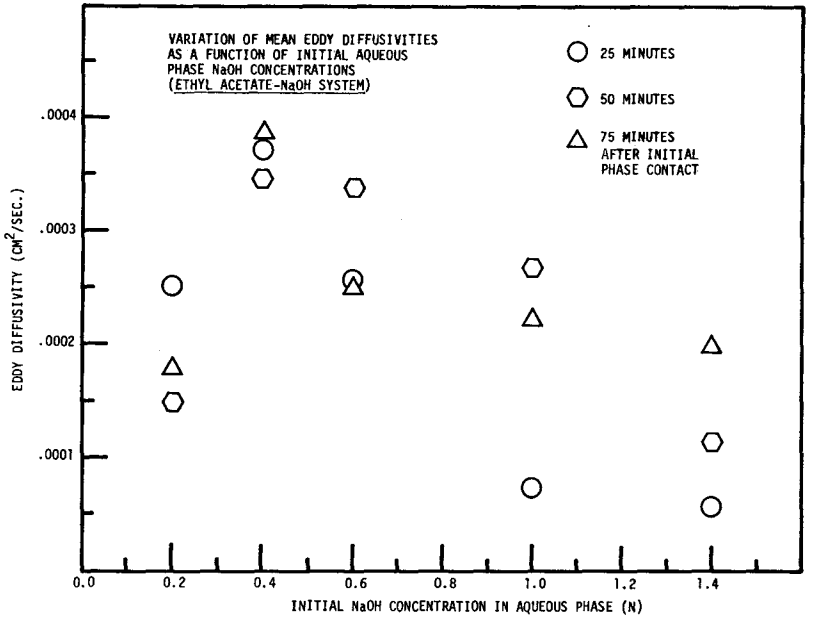
VARIATION OF MEAN EDDY DIFFUSIVITIES
AS A FUNCTION OF INITIAL AQUEOUS
PHASE NaOH CONCENTRATIONS
(ETHYL ACETATE-NaOH SYSTEM)
25 MINUTES
50 MINUTES
75 MINUTES
AFTER INITIAL
PHASE CONTACT
EDDY DIFFUSIVITY (CM²/SEC.)
.0004
.0003
.0002
.0001
0.0
0.2
0.4
0.6
0.8
1.0
1.2
1.4
INITIAL NaOH CONCENTRATION IN AQUEOUS PHASE (N)

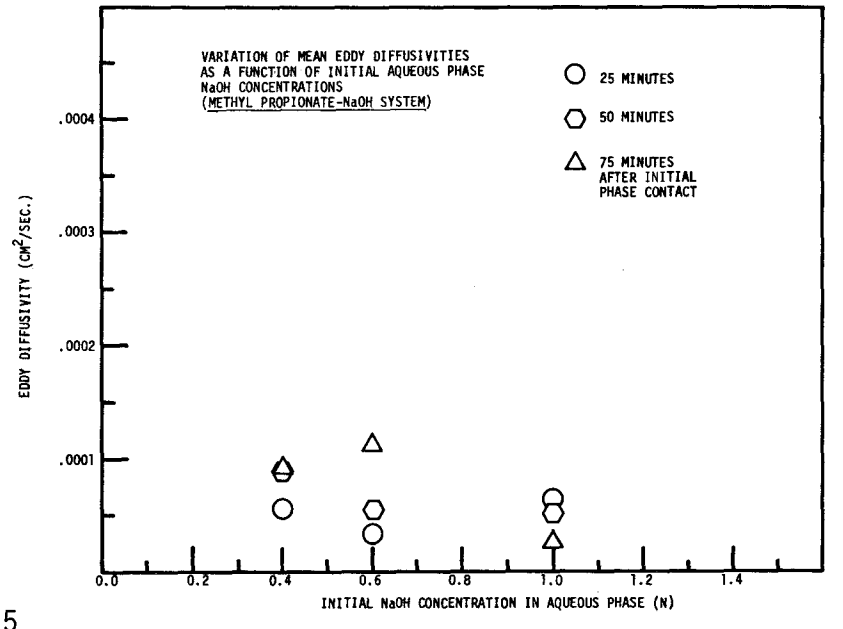
VARIATION OF MEAN EDDY DIFFUSIVITIES
AS A FUNCTION OF INITIAL AQUEOUS PHASE
NaOH CONCENTRATIONS
(METHYL PROPIONATE-NaOH SYSTEM)
25 MINUTES
50 MINUTES
75 MINUTES
AFTER INITIAL
PHASE CONTACT
EDDY DIFFUSIVITY (CM²/SEC.)
.0004
.0003
.0002
.0001
0.0
0.2
0.4
0.6
0.8
1.0
1.2
1.4
INITIAL NaOH CONCENTRATION IN AQUEOUS PHASE (N)

FIGURE 25

be plotted with the "time averaged mean eddy diffusivity" versus the caustic concentration level as shown in Figure 26. It is interesting to note that the shape of such a plot closely resembles the turbulent layer propagation rate curve (Figure 7).

For the system of methyl propionate-sodium hydroxide, the "mean eddy diffusivities" derived at various sodium hydroxide concentration levels also increase with phase contact times. However, the increase is insignificant as compared to the scattering of the data (Figure 25). The "mean eddy diffusivities" at different contact times slightly decrease with increasing sodium hydroxide concentration (Figure 25). The diffusivities range approximately between 2.5 to 11 times the molecular diffusivity of methyl propionate in water. Similar to the ethyl acetate-sodium hydroxide system, the "time averaged mean eddy diffusivity" was plotted against the caustic concentrations (Figure 26). It is realized, again, that the trend of such a plot is in agreement with that from the layer propagation experiments (Figure 7).

The above findings substantiate an important induction that the rate of turbulent layer growth is associated with the eddy diffusivities derived. Such an association between the two variables may be correlated as shown in Figure 27 for the ethyl acetate-caustic system and the methyl propionate-caustic system. The figure is almost self-explanatory. For each of the ethyl acetate-sodium hydroxide and the methyl

FIGURE 26

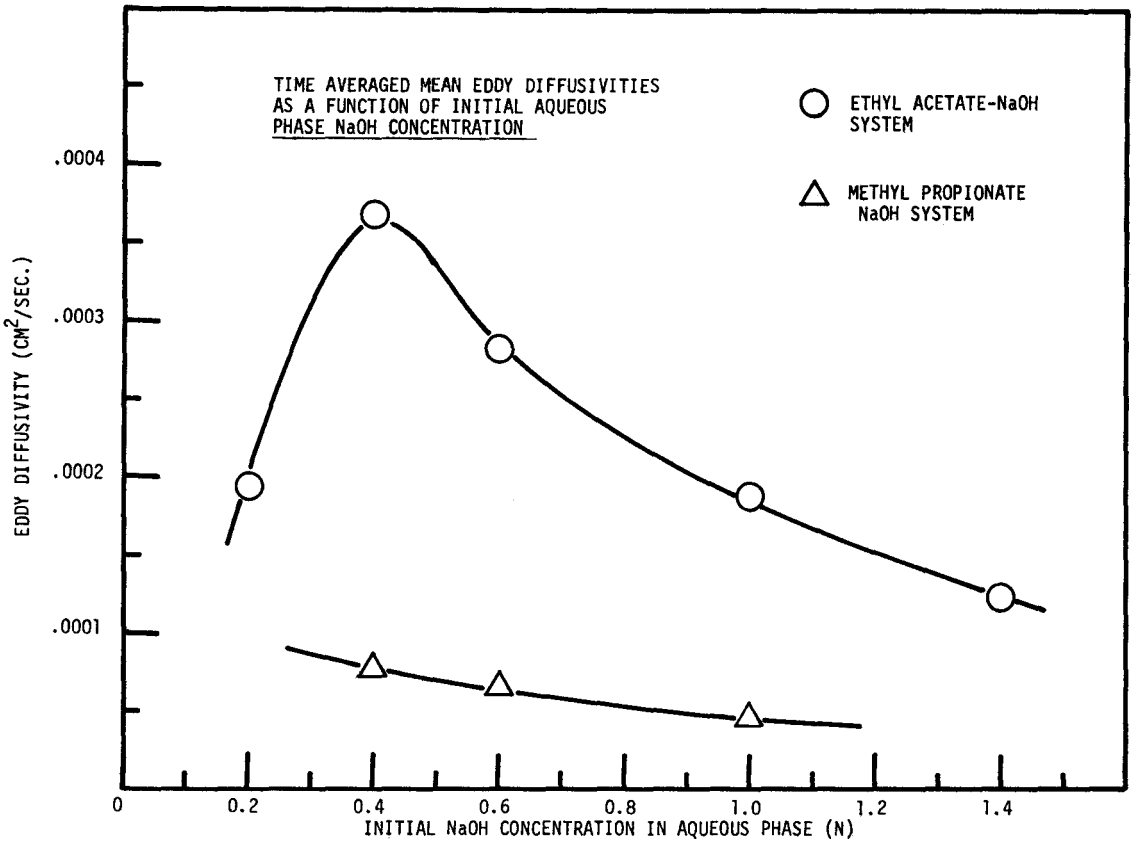

FIGURE 27

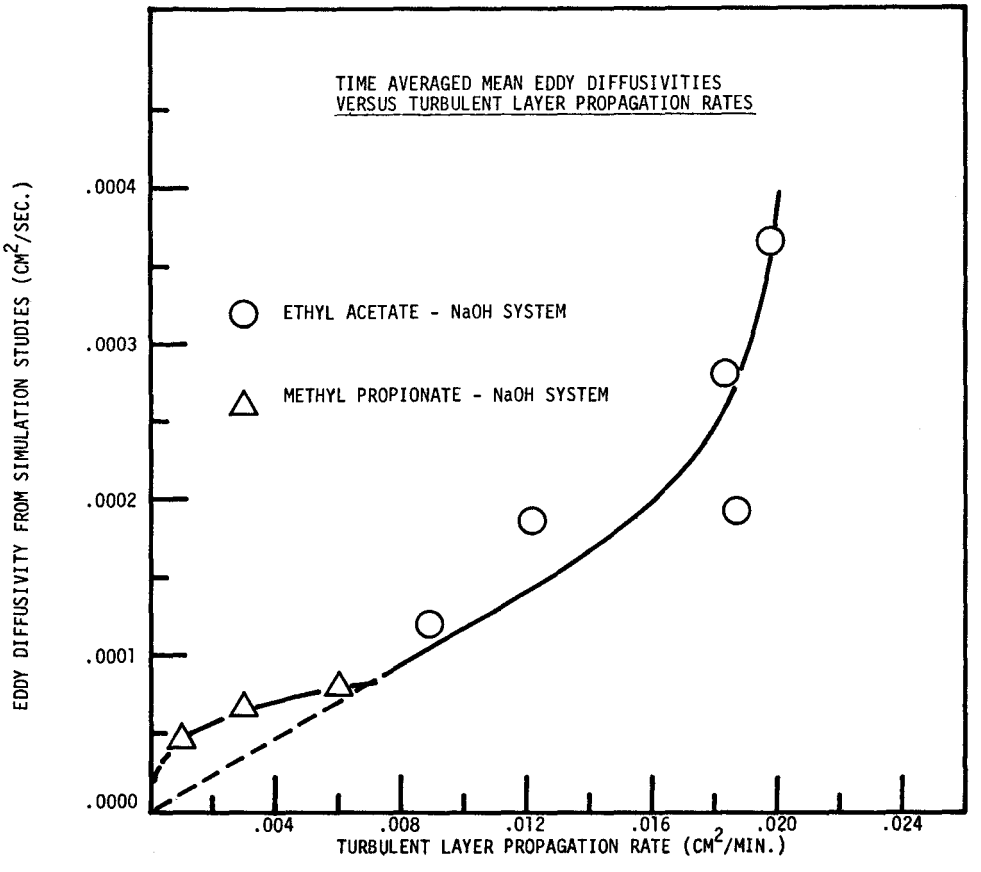

propionate-sodium hydroxide systems, the derived "time averaged mean eddy diffusivity" increases with the increasing speed of layer growth. The correlation relationships for both systems are non-linear and the correlation lines curve in different directions.

Due to the lack of knowledge and understanding concerning the nature of the turbulent systems, extrapolation of the correlation lines into regions beyond the experimental regime may be misleading as well as meaningless. Furthermore, the correlation lines are applicable only to their corresponding reaction systems under the same experimental conditions, although there is some evidence that the dimensions of the apparatus become irrelevant provided the cell has exceeded a certain critical size (Appendix V).

Despite all the restrictions discussed so far, the correlation lines are still obviously important. In a reaction system, provided the boundary concentrations are known, the correlation line relates the speed of layer growth, which is easy to measure, to the concentration profiles of the components across the layer which are both tedious and difficult to obtain. In order to obtain an approximate picture of the concentration distribution of the components within the turbulent layer in a slow reaction ester-caustic system, the following briefly outlined procedure is recommended.

I Measure the turbulent layer thickness at the particular

contact time when the profiles are desired. Simultaneously, take two liquid samples from the layer, one at, or very close to, each edge of the layer.

II Analyse the samples for component concentrations.

III Use the measured speed of layer growth to determine the "time averaged mean eddy diffusivity" from the correlation line (Figure 27).

IV Set up the analog circuit (Appendix IX).

V With the simulation criteria in mind, guess the values of C_{B_o} (probably very low, 10^{-3} N or less), C_{A_o} (should be higher than the experimental value) and $\frac{dC_A}{dx}\Big|_{x=0}$. Use $\frac{dC_B}{dx}\Big|_{x=0} = 0$ and the eddy diffusion coefficient to draw C_A and C_B profiles simultaneously. The profile of the sodium hydroxide at the reaction zone front should coincide with that experimentally determined. While the ester profile at the reaction zone front should generally be higher than the experimental value if a "hump shaped" profile is formed (refer to Figure 24 for example) and should read almost zero if no "hump shaped" profile is formed (refer to Figure 24 for example). The decision whether an ester profile should be "hump shaped" or not depends on previous experience with the liquid system.

VI Determine the boundary between zones "A" and "B" (refer to Section 4.2.3.4.3: Figure 23) as at the point where C_B rises abruptly.

VII Re-draw the "hump shaped" profile of C_A, whenever applicable, according to the simulation criteria. The re-drawn profile should have the experimentally determined ester concentrations at both ends. The total area under the re-drawn profile should be equal to that under the simulated profile. Also, at the same time, complete the drawing of C_B beyond the turbulent layer. The inflection point on the C_B profile, roughly at the zone front, may be re-constructed according to simulation experience.

VIII With the experimental value of C_{D_o} and $\left.\frac{dC_D}{dx}\right|_{x=0} = 0$, draw the profile of C_D. The area under the profile should represent the amount of salt which is equivalent to approximately 85% of the caustic disappeared. Profile at the reaction zone front should read the concentration of C_D as experimentally determined.

IX Guess the value of $\left.\frac{dC_C}{dx}\right|_{x=0}$. With the experimental value of C_{C_o}, draw the alcohol profile with the same eddy diffusivity used for the rest of the components. The concentration of C_C at the reaction zone front should coincide with the experimentally determined value.

The caustic, salt and alcohol profiles so obtained should represent fairly closely the actual concentration distribution of the components. On the other hand, the close representation of the ester profile may be achieved only through the previous knowledge of the shape of the profile in the liquid system.

4.2.3.4.4.4 Mass transfer of ester:

4.2.3.4.4.4.1 Ethyl acetate-sodium hydroxide system:

As seen in Figure 20, for a particular run, the total ester transfer increases as a function of time as normally expected; and among the runs, the total ester transfer increases as a function of the initial sodium hydroxide concentration. It is interesting to recall, at this point, that in the ethyl acetate-sodium hydroxide system, the speed of the turbulent layer propagation passes a maximum at approximately 0.4 N sodium hydroxide level (Figure 7). In other words, this qualitative comparison reveals the fact that the maximum speed of layer growth does not necessarily correspond to the maximum total ester transfer across the interface. Such a trend of inconsistency warrants the following further more detailed investigations.

Actually, the total ester transfer across the interface for a run at a particular time is calculated from two separate sources; the amount of ester present in the lower phase, as obtained by integrating the area under the ester profile and the amount of ester consumed by the reaction as obtained by integrating the area bound by the interface, the sodium hydroxide profile and the original sodium hydroxide concentration line. (Refer to Section 4.2.1.4.1.4 for detailed calculation methods.) If these two sources are calculated and plotted separately against time of contact with sodium hydroxide concentrations as a parameter, as shown

in Figure 28, it becomes clear that for a run and at a particular contact time, the thickness of the turbulent layer is related to the amount of ester present, but not to the total ester transferred across the liquid interface. Such an induction is not difficult to explain since in a fixed volume of the lower phase liquid, the amount of sodium hydroxide within increases with higher caustic concentration level runs. Therefore, in high caustic concentration runs (e.g. 1.0, 1.4 N), the turbulent layer thickness is relatively smaller as compared to the lower caustic concentration runs at the same contact time. Although the amount of ester present within the layer is less, the amount of ester consumed by the reaction is much higher. The increase of ester consumption by the reaction with higher caustic concentration runs (e.g. 1.0 N and 1.4 N sodium hydroxide) over-compensates the decrease of ester concentration present in the layer in the same runs. The resulting total ester transfer across the interface is therefore higher with the higher sodium hydroxide concentration runs.

4.2.3.4.4.4.2 Methyl propionate-sodium hydroxide system:

At a particular contact time, the amount of ester present in the lower phase is, again, qualitatively related to the thickness of the turbulent layer which decreases with increasing initial sodium hydroxide concentration levels (Figure 28). Similar to the ethyl acetate-sodium hydroxide runs, the amount of ester consumed by the sodium hydroxide

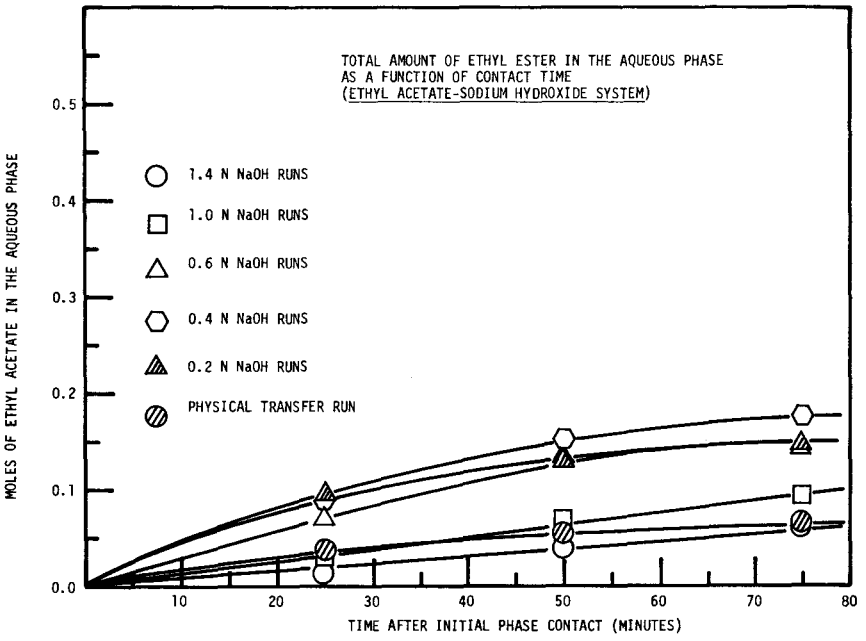
TOTAL AMOUNT OF ETHYL ESTER IN THE AQUEOUS PHASE
AS A FUNCTION OF CONTACT TIME
(ETHYL ACETATE-SODIUM HYDROXIDE SYSTEM)
1.4 N NaOH RUNS
1.0 N NaOH RUNS
0.6 N NaOH RUNS
0.4 N NaOH RUNS
0.2 N NaOH RUNS
PHYSICAL TRANSFER RUN
MOLES OF ETHYL ACETATE IN THE AQUEOUS PHASE
TIME AFTER INITIAL PHASE CONTACT (MINUTES)

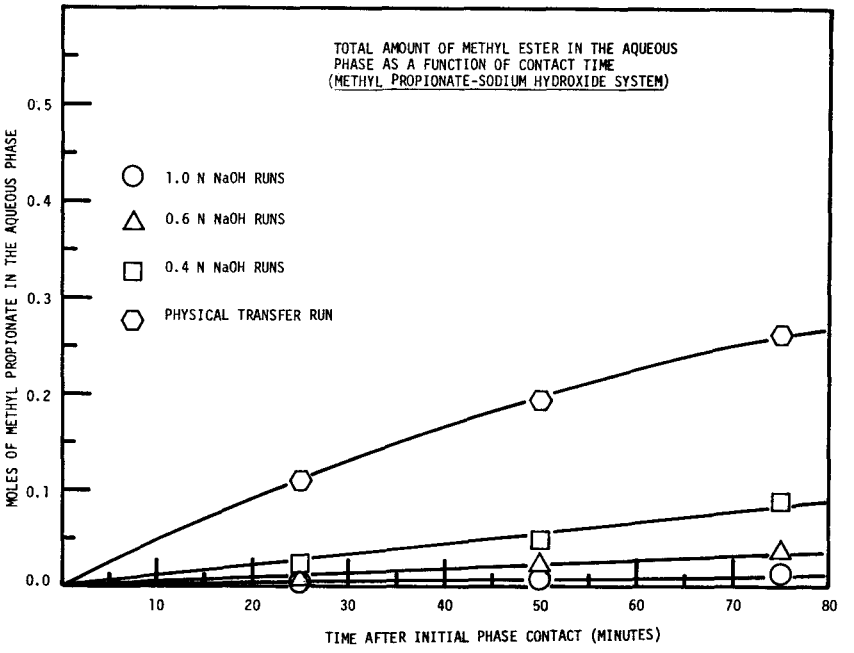
TOTAL AMOUNT OF METHYL ESTER IN THE AQUEOUS
PHASE AS A FUNCTION OF CONTACT TIME
(METHYL PROPIONATE-SODIUM HYDROXIDE SYSTEM)
1.0 N NaOH RUNS
0.6 N NaOH RUNS
0.4 N NaOH RUNS
PHYSICAL TRANSFER RUN
MOLES OF METHYL PROPIONATE IN THE AQUEOUS PHASE
TIME AFTER INITIAL PHASE CONTACT (MINUTES)

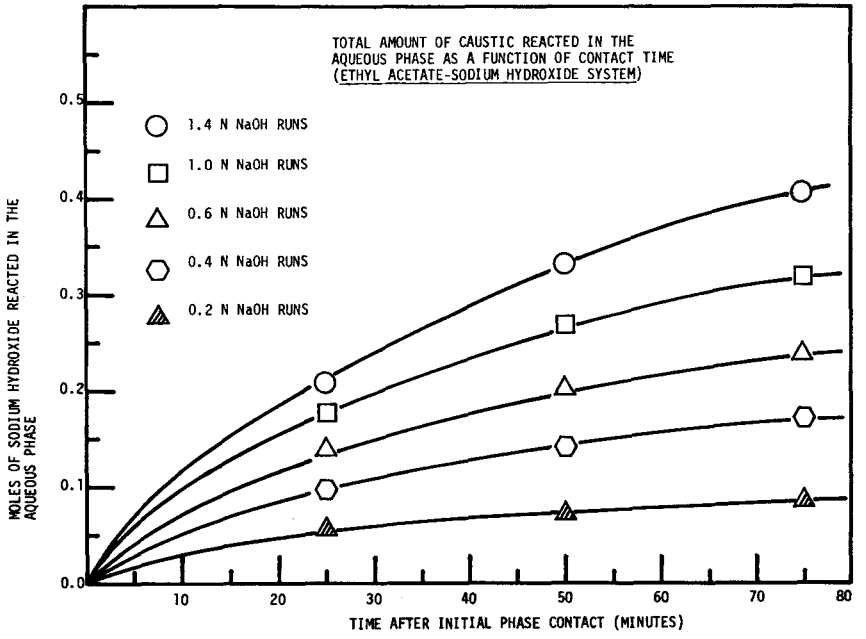
TOTAL AMOUNT OF CAUSTIC REACTED IN THE
AQUEOUS PHASE AS A FUNCTION OF CONTACT TIME
(ETHYL ACETATE-SODIUM HYDROXIDE SYSTEM)
1.4 N NaOH RUNS
1.0 N NaOH RUNS
0.6 N NaOH RUNS
0.4 N NaOH RUNS
0.2 N NaOH RUNS
MOLES OF SODIUM HYDROXIDE REACTED IN THE AQUEOUS PHASE
TIME AFTER INITIAL PHASE CONTACT (MINUTES)

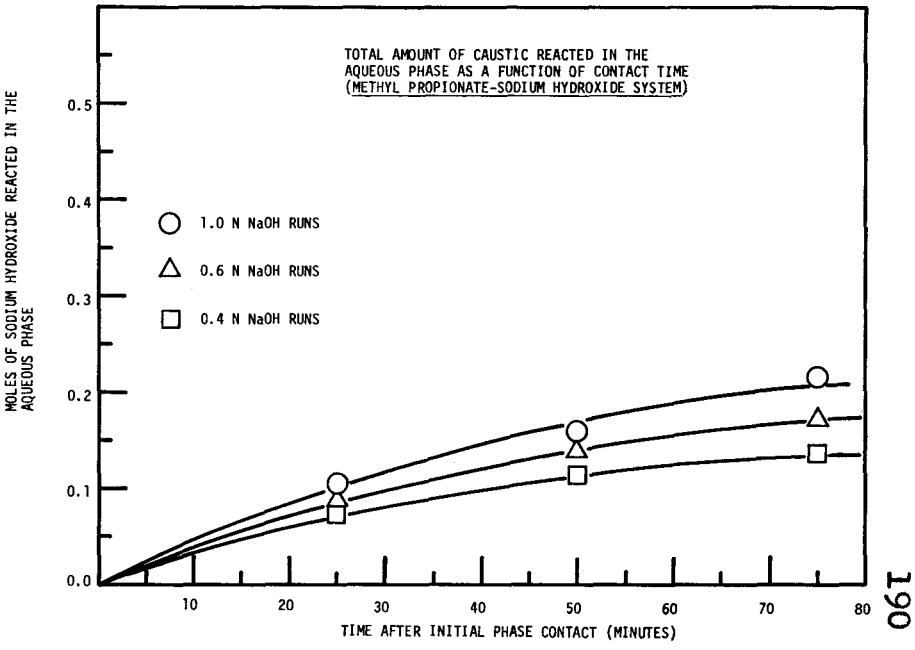
TOTAL AMOUNT OF CAUSTIC REACTED IN THE
AQUEOUS PHASE AS A FUNCTION OF CONTACT TIME
(METHYL PROPIONATE-SODIUM HYDROXIDE SYSTEM)
1.0 N NaOH RUNS
0.6 N NaOH RUNS
0.4 N NaOH RUNS
MOLES OF SODIUM HYDROXIDE REACTED IN THE AQUEOUS PHASE
TIME AFTER INITIAL PHASE CONTACT (MINUTES)

FIGURE 28

increases with increasing caustic concentration levels. (Refer to Figure 28.) In this system, however, the increase in the amount of ester which reacted is just high enough to slightly over-compensate the corresponding decrease in the ester present in the lower phase. As a result, the total ester transfer across the interface increases only very slightly with increasing sodium hydroxide concentration levels.

It is interesting to note that the total ester transfer with reaction (ranged up to 1.0 N sodium hydroxide) is slightly lower than the physical transfer despite the existence of both the interfacial and layer turbulence (Figure 20). This can probably be explained, apart from the usual solubility decrease as a result of the salt effect, by the fact that the physical properties of the system change drastically between the physical and the reaction transfer. In the physical run, the ester solution, having a density very close to that of the water, was observed to sink down towards the bottom of the aqueous phase in the form of random streaks. The increased contribution to the mass transfer by this flow (Section 4.2.3.3.3) is quite obvious. While in the reaction run, the density of the aqueous sodium hydroxide in the lower phase is higher than the ester solution. The streaking phenomenon ceases to prevail. The enhancement of the transfer, entirely due to the reaction and the turbulence in this case, is slightly lower than the enhancement

of the transfer due to streaking.

A comparison of the two ester-caustic systems shows that the total ester transfer with reaction in the ethyl acetate-sodium hydroxide system is, in general, higher than that in the methyl propionate-sodium hydroxide system. This is in agreement with the properties of the two systems. Ethyl acetate is more soluble in water, slightly more reactive with caustic. The effect of ethanol on the interface is probably stronger while the effect of sodium acetate is weaker than those caused by the products of the methyl propionate-sodium hydroxide system.

4.2.3.4.4.5 Comparison of the enhancement factors as measured from the experimental data and as predicted from the penetration theory:

For a particular reaction run, the total ester transferred across the interface up to any contact time can be determined experimentally from the concentration profile plots (Figures 18-19 and Appendix XVII). Thus the mass transfer rates, both the time averaged and the instantaneous ones can be calculated accordingly. (Refer to Section 4.2.1.4.1.4.) The respective mass transfer coefficients can then be obtained.

The time averaged ester transfer coefficients for all the reaction runs at 25 minutes, 50 minutes and 75 minutes of contact time so determined were compared with the time averaged physical transfer coefficients at the corresponding contact times. The resulting enhancement factors were

tabulated as shown in Table 10. A detailed sample calculation is given in Appendix X.

In the absence of both the layer and the interfacial turbulence, the enhancement factors can be predicted theoretically based on the method proposed by Brian P.L.T. et al. as described in the Theoretical Section (Chapter 3). A sample calculation is presented in Appendix X. For illustrative purposes, the theoretical enhancement factors for only three reaction runs were calculated for the two ester-caustic systems under study. The results are presented in Table X.2

The predicted and the experimentally determined enhancement factors were compared for the ethyl acetate-sodium hydroxide and the methyl propionate-sodium hydroxide systems. The results are shown in Table 10.

It is readily seen that for the ethyl acetate-sodium hydroxide system, the experimental enhancement factors are more than twice the values of those as predicted by the theoretical model. This is in accordance with the expectation from systems exhibiting interfacial turbulence. Alternatively, the effect of turbulence alone on mass transfer may be estimated by the subtraction of the theoretical from the experimental enhancement factor values. It was found that the enhancement due to the turbulence was higher (but in the same order of magnitude) than that due to reaction in the ethyl acetate-sodium hydroxide system. On the contrary,

TABLE 10

TIME AVERAGED ESTER TRANSFER RATES AND ENHANCEMENT FACTORS IN THE ETHYL ACETATE-SODIUM HYDROXIDE AND THE METHYL PROPIONATE-SODIUM HYDROXIDE SYSTEMS

Run	Ester transfer rates averaged over the period of contact time (moles/sec-cm^2) X 10^7			Enhancement factors $\phi_{avg.}$		
	25 minutes	50 minutes	75 minutes	25 minutes	50 minutes	75 minutes
EtAc - water	.69	.51	.40			
EtAc - 0.2 N NaOH	2.80	1.95	1.46	4.48	4.23	4.05
EtAc - 0.4 N NaOH	3.52	2.78	2.18	6.21	6.61	6.61
EtAc - 0.6 N NaOH	3.95	3.15	2.45	7.40	8.08	8.03
EtAc - 1.0 N NaOH	3.95	3.23	2.59	8.85 (3.40)	9.67 (3.47)	9.72 (3.50)
EtAc - 1.4 N NaOH	4.15	3.51	2.90	10.49 (4.94)	12.11 (5.15)	12.45 (5.22)
MePr - water	2.04	1.82	1.64			
MePr - 0.4 N NaOH	1.72	1.50	1.36	.96	.94	.95
MePr - 0.6 N NaOH	1.72	1.50	1.36	1.04	1.02	1.03
MePr - 1.0 N NaOH	1.91	1.65	1.45	1.33 (3.60)	1.29 (3.69)	1.24 (3.73)

Note - ( ) = theoretically predicted enhancement factors (Refer to Table X.2)

the experimental enhancement factors for the methyl propionate-sodium hydroxide system are much smaller than those predicted by the theoretical model. This discrepancy is explained by the fact that an abnormal physical mass transfer phenomenon was present as described in Section 4.2.3.3.3.

It should be realized, however, that in the aforementioned enhancement factor calculations, the multi-ion diffusion effects have not yet been taken into consideration.

Some of the enhancement factors for the ethyl acetate-1.0 N NaOH and ethyl acetate-1.4 N NaOH runs were subsequently re-calculated using the ionic penetration theory[B14]. The results indicated that the enhancement factors calculated from the ionic penetration theory were approximately 14% to 22% higher than the corresponding enhancement factors calculated based on the molecular penetration theory. A similar increase in the enhancement factors is expected for the methyl propionate-NaOH system. A sample calculation of the enhancement factors based on the ionic penetration theory is given in Appendix X: Note X.1.

4.2.3.4.4.6 Speed of the growth of the turbulent layer:

From each of the concentration profile graphs (Figures 18-19 and Appendix XVII), the distance between the interface and the reaction zone front (the point where the ester profile had just decreased to a negligible concentration) was measured. Unfortunately, due to an insufficient number of experimental datum points on the ester curve, extrapolation

or interpolation of the ester profile to zero concentration might sometimes be difficult and less accurate. Nevertheless, the distances spanned by the ester profiles were measured. Some of these measurements were compared with the turbulent layer thicknesses directly measured in separate experiments performed with the same liquid systems at corresponding concentration levels in the same apparatus (Appendix V). The results of comparison are shown in Table 11.

The comparison indicates that the edge of the turbulent layer as observed in the "direct measurement" experiments (Appendix V), as well as in the previous "optical cell" experiments[S8] corresponds, at least roughly, to the front of the reaction zone.

4.2.3.4.4.7 Comparison of experimental and theoretical reaction zone thickness:

As defined in Chapter 3 (Theoretical Principles), the reaction zone is the region where the concentrations of both reactants are substantial. The thicknesses of such regions can be measured experimentally from the concentration profile plots at 25 minutes, 50 minutes and 75 minutes of contact time for each reaction run and are recorded in Table 12.

Since the saponification reactions involved in the two liquid systems under study are so slow that the mass transfer situation may be considered approximately at steady state (Section 4.2.3.4.4.3), under such conditions, the reaction zone thickness can be calculated, based on the mathematical

TABLE 11

COMPARISON OF TURBULENT LAYER THICKNESS AS OBTAINED BY DIRECT MEASUREMENTS AND AS DERIVED FROM THE EXPERIMENTAL ESTER CONCENTRATION PROFILES

System & Normality of NaOH / Turbulent Layer Thickness (cm.) / Time (Minutes)	25	50	75
Ethyl acetate-sodium hydroxide			
0.2 N from profile	0.82	0.87	1.10
direct measurement	0.74	0.89	0.89
0.6 N from profile	0.80	0.98	1.02
direct measurement	0.64	0.87	0.92
1.0 N from profile	0.50	0.72	0.80
direct measurement	0.47	0.64	0.70
Methyl propionate-sodium hydroxide			
0.6 N from profile	0.29	0.60	0.64
direct measurement	0.29	0.48	0.57

model proposed by Friedlander et al.[F2] as described in the Theoretical Principles Section (Chapter 3). Mean eddy diffusivities of the reactants derived from the experimental concentration profiles (Section 4.2.3.4.4.3) and the time averaged experimental ester transfer rates were used for the calculations. A sample calculation is presented in Appendix X. It should be realised that the criterion of the reaction zone thickness prescribed by Friedlander et al. is somewhat different from that adopted in the present work. Friedlander et al. define the reaction zone as the region in which the flow of the upper phase is reduced from 95% of its initial value to 5% of its initial value. However, under normal concentration profile conditions (refer to Figure 1), this definition merely establishes a region of reaction where the concentrations of both the reacting species are significant.

Nevertheless, zone thicknesses so calculated were compared with those determined experimentally and it was found that the calculated results agreed approximately with the experimental reaction zone thicknesses both in the order of magnitude and in the trend with respect to caustic concentration levels as indicated in Table 12.

4.2.3.4.4.7.1 Validity of the assumption (quasi-steady state) involved in the calculation of the reaction zone thickness:

In the dimensionless form, equation (4a) (Chapter 3: Section 3.1) becomes

TABLE 12

COMPARISON OF THE REACTION ZONE THICKNESS AS MEASURED EXPERIMENTALLY AND AS APPROXIMATED FROM THE PSEUDO-STEADY STATE MODEL BASED ON TIME AVERAGED ESTER TRANSFER RATES

Run #	25 Minutes (cm.)		50 Minutes (cm.)		75 Minutes (cm.)	
	model	experimental	model	experimental	model	experimental
EtAc - 0.2 N NaOH	.56	.57	.45	.32	.56	.47
EtAc - 0.4 N NaOH	.68	.66	.70	.52	.82	.38
EtAc - 0.6 N NaOH	.51	.62	.66	.43	.59	.38
EtAc - 1.0 N NaOH	.22 (.09)	.37	.57 (.10)	.36	.53 (.11)	.25
EtAc - 1.4 N NaOH	.18 (.09)	.38	.31 (.09)	.44	.48 (.10)	.32
MePr - 0.4 N NaOH	.25	.46	.36	.40	.38	.26
MePr - 0.6 N NaOH	.18	.29	.26	.58	.43	.34
MePr - 1.0 N NaOH	.26 (.09)	.34	.24 (.10)	.35	.16 (.11)	.36

Note ( ) = Reaction zone thicknesses calculated based on molecular diffusivities and theoretical reaction transfer rates. (Refer to Section X.3.3, Appendix X for sample calculation.)

$$\frac{\tilde{l}^2}{D_A \tilde{t}} \frac{\partial C_A^*}{\partial t^*} = \frac{\partial^2 C_A^*}{\partial x^{*2}} - \frac{\tilde{l}^2 k \tilde{C}}{D_A} C_A^* C_B^* \qquad (4e)$$

where,

$\tilde{t}$ = characteristic time scale

$\tilde{l}$ = characteristic length

$\tilde{C}$ = characteristic concentration

Considering equation (4e) for the reaction zone and identifying $\tilde{l}$ with the reaction zone characteristic length[Cla], then

$$\frac{l^2 k \tilde{C}}{D_A} = 1$$

If $\tilde{t}$ is set to be the actual phase contact time, then in order to have a quasi-steady state in the reaction zone,

$$\frac{l^2}{D_A t} \ll 1 \qquad (4f)$$

Similar arguments may be made for the equations of the other reactant B and of the products. Thus the quasi-steady state approximation for all the species in the reaction zone is possible when the zone characteristic length is much less than the diffusion penetration thickness of the species.

The experimental values of the reaction zone thickness and the derived eddy diffusivity of the ester were substituted into expression (4f) for all the cases under study in the ethyl acetate-sodium hydroxide and the methyl propionate-sodium hydroxide systems. The calculated $(l^2/D_A t)$ values are tabulated in Appendix X: Note X.2. A sample calculation is given in Note X.2.

If the quasi-steady state criterion is arbitrarily set to be

$$\frac{l^2}{D_A t} \leq \frac{1}{10}$$

then the quasi-steady state condition is achieved in the reaction zone for all the cases under study (except for the case of methyl propionate-0.4 N sodium hydroxide: 25 minutes after phase contact).

4.3 - PART C

STEADY STATE MASS TRANSFER RATE MEASUREMENTS IN ESTER-AQUEOUS CAUSTIC SYSTEMS

In addition to the stagnant phase reaction systems study, steady state mass transfer experiments were carried out with both phases stirred. In this section, the simple apparatus for studying the rates of transfer of esters such as ethyl, methyl and propyl formate across a plane surface into water and into caustic solutions is described (Section 4.3.1). Quantitative measurements of the rate of transfer are reported (Section 4.3.2). Both the mass transfer coefficients and the enhancement factors for the experimental runs were calculated and compared with those obtained from the Van Krevelen and Hoftijzer's model[V1]. The results of the comparison are presented and discussed (Section 4.3.3).

4.3.1 Experimental Details

The same apparatus and experimental procedure were used to study the mass transfer rates in the formate-caustic systems as in the ethyl acetate-caustic system which has been reported in detail previously in Reference (S8). For this reason, only a brief description of the experimental details will be presented in the following sections.

4.3.1.1 Apparatus

Figure 29 shows the simple stirred apparatus used for saponification studies. The reactor itself consisted of a cylindrical pyrex glass vessel, indented to give two compartments of approximately the same volume (98-100 ml.). The indented part just above the tip of the glass hook gauge had a diameter of 4.8 cm. and an area of 18.1 cm^2. The stirrer was made of type 316 stainless steel and was of the paddle type, with the blades 2.4 cm. in diameter and 3.9 cm. apart. The whole reactor was thermostatted by water circulating through the outer glass jacket. For some runs in the ethyl formate-sodium hydroxide system, the conductivity of the lower phase solution was measured with a conductivity cell located immediately at the outlet of the reactor. Thus the instantaneous caustic concentration at the outlet of the reactor could be obtained through the calibration curves (Appendix XIX).

STEADY STATE TRANSFER APPARATUS

1. RESERVOIR
2. TYGON OR GLASS TUBING
3. CONSTANT HEAD DEVICE
4. FLOWMETER
5. TEMP. CONTROLLER
6. GLASS COIL
7. WATER BATH
8. OUTER GLASS JACKET
9. CONSTANT SPEED MOTOR
10. MERCURY CUP
11. GLASS HOOK GAUGE
12. REACTOR
13. FLOW REGULATOR
14. STEM
15. CLAMP
16. STOPCOCK

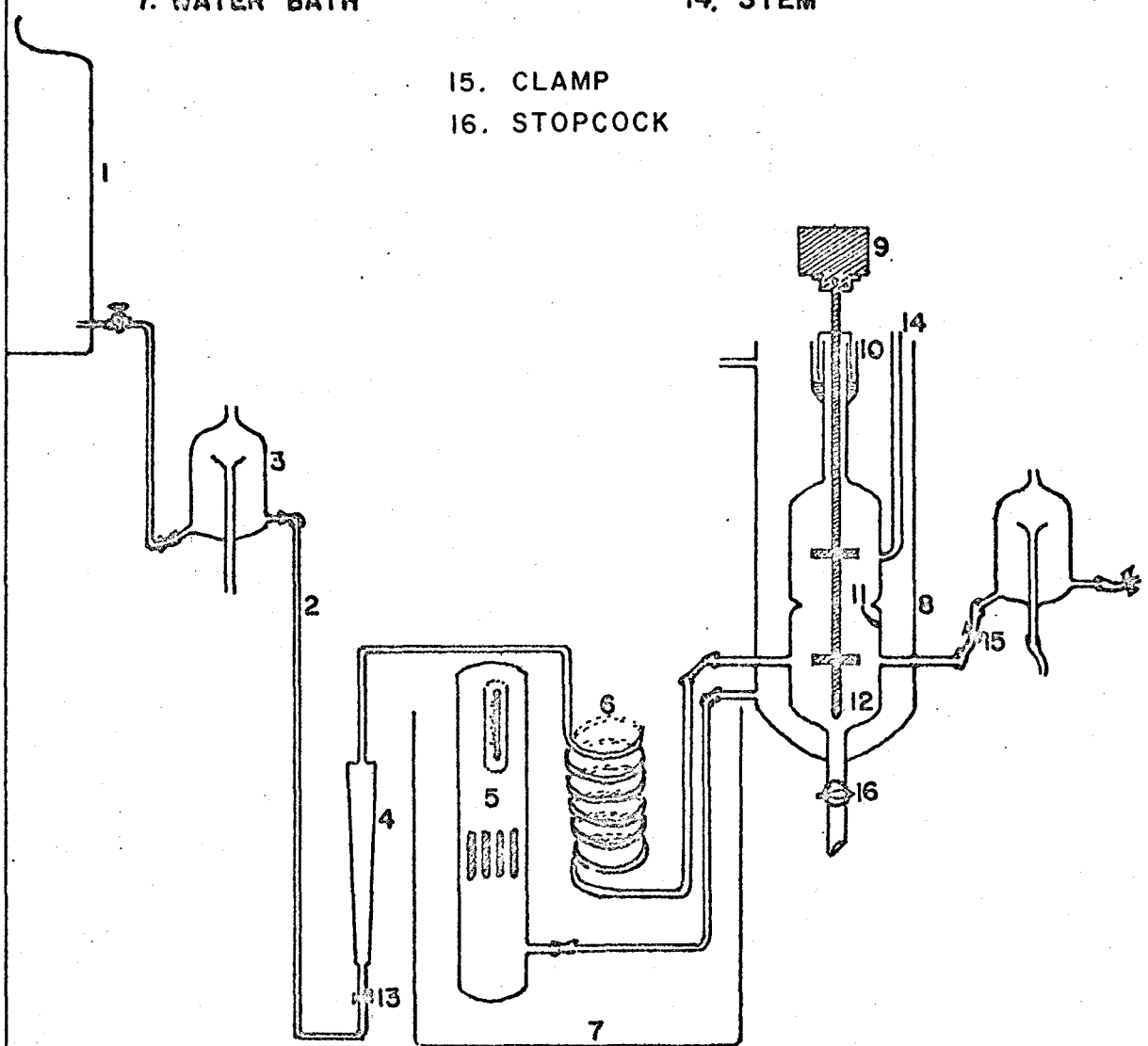

4.3.1.2 Procedure

In operation, the aqueous caustic solution flowed from the feed tank, through a constant head device, a rotameter and a temperature regulating glass coil into the lower compartment of the mass transfer cell, thence out through a second head levelling device. Ester, presaturated with water at the experimental temperature, floated in the upper compartment. The ester-caustic solution interface was located accurately by using the glass hook gauge and controlled by the constant head device on the discharge of the caustic layer. In order to have a reasonably high mass transfer rate as well as a plane liquid-liquid interface, the set of constant operating conditions found most satisfactory was a lower phase flowrate of 1.5 litres/hour and a stirrer speed of 141 r.p.m. for the systems of ethyl formate-caustic and propyl formate-caustic; while for the methyl formate-sodium hydroxide system, experiments were conducted with stirring speeds at 141 r.p.m. and at 90 r.p.m. respectively.

Each experiment was run for at least 20 minutes before taking any measurements in order that the system could come to a steady state (lower phase reactor retention time was approximately 4 minutes). During the run, the upper phase transferred into the lower phase. Therefore the volume of the upper phase decreased. The hydrodynamic equilibrium in the system was upset and the interface went up. A small amount of the upper phase liquid was added in at short intervals

via the glass stem (see Figure 29) using a 5-ml. syringe. These additions were made to keep the level of the interface always at the tip of the hook gauge. The amount added would be equal to the amount transferred after a correction has been made for the small vapor loss of the ester through the open ends of the upper compartment. Thus the transfer rate could be calculated if the time between additions were known.

4.3.1.3 Number of Ester-Caustic Systems Investigated

Mass transfer experiments were performed at 25 ± 0.05°C with the ethyl, methyl and propyl formate-caustic systems respectively and at various sodium hydroxide concentrations. In addition, steady state physical transfer rates of the esters into the water phase were individually measured. Both the esters and the sodium hydroxide used were of reagent grade. The esters were purified by distillation in a packed column. Double-distilled water was used (Appendix I).

With the ethyl formate-sodium hydroxide system, an additional series of transfer runs was also performed using once-distilled water for the preparation of the two reacting phases.

4.3.1.4 Method of Calculation

4.3.1.4.1 Mass Transfer Rates

For each run, the time required for each 5-ml. of the upper-phase liquid to transfer into the lower phase was noted. These time intervals were plotted against time after the start of the experiment (i.e. after the first measurement was taken). A typical plot is shown in Figure 31. The steady state transfer rate was calculated from the graph.

The transfer rates from the various runs were corrected for the vapor loss of the ester through the open ends of the upper compartment. The rates were also corrected for the small amount of water accompanying the transfer of ester across the interface.

4.3.1.4.2 Mass Transfer Coefficients

The mass transfer rate data were used to evaluate the transfer coefficients using the following equation:

$$\frac{N_A}{3600 \times A} = k_L \frac{(C_{A_i} - C_A)}{1000} \qquad (22)$$

where

N_A = mass transfer rate of ester , moles/hour

A = interfacial area , cm^2.

k_L = mass transfer coefficient with chemical reaction , cm/sec.

C_{A_i} = interfacial concentration of the ester , moles/litre

C_A = lower phase bulk concentration of the ester , moles/litre

The interfacial concentration of the ester was measured experimentally (Appendix XIII). The caustic concentrations (and thus the ester concentrations by mass balance) in the lower phase were measured at steady state for a few runs in the ethyl formate-sodium hydroxide system (Appendix XIX) and found to be in agreement with the calculated values. The computed concentrations were made by assuming the lower phase to be well-mixed and the components reacted homogeneously. Consequently, the concentrations of both reactants for each run were calculated by solving the following simultaneous equations:

$$FC_{B_o} - FC_B = kC_AC_BV \qquad (23)$$

$$N_A - FC_A = kC_AC_BV \qquad (24)$$

where

V = volume of the lower compartment of the reaction cell, litres

k = reaction constant, (litres/mole)/hr.

F = flowrate of the lower phase, litres/hr.

C_{B_o} = concentration of input sodium hydroxide, moles/litre

Based on the agreement of the calculated and the measured values of the sodium hydroxide concentration in the lower phase in both the ethyl formate-sodium hydroxide system (Appendix XIX) and in the ethyl acetate-sodium hydroxide system[S8], the steady state lower phase ester concentrations thus computed for all subsequent runs in the ethyl formate-sodium hydroxide and methyl formate-sodium hydroxide systems

were used for the mass transfer coefficient calculations.

4.3.1.4.3 The Enhancement Factors

For each ester-caustic system, the mass transfer coefficients calculated from the reaction runs were compared with the one for the physical transfer run without reaction.

$$\phi = \frac{k_L}{k_L^V} \qquad (25)$$

The experimental enhancement factors were compared with the theoretical ones predicted from the Van Krevelen and Hoftijzer's model(V1).

4.3.2 Results

4.3.2.1 Ethyl Formate-Sodium Hydroxide System

4.3.2.1.1 Mass Transfer Rate Measurements

4.3.2.1.1.1 Solutions prepared from once distilled water (Group I):

A total of 11 runs were performed and the transfer rate results obtained are presented in Figure 30. For each run, a steady state mass transfer rate was achieved only at a long period after the start of the experiment; although the variation of the rate was already quite small when the phase contact time was 50 minutes or longer. Because of the abnormally long period of time the system took to achieve steady state, the transfer experiments were repeated with both of the reacting phases prepared from double-distilled water.

4.3.2.1.1.2 Solutions prepared from twice distilled water (Group II):

A total of 20 runs were performed. In each of these runs, steady state was achieved at 30 to 50 minutes after the start of the run. A typical data plot is shown in Figure 31. The calculated transfer rate data are presented in Figure 30.

4.3.2.1.2 Enhancement Factors

Mass transfer coefficients for individual runs were calculated for both sets of experiments. The transfer coefficient of each reaction run was compared with the physical transfer coefficient of the same set. The resulting enhancement factors were plotted and are presented in Figure 32.

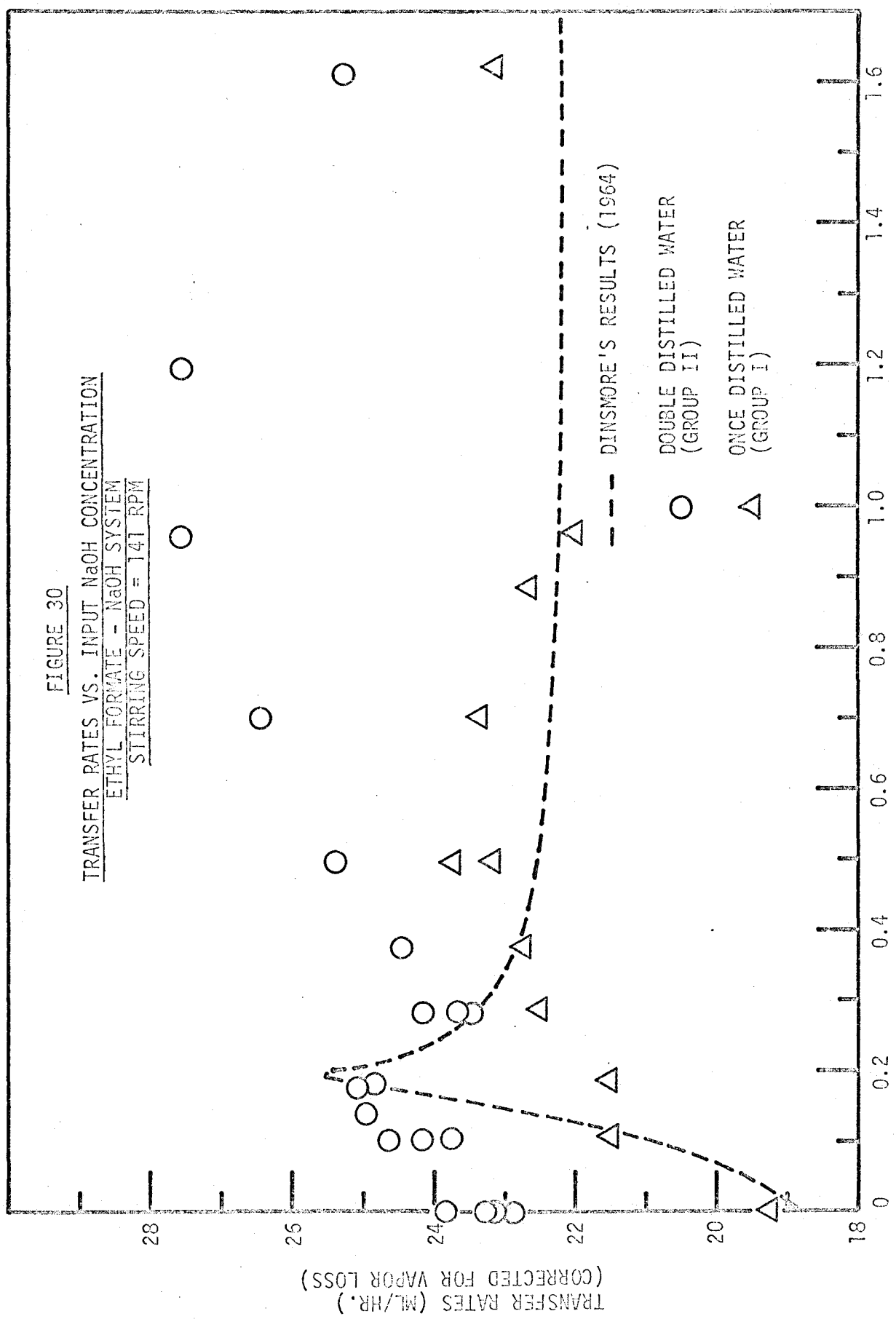
FIGURE 30
TRANSFER RATES VS. INPUT NaOH CONCENTRATION
ETHYL FORMATE - NaOH SYSTEM
STIRRING SPEED = 141 RPM
DINSMORE'S RESULTS (1964)
DOUBLE DISTILLED WATER (GROUP II)
ONCE DISTILLED WATER (GROUP I)
TRANSFER RATES (ML/HR.) (CORRECTED FOR VAPOR LOSS)
INPUT NaOH CONCENTRATION (NORMALITY)
18
20
22
24
26
28
0
0.2
0.4
0.6
0.8
1.0
1.2
1.4
1.6

FIGURE 31

RECIPROCAL OF REACTION MASS TRANSFER RATE VS. TIME

ETHYL FORMATE - 0.5N NaOH (GROUP II, TWICE DISTILLED WATER)

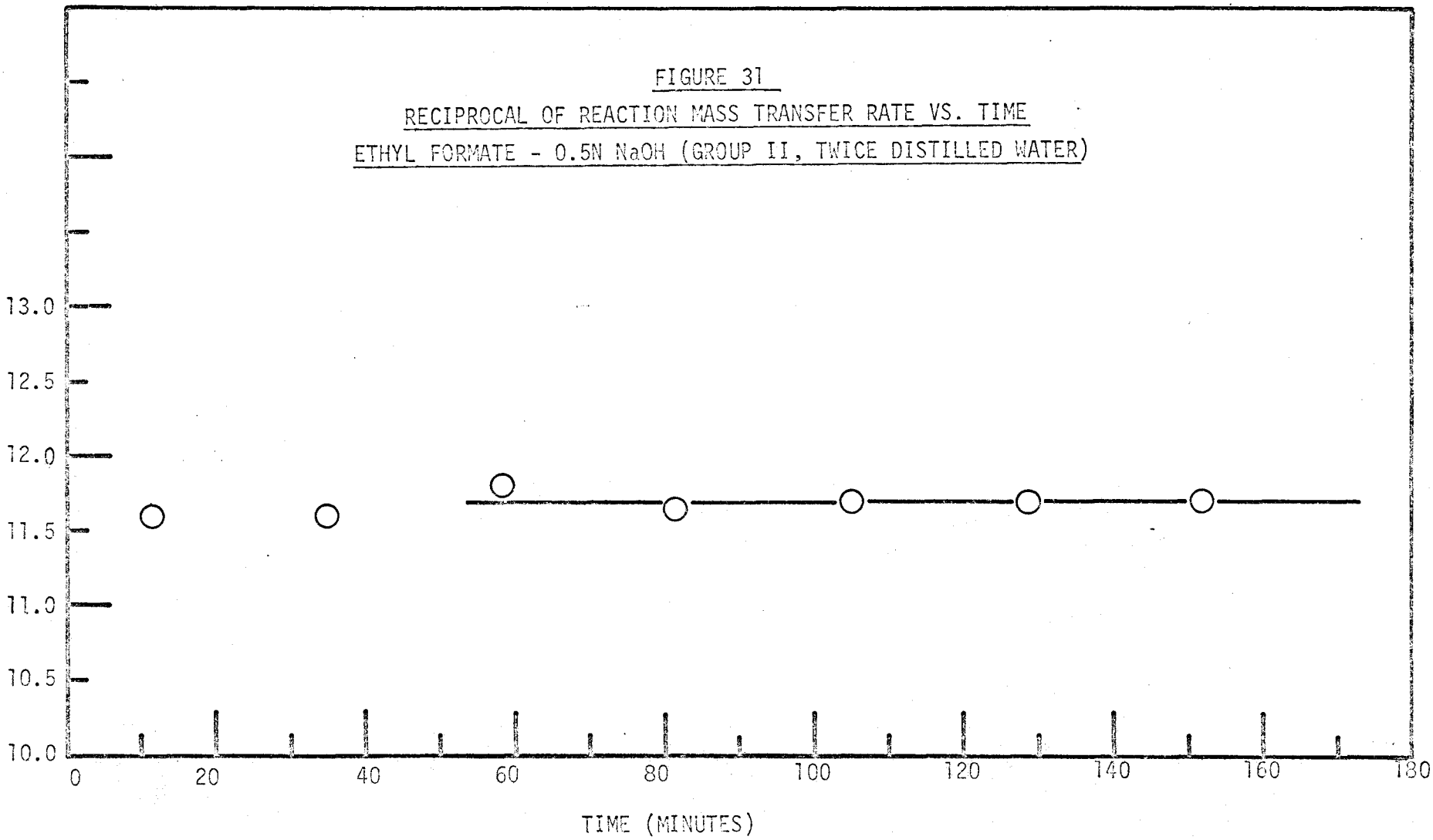

FIGURE 32 COMPARISONS OF THEORETICAL AND EXPERIMENTAL ENHANCEMENT FACTORS ETHYL FORMATE - NaOH SYSTEM

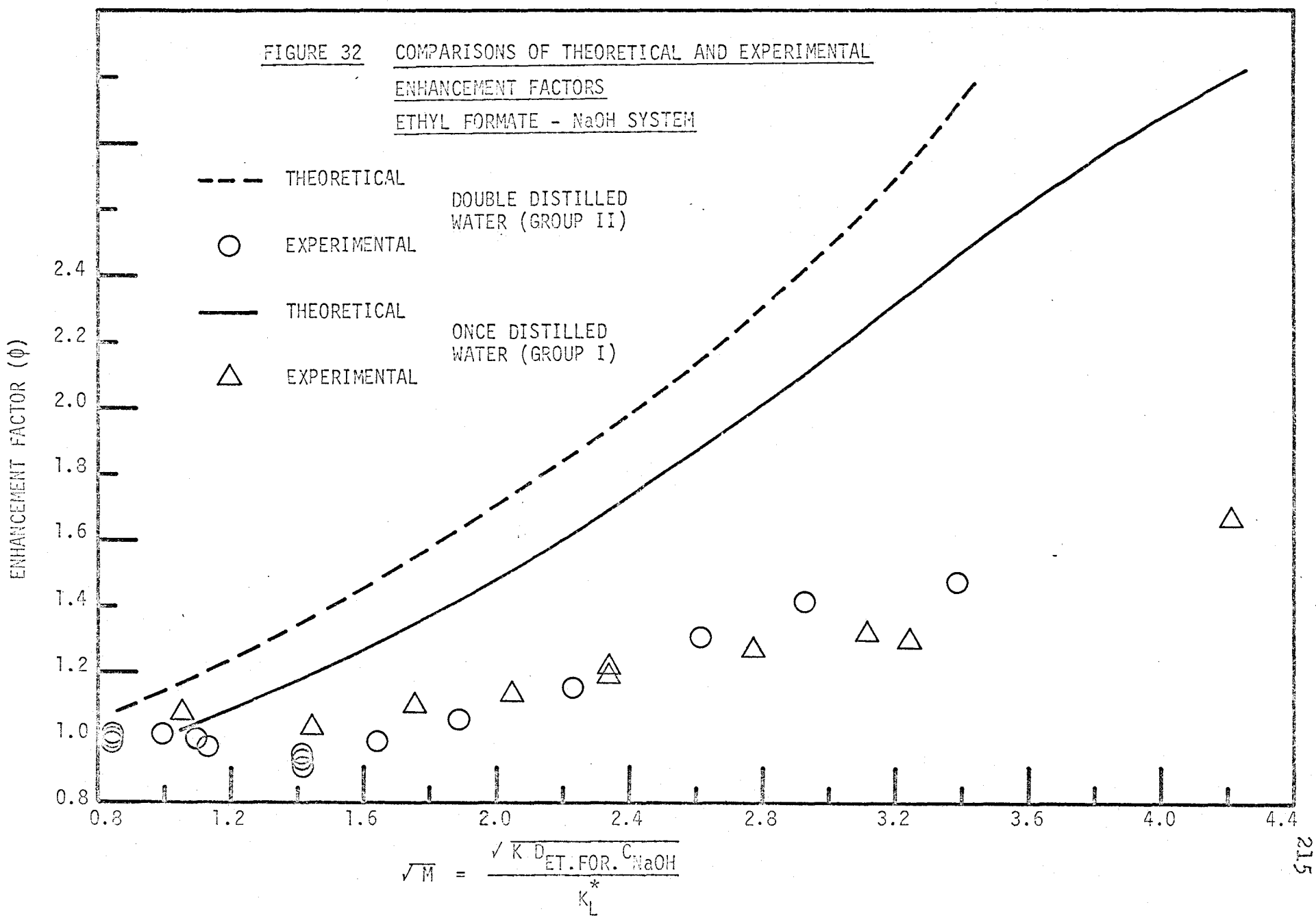

4.3.2.2 Methyl Formate-Sodium Hydroxide System

4.3.2.2.1 Mass Transfer Rate Measurements

A total of 4 runs (Group I) were performed with the stirrer speed set at 141 r.p.m. The results are presented in Figure 33. During the runs, the liquid-liquid interface was observed to be quite wavy.

The stirrer speed was then reduced to 95 r.p.m. and a series of runs (Group II) was repeated at various input caustic concentrations. The transfer rate data are presented in Figure 33.

4.3.2.2.2 Enhancement Factors

Mass transfer coefficients and the corresponding enhancement factors were calculated for both sets of the experiments. The enhancement factors so calculated are presented in Figure 34.

FIGURE 33

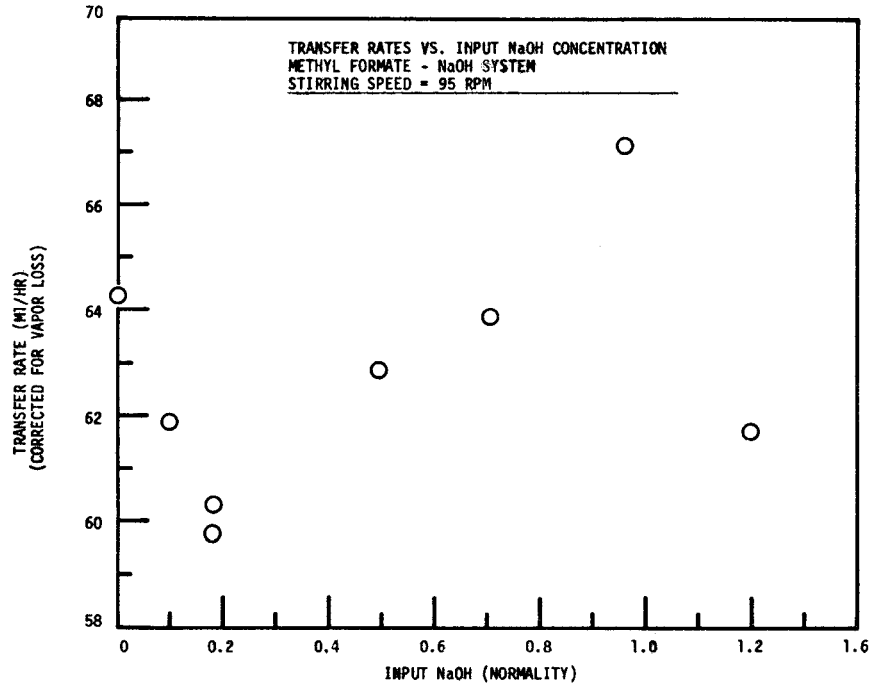
TRANSFER RATES VS. INPUT NaOH CONCENTRATION
METHYL FORMATE - NaOH SYSTEM
STIRRING SPEED = 95 RPM
TRANSFER RATE (MI/HR)
(CORRECTED FOR VAPOR LOSS)
70
68
66
64
62
60
58
0
0.2
0.4
0.6
0.8
1.0
1.2
1.6
INPUT NaOH (NORMALITY)

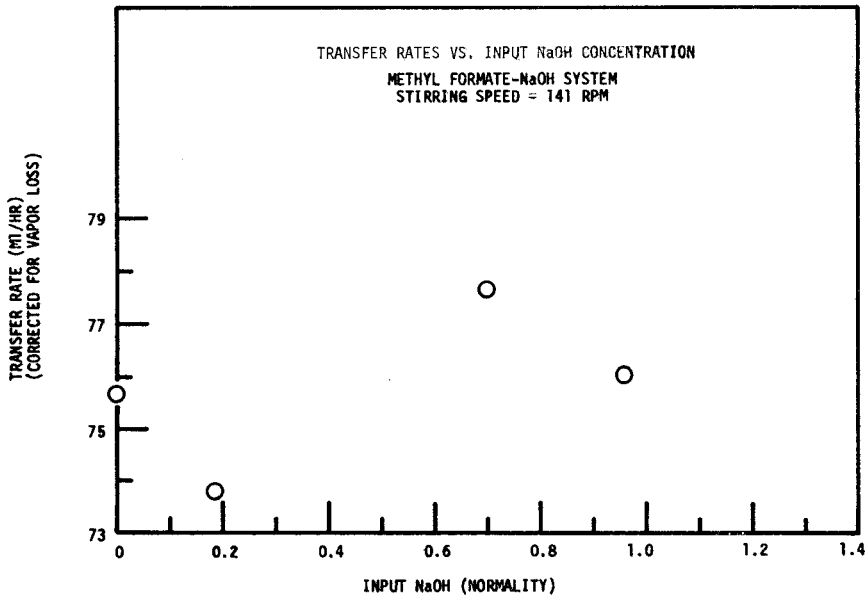
TRANSFER RATES VS. INPUT NaOH CONCENTRATION
METHYL FORMATE-NaOH SYSTEM
STIRRING SPEED = 141 RPM
TRANSFER RATE (MI/HR)
(CORRECTED FOR VAPOR LOSS)
79
77
75
73
0
0.2
0.4
0.6
0.8
1.0
1.2
1.4
INPUT NaOH (NORMALITY)

FIGURE 34

COMPARISON OF THEORETICAL AND EXPERIMENTAL ENHANCEMENT FACTORS

METHYL FORMATE - NaOH SYSTEM

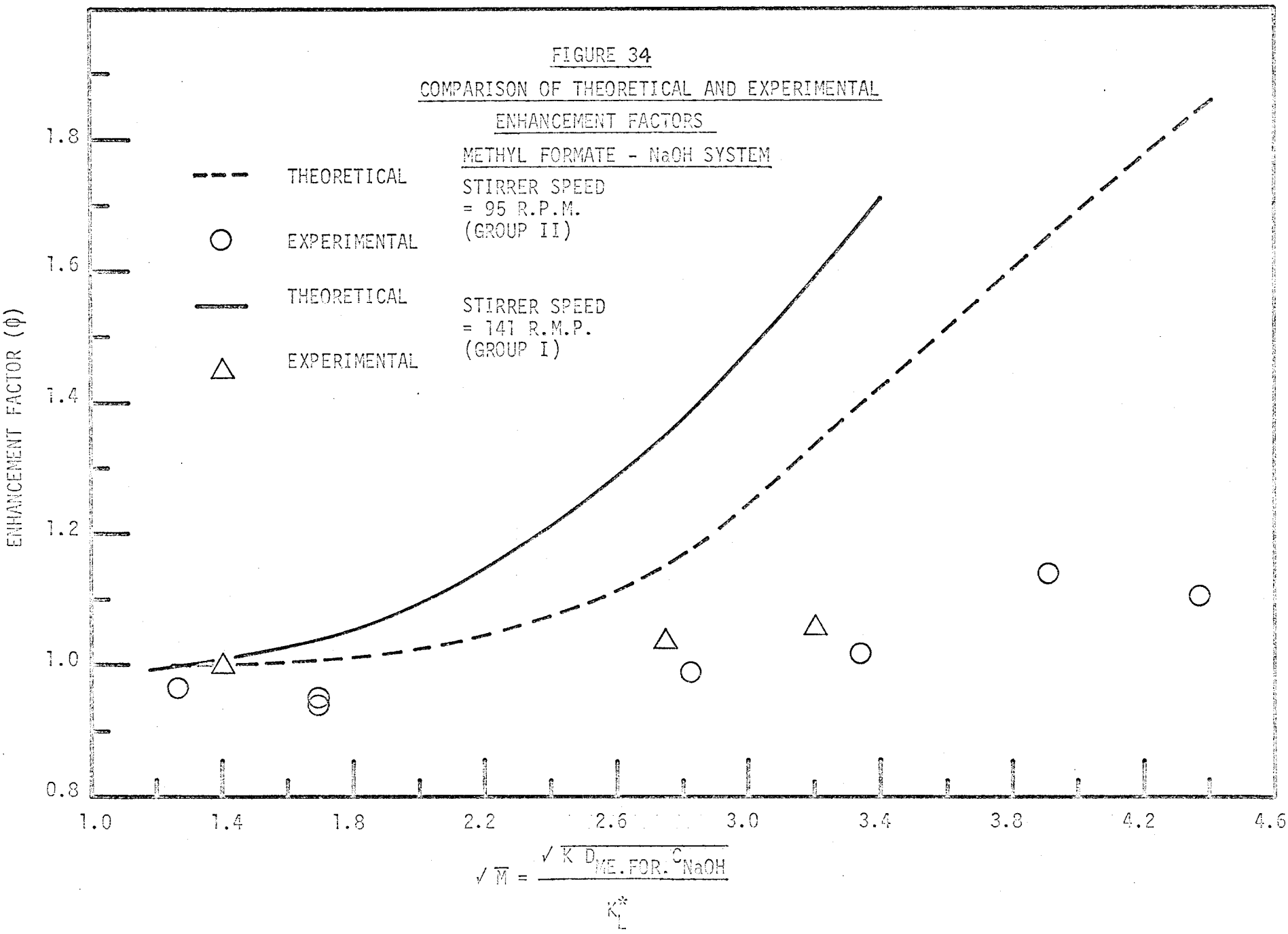

4.3.2.3 Propyl Formate-Sodium Hydroxide System

4.3.2.3.1 Mass Transfer Rate Determinations

A total of 12 runs were performed and the results are presented in Figure 35.

FIGURE 35

TRANSFER RATES VS. INPUT NaOH CONCENTRATION

PROPYL FORMATE - NaOH SYSTEM

STIRRING SPEED = 141 R.P.M.

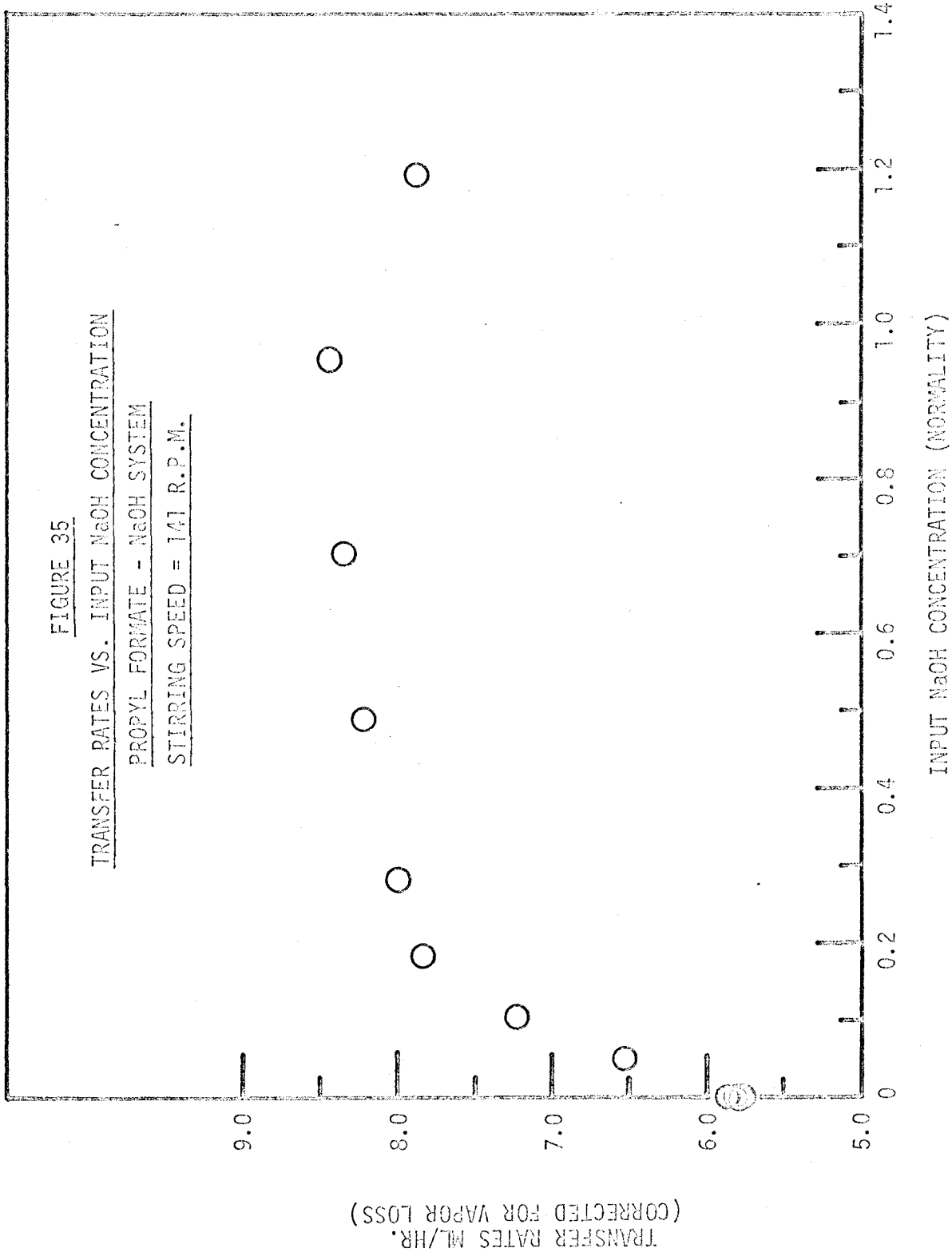

4.3.3 Discussion of Results

4.3.3.1 General Assumptions

4.3.3.1.1 Measurement of Steady State Mass Transfer Rates

The transfer rates are calculated based on the rate of addition of the ester phase saturated with water to the upper compartment of the reactor to keep the level of the interface always at the tip of the hook gauge. During the reaction, alcohol is produced. Part of the alcohol formed diffuses back into the upper ester phase; thus, the transfer rate measured is lower than the actual transfer rate. Furthermore, the solubility of the water in the ester phase may change with the presence of alcohol. This is particularly more so with systems of higher ester transfer rates and reaction velocities because more alcohol is being produced. The interface transfer of water due to the change of solubility will, no doubt, cause errors in the measurement of transfer rates. All these errors can be evaluated only with the knowledge of the ternary ester-alcohol-water phase diagrams.

Alternatively, if the transfer system is allowed to run for a sufficiently long period of time, a dynamic equilibrium will be reached whereby the concentration of alcohol and thus the solubility of water in the ester phase will be constant. A steady state transfer situation will then prevail as reflected in a typical transfer rate plot shown in Figure 31.

4.3.3.1.2 Salt Effects

Salt effects of sodium hydroxide on the solubilities of

the formate esters cannot be measured experimentally since they react with each other. Furthermore, the salt effects of caustic on the non-electrolyte are difficult to evaluate using the existing Kirkwood's[K5] or Deybe's[D4] methods due to limited thermodynamic data available. Nevertheless, a comparison of a large group of experimental data on salt effects[H5][L4] indicates that the salt effects of sodium hydroxide on ethyl acetate should be in the same order of magnitude as sodium acetate on ethyl acetate. Similarly, in this work, it is assumed that the salt effects of both sodium hydroxide and sodium formate on a particular kind of formate ester are the same. The solubilities of esters in aqueous salt solutions were measured as described in Appendix XIII.

4.3.3.1.3 Alcohol Effects

Available literature data[S17] indicate that the presence of alcohol (formed as the reaction product) will increase the solubility of the ester in the aqueous lower phase. However, since the steady state lower phase alcohol concentrations in the experimental runs are dilute (ranging from 0.2 to 0.7 N for the ethyl formate-sodium hydroxide and the methyl formate-sodium hydroxide systems), it is assumed that the effects of alcohol on the solubilities of the esters are insignificant in the calculation of mass transfer coefficients.

4.3.3.1.4 Application of the "Film Theory" to the Ester-Caustic Systems

In applying the Van Krevelen and Hoftijzer's model to each

of the ester-caustic systems studied, the molecular diffusivities of the ester and the caustic are required (with reference to Chapter 3: Section 3.1.2.2). Due to the limited amount of available literature data on molecular diffusivities of the ester-caustic systems, the diffusion coefficients of ethyl formate, methyl formate are assumed to be the same as that of ethyl acetate. Furthermore, it is assumed that the diffusion coefficients are not affected by the presence of multi-ions. The diffusivities of ethyl acetate and sodium hydroxide in water, taking into account their concentration dependencies, are estimated to be 0.8×10^{-5} and 1.91×10^{-5} $cm^2/sec.$ respectively (Appendix X: Section X.2.3).

4.3.3.2 Ethyl Formate-Sodium Hydroxide System

4.3.3.2.1 Comparison of the Transfer Rates Between Groups I and II

A comparison of the results obtained from the solutions prepared from once-distilled water and from the solutions prepared from twice-distilled water reveals that transfer rates between the two groups are not the same even at identical input sodium hydroxide concentrations; although reproducible results are obtained within each individual group. Generally, the transfer rates of the group using twice-distilled water are higher as observed in Figure 30.

The exact reasons for the difference in transfer rates between the two groups are not clear. The once-distilled water, supplied from the central system of the building, may have picked up some contaminants from the long sections of the pipes. These contaminants which may be surface active agents or compounds of higher molecular weights, may be reduced satisfactorily by re-distillation (Appendix I: I-5).

4.3.3.2.2 Comparison of Transfer Rate Results Obtained by Other Workers

Transfer rate data on the ethyl formate-sodium hydroxide system using the same stirred cell apparatus were also obtained by Dinsmore[DI5]. His results, using solutions prepared from once-distilled water, were replotted in Figure 30. It is evident that Dinsmore's data generally agree with the present Group I data obtained also by using once-distilled water.

4.3.3.2.3 Comparison of the Experimental and Theoretical Enhancement Factors

With the exception of a few runs at the dilute input caustic concentrations, all the results from the runs of both Group I and Group II show an enhancement of transfer coefficients due to the reaction. However, the experimental enhancement factors are much lower than those predicted from the Van Krevelen and Hoftijzer's model as indicated in Figure 32.

The overlapping of the two groups of experimental enhancement factor data indicates that in spite of the difference in the absolute values of the transfer rate existing between the two groups of experiments, their degrees of transfer enhancement are the same.

The mass transfer enhancement observed in the ethyl formate-caustic system appears to contradict the retardation of transfer results previously reported for the ethyl acetate-caustic system[89]. On the other hand, it should also be realized that the reaction rate in the ethyl acetate-sodium hydroxide system is so small that the theoretical enhancement factor for the system is practically equal to 1. Therefore, in comparing the experimental with the theoretically predicted enhancement factor values, both the systems of ethyl formate-caustic and ethyl acetate-caustic actually show similar trends of transfer retardation with chemical reaction.

4.3.3.2.4 Possible Factors Governing the Reduced Enhancement of Transfer Coefficients

The following factors are proposed based on the previous

research experience with the ethyl acetate-sodium hydroxide system[S8]. Each of these factors will contribute partially towards the understanding of the discrepancy between the experimental and the theoretical enhancement factors. While some of these explanations are speculative, further experimental work must be performed to evaluate the effects of individual factors on the transfer retardation so that a more fully satisfactory explanation to the discrepancy may be acquired.

4.3.3.2.4.1 Effect of experimental conditions:

The variation of the experimental conditions in the reaction transfer runs, such as the density, viscosity and interfacial tension with sodium hydroxide concentrations, have not yet been accounted for in the theoretical prediction calculations. The concentration dependencies of the reactant diffusivities, on the other hand, have been accounted for (Section 4.3.3.1.3).

4.3.3.2.4.2 Effect of the product salt:

Apart from the usual salt effect of decreasing the ester solubility, the presence of the product salt was also observed to modify the hydrodynamic conditions, thus reducing the transfer rate by decreasing the turbulent liquid motion at and near the liquid-liquid interface[S8].

It may also be speculated that the adsorption of sodium formate at the interface may, to some extent, result in the formation of a mobile surface barrier, and cause a reduction in transfer.

4.3.3.2.4.3 Effect of the impurities:

The ever present impurities, although maybe in trace amounts in this case from NaOH pellets, may also affect the interfacial properties and cause transfer retardation.

4.3.3.2.4.4 Assumptions involved in the application of the "film theory":

The assumptions of a constant ester diffusivity value (equal to that of ethyl acetate in water) for all ester-caustic systems under study and negligible multi-ion effects render the theoretical analysis to be semi-quantitative.

4.3.3.3 Methyl Formate-Sodium Hydroxide System

Similar to the ethyl formate-sodium hydroxide system, with the exception of a few runs at the dilute input caustic concentration range, the results indicate the increase of enhancement factors with increasing input sodium hydroxide concentrations. The measured enhancement factors for both groups of experiments are, again, lower than those predicted from the theoretical model as shown in Figure 34.

The overlapping of the two sets of enhancement factor data indicates that although the absolute values of the transfer rates are different when the transfer experiments are performed at different stirrer speeds, yet, the degrees of enhancement due to the reaction are the same. The stirrer speeds for both groups of experiments are high enough to ensure vigorous mixing in each of the two liquid phases.

The reasons for the reduced transfer enhancement for the methyl formate-sodium hydroxide system are believed to be similar to those speculated for the ethyl formate-sodium hydroxide system.

4.3.3.4 Propyl Formate-Sodium Hydroxide System

Judging from the transfer rate data (Figure 35), similar enhancement factor results are expected for the propyl formate-sodium hydroxide system as with the previous two ester-caustic systems.

Reaction rate constant information for the ester-caustic system is not available. An attempt to measure the rate constant of the batchwise saponification reaction using the conductivity method(D8)(R6) was not successful due to the fast reaction rate. As a result of the lack of knowledge on the reaction rate, the enhancement factors for this system were not calculated.

4.4 - PART D

MEASUREMENT OF THE LIQUID DIFFUSION COEFFICIENTS

In the theoretical calculations of this dissertation, diffusion coefficients of various components in the solutions, particularly those of the esters, are frequently involved. Although some theories for the prediction of diffusion coefficients of liquids exist in the literature, they are, however, by no means adequate for accurate predictions. It was therefore decided, as part of the project, to design and construct a diffusion cell which enabled the quick experimental measurement of the binary diffusion coefficient and possibly the ternary diffusion coefficient as a function of concentration in the liquid-liquid and gas-liquid systems with reasonable accuracy. The apparatus was so designed as to adopt the moiré pattern method originally developed by Sato[S2] for the determination of diffusion coefficients.

Only the preliminary experiments to obtain the diffusion coefficient results were carried out. Some experiments of an exploratory nature in the one-phase three-component systems were also studied in this project. In addition, the interfacial phenomena involved in the two-phase ester-caustic systems were investigated using this cell.

The apparatus was subsequently used to evaluate the moiré pattern method in detail using several one-phase binary liquid systems by a MastersDegree candidate[L2] of this Department.

4.4.1 Experimental Details

4.4.1.1 Apparatus

The diffusion cell consisted mainly of two parts, one (block 2), being smaller, was enclosed by the main body (1) as shown in Figure 36. The smaller block was made of Teflon reinforced by a stainless steel structure. The remaining part was made of stainless steel (type 316). The smaller block could also slide smoothly onto the other. Both the front and the back of the main body were mounted with optically flat glass plates. Rubber gaskets were used between the stainless steel frame (4) and the glass (5) as shown in Figure 36. The whole cell measured 12.7 cm. long, 8.2 cm. wide and 4.8 cm. deep. The test section was 2.5 cm. deep, 0.65 cm. wide and 4.3 cm. from tip to tip. The upper compartment, being shorter, was 1.75 cm. long.

The experimental set-up was arranged as shown in Figure 37. The cell was placed inside the water bath to ensure a constant temperature. A thermostat was used to regulate the temperature. Light beams, from the point source (Sylvania concentrated arc lamp K 25) became parallel after passing through the convex lens (B). The moiré pattern image on the ground glass (F) was photographed using a Pentax camera (H) equipped with close-up extension tube No. 2. The settings on the camera should be f4 and $\frac{1}{2}$ second for plus-x film.

SCHEMATIC DIAGRAM OF THE DIFFUSION CELL

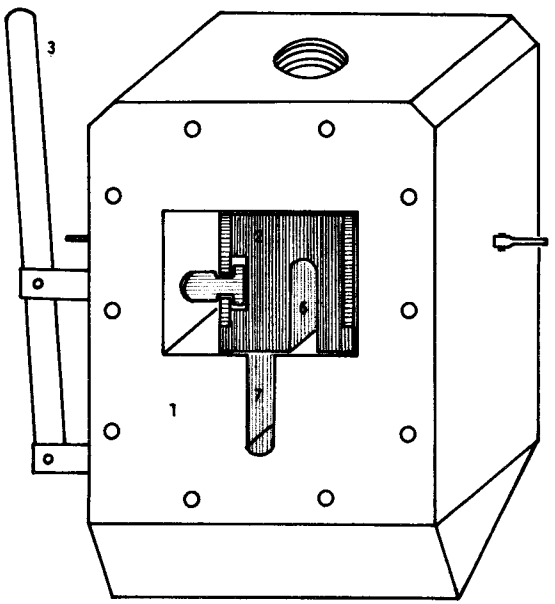

1 Stainless Steel (Type 316) Main Body
2 Teflon Block (Stainless Steel Reinforced)
3 Lever
6 Upper Compartment of the Test Section
7 Lower Compartment of the Test Section

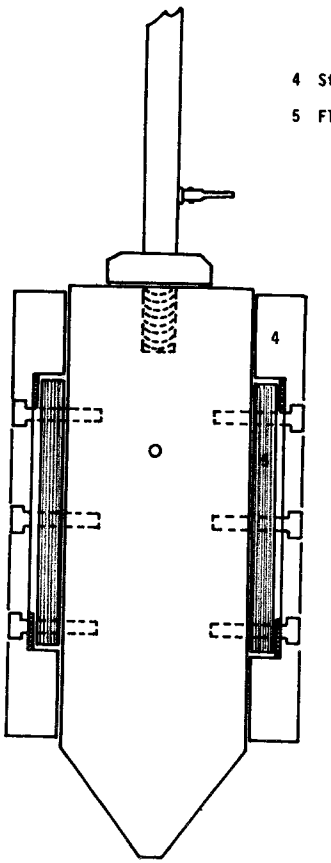

4 Stainless Steel Frame
5 Flat Pyrex Glass Plates

SIDE VIEW OF THE DIFFUSION CELL

FIGURE 36

A Sylvania Concentrated Arc Lamp K25
B Convex Lens
C Glass Windows
D Diffusion Cell
E Moire Plates
F Ground Glass Plate
G Temperature Controller
H Pentax Camera with Close-Up Extension Tube No.2
I Water Bath

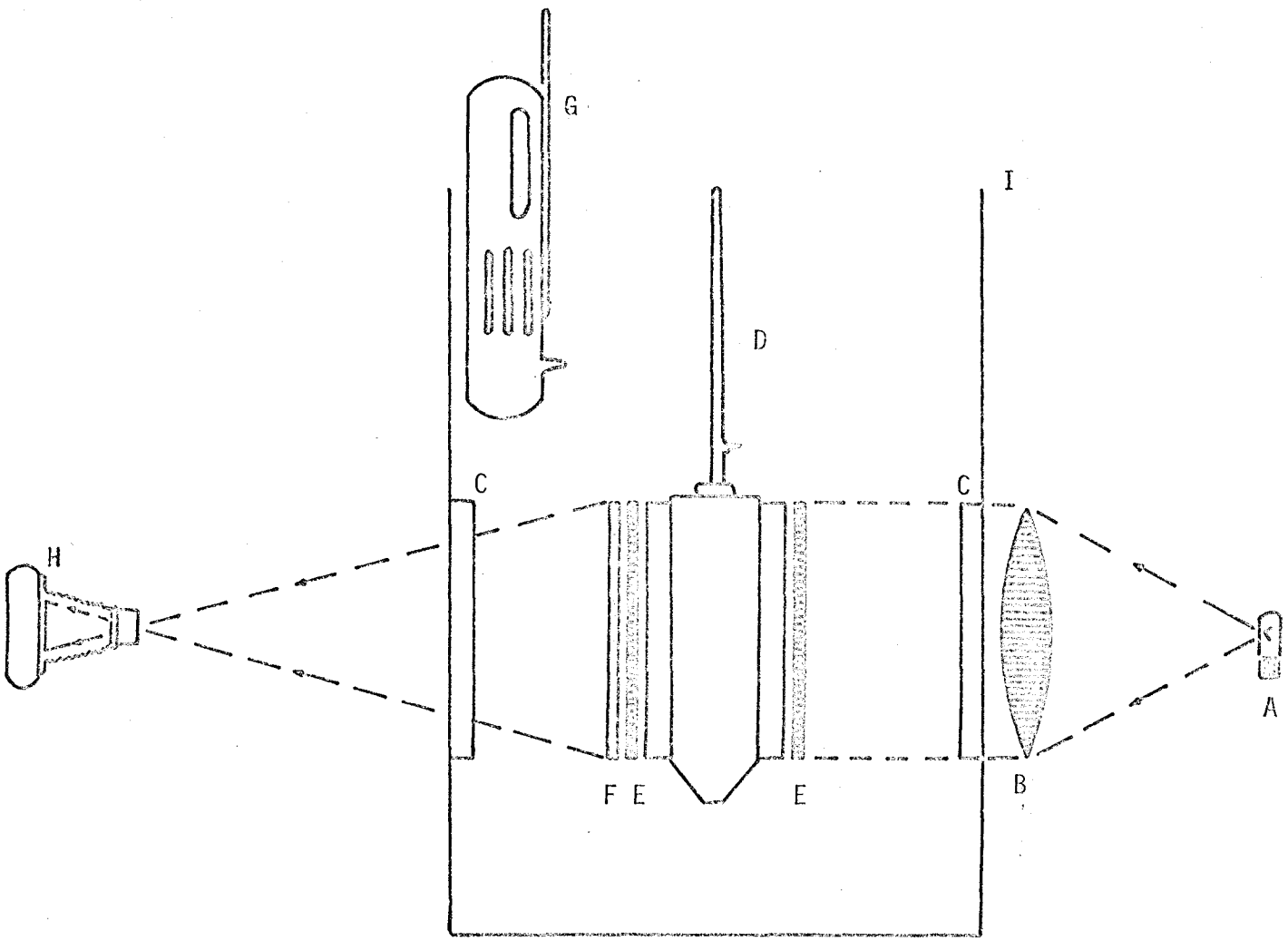

FIGURE 37 THE EXPERIMENTAL SET UP

4.4.1.2 Procedure (with reference to Figure 36)

All parts of the cell were cleaned with soap solution, ethyl acetate, concentrated chromic acid and finally rinsed with distilled water. The parts were then dried in air.

When the cell was already assembled, block (2) was moved to a position in which the upper half of the test section (6) was aligned with the lower half (7). Then, the lower compartment of the test section (7) in block (1) was filled with the solution of a higher density. Block (2) was pushed to the right in order to isolate the two compartments. The upper compartment (6) in block (2) was rinsed and then was filled with the lighter solution through the top opening. The whole cell was placed inside the water bath. Block (2) was then pushed very slowly and steadily to the left using the lever (3). Caution should be taken to avoid inducing a convection current as a result of the drag when moving the block. When the upper compartment was aligned with the lower one, the rest of the space in the main block (1) was filled with the same test solution as for the upper compartment to ensure that no liquid could leak out of the upper compartment (6) during the long period of an experiment. Time t = 0 was noted when half of the upper compartment (6) overlapped the lower one (7). The light source was turned on and pictures were taken at set intervals of time. The film was later developed and magnified over a microfilm reader. The moiré pattern was traced out.

4.4.1.3 Principle of the Moiré Pattern(S2)(07)(R4)(G13)

Theory on the moiré pattern has been treated by Rayleigh in detail(R4). The conversion of the moiré pattern curves into concentration profiles has been discussed by Sato et al.(S2) and later by Le (L2). A very brief qualitative explanation as summarized from Sato's paper is given below:

A glass plate having equidistant parallel lines, 100 lines per inch is put horizontally on one side (the light source side) of the diffusion cell and a similar plate is put on the other side of the cell in such a manner that the two sets of lines intersect with a small angle. When a parallel light beam is cast through the plates and the cell, a family of parallel straight stripes are visible when the solution inside the test cell is uniform: this is the so-called "moiré phenomenon". The stripes will be curved when a concentration gradient exists in the test solution. If the refractive index of the solution is a linear function of concentration, and the displacement of light beam is proportional to the refractive index gradient, as is usually the case, it may be considered that any one of the above-mentioned curved stripes represents the relation $\frac{dC}{dx}$ vs. x.
Upon integration of the area under the curve, the concentration profile can be obtained readily. The diffusion coefficient can be calculated using either equation (17) or (18). For a detailed method of diffusion coefficient calculations, References (S2), (L2) and (S10) should be consulted.

4.4.2 Liquid Systems under Study and the Experimental Results

Preliminary experiments on the measurement of diffusion coefficients were performed with the following one-phase binary liquid systems: sucrose-water, sodium chloride-water, ethyl acetate-water, butyl lactate-water, carbon tetrachloride-benzene and chloroform-benzene. In addition, the reaction systems of ethyl formate-sodium hydroxide and ethyl acetate-sodium hydroxide under one-phase condition were also studied. Results were summarized in a Summer Report (S10). As expected, the ester-caustic systems in the absence of a liquid-liquid interface did not exhibit turbulent layer phenomena (Section 4.1.4.3.1.3).

Further diffusion coefficient measurement runs were carried out with water and methyl formate, methyl acetate, methyl propionate, ethyl formate, ethyl acetate, ethyl propionate, propyl formate respectively. The experiments were semi-quantitative. In general, it was found that the diffusion coefficient versus concentration curves decreased with the increasing order of the member of the methyl-ethyl-propyl homologous series and similarly with the increasing order of the member of the formate-acetate-propionate homologous series.

As an exploratory study, one-phase ternary liquid systems were also investigated. Ethyl acetate diffusing in uniform concentration of aqueous sodium acetate solution and ethyl formate diffusing in uniform concentration of aqueous sodium

formate were individually studied. It was tentatively concluded that for the ethyl acetate diffusing in aqueous sodium acetate solution, the moiré pattern method of determining the diffusion coefficient might be applicable up to 0.05 N of sodium acetate concentration; while for the diffusion of ethyl formate in aqueous sodium formate solution, the method might be applicable up to 0.2 N of the sodium formate concentration. Beyond the concentration limit of the salt, irregular moiré patterns were developed. More experiments must be performed before the moiré pattern method could safely be extended to one-phase ternary liquid systems.

Two-phase ester-caustic systems (such as ethyl acetate-sodium hydroxide and ethyl formate-sodium hydroxide) were also investigated. The turbulent layers developed in these systems were quite thin as compared to those obtained in the optical cell runs (Section 4.1.2). The smaller turbulent layer thickness in the diffusion cell is probably due to the wall effects.

The apparatus was subsequently used by a MastersDegree candidate[L2] of this Department to re-measure the diffusion coefficients of some of the binary liquid systems previously studied[S10]. His preliminary results indicated that such a diffusion cell design was workable. However, the scattering of data could be more than ± 10% of the mean diffusion coefficient values due to the inaccuracy in the drawing and the measuring of moiré lines from the photographs. A typical

é photograph is shown in Figure 38 and a sample of the ..sults on the ethyl acetate-water system is presented in Figure 39.

FIGURE 38

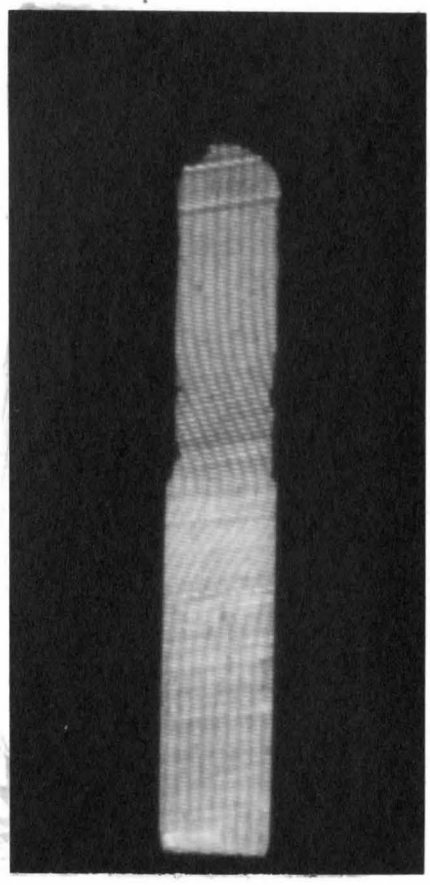

A TYPICAL MOIRÉ PHOTOGRAPH
OF SUCROSE - WATER SYSTEM

FIGURE 39

EFFECT OF CONCENTRATION ON DIFFUSION COEFFICIENT (OBTAINED FROM REFERENCE (L2)) ETHYL ACETATE - WATER SYSTEM, 25°C

PREDICTED VALUE OF D AT INFINITE DILUTION:
0.92×10^{-5} CM^2/SEC. (OTHMER - THAKER)

EXPERIMENTAL $D_{AVG.} = (\int_0^C D\, dC)/C = 0.8 \times 10^{-5}$ CM^2/SEC.

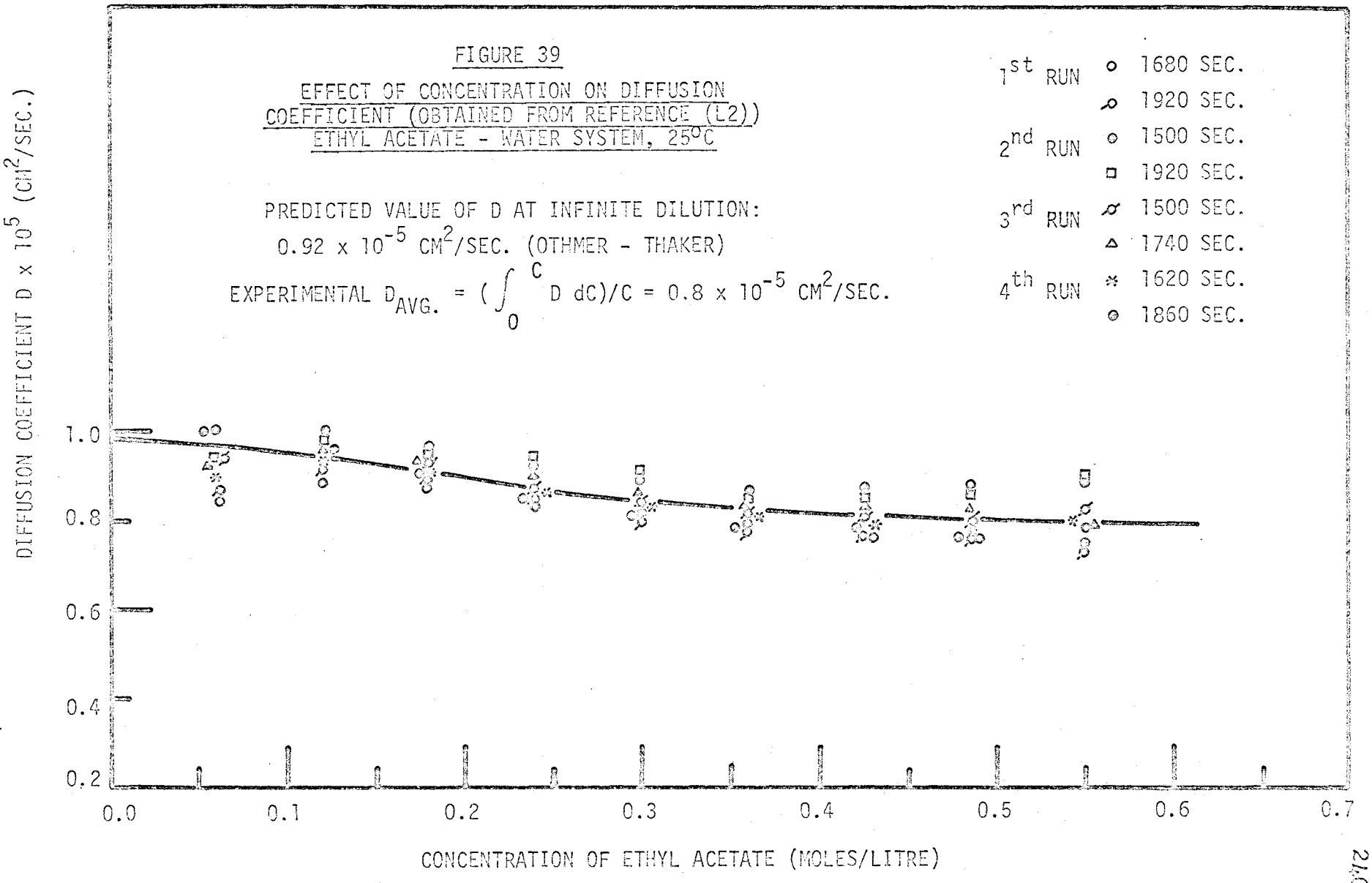

CHAPTER 5

CONCLUSIONS

5.1 Unsteady State Mass Transfer Study (4.1 - PART A and 4.2 - PART B)

A turbulent reaction layer was formed on contact of two stagnant, reactive, partially miscible phases in the ester-aqueous caustic systems with a slow second-order irreversible chemical reaction. The layer thickness (in the aqueous phase) was linearly proportional to the square root of the phase contact time for at least the initial part of each run. The rate of the turbulent layer propagation was a function of the input caustic concentration, the reaction velocity (which governed the amount of reaction products and the heat generated by the reaction), the physical properties of the salt and alcohol released, the solubility of the ester, the density and viscosity of the aqueous phase.

The clear-cut boundary observed between the layer and the bulk sodium hydroxide phase was due to the existence of the abrupt concentration profiles of the reactants and the products at the layer front. The occurrence of the interfacial turbulence was mainly due to the localized variation of the interfacial tension at the liquid-liquid interface. This localized variation was due to the non-uniform distribution of the product alcohol, the heat of reaction and possibly, to

some extent, the heat of solvation. The turbulent liquid motion inside the layer beneath the interface was created by the buoyancy flow of "alcohol-rich liquid pockets" and the "hot liquid" heated up by the heat of the reaction.

At the longer phase contact time of a run, the turbulent layer subdivided into two zones; a turbulent diffusion zone with abnormal component concentration profiles and a reaction zone.

Simulation of the experimental concentration profiles within the turbulent layer (obtained at various caustic concentration levels and phase contact times) of the two ester-caustic systems employing a quasi-steady state transfer with chemical reaction model yielded the values of "mean eddy diffusivity" of the components ranging from 6 to 39 X 10^{-5} cm^2/sec. for the ethyl acetate-sodium hydroxide system and 2.5 to 11 X 10^{-5} cm^2/sec. for the methyl propionate-sodium hydroxide system. Furthermore, the "time averaged mean eddy diffusivity" could be correlated with the layer propagation rate of the same system.

The experimental enhancement factors calculated from the mass transfer data of the ethyl acetate-sodium hydroxide system were two to three times higher than the theoretically predicted ones which were derived from a model based on the transfer with chemical reaction only. Thus the enhancement of mass transfer due to the turbulence alone was slightly higher (but in the same order of magnitude) than that due to reaction for

this system. Despite the similarity in physical properties and the reaction velocities of the two systems under study, the experimental enhancement factors for the methyl propionate-sodium hydroxide system were much lower than the theoretically predicted ones due to the abnormally large physical transfer in the methyl propionate-water system. Consequently, the transfer enhancement due to the turbulence alone could not be estimated in the methyl propionate-caustic system.

The measured reaction zone thicknesses for both ester-caustic systems were comparable with those calculated from a model using the experimental mean eddy diffusivities and mass transfer rates; but were much larger than those calculated from the same model when using the molecular diffusivities and theoretical reaction transfer rates.

5.2 Steady State Mass Transfer Study (4.3 - PART C)

In the steady state mass transfer study of the two-phase ester-caustic systems with both phases stirred, it was found that all three formate-sodium hydroxide systems exhibited, at the higher input caustic concentration range, transfer coefficient enhancement due to reaction. However, the enhancement factors obtained were lower than those predicted from the theoretical model. The purity of the distilled water used for the experiments markedly influenced the absolute rates of inter-phase mass transfer, but not the enhancement of mass transfer coefficient due to chemical reaction. Similar conclusions were applicable to the effect of changing the stirrer's r.p.m., provided that the stirrer speeds for the experiments were high enough to ensure a well-mixed condition in each of the two phases and yet maintaining a stable, plane liquid-liquid interface.

The discrepancy arising between the experimental and the theoretical enhancement factor values were speculated to be due to the following factors:

I . Failure to account for the change of experimental conditions (e.g. the change of density, viscosity and interfacial tension with the sodium hydroxide concentrations) in the theoretical analysis.

II Inaccuracy in the assumption of diffusion coefficient values in the theoretical analysis.

III Modification of hydrodynamic conditions at and near the

interface in the reaction runs. The modification was due to the presence of the product salt and a trace amount of impurities from the reagent grade sodium hydroxide pellets.

CHAPTER 6

RECOMMENDATIONS

6.1 Unsteady State Mass Transfer Study

6.1.1 Further Investigations on the Cause and Nature of the Turbulent Layer in Ester-Aqueous Caustic Systems (4.1 - PART A).

6.1.1.1 Layer Propagation Measurements on more Ester-Caustic Systems

Data on the layer propagation rate should be obtained for more ester-caustic systems with physical and chemical properties different from those systems currently under study.

To investigate the layer propagation of systems with both slow reaction velocities and slow rates of layer propagation (such as the caustic-ethyl propionate system or perhaps, systems consisting of the caustic and one of the esters of the higher members in the homologous series than the ethyl propionate), the optical cell wall should be coated with a thin layer of anti-wetting agent to reduce the thickness of the meniscuses of the interface and the turbulent layer front. These meniscuses show up in the moiré pattern photographs as thick dark bands (Figure 5) and cause errors in the determination of the turbulent layer thickness (with reference to Section 4.1.2.3.1.1). The anti-wetting agent used for the coating should be inert and insoluble in the ester-caustic systems. Previous attempts to coat the cell wall with silicone derivatives,

with a suspension of Teflon particles, and with vinylidene fluoride respectively, gave unsatisfactory results(88).

For systems with fast reactions and fast rates of layer propagation (such as methyl formate-sodium hydroxide system), the present method of contacting the two phases is not suitable (with reference to Section 4.1.2.2.1.1). Perhaps a sliding cell should be constructed. The cell can be similar to that of the diffusion cell (Figure 36: 4.4. - PART D) in design but with the dimensions of the test section similar to that of the optical cell (5 cm. X 5 cm. X 5 cm.) in order to reduce the wall effects.

6.1.1.2 Investigations on the Effects of Salt and Density on the Layer Propagation Rate

Various factors governing the rate of turbulent layer propagation have been studied (Section 4.1.4.3). In those investigations, the salt and density effects are always combined. Experiments should be devised, if possible, to attempt to isolate the effects of salt and density (such as by loading the aqueous phase with a non-ionic compound which will increase the density of the solution but with little or no salt effects).

6.1.1.3 The Effects of Heat of Reaction and Alcohol on the Layer Propagation Rate

The effects of heat and alcohol on the layer propagation rate are difficult to evaluate quantitatively; yet, they are considered to be the major factors contributing to the occurrence of the interfacial turbulence which, in turn, promotes the rate of layer propagation. Qualitative

experiments are proposed to measure the layer propagation of the ester-caustic systems whereby an appropriate amount of aqueous alcohol solution is injected from a syringe (or several syringes) through several hypodermic needles with their outlet tips placed in the vicinity of the turbulent layer front. The alcohol should be injected at a slow, but discontinuous rate - i.e. in small, discrete volumes at short intervals. At the same time, heating elements are placed in the vicinity of the layer front. A small amount of electric current is passed through the elements intermittently. The liquid surrounding the elements will be heated up slightly ($\frac{1}{2}^{o}$C) and ascends to the interface. Such a phenomenon is similar to the reaction run situation whereby pockets of liquid within the turbulent layer are heated up locally by the heat of reaction and ascend to the interface.

6.1.2 Further measurements on the Concentration Distribution within the Turbulent Layer in the Ester-Aqueous Caustic Systems (4.2 - PART B)

6.1.2.1 Concentration Profile Measurements on more Ester-Caustic Systems

Data on the components' concentration distribution within the turbulent layer should be obtained for more ester-caustic systems other than those currently studied. However, the new systems studied with the present experimental set-up should not have too fast rates of layer propagation (with reference to Section 6.1.1.1).

To obtain the concentration distribution in an ester-

caustic system with fast reaction (e.g. ethyl formate-sodium hydroxide system), the existing apparatus or sampling technique should be modified (such as shortening the portion of each sampling needle above the brass supporting plate) in order to reduce the amount of reaction of the liquid sample travelling inside the needle before reaching the syringe to be neutralized. If the experimental set-up is not modified, the amount of liquid sample reacted in the sampling needle should, at least, be calibrated and corrected in the drawing of concentration profiles.

6.1.2.2 Improvement on the Experimental Techniques and the Apparatus to give Better Results

Simultaneous sampling at several key positions within and at the edges of the turbulent layer will yield the concentration profile directly without the tedious processes of extrapolations and cross-plots presently employed (with reference to Section 4.2.1.4). The change to simultaneous sampling will require the modification of the apparatus to accommodate several "sampling devices" (Figure 12). A mechanical instrument will have to be built in order to pull several plungers of the syringes at the same time. Care should be exercised in sampling the appropriate volume of the liquid and at the right time so as to avoid an excessive loss of the liquid in a short time through sampling and cause a sharp drop of the interface. A sufficient time lapse should be allowed for the aqueous phase to replenish its sampling loss

through the transfer of the ester solution across the liquid-liquid interface before the next round of sampling.

Future experiments should be planned with the layer propagation measurement and the concentration probing (by sampling) being performed at the same time.

It would be more convenient if delicate instruments could be devised and inserted into the turbulent layer to measure the concentration of the reactants without sampling. One type of instrument suggested for measuring the sodium hydroxide concentration is an accurate pH meter, capable of recording readings up to 0.01 pH and with a very fine electrode (e.g. Beckman Special model electrode, which has a sensing tip of $\frac{1}{2}$ mm. both in length and in diameter).

6.1.2.3 The Effects of Alcohol and the Heat of Reaction on the Ester Transfer Rate

To estimate, semi-quantitatively, the enhancement of transfer due to turbulence caused by the alcohol alone, experiments may be performed with the ester-aqueous salt solution system. The concentration of the salt in the aqueous solution should be equal to that in the actual experimental reaction run under comparison. As an example, in order to estimate the alcohol effects in the ethyl acetate-1.0 N sodium hydroxide run, alcohol is injected into the ethyl acetate- ~0.85 N sodium acetate system (with reference to Figure 18) in a way similar to that described in Section 6.1.1.3. The rate of injection should be roughly equivalent

to the production rate of alcohol in the ethyl acetate-1.0 N sodium hydroxide run. The concentration profiles of the ester at various phase contact times are measured. The ester transfer rates are calculated and compared with those obtained from the ethyl acetate-water system and the ethyl acetate-1.0 N sodium hydroxide system respectively.

Similarly, following the same procedure as described in Section 6.1.1.3, the effects of heat of reaction on the enhancement of ester transfer can be approximated.

If the abnormally high ester transfer in the ethyl acetate-caustic system is due to the interfacial and layer turbulences which, in turn, are caused mainly by the alcohol and the heat of reaction (with reference to Section 4.2.3.4), then the ester transfer due to diffusion (measured from the ethyl acetate-water system: Figure 20) plus the transfer due to the turbulence created by the presence of alcohol and heat (measured from the aforementioned experiments) plus the transfer due to reaction (theoretically predicted) would be equal to the experimentally measured ester transfer in the ethyl acetate-1.0 N sodium hydroxide system.

6.1.3 Mathematical Modelling

With the accumulated knowledge concerning the cause and nature of the turbulent layer in the ester-caustic systems, theoretical models should be formulated in order to predict the rates of layer propagation, the ester transfer rates and, if possible, the general shapes of the component concentration

profiles in the aqueous phase. Presumably one of the simplest models proposed would be diffusion with reaction with a convective flow of ester across the liquid-liquid phase and a convective flow of liquid in the aqueous phase towards and parallel to the interface at prescribed velocities. Alternatively, a transfer with reaction model should be attempted whereby the interfacial turbulence is visualized as eddies at and near the interface. An optical study (by suspending very fine particles in the liquid system) of the velocity and direction of the ascending pockets of alcohol and "hot liquid" before and after hitting the interface from experiments described in Section 6.1.1.3 may cast some enlightenment on prescribing the magnitude and direction of the convective flows or the eddies in the models. In addition, the following references may be helpful in the formulation of theoretical models, (R11)(F1)(S29).

6.2 Steady State Mass Transfer Study (4.3 - PART C)

6.2.1 Extension of the Present Experimental Work

It is evident that much work is left to be done in order to fully understand the factors governing the discrepancy between the theoretical and the experimental enhancement factors as observed in the formate-caustic systems in the steady state transfer experiments. All the possible factors speculated in Section 4.3.3.2.4 should be checked out by further experiments.

In addition, physical and reaction mass transfer experiments should be performed with esters of the higher members or the branched members of the homologous series. Also, transfer experiments should be performed with other kinds of alkaline solutions (e.g. potassium hydroxide) as the lower phase. Some runs should be performed with purified sodium hydroxide(P8). All these experiments will help to reveal the importance of ester solubility, reaction rate, steric effects of the molecules and the contaminants to the steady state interphase ester transfer.

Experiments may be repeated with the same formate-caustic systems studied but using other types of apparatus (with the appropriate theoretical analyses, of course) such as the wetted-wall column or liquid-liquid laminer jet etc. These apparatus have the advantages of studying the unsteady state transfer in short contact time and under well-defined hydrodynamic conditions. The continuous surface renewal will eliminate or minimize the accumulation of impurities and the

adsorption of the salt at the interface.

6.2.2 Analysis of Data using Other Theoretical Models

In view of the discrepancy of enhancement factors existing between the experimental and the theoretical analyses (using the film model), it is proposed that part of the experimental data be re-analysed, using a model of transfer accompanied by fast pseudo-first-order reaction(D1)(N1)(V1). Due to the high solubilities of esters in the aqueous solution in both the ethyl formate-sodium hydroxide and the methyl formate-sodium hydroxide systems, the pseudo-first-order reaction model is not suitable for these two systems except at very high caustic concentrations. On the other hand, the model may be applicable to the analysis of data in the propyl formate-sodium hydroxide because of the limited solubility of the propyl ester in the aqueous solution.

In addition, the feasibility of using models other than the film model to analyse the present experimental data should, perhaps, be investigated. The models to be employed should describe the actual experimental conditions more realistically such as taking into account the following:

I. The change of the physical properties of the systems with increasing caustic concentration levels. (The change of physical properties will affect the component diffusion coefficients and the hydrodynamic conditions.)

II. Turbulent liquid motion right up to the interface.

6.3 Measurement of the Liquid Diffusion Coefficients (4.4 - PART D)

6.3.1 Improvement on the Present Existing Apparatus (With reference to Figure 36)

6.3.1.1 Modification of the Apparatus to Minimize Liquid Leakages

After loading the separate compartments of the diffusion cell with the test liquids (but before the two compartments were aligned to start the diffusion run), a minute amount of the liquid from the upper compartment was observed to creep through the imperfect contact between the Teflon block (2) and the glass plate and run into the space in the main body (1). Another leak, though very minor, was also observed between the bottom-end of the Teflon block (2) and the stainless steel main body (1). These leakages will undoubtedly cause errors in the diffusion coefficient measurements and should be remedied by the four modifications to the apparatus proposed in the following:

I. The stainless steel main-body (1) can be replaced with a Teflon one reinforced by a stainless steel structure. This modification will provide a tighter seal against the leakage of the liquids from the test section.

II. Pressure should be applied on top of the Teflon block (2) so as to minimize the leakage of the liquid from the upper compartment (6) into the lower compartment (7) when filling the upper compartment for a diffusion run.

The pressure application can be achieved by fitting a spring device between the top of the Teflon block (2) and the main body (1) as sketched in Figure 40.

III. The rectangular space in the stainless steel main body (1) should be lengthened slightly on the right side so that the Teflon block (2) may be pushed further to the right side during the filling period of the test solutions. The increase in distance between the two compartments should reduce the leakage of the liquid from the upper compartment into the lower compartment before the start of the diffusion run.

IV. Both sides of the Teflon block (2) should have the types of surfaces sketched in Figure 40. Surface "A" is indented. The tight contact between surface "B" and the glass plates will further prevent the leakage of the liquid from the upper compartment.

6.3.1.2 Modification of the Apparatus to Provide a Better Way of Filling the Test Solutions

In order to facilitate the filling of the test solutions in separate compartments and also to avoid the unnecessary rinsing of the upper compartment, additional holes of small diameters may be drilled as sketched in Figure 41.

6.3.2 Improvement on the Analysis of Data

Errors in the measurement of diffusion coefficients are introduced due to the inaccuracy in the tracing and the measuring of the moiré curves from the photographs (with reference to Section 4.4.1.2). In order to minimize such

FIGURE 40

A. SURFACE A (INDENTED)
B. SURFACE B
C. SPRING DEVICE

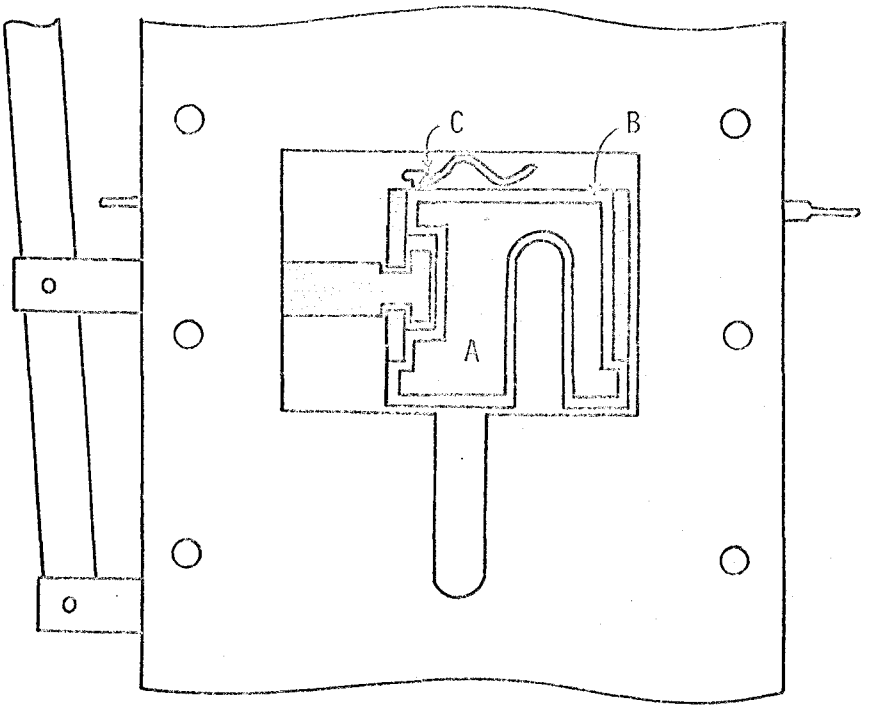

FIGURE 41

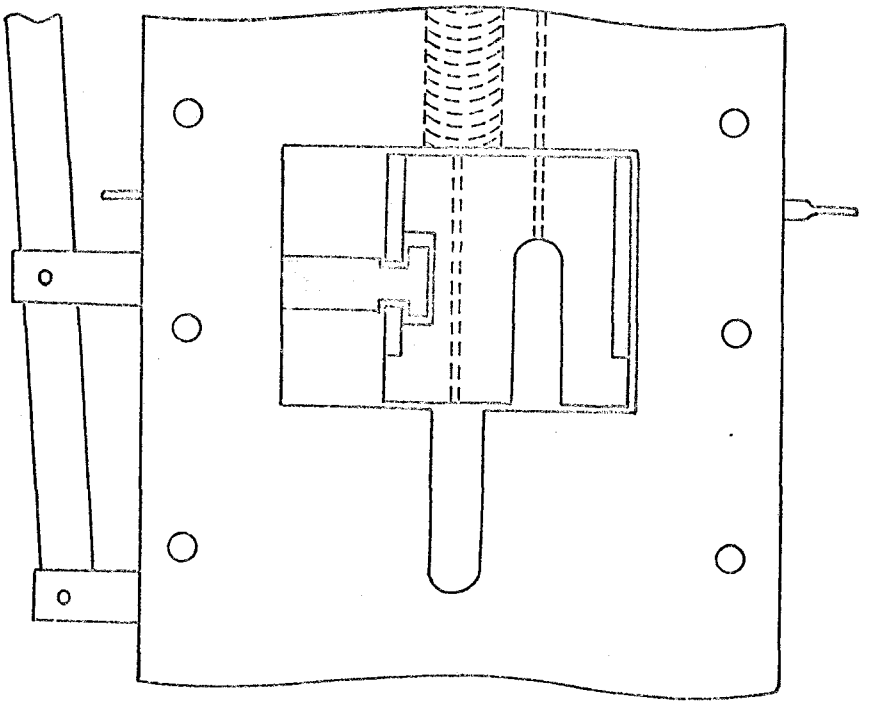

PROPOSED MODIFICATIONS OF THE DIFFUSION CELL (WITH REFERENCE TO FIGURE 36)

errors, the thickness of the moiré lines must be reduced. This reduction can be achieved, to some extent, by increasing the angle of the intersection of the two moiré glass plates. Further refinement of the moiré lines can only be achieved by reducing the spacing between the successive lines in the moiré glass plates.

6.3.3 Extension of the Present Experimental Systems

A variety of one-phase binary liquid systems should be investigated in order to test the limitations of the cell and the moiré pattern method for the determination of diffusion coefficients.

The diffusion measurement in one-phase ternary systems (similar to the diffusion of ethyl ester in aqueous salt solution as described in Section 4.4.2) should be further explored.

The diffusion measurement in two-phase ternary systems (similar to the diffusion of acetic acid across the water-toluene interface as described by S. Hoshino et al.[H15]) should also be investigated.

CHAPTER 7

SUMMARY OF CONTRIBUTIONS TO KNOWLEDGE

Simultaneous mass transfer and chemical reaction at a plane liquid-liquid interface involving the saponification of simple esters transferring into aqueous caustic solutions have been investigated.

In the unsteady state transfer study, the cause and nature of the turbulent reaction layer formed on contact of two stagnant phases have been elucidated. Measurements of the initial layer growth rate on various ester-caustic systems and at different caustic concentration levels were obtained. Various contributing factors to the rate of layer propagation were determined. An apparatus was constructed and experimental techniques were developed to probe the concentration distribution of the reactants and the products in the systems with slow chemical reaction velocities as well as to measure the concentration profiles in the two-phase physical transfer systems. The sampling techniques developed were checked out by the close agreement between the theoretical and the measured concentration profiles of n-butanol in water in the two-phase binary liquid system. Concentration distribution data of individual components in two ester-aqueous caustic systems were obtained at various phase contact times and at caustic concentration levels ranging

from 0 to 1.4 N. From these concentration profiles, ester transfer rates, enhancement factors, turbulent layer thicknesses and reaction zone thicknesses were derived for each system. A quasi-steady state transfer-with-reaction model was employed for the simulation of the experimental concentration profiles. The eddy diffusivities of the components obtained from the simulation studies were correlated with the layer propagation rate of the same system. The magnitude of the enhancement of mass transfer due to turbulence alone as compared to that due to reaction was estimated in terms of enhancement factors for the ethyl acetate-sodium hydroxide system.

In the steady state transfer study using stirring in both phases, transfer rate data and enhancement factor data were obtained for three formate-sodium hydroxide systems at various caustic concentration levels. The effects of the stirring rate and the impurities from distilled water on the transfer rates and the enhancement factors in a system were also investigated.

In addition to the mass transfer studies, a diffusion cell was designed and built to enable the quick experimental measurements of binary diffusion coefficients and possibly ternary diffusion coefficients as a function of concentration in liquid-liquid and gas-liquid systems with reasonable accuracy. The apparatus was so designed as to adopt the moiré pattern method for the determination of diffusion coefficients.

APPENDIX I

THE CHEMICALS USED IN THE EXPERIMENTS

The following descriptions refer to the chemicals and water used in the turbulent layer (PARTS A & B), diffusion coefficient (PART D), and the semi-continuous mass transfer (PART C) experiments. The salts were used for the measurement of ester solubilities in aqueous salt solutions (Appendix XIII).

I.1 Esters

Ethyl acetate

Baker analysed reagent

F.W. 88.11 $CH_3COOC_2H_5$

Density: 0.893 gm/ml at 25°C

Boiling range: 77.1 to 77.3°C

Ethyl formate

Baker analysed reagent

F.W. 74.081 $HCOOC_2H_5$

Density: 0.917 gm/ml at 25°C

Ethyl propionate

Eastman Organic Chemicals Company Cat. No. 125

F.W. 102.14 $CH_3CH_2COOC_2H_5$

Methyl formate

Eastman Organic Chemicals Company Cat. No. S1227, spectro grade.

F.W. 60.05 $HCOOCH_3$

Methyl acetate

B.D.H. Laboratory reagent grade

F.W. 74.08 CH_3COOCH_3

Density: 0.929 to 0.933 gm/ml at 20°C

Assay: not less than 97%

Methyl propionate

Eastman Organic Chemicals Company Cat. No. 746.

F.W. 88.11 $CH_3CH_2COOCH_3$

Propyl formate

Eastman Organic Chemicals Company Cat. No. 1419

F.W. 88.11 $HCOOCH_2CH_2CH_3$

Redistilled esters

The batchwise apparatus for the purification of the esters was as shown in Figure I.1.

Approximately 4½ litres of the fresh ester were put into a 5-litre round bottom flask surrounded by two Glas-col hemispherical heating mantles. Fractionation was done in a 32-inch long column packed with a mixture of small glass beads and glass raschig rings. The column was equipped with a nichrome wire heating coil. Both the pot and the column were electrically heated and the power supply was regulated by powerstats. The ester vapor overhead was cooled by a cold-finger type condenser.

During the purification, the column was operated at a temperature which was a little above the boiling point of the ester. Reflux ratio of 1:1 was used until the ester vapor at constant boiling temperature was obtained. Zero external reflux was then used. The distillation was continued until the ester vapor temperature was ½°C above the normal boiling temperature of

FIGURE I.1

APPARATUS FOR THE DISTILLATION OF THE ESTERS

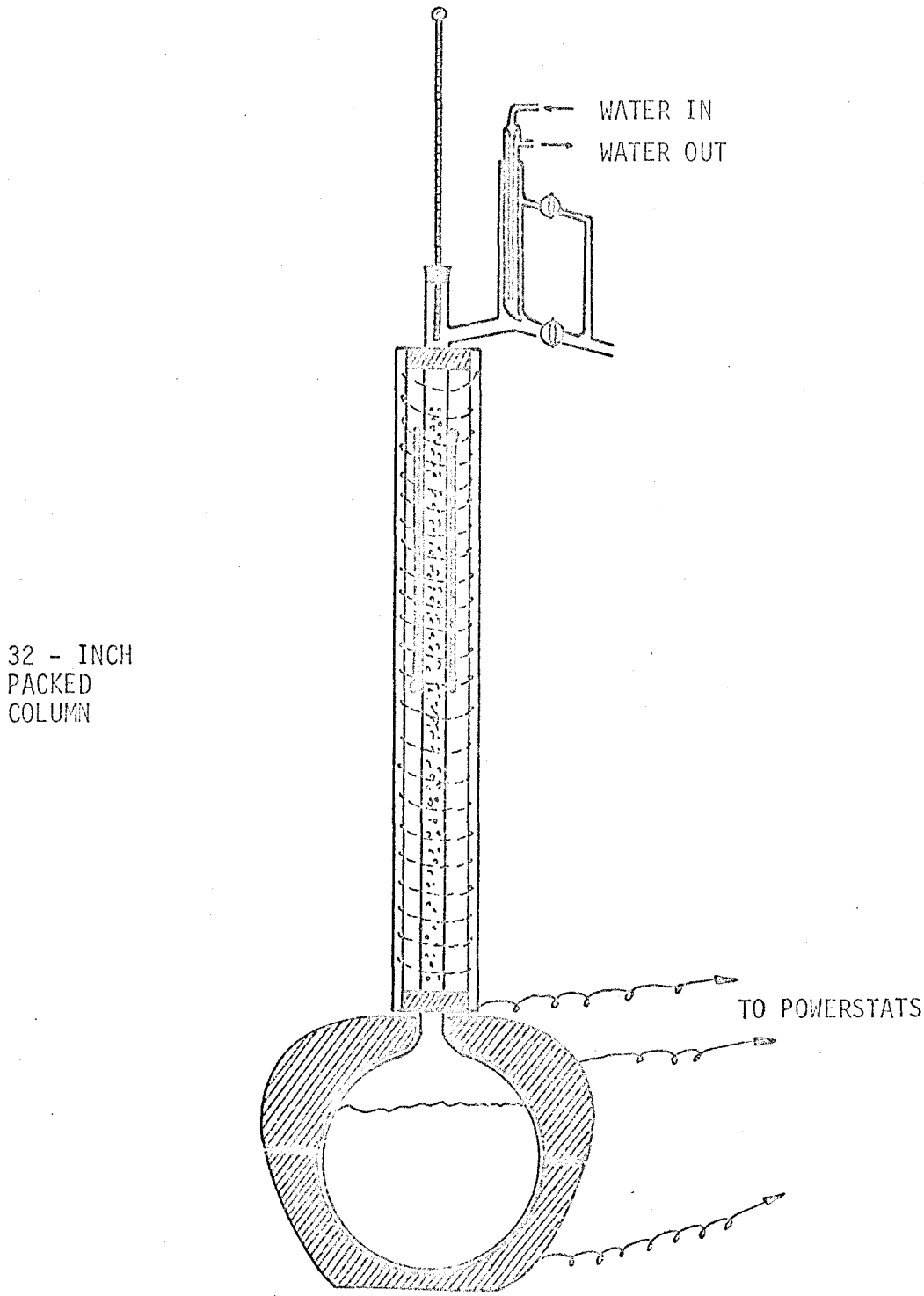

its pure form.

I.2 Caustic

Sodium hydroxide pellets

Fisher certified, A.C.S.

F.W. 39.999 NaOH

Potassium hydroxide pellets

Fisher certified, A.C.S.

F.W. 56.108 KOH

I.3 Salts

Sodium formate

Fisher certified

F.W. 68.01 HCOONa

Sodium acetate

Fisher certified, fused anhydrous

F.W. 82.037 CH_3COONa

Sodium propionate

Fisher FF

F.W. 96.064 C_2H_5COONa

I.4 n-Butanol

n-Butanol used for the physical mass transfer experiments was supplied by Fisher Scientific Co. with the following specifications:

Fisher certified A.C.S. Cat. No. A-399

F.W. 74.12 $CH_3CH_2CH_2CH_2OH$

Boiling range 117.4 to 117.9°C.

The certified grade butanol was redistilled in a 24-inch long

packed column before using.

I.5 Water

Distilled water supplied from the central system of the building was re-distilled continuously through a Corning all pyrex glass water still (model No. AG-2). Output from the water still was stored in a 20-litre pyrex bottle with a Teflon-plug stopcock at the bottom.

APPENDIX II

SAMPLE CALCULATION OF THE MEASUREMENT OF LAYER PROPAGATION

The following sample calculation refers to the measurement of the turbulent layer thickness as a function of the phase contact time in a typical run of an ester-caustic system (4.1 - PART A: SECTION 4.1.2). Photographs of the turbulent layer, taken at intervals during the run, were enlarged. The layer thicknesses were measured.

Data for the calculation were taken from Run No. 6.

System: Methyl acetate - 0.407 N sodium hydroxide.

Temperature: $24 \pm 1^{\circ}C$

Photograph No. 3 was taken at 6.0 minutes; the three measurements of the layer thickness were 4.0, 4.4 and 4.3 cm. respectively

The internal width of the cell = 4.82 cm.

The width of the cell when projected onto the wall for measurement = 55.0 cm.

$\therefore$ The magnification factor = $\frac{55.0}{4.82} = 11.41$

The error analysis on the layer thickness measurement was performed using a method similar to that shown in Appendix VII.

$\therefore$ The actual thickness of the layer:

$$4.0 \pm .05 \times \frac{4.82 \pm .01}{55.0 \pm .05} = .351 \pm .004 \text{ cm.}$$

$$4.4 \pm .05 \times \frac{4.82 \pm .01}{55.0 \pm .05} = .386 \pm .004 \text{ cm.}$$

$$4.3 \pm .05 \times \frac{4.82 \pm .01}{55.0 \pm .05} = .377 \pm .004 \text{ cm.}$$

$\therefore$ Average layer thickness = .371 $\pm$ .004 cm.

$\therefore$ Square of the average layer thickness = .138 $\pm$ .003 $cm.^2$

Data of Run No. 6 after converted back to actual layer thicknesses are given in Table II.1.

TABLE II.1

Experimental Data: Measurement of Turbulent Layer Propagation

Run #6

Upper phase: methyl acetate saturated with water

Lower phase: 0.407 N NaOH

Temperature: 24 ± 1°C

Picture No.	Time (minutes)	Layer thickness measurement No. 1 (cm)	Layer thickness measurement No. 2 (cm)	Layer thickness measurement No. 3 (cm)	Average Layer thickness (cm)	(Average Layer thickness)^2 (cm)^2
1	1.0	.123	.105	.105	.111	.012
2	3.2	.307	.307	.307	.307	.094
3	6.0	.351	.386	.377	.371	.138
4	10.0	.473	.482	.526	.494	.244
5	17.5	.701	.745	.701	.716	.513
6	25.0	.938	.920	.964	.941	.885
7	32.0	1.052	1.139	1.139	1.110	1.232
8	40.0	1.227	1.227	1.227	1.227	1.505
9	50.0	1.358	1.358	1.446	1.387	1.924
10	65.0	1.577	1.525	1.542	1.548	2.396
11	83.0	1.665	1.753	1.709	1.709	2.921
12	97.0	1.797	1.884	1.849	1.843	3.397
13	183.0	1.884	2.016	1.928	1.943	3.775

APPENDIX III

DETAILED DESCRIPTION OF THE APPARATUS

III.1 Qualitative and Quantitative Investigations of the Turbulent Layer in the Ester-Caustic Systems

III.1.1 The Phase Contactor (or the Caustic Delivery Tube)

The phase contactor was made out of the design and dimensions shown in Figure III.1. The reservoir of the phase contactor had a capacity of 100 ml. When filling the reservoir, the sintered glass disc portion was lowered into the sodium hydroxide solution. The stopcock (1) was turned to the pipette filler side (a) and the sodium hydroxide was drawn up until the liquid level reached the prescribed mark. When the contactor was used to fill the optical cell, the stopcock (1) was turned to the capillary tube side (b). The capillary tube would control the intake of air into the reservoir (which, in turn, would control the flowrate of sodium hydroxide solution into the optical cell).

If, for every experiment, the initial sodium hydroxide level in the phase contactor was the same, then the filling rate of the lower phase (and thus the same degree of phase contact mixing) could be reproduced quite closely despite the slight variation of density of the caustic solutions at different concentration levels. The spherical reservoir was so designed that a large decrease in liquid volume would result in only a slight decrease in the liquid hydrostatic level and at the same time a minimum surface area for heat transfer was provided.

FIGURE III.1

THE CAUSTIC DELIVERY TUBE

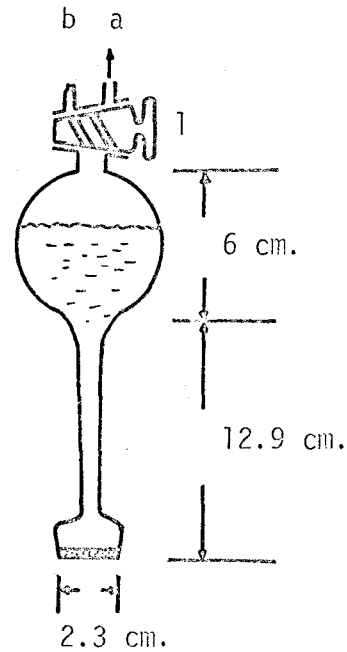

1 Stopcock

a Connected to a Pipette Filter when loading the Caustic Solution

b Capillary Tube

III.2 Measurement of Concentration Distribution in the Turbulent Layer

III.2.1 The test cell (with reference to Figure III.2)

In order to minimize the errors arising from sampling loss, a rather large cell was used for the experiment. The dimensions of the cell were so chosen that for a normal reaction run the volume of liquid loss in the lower phase due to sampling as well as due to back transfer of the alcohol to the upper phase would be compensated by the volume increase in the lower phase as a result of the ester transferred from the upper phase. The cell was made of pyrex glass having an inside diameter of 21.2 cm. and measured 7 cm. from bottom to top. The mid bottom of the cell was made of fritted glass disc (pyrex coarse grade) through which the lower aqueous phase could be introduced into the cell. The sintered glass disc was 9 cm. in diameter. The bottom of the disc was connected with a piece of 9 mm. tubing extending downwards to about 4 cm. long with a female ball joint at the end.

III.2.2 The Hypodermic Sampling Needles and the Supporting Plate

The 0.51 cm. thick circular brass plate was made to cover the top of the cell. A circular groove of 0.24 cm. deep and having the exact diameter of the cell was machined at the bottom surface of the plate. When the plate was placed on top of the cell, the groove would fit the rim of the cell and cover it tightly, thus eliminating the evaporation

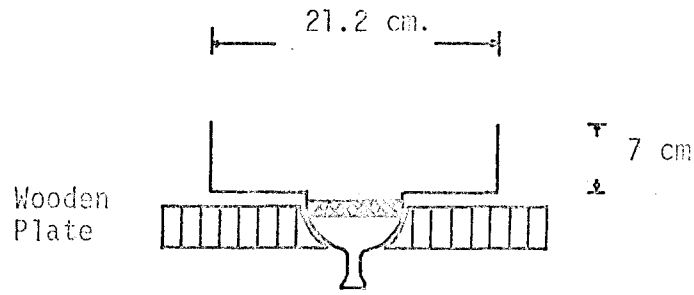

FIGURE III.2

CROSS-SECTION OF THE TEST CELL AND
THE SUPPORTING WOODEN PLATE

of the upper phase. Two brass rods were soft-soldered to the side of the plate for easy handling. The attachment of the rods would also facilitate the fastening of the plate to the tripod stand as shown in Figure 11.

Sixteen holes of 0.4 cm. in diameter were drilled through the plate in the pattern as shown in Figure III.3. The holes were then threaded. In each of fifteen of the holes, a sampling tube was inserted. The sampling tube was made of stainless steel tubing, type 316, 0.028-inch O.D. A pre-measured length of the tube was passed through and silver-soldered to the middle of a bolt which, in turn, was screwed into the hole in the plate. After the needle together with the bolt had been screwed to the desirable position, the bolt was soft-soldered to the plate as shown in Figure 12. The top end of the stainless steel tube was connected with, and silver-soldered to, a No. 18 B-D hypodermic needle, on top of which a B-D spring loaded stopcock (MS09) was fitted. The height of each needle above the plate was made the same. The bottom ends of the stainless steel needles were bent 90°, so that liquid samples could be sucked in horizontally. The directions of all the needle inlets were so oriented that maximum distance could be obtained between any two sampling inlets (Figure III.3). The last (the sixteenth) hole was fitted with a solid stainless steel rod 0.16 cm. in diameter. The rod, having a sharp point at the lower end, was used as a gauge to indicate the location of the liquid-liquid interface.

FIGURE III.3

SAMPLING NEEDLES ARRANGEMENT

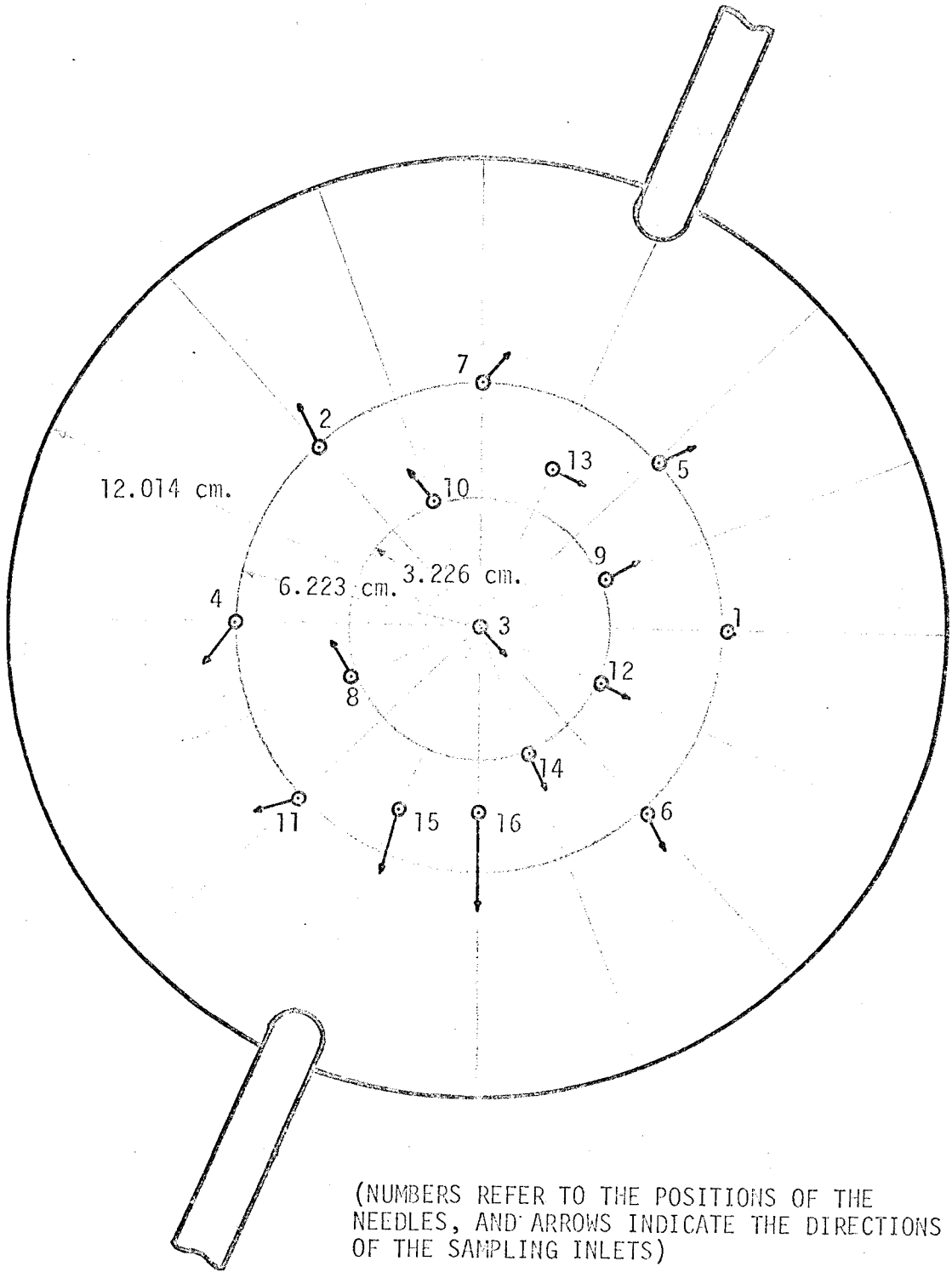

(NUMBERS REFER TO THE POSITIONS OF THE NEEDLES, AND ARROWS INDICATE THE DIRECTIONS OF THE SAMPLING INLETS)

III.2.3 The Tripod Stand (with reference to Figure 11)

The cell was rested on a wooden plate which had an opening in the centre in order to accommodate the bottom part of the cell. The plate, in turn, was supported by a tripod iron frame bolted tightly to the floor of the building. The brass needle supporting plate was fastened to the tripod frame by two clamps.

The cell, the plate, and the frame were detached from the rest of the experimental setup so that any vibrational disturbances created by the mechanical movement on the table would not be transmitted to the system under test.

III.2.4 The Sampling Device (Numbers in the following description refer to Figure 12. In addition, Figure 11 should also be consulted whenever necessary.)

The main function of this device was to create mixing between a liquid sample and a known amount of hydrochloric acid, so that any residual sodium hydroxide in the sample was immediately neutralized and the saponification reaction was thus halted. The liquid sample was sucked through the sampling tube into a syringe already containing a known amount of hydrochloric acid. The mixing inside the syringe was produced by a small stirring magnet bar coated with Teflon (3). Dimensions of the bar were $1/8$ X $1/8$ X $3/8$ inches. Motion of the stirrer was induced by another two large rotating magnets (2) housed in a donut shaped Lucite block (8) and in the direction opposite to each other. In the centre

opening of the block, part of the inside wall of the "Lucite donut" was tightly fitted to the outer rim of an SKF (No. 6905 LC) ball bearing (6). The inner wall of the ball bearing was, in turn, tightly attached to a brass cylindrical sleeve (7). A groove was machined around the circumference of the Lucite block, so that an O ring (1) could be installed to connect the block to a variable speed motor. In this way, the Lucite donut with its two magnets could be revolved freely while the brass sleeve in the middle of the donut was fixed. During the sampling, the B-D Cornwall syringe was inserted through the stationary brass sleeve and connected to the spring-loaded stopcock attached on top of the sampling needle. The Teflon-coated stirrer revolving inside the syringe would provide vigorous mixing of liquids. The whole sampling device was mounted on a frame which could be moved horizontally on the table with ease as to facilitate the sampling from needle to needle. The legs of the frame were cushioned with soft rubber to absorb most of the mechanical vibration from the electric motor.

III.2.5 The "Cornwall" syringe (Numbers in the following description refer to Figure 11)

During sampling, in order to obtain a representative sample from a concentrated small region surrounding the needle inlet rather than from a wide area, the liquid must be sucked in very slowly and over a fairly long period of time. A Cornwall syringe nicely served such a purpose.

By controlling the rate of unscrewing the nut (1) on top of the metal cover, the spring-loaded plunger would lift up very slowly and steadily, sucking liquid into the syringe. Because the plunger was spring-loaded, the plunger would not sag down at all due to gravity force even if it were unattended; thus eliminating the danger of pushing the liquid already inside the sampling needle back to the cell and causing local mixing and the associated effects.

APPENDIX IV

EXPERIMENTAL DETAILS FOR THE MEASUREMENT OF CONCENTRATION DISTRIBUTION IN THE TURBULENT LAYER

IV.1 Preparatory Procedure for the Reaction Runs

IV.1.1 Preparation of the Two Reacting Phases

Sodium hydroxide solution of prescribed normality was freshly prepared for each run by dissolving a weighed amount of the certified grade pellets in double distilled water. Two samples were taken from each batch in order to determine the exact normality of the prepared solution. The solution was then allowed to stand until it was cooled down to room temperature. It was then poured into the reservoir (Figure 11), ready for use.

Ester, freshly distilled in a 32-inch packed column (Appendix I), was shaken vigorously with double distilled water for ten minutes in room temperature. The mixture was allowed to settle. The water-saturated ester phase was separated from the water phase by decantation.

IV.1.2 Measurement of Needle Inlets Positions

Before starting a run, the sampling needles together with the supporting brass plate were thoroughly cleaned with concentrated chromic acid, double distilled water, and then allowed to dry. The plate was put on a special tripod stand as shown in Figure IV.1. The legs of the tripod were adjusted until the brass plate was suspended horizontally as indicated by two levellers temporarily attached on top of the plate.

FIGURE IV.1

TRIPOD STAND FOR MEASURING THE
SAMPLING NEEDLE INLET POSITIONS

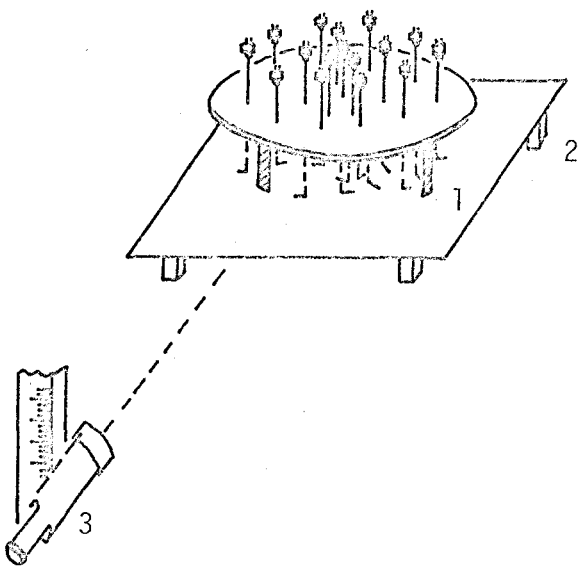

1 3 Legs to support the Needles and Plates

2 Adjustable Legs for Levelling

3 Cathetometer

The levellers were placed perpendicular to each other. Not all of the 15 sample needles were used for every run, as will be described later in Section IV.2. B-D spring-loaded stopcocks (MS09), pre-cleaned with ethyl acetate, chromic acid and distilled water, were adapted only to those needles used for the particular run. The vertical distance of each needle inlet with respect to the sharp tip of the point gauge was measured using a cathetometer.

IV.1.3 Preparation of the Sampling Tubes as well as the Syringes

About 25 sampling tubes (pyrex No. 7090) were cleaned and dried. The tubes were approximately 40 ml. in capacity and were provided with screw caps. To each tube, exactly 15 ml. of double-distilled water together with one drop of controlled volume of phenolphthalein were added. The tube was then tightly capped and stored in the ice bath.

The ice bath was a rectangular container made of galvanized iron sheet and measured 7 inches wide, 48 inches long, 5 inches high, with an outlet installed at the bottom of the bath for the drainage of melted ice. The bath was housed in a wooden box with insulating foam all around the sides and the bottom. The top of the bath was covered by a piece of wood with 48 holes arranged in four columns and twelve rows. The diameter of the holes was 1 inch. The sampling tubes were inserted through the holes with the screw cap parts above the wooden cover; while the lower three-quarters

of the tubes with samples inside were immersed in the ice water mixture.

Four to five Cornwall syringes were used for each experiment. Before each experiment, the syringes were dismantled and cleaned. The graduated scale on each syringe was calibrated separately against a known volume of water measured from a burette (Appendix VII). The volume of each Teflon stirring bar in each syringe was also accounted for during calibrations. Standard hydrochloric acid solutions were prepared at two concentration levels. One solution was ten times more concentrated than the other. Normally, known volumes (1.87 ml.) of the dilute hydrochloric acid solution were used to load the first three syringes which were used for sampling in locations inside the turbulent layer. On the other hand, the same amount of the more concentrated hydrochloric acid solution was used to load each of the other two syringes which were used for sampling in locations in the vicinity or beyond the reaction zone front.

IV.2 Concentration Probing Procedure for the Reaction Runs

(Numbers in the following description refer to Figure 11. A detailed description of the apparatus is given in Appendix III)

The test cell, cleaned with concentrated chromic acid and thoroughly rinsed with double-distilled water, was placed in a preset position and supported by the wooden plate (9). The cell was then connected to the feed tube which was made of 9 mm. pyrex glass. The stopcock (10) was turned on and a

small amount of the sodium hydroxide solution from the reservoir (8) was fed through the sintered glass disc into the cell. The stopcock (10) was then turned off and the sodium hydroxide solution in the cell above the disc was sucked off by a clean Teflon tube connected to a water aspirator. The filling and sucking process was repeated five times to make sure that both the air and water trapped inside the pores of the sintered glass disc as well as the feed line were cleared out.

Then 500 ml. of water-saturated ester was gently poured into the cell along the wall. Direct pouring of ester onto the sintered disc area was carefully avoided to ensure minimum mechanical mixing of the two contacting phases. The brass plate holding the needles was put on top and covered up the cell quite tightly. The plate was fastened to the tripod stand by means of two clamps (11) which were also used to adjust it to a perfectly horizontal position. The distance of the tip of the point gauge from the bottom of the cell was carefully checked using the cathetometer for each run. B-D stopcocks (5), fitted on top of those needles chosen for sampling in the particular run, were closed so that neither ester nor caustic solution could get into the needles while the cell was in the process of being filled up.

The stopcock (10) was then opened and the timer was started. The sodium hydroxide solution was fed into the cell in three stages, each at controlled flowrates. For the first four minutes, the flowrate was set at 0.042 litres/minute

by means of adjusting the stopcock (10). For the next five minutes, the flowrate was set at 0.166 litres/minute. Finally, it was adjusted to 0.187 litres/minute until the ester-aqueous sodium hydroxide interface just touched the tip of the point gauge. The total filling time was approximately fourteen minutes. The relatively low flowrate used at the beginning was essential in order to reduce the mechanical mixing of liquids during the initial contact of the two phases. In the meantime, the sampling device was put into position and the motor was turned on. The speed of the motor was adjusted by a variac.

When taking a sample, a Cornwall syringe (1), prefilled with a known amount of standard hydrochloric acid solution was inserted through the brass sleeve of the sampling device (the sampling device is shown in Figure 12) and twist locked to the B-D stopcock (5). The nut on top of the syringe was screwed in a counter-clockwise direction for one revolution, thus causing the plunger to lift a short distance upward and create a small suction inside the syringe. When the B-D stopcock was opened, the negative pressure inside the syringe would ensure that no hydrochloric acid could be forced out of the sampling system. About 1.2 ml. to 1.5 ml. of the sample (later accurately measured) was drawn in steadily over a period of roughly two minutes. Vigorous mixing inside the syringe was created by the Teflon magnetic stirrer, and any unreacted sodium hydroxide present inside the sample was

immediately neutralized by excess hydrochloric acid. After the desired volume of sample was obtained, stopcock (5) was closed. The exact volume of the sample obtained was read from the graduated scale (calibrated; Appendix VII) on the syringe. The time was noted before and after the sampling, and the average of these two times was considered as the time at which the sample was taken. The sample from the syringe was then transferred to a pyrex No. 7090 sample tube and stoppered. The sample was intimately mixed with 15 ml. of ice-cold distilled water to slow down the hydrolysis rate. The sample tube was then stored in the ice bath. The syringe was then rinsed several times with double-distilled water, two to three times with standard hydrochloric acid solution of the same normality as the one used for sampling. The syringe was then filled with the pre-determined amount of hydrochloric acid again and was ready for the next sampling.

Each experiment was allowed to run up to about 90 minutes after the phase contact. Usually, about 20 samples were taken for each run. Five samples were taken from each needle at various contact times. One sample was taken at a time. Samples were taken consecutively from the chosen set of needles until each needle had been sampled once. Then the next cycle of sampling was repeated. At the end of the experiment, both the brass plate with needles and the test cell were cleaned with concentrated chromic acid and rinsed with a large amount of double-distilled water.

All the experimental steps were essential, and an assistant for the experimental work was required. The author concentrated on taking samples, recording time and volumes of samples, while his assistant transferred the samples into the tubes and cleaned and re-loaded the several syringes in turn.

IV.3 Analysis of Samples from the Reaction Runs

In order to determine the concentrations of both the reactants and the products in a sample, the following methods of analysis were developed.

IV.3.1 Sodium Hydroxide

Sodium hydroxide in a sample was neutralized with the known amount of hydrochloric acid in the syringe. The excess hydrochloric acid was back-titrated to the end point using standard sodium hydroxide solution and a 10 ml. capacity burette. The controlled volume of phenolphthalein (one volume-calibrated drop from a dropping bottle), previously added together with the water for dilution in the sample tube, served as the indicator.

IV.3.2 Ester and Alcohol

The sample, after being neutralized with standard sodium hydroxide solution, was diluted further with 15 - 20 ml. of ice-cold double-distilled water to a total volume of about 40 ml. At this point, the total volume of the sample was noted accurately. The sample contained ester, sodium chloride, salt, product alcohol, ethanol from phenolphthalein solution

and a large amount of water. Ten microlitres of the well-mixed sample solution was charged into a Beckman GC-2A chromatograph. The appropriate column would separate the ester, alcohol and water (Note IV.1 at the end of this Appendix), while the sodium chloride and the salt would stay either in the injection pot or inside the column. The accumulation of the chloride and the salt in the column would eventually alter the column's characteristics, such as the decrease of the degree of separation and the prolonging of the components' retention times. However, since the samples analysed were both quite dilute in concentration and small in volume, many samples would be passed through the column before a significant amount of the salts could be accumulated. Standard samples of aqueous ester and alcohol solutions were injected at intervals between sets of samples. The column would be replaced at the first sign of its change of characteristics.

Output signals from the chromatograph were connected to a Honeywell recorder (Honeywell model No. Electronik 19, multirange, single point). Peak areas of the chromatograms were identified and measured, using a planimeter. The measured peak areas could be readily converted to their respective concentrations by means of calibration charts which were prepared by passing samples of standard solutions through the chromatograph under similar operating conditions. For the system of ethyl acetate - sodium hydroxide, the

ethanol concentration in the analysis was a combination of the alcohol contributed by the sample itself and by the phenolphthalein solution added. The amount of ethanol from the phenolphthalein solution in the sample could be found from yet another calibration curve. Finally, the actual ethanol concentration in the sample was then calculated from the difference between the total ethanol concentration and the ethanol concentration contributed by the phenolphthalein solution. A typical sample calculation is found in Appendix VII.

IV.3.3 Salt

Concentration of either sodium acetate or sodium propionate in a sample was obtained by conductometric titration (Note IV.2 at the end of this Appendix). The whole sample (minus the 10 µl. for chromatographic analysis) was poured into a 400 ml. beaker and made up to a volume of approximately 350 ml. with double-distilled water. The solution was vigorously stirred with a Teflon-coated magnetic stirrer. A known volume of standard solution of the hydrochloric acid was added at intervals and the conductivity of the solution was measured after each addition of hydrochloric acid. The process of titration continued until an abrupt increase in conductivity of the solution was noted. For each sample, a graph of conductivity of the solution versus the amount of standard hydrochloric acid solution added was plotted. The end point was located at the sharp break of

the curve. Salt concentration in the sample could thus be calculated. A typical sample calculation is shown in Appendix VII.

IV.4 Analysis of Samples from the Physical Runs

Determination of concentrations of ethyl acetate, methyl acetate or n-butanol in the aqueous solution samples was achieved by means of refractive index method.

A Bausch and Lomb dipping refractometer was used for the purpose. Prism A was specially adapted with an auxiliary prism, so that only a few drops of the sample would be adequate for the analysis. Water from the constant temperature bath at 25°C was circulated through the prism holders during analysis. Monochromatic light from sodium vapor lamp was used for illumination. The scale readings obtained from the refractometer were converted directly into concentrations by means of calibration charts prepared by measuring respective sets of standard solutions at the same temperature.

NOTE IV.1

CHROMATOGRAPHIC ANALYSIS

In the concentration probing experiments (4.2 - PART B), samples were taken from the turbulent layer and analysed for the ester and the alcohol contents by means of a chromatograph.

Ethyl acetate-sodium hydroxide system

Concentrations of ethyl acetate and ethanol in water from each sample were analysed by means of a Beckman GC-2A chromatograph. Two kinds of chromatography columns were tested; 5% tetraethylene glycol dimethyl ether on fluropak 80 and 5% carbowax 1500 on fluropak 80. The carbowax column was found to be better for separating the components of the system. After a few experimental trials, the standard operating conditions were established for the analysis. The column packing was set to be 15% carbowax 1500 on Chromosorb T support. Approximately 49 grams of the prepared column packing was used to fill a 7-feet, $\frac{1}{4}$-inch stainless steel column. The temperature in the chromatograph was set at 100°C with the helium flowrate at 40 c.c./minute at 20 psi. The detector current was set at 350 mA. The output from the chromatograph was connected to a Honeywell recorder with the chart speed set at 1-inch per minute. Under these operating conditions, the ethyl acetate peak would appear at 3.7 minutes, and the ethanol peak would appear at 5.6 minutes after the sample injection. The water, on the other hand, would start to come out of the column at 13 minutes. Because of the large amount of water in the sample, it would take 55 minutes

after the injection before all the water could pass through the column.

It should be realised that these standard operating conditions, although found to be experimentally acceptable, may not necessarily be the optimum conditions. As an example, the 15% liquid phase would probably over-saturate the surface of the Teflon support. However, no further search for the optimum operating conditions was made since the purpose was served.

A newly packed column should be baked at the operating temperature and under the helium gas flow for at least 24 hours before using. Chromatograms obtained from the first few injections of the samples into the new column should be discarded. Furthermore, whenever a new column was used, a new set of calibration charts should be prepared with standard solutions.

Methyl propionate-sodium hydroxide system

Samples from this system contained aqueous solutions of methyl propionate, methanol, sodium chloride, sodium propionate and ethanol added in as phenolphthalein indicator.

The appropriate liquid phase substrate for this system was found to be polypropylene glycol. After a few experimental trials, the standard operating conditions were determined. The column packing was set to be 14.5% polypropylene glycol on Chromosorb T support. Approximately 73.8 grams of the prepared material was used to pack 15 feet of $\frac{1}{4}$-inch copper tubing. The temperature in the chromatograph was set at 92°C. The helium gas flowrate was set at 40 c.c./minute at 23.5 psi. The

detector current was set at 350 mA. In a typical sample injection, the methanol would appear at 18.7 minutes, followed by the methyl propionate at 23.6 minutes and finally, the ethanol together with water would start to appear at 29 minutes. Each injection would require 95 minutes before the chromatograph was ready for the next sample.

Again, the standard operating conditions may not be the optimum conditions, but were considered satisfactory for these runs.

NOTE IV.2

CONDUCTOMETRIC TITRATIONS OF SODIUM ACETATE AND SODIUM PROPIONATE

Samples taken from the turbulent layer in the concentration probing experiments (4.2 - PART B) were analysed for their salt contents by means of conductometric titrations.

When hydrochloric acid was added to a solution of sodium acetate or sodium propionate, the acetate or propionate was replaced by the chloride ion forming sodium chloride and acetic acid or propionic acid respectively. The conductivity of the solution increased slightly due to the fact that the chloride ions were more conductive than the acetate ions. After all the acetic acid or the propionic acid had been liberated, continued addition of hydrochloric acid gave rise to a strong increase in conductance. Thus by tracing the plot of conductivity of the solution versus the amount of hydrochloric acid added, the end point could be located at the sharp break of the curve.

Caution was exercised during the conductometric titration of the salt solution to ensure that the temperature of the solution be kept constant and the volume of hydrochloric acid added be as small as possible (preferably not more than 6 to 8 ml.) since conductivity of the solution changed with dilution.

A conductivity meter capable of continuous measurements (Radiometer model No. CDM2) with a three-ring conductivity cell (model No. $CDC10_4$) was employed for the measurement. The solution

was stirred by a magnetic stirrer. Hydrochloric acid was metered through a "Kimax" automatic burette, 10 ml. capacity.

APPENDIX V

LAYER PROPAGATION MEASUREMENTS IN THE ROUND TEST CELL OF 21.2 cm. IN DIAMETER

Five experiments on the measurement of layer propagation were performed using the big round test cell (21.2 cm. in diameter). Three runs were performed on the ethyl acetate-aqueous sodium hydroxide system at 0.2, 0.6 and 1.0 N caustic concentration levels. Two runs were performed with the methyl propionate-aqueous sodium hydroxide system with the lower phase concentrations at 0.2 N and 0.6 N respectively.

The two liquid phases were contacted in the same way as described in the concentration probing experiments (4.2 - PART B:Section 4.2.1.2). For each run, layer thicknesses were measured as a function of contact time using two vernier calipers situated at different positions along the outer wall of the cell. The average of the two measurements from the two calipers was taken.

Results of the turbulent layer propagation measurements on the two liquid systems studied were plotted as shown in Figures V.1, V.2, V.3, and V.4.

All the layer propagation data thus obtained were compared with those obtained from the cubical optical cell experiments (Section 4.1.2.2). Results of the comparisons were best illustrated by the following Table V.1.

Study of the results in Table V.1 suggested that the speed of the layer growth for a liquid system was independent of the

FIGURE V.1

TURBULENT LAYER THICKNESS VS. PHASE CONTACT TIME
ETHYL ACETATE - NaOH SYSTEM

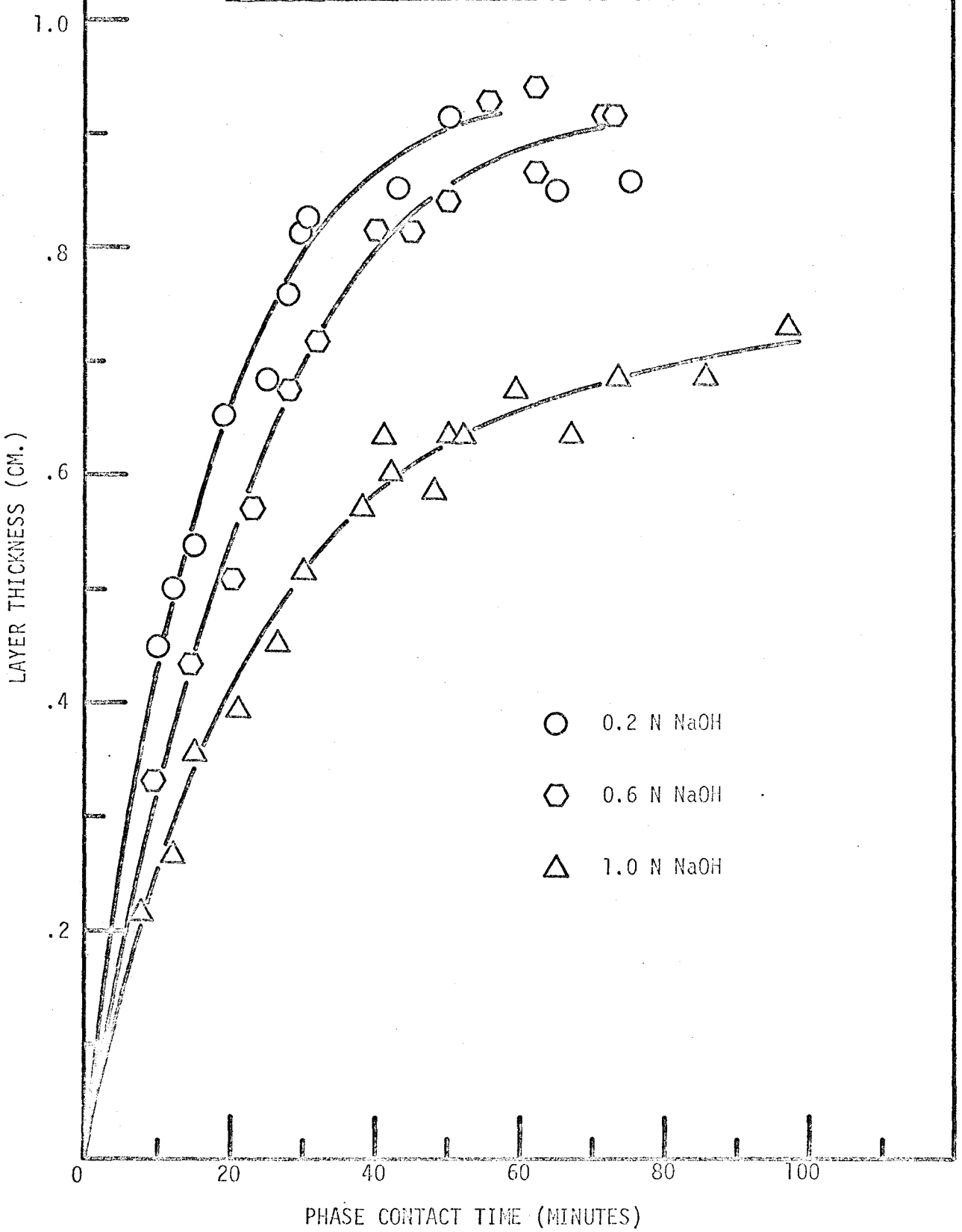

FIGURE V.2

TURBULENT LAYER THICKNESS VS. PHASE CONTACT TIME
METHYL PROPIONATE - NaOH SYSTEM

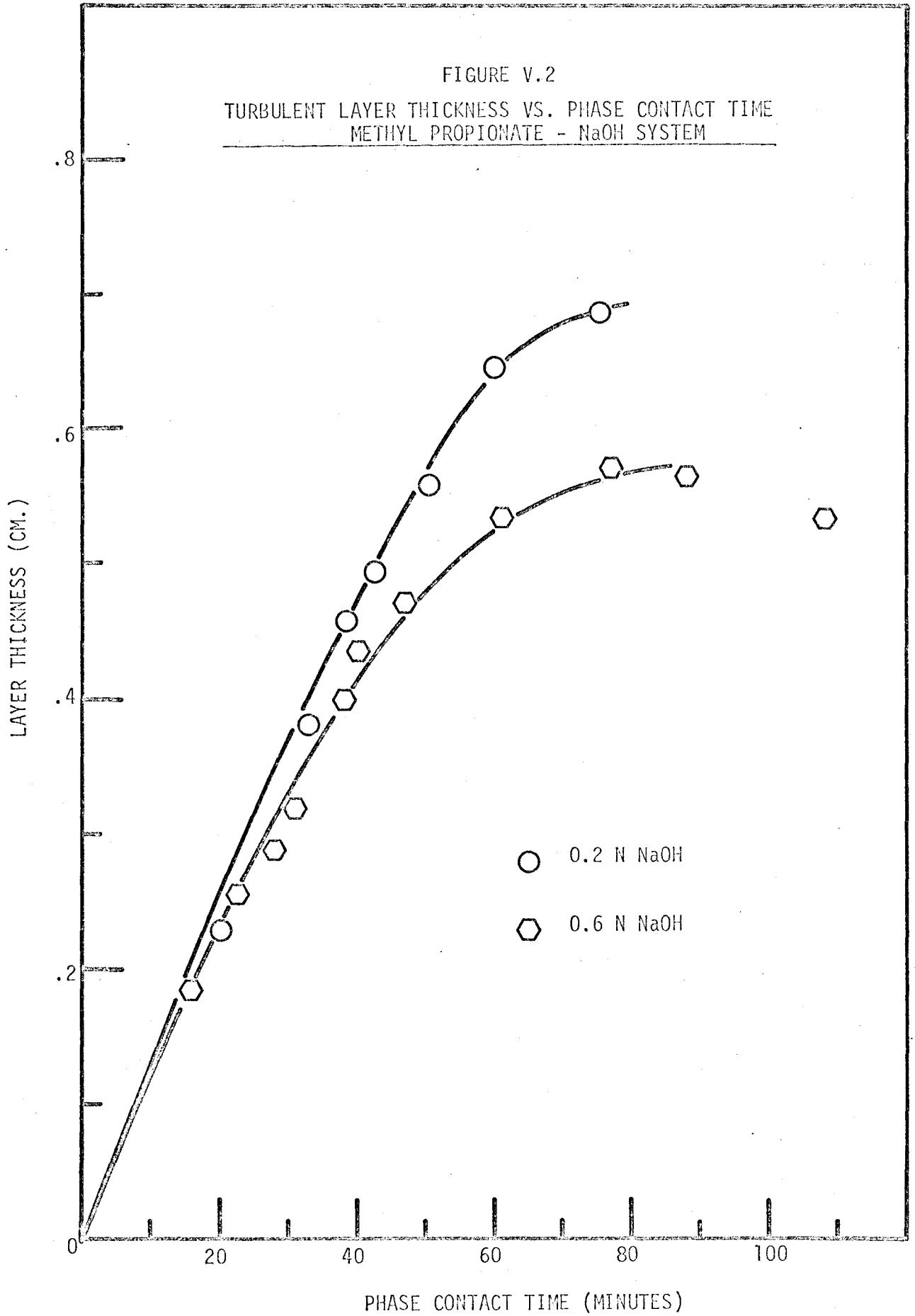

FIGURE V.3

(TURBULENT LAYER THICKNESS)^2 VS. PHASE CONTACT TIME

ETHYL ACETATE - NaOH SYSTEM

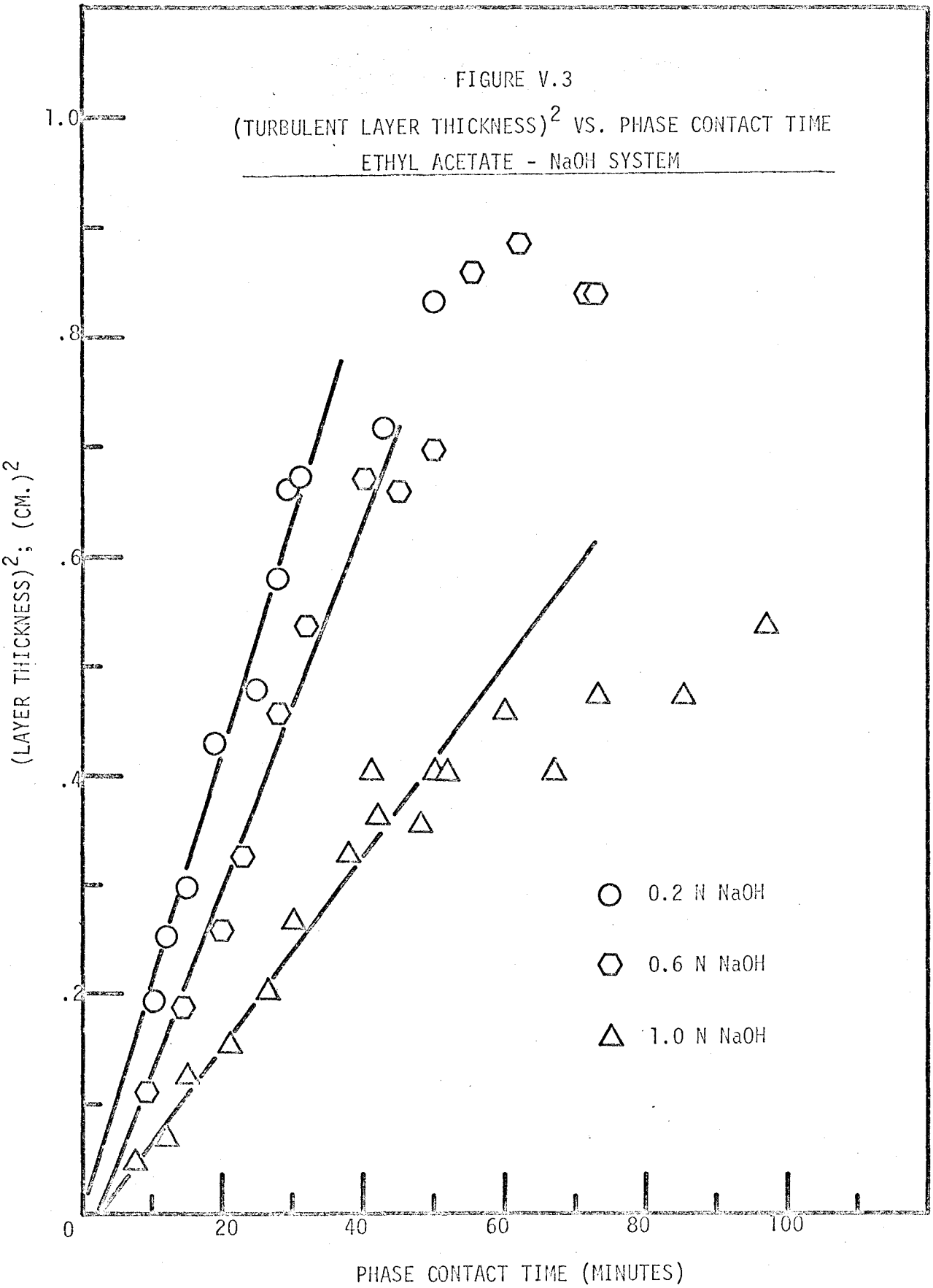

FIGURE V.4
(TURBULENT LAYER THICKNESS)^2 VS. PHASE CONTACT TIME
METHYL PROPIONATE-NaOH SYSTEM

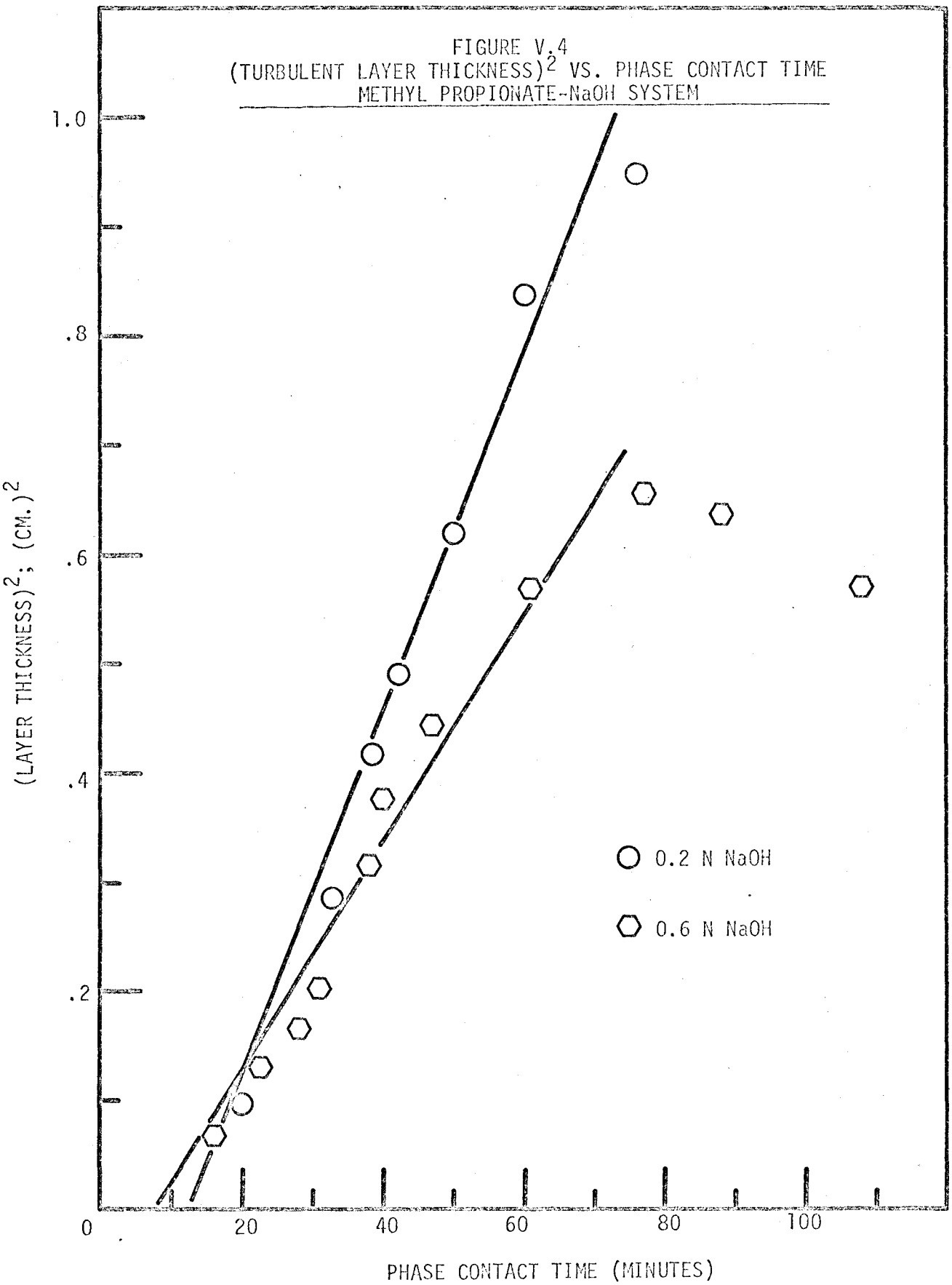

TABLE V.1

COMPARISON OF THE TURBULENT LAYER PROPAGATION SPEED IN THE ROUND CELL (21.2 cm. IN DIAMETER) AND IN THE OPTICAL CELL (4.8 cm. X 4.9 cm.)

V.1.1 Ethyl acetate- NaOH system

conc. of NaOH (N) / slope cm^2/min / cell size	0.2	0.6	1.0
Big cell 353 cm^2	0.0211	0.0168	0.009
Optical cell 24 cm^2	0.0193	0.0191	0.0113
~ % deviation	-10%	+12%	+25%

V.1.2 Methyl propionate-NaOH system

conc. of NaOH (N) / slope cm^2/min / cell size	0.2	0.6
Big cell 353 cm^2	0.0159	0.0097
Optical cell 24 cm^2	0.0138	0.0033
~ % deviation	-13%	-65%

interfacial area provided the test cell size exceeded a certain critical dimension. It was noted that the drastic reduction in layer growth of the ester-caustic systems in sliding diffusion cell was observed (interfacial area = 1.625 cm^2; PART D) as compared to that in optical cell while the experiments were performed under similar conditions.

Some errors were inevitably induced when direct measurements of the turbulent layer were made using vernier calipers due to the uncertainty (parallax) in judging the location of the layer front by eye within a short period of time. This error was greater when the layer thickness was smaller. Such was the case in the methyl propionate-sodium hydroxide system. For this reason, it was expected that the layer propagation data from the big cell were not as accurate as those obtained from optical cell experiments.

APPENDIX VI

TEMPERATURE PROFILE ACROSS THE TURBULENT LAYER FOR THE ETHYL ACETATE-SODIUM HYDROXIDE SYSTEM

Preliminary measurements of the temperature inside the turbulent layer[S8] in the cubic optical cell indicated that perhaps as much as 1°C difference existed across the turbulent layer of the ethyl acetate-sodium hydroxide system; and the hottest region was probably located near the lower zone front. In order to corroborate such findings and acquire further information on the temperature distribution in an ester-caustic reaction system, a temperature measuring experiment was repeated in the large test cell (21.2 cm. in diameter). A chromel-alumel thermocouple was connected to a multirange, single point recorder (Honeywell model No. Electronik 19). The range was set at 0.1 mV full scale. The thermocouple was calibrated against a thermometer capable of reading accurately to 1/100°C.

Ethyl acetate (pre-saturated with water)-1.0 N NaOH system was chosen for this study. The two liquid phases were contacted in the same way as described previously (4.2 - PART B: Section 4.2.1.2). The level indicating gauge from the brass plate for supporting sampling needles was taken out, leaving a small hole to insert the two thermocouple junctions. Initially, both the hot and the cold junctions of the thermocouple were placed half way in the ethyl acetate phase. Subsequently, the hot junction was moved manually downward at a slow but steady rate. The temperature difference between the two junctions

rather than the individual absolute temperature was recorded continuously. The recording chart represented, at least qualitatively, the temperature difference profile as a function of vertical distance in the cell.

It was found that at the beginning of the experiment, the temperature rise was approximately 0.36°C and was quite uniform inside the thin turbulent layer. At about 30 to 40 minutes of contact time, the maximum temperature region inside the layer tended to move towards the lower zone front. Presumably at this time the convective liquid current inside the layer was effective, causing the temperature profile to be slightly irregular with time. Towards the end of the run (60-80 minutes), the temperature profile tended to spread out. Typical profiles at different contact times were shown in Figure VI.1.

From the concentration probing experiments, the amount of the sodium hydroxide consumed up to 70 minutes of contact time was estimated to be 0.335 moles for this system (Figure 20) Since ΔH reaction is to be 13.1 kcals./mole[B5], the heat released by the reaction was calculated to be 4385 cals. Assume that all the heat released by the reaction was transferred by turbulent motion to, and evenly distributed into, the upper phase as well as the aqueous region between the interface and up to 2.5 cm. below the interface. Then a temperature difference of as high as 3.1°C could exist between the bottom of the caustic phase and the middle of the ester phase where the reference junction of the thermocouple was situated. In

FIGURE VI.1

QUALITATIVE STUDY OF TEMPERATURE DISTRIBUTION

IN THE TURBULENT LAYER OF ETHYL ACETATE - 1.0N NaOH SYSTEM

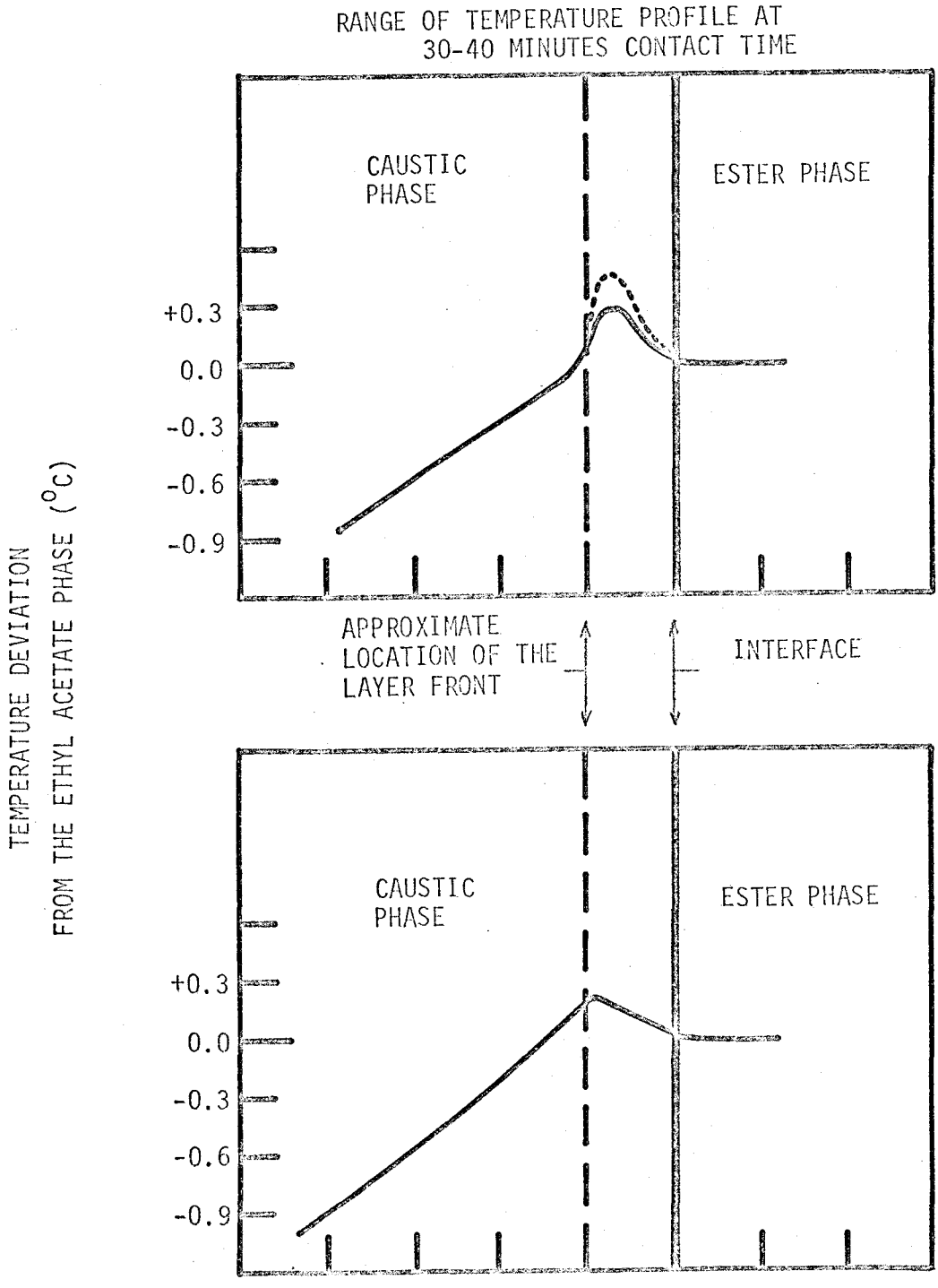

this case, probably some of the heat of reaction diffused towards the bottom of the aqueous phase reduced the temperature difference across the liquid phases to $1.5^{o}C$. The amount of heat diffused out of the system via the cell wall as well as by the evaporation of the upper phase was probably small.

APPENDIX VII

SAMPLE CALCULATIONS AND ERROR ANALYSES FOR THE CONCENTRATION PROBING EXPERIMENTS

The following error analyses are performed in order to determine the precision limits on the measured concentrations of various components in the concentration probing experiments. (4.2 - PART B).

Notation

V_1 = Volume of the hydrochloric acid inside the syringe before sampling.

N_1 = Normality of the hydrochloric acid solution.

V_2 = Volume of the sodium hydroxide required to neutralize the excess hydrochloric acid in the titration.

N_2 = Normality of the sodium hydroxide solution.

*V = Total volume of the sample in the syringe after sampling. (volume of the sample + volume of added HCl) = V + 0.27

V_4 = Total volume of the sample in the sampling tube (volume of the sample, plus volume of added HCl, plus volume of sodium hydroxide solution for back titration, plus volume of water added for dilution).

N_4 = Normality of the ester in the sampling tube solution (analysed by the chromatograph).

N_5 = Normality of the total alcohol content in the sampling tube solution (analysed by the chromatograph)

N_6 = Normality of the ethanol added into the sampling tube solution in the form of phenolphthalein solution (calibrated).

V_3 = Volume of the hydrochloric acid used for salt titration.

N_3 = Normality of the hydrochloric acid used for salt titration.

dV_1, etc., = Maximum error involved in measuring the volume of hydrochloric acid (V_1), etc.

*As read directly from the graduated scale on the syringe (refer to Note VII.1).

VII.1 Caustic Concentration

(Refer to 4.2 - PART B.)

The normality (equivalent to the concentration in this case) of the sodium hydroxide in the sample is expressed by the following formula:

$$C_{NaOH} = \frac{V_1N_1 - V_2N_2}{V - V_1 + 0.27^*} \qquad \text{(VII.1)}$$

and the maximum error range can be calculated from the following formula (M6)(V5)

$$dC_{NaOH} = \left(\frac{\partial C_{NaOH}}{\partial V_1}\right)dV_1 + \left(\frac{\partial C_{NaOH}}{\partial V_2}\right)dV_2 + \left(\frac{\partial C_{NaOH}}{\partial N_1}\right)dN_1 + \left(\frac{\partial C_{NaOH}}{\partial N_2}\right)dN_2 + \left(\frac{\partial C_{NaOH}}{\partial V}\right)dV \qquad \text{(VII.2)}$$

Also,

$$\sigma^2(C_{NaOH}) = \left(\frac{\partial C_{NaOH}}{\partial V_1}\right)^2\sigma^2(V_1) + \left(\frac{\partial C_{NaOH}}{\partial V_2}\right)^2\sigma^2(V_2) + \left(\frac{\partial C_{NaOH}}{\partial N_1}\right)^2\sigma^2(N_1) + \left(\frac{\partial C_{NaOH}}{\partial N_2}\right)^2\sigma^2(N_2) + \left(\frac{\partial C_{NaOH}}{\partial V}\right)^2\sigma^2(V) \qquad \text{(VII.3)}$$

where σ^2 is the variance of the variable.

Multiply equation (VII.3) by $(1.96)^2$ and take the root,

$$1.96\sigma(C_{NaOH}) = \left[\left(\frac{\partial C_{NaOH}}{\partial V_1}\right)^2(1.96\sigma(V_1))^2 + \left(\frac{\partial C_{NaOH}}{\partial V_2}\right)^2(1.96\sigma(V_2))^2 + \left(\frac{\partial C_{NaOH}}{\partial N_1}\right)^2(1.96\sigma(N_1))^2 + \left(\frac{\partial C_{NaOH}}{\partial N_2}\right)^2(1.96\sigma(N_2))^2 + \left(\frac{\partial C_{NaOH}}{\partial V}\right)^2(1.96\sigma(V))^2\right]^{0.5} \qquad \text{(VII.4)}$$

From equation (VII.4), it is evident that if the precision limits for each independent variable are at 95% confidence level (1.96σ) or at any other level, then the precision limits

* Refer to note at the end of this Appendix: (Note VII.1).

for the (C_{NaOH}) so calculated from equation (VII.4) are also at 95% confidence level or at the same level of the independent variable. Error range calculated in such a way is called the probable error.

By differentiating equation (VII.1) with respect to all the variables and taking positive signs for each group (in order to get maximum errors).

$$dC_{NaOH(max.)} = \frac{(V - V_1 + 0.27)N_1 + (V_1N_1 - V_2N_2)}{(V - V_1 + 0.27)^2} dV_1 + \frac{N_2}{(V - V_1 + 0.27)} dV_2 + \frac{V_1}{(V - V_1 + 0.27)} dN_1 + \frac{V_2}{(V - V_1 + 0.27)} dN_2 + \frac{V_1N_1 - V_2N_2}{(V - V_1 + 0.27)^2} dV \qquad \text{(VII.5)}$$

Data for this sample calculation are taken from Run #3-2, sample #21.

$V_1 \pm dV_1 = 1.870 \pm 0.025$ **

$V_2 \pm dV_2 = 2.970 \pm 0.0125$

$N_1 \pm dN_1 = 0.050 \pm 0.00025$ ***

$N_2 \pm dN_2 = 0.025 \pm 0.000125$ ***

$V \pm dV = 2.800 \pm 0.025$

Substituting the data into equations (VII.1) and (VII.5) respectively,

$$C_{NaOH} = \frac{(1.87 \times 0.05) - (2.97 \times 0.025)}{(2.8 - 1.87 + 0.27)} = .016_{04}$$

and,

** Refer to Note VII.2 at the end of this Appendix

*** Refer to Note VII.3 at the end of this Appendix

$$dC_{NaOH(max.)} =$$

$$\frac{(2.80 - 1.87 + 0.27)(0.05)+(1.87 \times 0.05)-(2.97 \times 0.025)}{(2.80 - 1.87 + 0.27)^2}(0.025)$$

$$+ \frac{0.025}{(2.80 - 1.87 + 0.27)}(0.0125) + \frac{2.80}{(2.80 - 1.87 + 0.27)}(0.00025)$$

$$+ \frac{2.97}{(2.80 - 1.87 + 0.27)}(.000125)$$

$$+ \frac{(1.87 \times .05)-(2.97 \times .025)}{(2.80 - 1.87 + 0.27)^2}(.025) = .002_{67}$$

The probable $dC_{NaOH} = .001_{52}$

% of maximum error = 16.64

% of probable error = 9.50

VII.2 Ester Concentration

(Refer to 4.2 - PART B).

The normality (concentration) of the ester in the sample is expressed by the following formula:

$$C_{EtAc} = \frac{N_4 V_4}{(V - V_1 + 0.27)} \qquad \text{(VII.6)}$$

and,

$$dC_{EtAc(max.)} = \frac{N_4 V_4}{(V - V_1 + 0.27)^2}dV + \frac{N_4 V_4}{(V - V_1 + 0.27)^2}dV_1$$

$$+ \frac{V_4}{(V - V_1 + 0.27)}dN_4 + \frac{N_4}{(V - V_1 + 0.27)}dV_4 \qquad \text{(VII.7)}$$

and the probable error ($dC_{EtAc(probable)}$) is equal to the square root of the sum of squares of each term in equation (VII.7).

Data for this sample calculation are taken from Run #3-2, sample #21.

The ester concentration in a sampling tube is obtained by injecting 10 μl. of the sample solution into the chromato-

graph. The area of the chromatogram obtained is converted into concentration data by means of a calibration chart which, in turn, is prepared by passing samples of standard solutions through the chromatograph under similar operating conditions.

The following practical example is given to illustrate the estimation of the error range of ester concentration in a sample solution:

For the standard ester solution "E", which is prepared with 2.3 ml. of ethyl acetate/litre solution, three separate sample injections are made. Three chromatograms are obtained with areas of 0.404, 0.421 and 0.402 planimeter units respectively. The mean value is 0.409 units.

Since the difference between duplicate area measurements on the same chromatogram is usually very small (typically 0.25%), and if the error involved in the injection of exactly 10 µl. of the sample from the microsyringe is assumed negligible, then the variation of the three chromatogram areas obtained by repeated injections of the same sample solution reflects the reproducibility of the chromatographic instruments.

If these three sample calibrations are representative (i.e. the statistical analysis on the three repeated calibrations, based on the normal distribution curve, will yield the same result as on a large number or infinite number of repeated calibrations), and if the same degree of reproducibility as obtained between the calibration runs and the actual analysis runs, then the standard deviation of the areas, representing

the ester concentrations, at 0.409 units level is

$\sigma = \left[((.404-.409)^2+(.421-.409)^2+(.402-.409)^2)/(3-1)\right]^{\frac{1}{2}} =$

0.010_{44} units.

Arbitrarily taking the error range to be 1.5σ, which will contain 86.62% of the data, then the estimated error range is $1.5\sigma = .015_7$ units.

Converting the area units into normality, the ester concentration in solution "E" is $0.023_{75} \pm .000_9$.

The % error is 3.79.

Similar error analyses are performed on the calibrations of the rest of the standard solutions. The errors obtained for all calibrations of the standard solutions are averaged to be 3%. The error involved in preparing the standard solutions is estimated to be 1%. The two errors are additive. Therefore the average error range of the ester concentration is estimated to be 4%.

Data for this calculation are taken from Run #3-2, sample #21:

$$V_1 \pm dV_1 = 1.87 \pm 0.025$$

$$V \pm dV = 2.80 \pm 0.025$$

$$V_4 \pm dV_4 = 41.02 \pm 0.100$$

$$N_4 \pm dN_4 = 0.014 \pm (0.014 \times .04)$$

Substituting the data into equations (VII.6) and (VII.7),

$$C_{EtAc} = \frac{0.014 \times 41.02}{(2.80 - 1.87 + 0.27)} = .478_{57}$$

and,

$$dC_{EtAc(max.)} = \frac{0.014 \times 41.02}{(2.80 - 1.87 + 0.27)^2}(0.025)$$

$$+ \frac{0.014 \times 41.02}{(2.80 - 1.87 + 0.27)^2}(.025) + \frac{41.02}{(2.80 - 1.87 + 0.27)}(.00056)$$

$$+ \frac{.014}{(2.80 - 1.87 + 0.27)}(0.125) = .040_{25}$$

The probable $dC_{EtAc} = .023_{81}$

$\therefore$ % of maximum error = 8.41

% of probable error = 4.97

VII.3 Ethanol Concentration

(Refer to 4.2 - PART B.)

The normality (concentration) of the alcohol in the sample is expressed by the following formula:

$$C_{EtOH} = \frac{(N_5 - N_6)V_4}{(V - V_1 + 0.27)} \qquad \text{(VII.8)}$$

and,

$$dC_{EtOH(max.)} = \frac{V_4}{(V - V_1 + 0.27)}dN_5 + \frac{V_4}{(V - V_1 + 0.27)}dN_6$$

$$+ \frac{N_5 - N_6}{(V - V_1 + 0.27)}dV_4 + \frac{(N_5 - N_6)V_4}{(V - V_1 + 0.27)^2}dV$$

$$+ \frac{(N_5 - N_6)V_4}{(V - V_1 + 0.27)^2}dV_1 \qquad \text{(VII.9)}$$

The probable error is calculated as described previously.

Data for this sample calculation are taken from Run #3-2, sample #21:

The method used to estimate the error involved in the calibration of ethanol concentration is similar to that used in the ester calibrations. It is found that the errors averaged to be 2.3%. The error involved in preparing the

standard solutionsis 1%. Therefore the average error range of the ethanol concentration is estimated to be 3.3%.

It should be mentioned that in both the ethyl acetate and the alcohol calibrations, the chromatogram areas are linearly proportional to concentrations. Therefore subtraction of a chromatogram area from the other, and then conversion to concentration datum is the same as converting the two chromatogram areas to concentration data first, and then doing the subtraction.

$$V_1 \pm dV_1 = 1.87 \pm 0.025$$
$$V \pm dV = 2.80 \pm 0.025$$
$$V_4 \pm V_4 = 41.02 \pm 0.100$$
$$N_5 \pm dN_5 = .0202 \pm (.0202 \times .033)$$
$$N_6 \pm dN_6 = .0104 \pm (.0104 \times .033)$$

Substituting the data into equation (VII.8) and (VII.9),

$$C_{EtOH} = \frac{(0.0202 - .0104)\ 41.02}{(2.80 - 1.87 + 0.27)} = 0.335$$

and,

$$dC_{EtOH(max.)} = \frac{41.02}{(2.80-1.87+0.27)}(.000667) + \frac{41.02}{(2.80-1.87+0.27)}(.000343) + \frac{(0.0202-0.0104)}{(2.80-1.87+0.27)}(0.100) + \frac{(.0202-.0104)(41.02)}{(2.80-1.87+0.27)^2}(.025) + \frac{(.0202-.0104)(41.02)}{(2.80-1.87+0.27)^2}(.025) = .049_3$$

The probable $dC_{EtOH} = .027_{48}$

$\therefore$ % of maximum error = 14.72

% of probable error = 8.20

VII.4 Salt Concentration

(Refer to 4.2 - PART B.)

The normality (concentration) of the salt in the sample is expressed by the following formula:

$$C_{salt} = \frac{N_3 V_3}{(V - V_1 + 0.27)} \qquad \text{(VII.10)}$$

and,

$$dC_{salt(max.)} = \frac{N_3 V_3}{(V - V_1 + 0.27)^2} dV + \frac{N_3 V_3}{(V - V_1 + 0.27)^2} dV_1 + \frac{N_3}{(V - V_1 + 0.27)} dV_3 + \frac{V_3}{(V - V_1 + 0.27)} dN_3 \qquad \text{(VII.11)}$$

Data for this sample calculation are taken from Run #3-2, sample #21:

$V \pm dV = 2.80 \pm 0.025$

$V_1 \pm dV_1 = 1.85 \pm 0.025$

$V_3 \pm dV_3 = 4.89 \pm 0.0125$

$N_3 \pm dN_3 = 0.125 \pm 0.000625$

Substituting the data into equations (VII.10) and (VII.11) respectively,

$$C_{NaAc} = \frac{(0.125)\ (4.89)}{(2.80 - 1.87 + 0.27)} = .509_{38}$$

and,

$$dC_{NaAc(max.)} = \frac{0.125 \times 4.89}{(2.80 - 1.87 + 0.27)^2}(0.025) + \frac{0.125 \times 4.89}{(2.80 - 1.87 + 0.27)^2}(0.025) + \frac{0.125}{(2.80 - 1.87 + 0.27)}(.0125) + \frac{4.89}{(2.80 - 1.87 + 0.27)}(.000625) = .025_{07}$$

The probable $dC_{NaAc} = .015_{28}$

$\therefore$ % of maximum error = 4.92

% of probable error = 3.00

As is evidenced from the calculations, most of the error is contributed by the inaccuracy in reading the volume of the sample in the "Cornwall syringe."

Study of the equations (VII.5), (VII.7), (VII.9) and (VII.11) reveals that the estimated error ranges of various components are not simple functions of concentrations. As a result, representative sets of error calculations for all the components from each run are performed and the results are shown in Figures VII.1, VII.2, VII.3 and VII.4. For each component, the deviations between runs are probably small enough to permit an average curve to be drawn through all the data points.

The error analyses for the ester, caustic and salt concentrations in the methyl propionate-sodium hydroxide system are assumed similar to those of the ethyl acetate-sodium hydroxide system. The estimated error ranges curves for the three aforementioned components in the ethyl acetate-caustic system also apply to the methyl propionate-caustic system. On the other hand, the methanol concentration in the sample is analysed independently of the ethanol concentration being added in as phenolphthalein solution (Refer to Appendix IV, Note IV.1). Consequently, the error analysis of the methanol concentration is assumed similar to that of the ester concentration and is shown in Figure VII.5.

FIGURE VII.1

MAGNITUDE OF THE PROBABLE ERROR RANGE INVOLVED IN THE MEASUREMENT OF NaOH CONCENTRATIONS

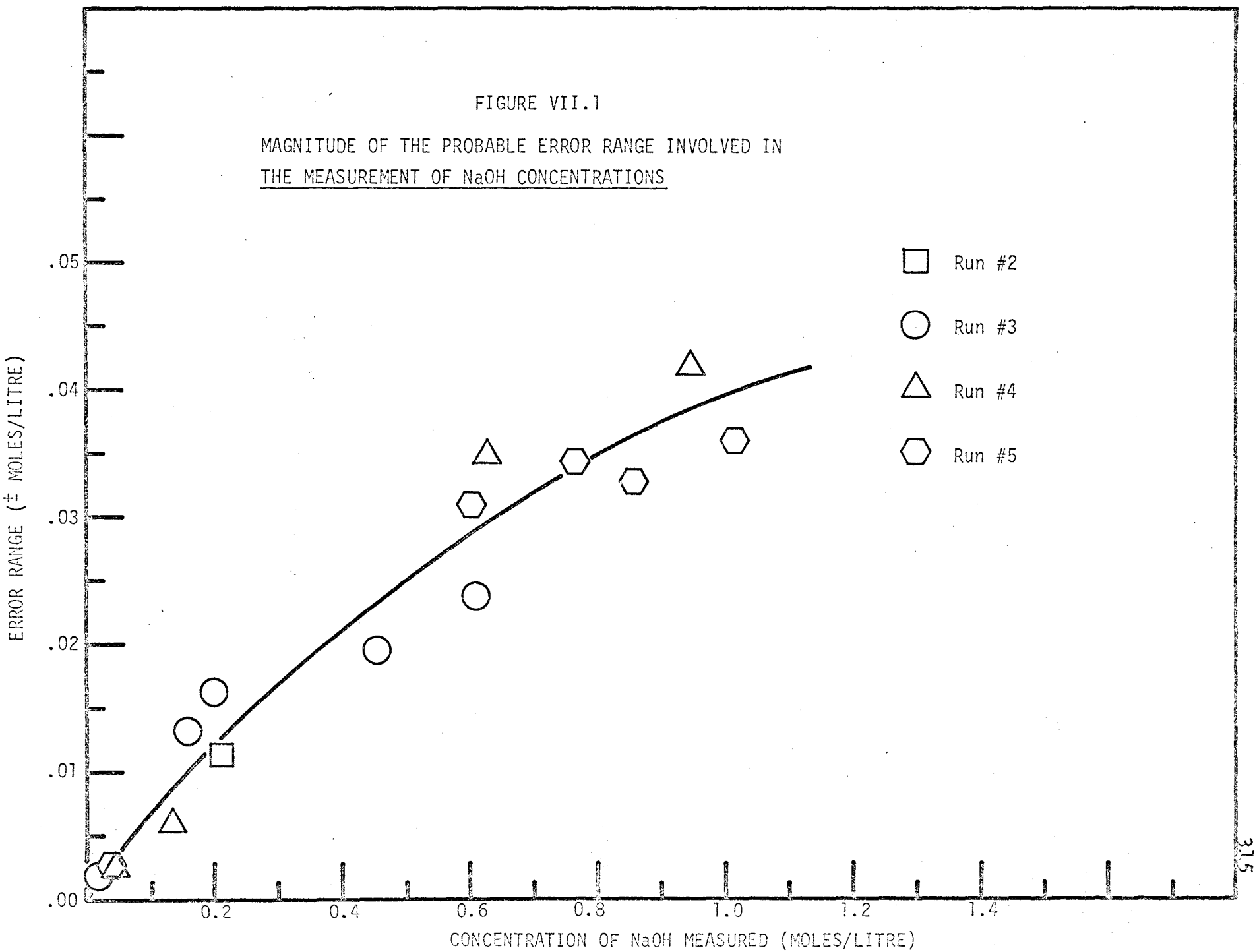

FIGURE VII.2

MAGNITUDE OF THE PROBABLE ERROR RANGE INVOLVED IN THE MEASUREMENT OF ESTER CONCENTRATION

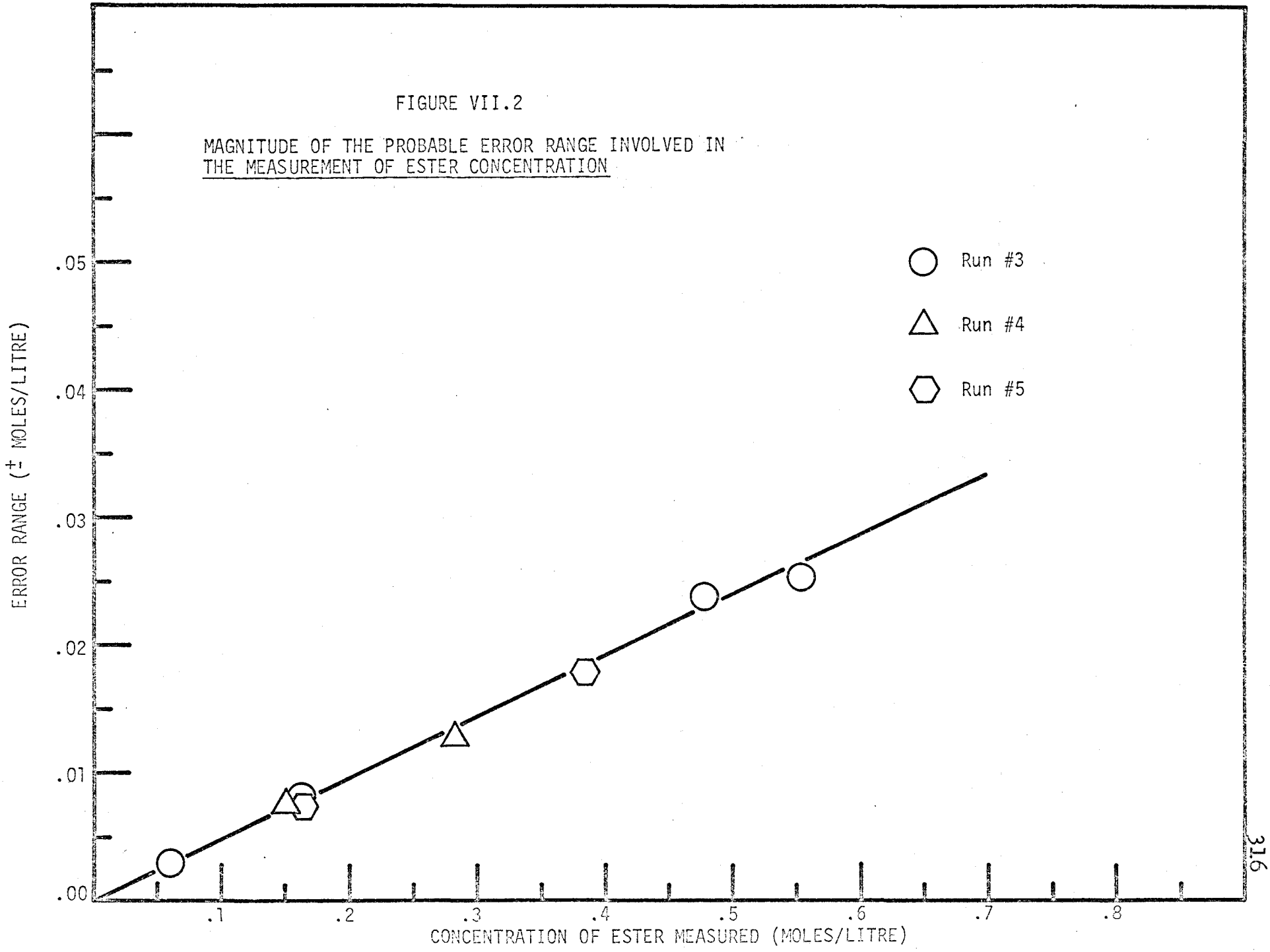

FIGURE VII.3

MAGNITUDE OF THE PROBABLE ERROR RANGE INVOLVED IN THE MEASUREMENT OF ETHANOL CONCENTRATION

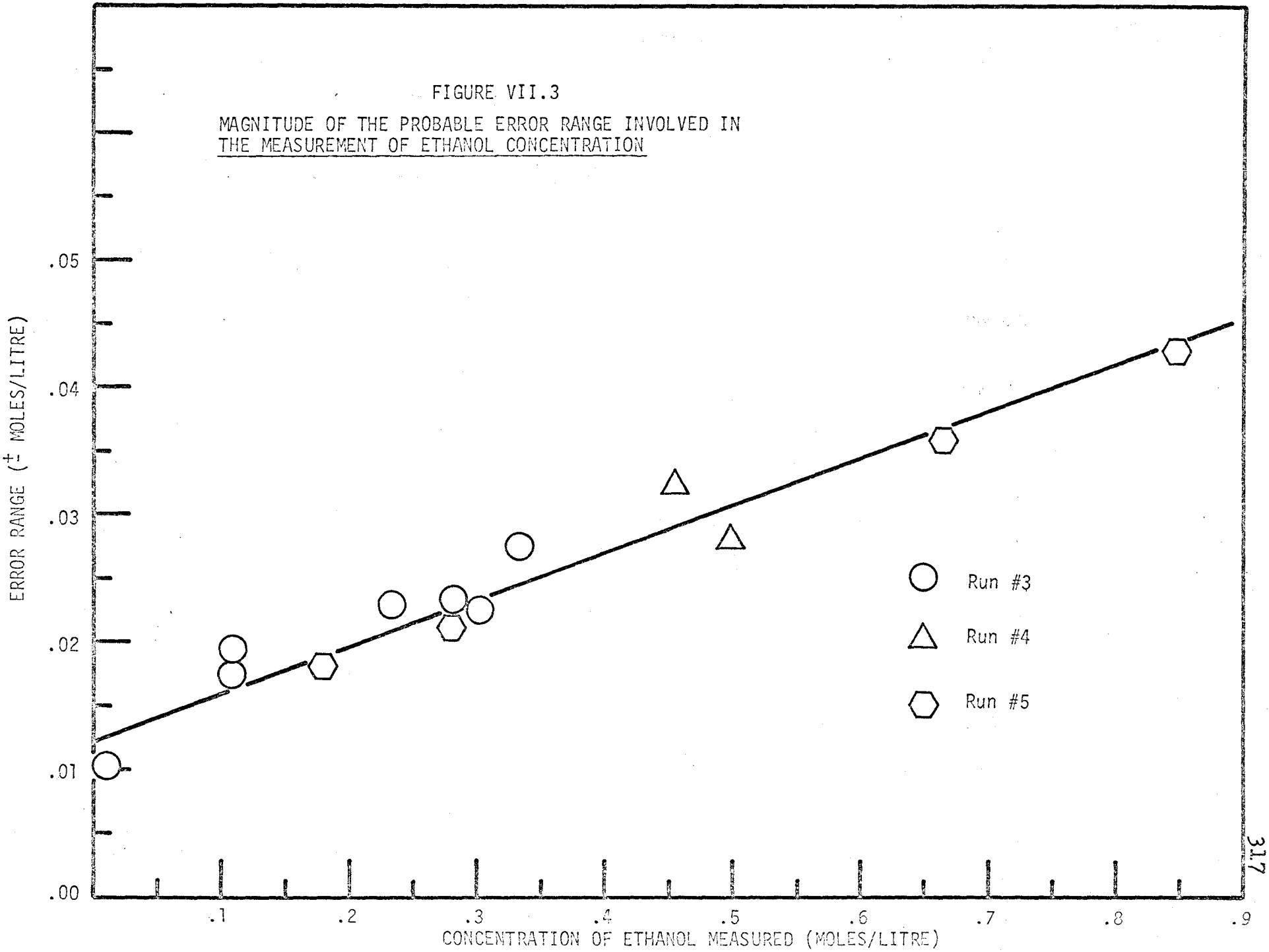

FIGURE VII.4

MAGNITUDE OF THE PROBABLE ERROR RANGE INVOLVED IN THE MEASUREMENT OF SALT CONCENTRATIONS

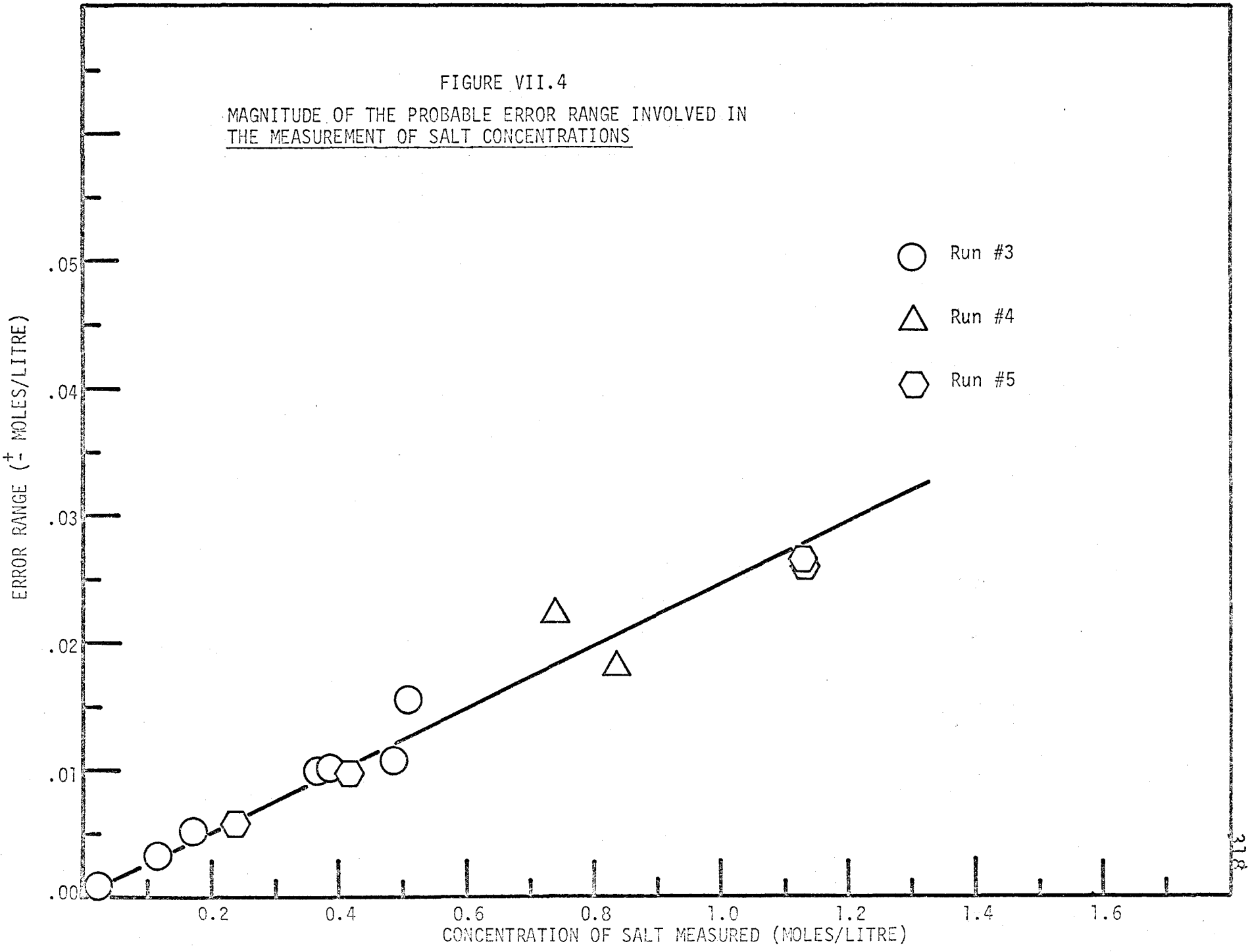

FIGURE VII.5

MAGNITUDE OF THE PROBABLE ERROR RANGE INVOLVED IN THE MEASUREMENT OF METHANOL CONCENTRATION

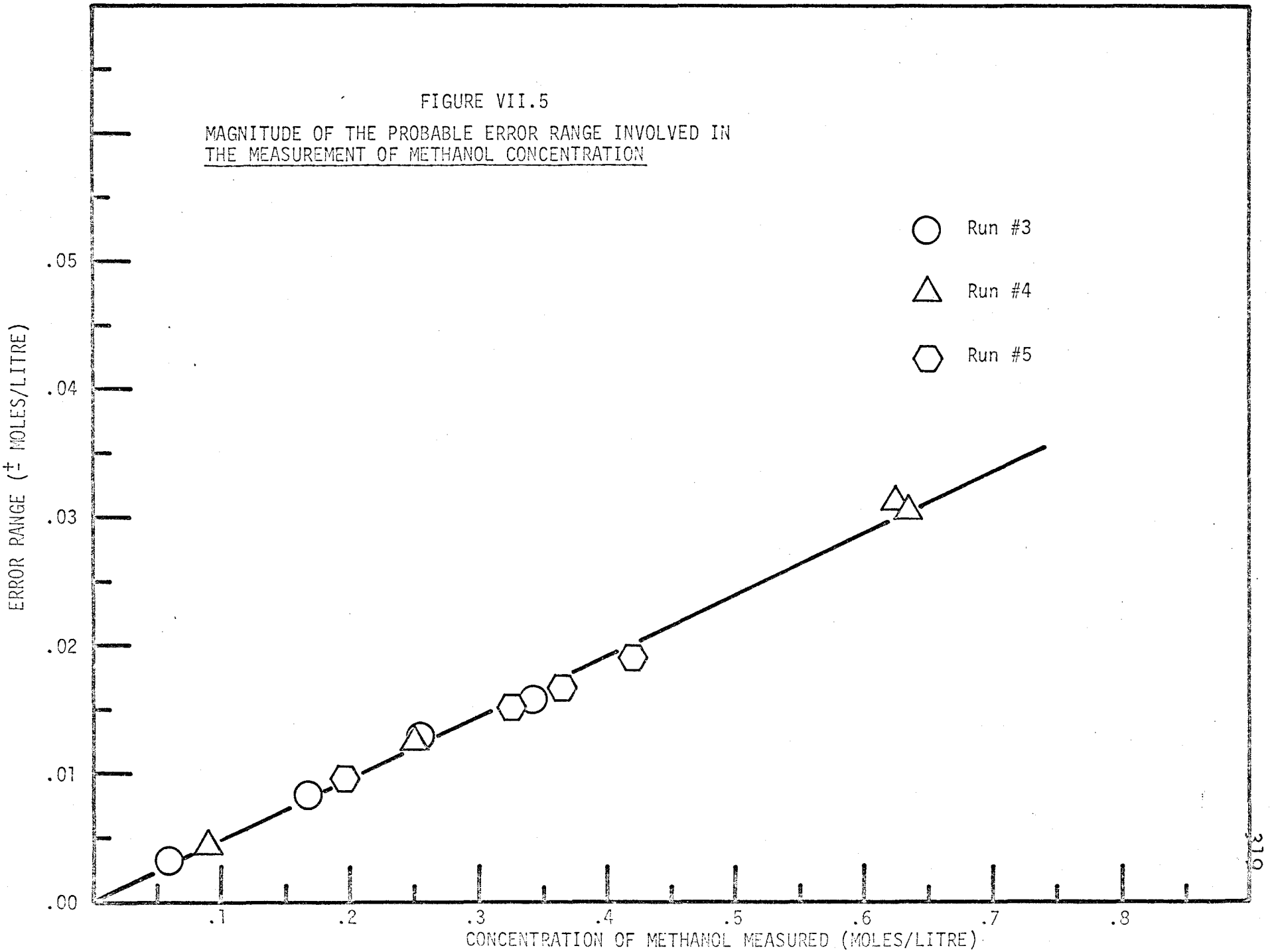

Note VII.1

Calibration of the volumes of the syringes (with a Teflon stirring bar in each syringe) against a known volume of water measured from a burette was made. It was found that the amount of water reading 1.6 ml. in the syringe was actually 1.87 ml. as measured from the burette. Therefore, a correction of 0.27 ml. had to be applied in the volume calculations.

The errors involved in metering the water from the 10 ml. burette were probably small. (A syringe was calibrated several times and the results of calibrations were practically 100% reproducible.)

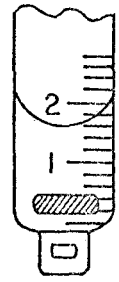

In addition, the volumetric readings on the Cornwall syringes (with a Teflon stirring bar in each syringe) were calibrated by an alternative method. A certain volume of the standard caustic solution of accurately known normality was drawn into the syringe. The volume of the sample solution was read, and the solution was then titrated against the standard hydrochloric acid solution. The volume of the sample solution was back-calculated based on the titration data. Results of the calibrations are shown in Table VII.1.

Note VII.2

The uncertainty range in reading the sample volume in the Cornwall syringe is probably ± 0.05 ml., which is half of

TABLE VII.1

ESTIMATION OF THE ERROR RANGE IN MEASURING THE SAMPLE VOLUME IN CORNWALL SYRINGES

Sample volume as measured by Cornwall syringe scales ml.	Number of repeated titration experiments	Volume of sample back-calculated based on titration data ml.	Standard deviation of the calculated sample volume σ; (68% of data included) ml.	1.5σ (87% of the data included) ml.
1.70	16	1.970	.016	.024
1.60	8	1.870	.013	.020
3.00	5	3.270	.021	.032

the minimum scale division on the syringe. However, with experience gained in reading the sample volumes in the syringes, the estimated error range may, perhaps, be justifiably reduced to ± 0.025 ml. Titration experiments were performed to check the validity of the justification. Individual samples of standard sodium hydroxide solution were put into the syringe consecutively. The volumes of the samples were measured by the syringe scale readings. Each sample was then titrated against standard hydrochloric acid solution in order to determine its actual volume. Results of the titration experiments are shown in Table VII.1.

Standard solutions of the acid and the base used for these experiments were double checked and cross titrated. The error involved in pipetting solutions is assumed negligible. Furthermore, the error in reading the volume of the titre in a 10-ml. burette was also estimated to be negligible.

It is evident from the results that the estimated error range of the sample volume in the syringe should be ± 0.025 ml.

A separate set of experiments was performed to simulate the actual experimental procedure of determining the sodium hydroxide concentration in the samples. The Cornwall syringe was preloaded with a known volume (as read from the calibrated syringe scales) of standard 0.5 N hydrochloric acid solution. The hydrochloric acid solution inside the syringe was then partially neutralized with a known volume (as read from the calibrated syringe scales) of standard 0.5 N sodium hydroxide

solution which served as the sample solution. The mixed solution was, eventually, titrated to the end point with 0.25 N standard sodium hydroxide solution. The concentration of the 0.5 N sodium hydroxide solution was back-calculated based on the titration data.

The results of 17 repetitive runs with solution volumes comparable to those used in the actual concentration probing experiments indicated that the calculated 0.5 N sodium hydroxide concentration was 0.493_8 N and the spread which included 87% of the data (1.5σ) was $\pm$ 0.012_8 N.

Based on the error analysis of sodium hydroxide concentration calculations with the estimated error range of the sample volume to be $\pm$ 0.025 ml., the probable uncertainty of the calculated sodium hydroxide concentration is $\pm$ 0.025 N (Figure VII.1). This uncertainty range well covers the actual experimental error range.

Note VII.3

The uncertainty range in the normality of the prepared caustic and acid solutions is estimated to be $\pm$ 0.5% of the normality of the solution concerned. This estimation is substantiated by experimental data. Five samples of 0.25 N sodium hydroxide solution were titrated against the double checked 0.5 N standard hydrochloric acid solution. The back-calculated sodium hydroxide concentrations were averaged to be 0.25075 N with a standard deviation (σ) of $.00015_9$ N.

Therefore, the uncertainty range which included 87% of the data would be 1.5σ or $\pm .00023_9$ N.

The estimated error range based on $\pm$ 0.5% of the solution concentration would be $\pm$ 0.00125 N, which well covers the actual experimental deviation range.

APPENDIX VIII

ESTIMATION OF THE EXTENT OF REACTION WITHIN THE SAMPLING NEEDLE DURING SAMPLING IN THE CONCENTRATION PROBING EXPERIMENTS

When a sample is being taken, liquid travels along the tube and reacts before it reaches the syringe and is neutralized. If plug flow conditions inside the sampling needle are assumed, then the original reactant concentrations before entering the sampling needle can be calculated as follows:

Outside diameter of the sampling needle = 0.028 inch

Wall thickness = 0.006 inch

Internal diameter of the needle = 0.016 inch

Cross-sectional area $= \pi(0.016 \times 2.54)^2/4$

$= .00129_5$ cm.^{2}

Assuming 1.5 ml. of sample taken over a period of 2 minutes,

$\therefore$ Volumetric flowrate of sample = 0.75 ml./minute

$\therefore$ contact time $= \frac{V}{v} = .0172$ minutes

Assuming negligible volume change during reaction, then plug flow reaction equation is the same as batch reaction equation;[I2]

$$k = \frac{1}{(b-a)t} \ln \frac{a}{a-x} \frac{b-x}{b} \qquad \text{(VIII.1)}$$

where

k = reaction constant, litres/(mole-minute)

b = original concentration of sodium hydroxide, moles/litre

a = original concentration of ethyl acetate, moles/litre

t = reaction time, minutes

x = amount reacted in the sampling needle, moles/litre.

Reactant concentrations data for this calculation are taken from needle #12 (0.525 cm. below the interface) at 25 minutes of contact time in Run #3 (ethyl acetate - 0.6 N sodium hydroxide).

b-x = 0.23 moles/litre

a-x = 0.15 moles/litre

b-a = 0.08 moles/litre

k $\cong$ 6.0 litre/mole-minute (refer to Figure VIII.1)

Substituting the values into equation (VIII.1),

$$6.0 = \frac{1}{(0.08)(.0172)} \ln \frac{a}{(0.15)} \frac{(0.23)}{(a+0.08)}$$

$a = 0.153_{632}$ moles/litre

$b = 0.233_{632}$ moles/litre

$x/a = .0236_{383}$

$x/b = .0155_{441}$

Four sets of reactant concentrations data are calculated and the results are tabulated in Table VIII.1.

Reactant concentration changes before and after corrections are so small that they do not influence the data points on the graphs.

FIGURE VIII.1

REACTION RATE CONSTANT VS. TEMPERATURE

ETHYL ACETATE - NaOH SYSTEM

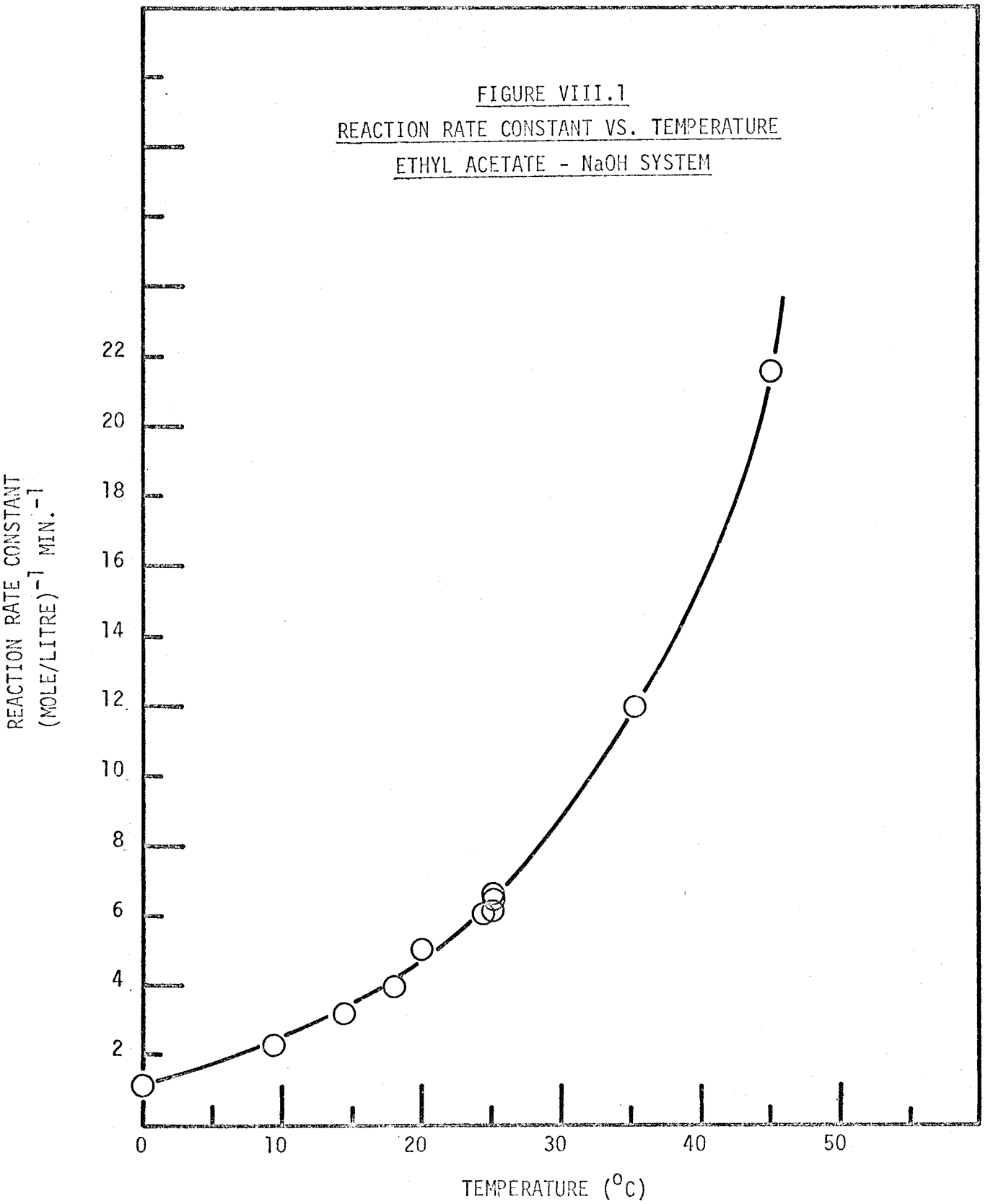

TABLE VIII.1

AMOUNT OF REACTANTS DISAPPEARED IN THE SAMPLING NEEDLE DURING SAMPLING

Data set No.	1	2	3	4
Measured ethyl acetate conc., (a-x), moles/litre	.15	.075	.018	.17
Measured sodium hydroxide conc., (b-x), moles/litre	.23	.275	.62	.14
Original ester conc., a, moles/litre	$.153_{632}$	$.077_{1676}$	$.019_{1905}$	$.172_{496}$
Original sodium hydroxide conc., b, moles/litre	$.233_{632}$	$.277_{168}$	$.621_{191}$	$.142_{496}$
Amount reacted, moles/litre	$.003_{632}$	$.002_{168}$	$.001_{191}$	$.002_{496}$
percentage of ester reacted, $100(x/a)$	2.36	2.80	6.20	1.44
percentage of sodium hydroxide reacted, $100(x/b)$	1.55	.78	.19	1.75

APPENDIX IX

ANALOG STUDY

The experimental concentration profiles of the reactants and the products in the turbulent layer were simulated on an analog computer. A quasi-steady state mass transfer with chemical reaction model was employed. The study was carried out with the aid of an Electronic Associates Inc. TR-10 computer and a Variplotter.

A worked example of the analog study is given below with the data taken from Run #3 (ethyl acetate - 0.6 N sodium hydroxide), 25 minutes after phase contact.

One of the troublesome parts in applying a TR-10 computer is in scaling. Since the computer can produce a maximum voltage of only 10, every numerical value has to be scaled so that the corresponding representing voltage is less than 10. Furthermore, the product of two variable voltages is automatically divided by 10 in order to avoid over-voltages.

Let the machine constant be $^1/_{10}$, if the maximum layer thickness to be simulated is 1.0 cm. then the solution time will be 10 seconds.

Let C_A = concentration of ethyl acetate

C_B = concentration of sodium hydroxide

C_C = concentration of ethanol

C_D = concentration of sodium acetate

x = turbulent layer thickness

D_{Ei} = eddy diffusivity of species i

Table IX.1 can then be set up

	Machine variable	Maximum value across the layer (moles/litre)	Representing voltage (volts)
C_A	$10\ C_A$	0.563	5.63
C_B	$10\ C_B$	0.600	6.00
C_C	$10\ C_C$	0.332	3.32
C_D	$10\ C_D$	0.505	5.05
x		1.0 (cm.)	

For the simulation of C_A,

equation (5a) is scaled as the following:

$$\frac{100}{10}\frac{d^2(10C_A)}{d\tau^2} = \frac{k}{D_{EA}}\frac{10}{100}\frac{(10C_A)(10C_B)}{10}$$

$$\therefore \quad \frac{d^2(10C_A)}{d\tau^2} = \frac{k}{D_{EA}}\frac{1}{100}\frac{(10C_A)(10C_B)}{10} \qquad \text{(IX.1)}$$

Similarly, equations (5b)(5c)(5d) are scaled as the following:

$$\frac{d^2(10C_B)}{d\tau^2} = \frac{k}{D_{EB}}\frac{1}{100}\frac{(10C_A)(10C_B)}{10} \qquad \text{(IX.2)}$$

$$\frac{d^2(10C_C)}{d\tau^2} = -\frac{k}{D_{EC}}\frac{1}{100}\frac{(10C_A)(10C_B)}{10} \qquad \text{(IX.3)}$$

$$\frac{d^2(10C_D)}{d\tau^2} = -\frac{k}{D_{ED}}\frac{1}{100}\frac{(10C_A)(10C_B)}{10} \qquad \text{(IX.4)}$$

The circuit diagram is shown in Figure IX.1. In order to increase the values in potentiometers Nos. 9, 10, 11 and 12 (Refer to Figure IX.1) by a factor of 10, the feedback

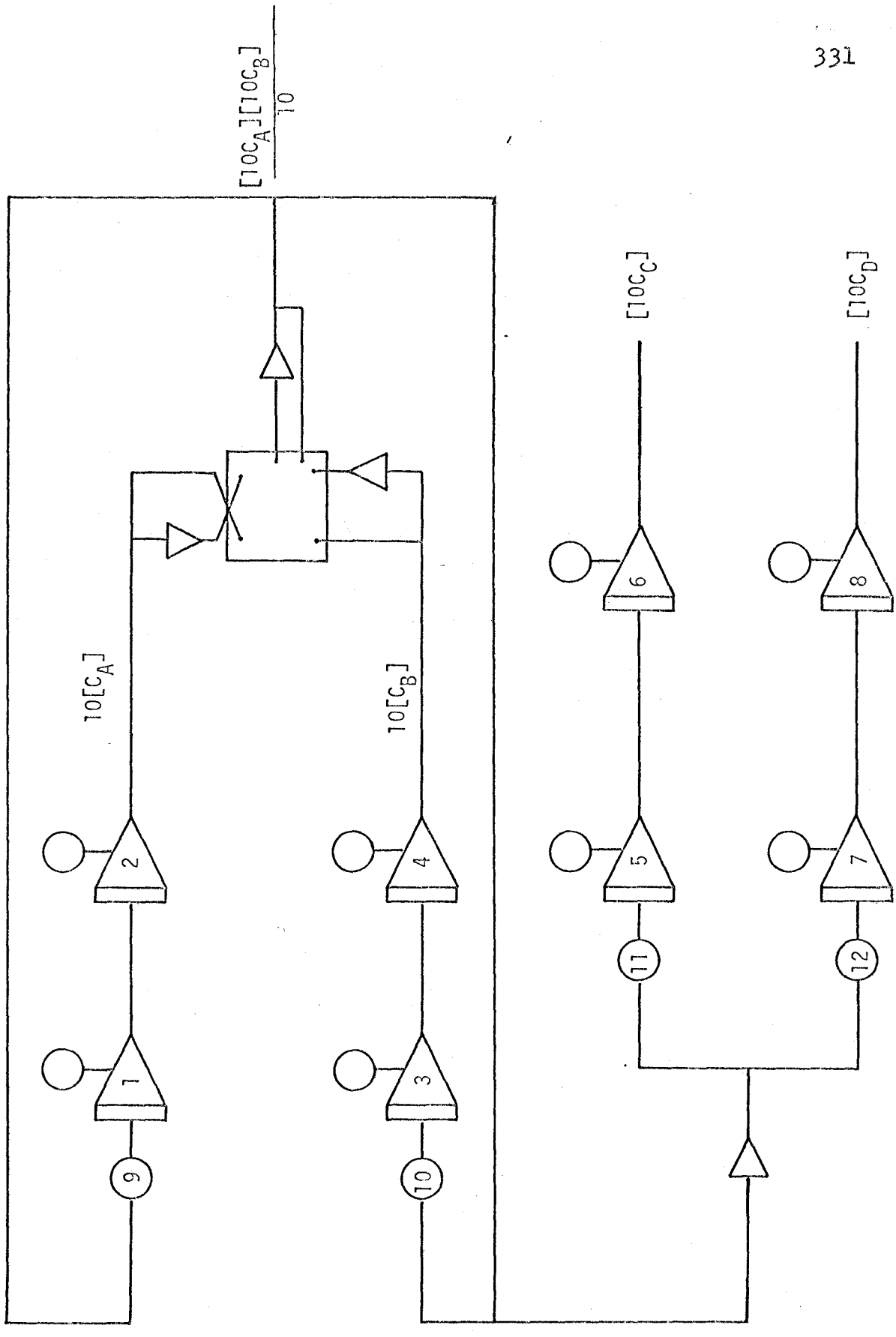

FIGURE IX.1
ANALOG CIRCUIT DIAGRAM

resistors to integrators Nos. 1, 3, 5 and 7 were changed to 10 K Ohms (instead of the usual 100 K Ohms).

The resulting analog simulation plots are shown in Figure IX.2. The results obtained from the simulation are as follows:

$C_{A_o} = 0.563$ moles/litre

$C_{B_o} = 0.0046$ moles/litre

$C_{C_o} = 0.2715$ moles/litre

$C_{D_o} = 0.505$ moles/litre

$\frac{k}{D_{EA}} = 217.4$; $\frac{k}{D_{EB}} = 483.1$; $\frac{k}{D_{EC}} = 680.2$;

$\frac{k}{D_{ED}} = 476.2$ litre/mole - cm.^{2}

$\therefore$ Taking k = 0.1 litre/mole - sec. (Appendix VIII),

$D_{EA} = 0.000460$ cm^2/sec

$D_{EB} = 0.000207$ cm^2/sec

$D_{EC} = 0.000147$ cm^2/sec

$D_{ED} = 0.000210$ cm^2/sec

The values of eddy diffusivities of the various components derived from the profiles in this example are not very close to each other. However, it should also be realized that this particular set of eddy diffusivities derived is by no means among the best sets whose diffusivity values for various components are much closer to each other.

More examples of the simulated concentration profiles are shown in Figures IX.3 and IX.4. Tables of derived sets of eddy diffusivities are shown in Appendix XVI.

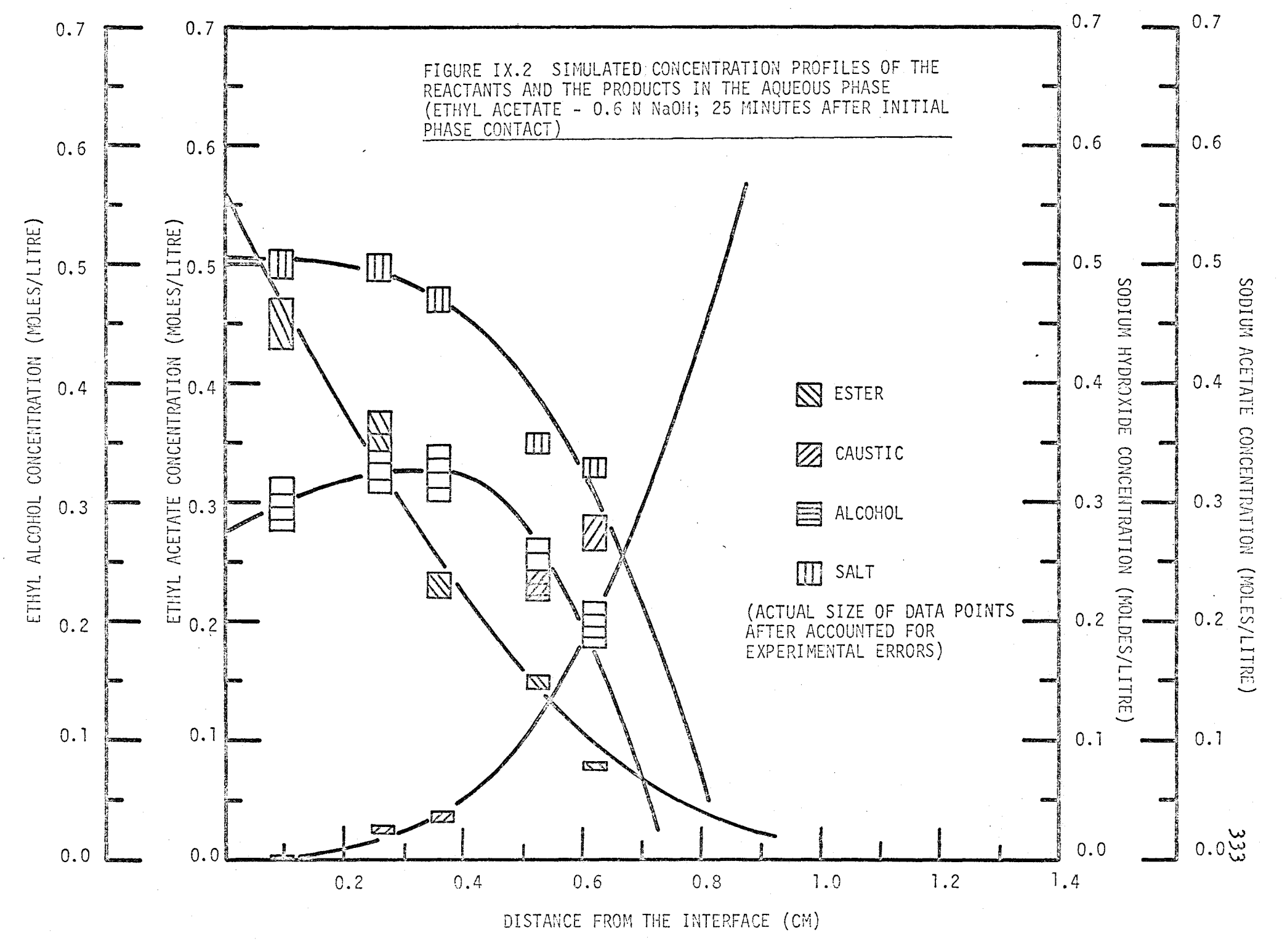
FIGURE IX.2 SIMULATED CONCENTRATION PROFILES OF THE REACTANTS AND THE PRODUCTS IN THE AQUEOUS PHASE (ETHYL ACETATE - 0.6 N NaOH; 25 MINUTES AFTER INITIAL PHASE CONTACT)
ETHYL ALCOHOL CONCENTRATION (MOLES/LITRE)
ETHYL ACETATE CONCENTRATION (MOLES/LITRE)
SODIUM HYDROXIDE CONCENTRATION (MOLES/LITRE)
SODIUM ACETATE CONCENTRATION (MOLES/LITRE)
0.0
0.1
0.2
0.3
0.4
0.5
0.6
0.7
0.2
0.4
0.6
0.8
1.0
1.2
1.4
DISTANCE FROM THE INTERFACE (CM)
ESTER
CAUSTIC
ALCOHOL
SALT
(ACTUAL SIZE OF DATA POINTS AFTER ACCOUNTED FOR EXPERIMENTAL ERRORS)

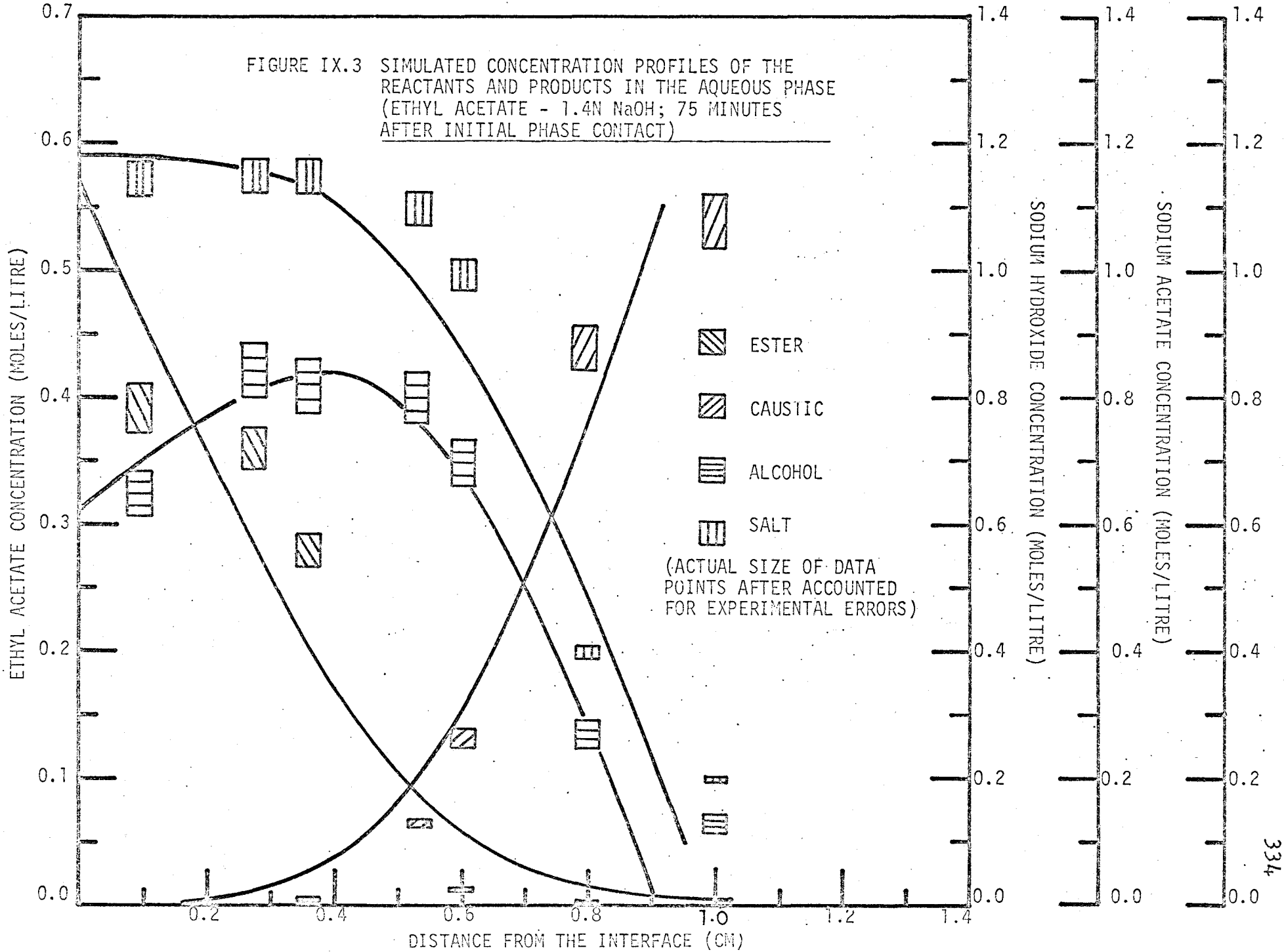

FIGURE IX.3 SIMULATED CONCENTRATION PROFILES OF THE REACTANTS AND PRODUCTS IN THE AQUEOUS PHASE (ETHYL ACETATE - 1.4N NaOH; 75 MINUTES AFTER INITIAL PHASE CONTACT)

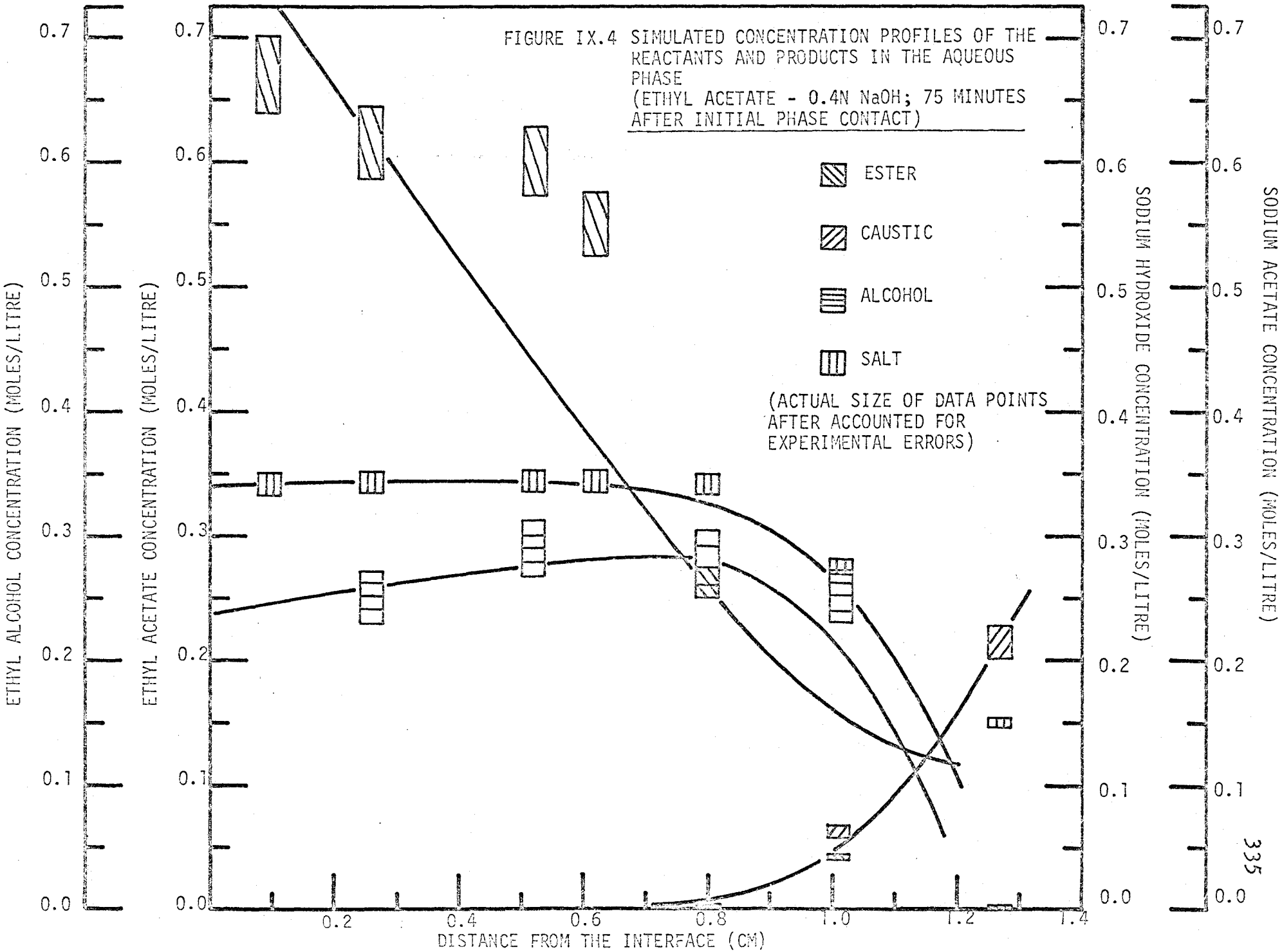

FIGURE IX.4 SIMULATED CONCENTRATION PROFILES OF THE REACTANTS AND PRODUCTS IN THE AQUEOUS PHASE
(ETHYL ACETATE - 0.4N NaOH; 75 MINUTES AFTER INITIAL PHASE CONTACT)

APPENDIX X

CALCULATION OF THE ENHANCEMENT FACTORS AND THE REACTION ZONE THICKNESSES IN THE CONCENTRATION PROBING EXPERIMENTS

(Refer to Chapter 4: 4.2 - PART B)

In this appendix, sample calculations of the experimental mass transfer rates and mass transfer coefficients are presented (data for the calculations are taken from Figure 20: Total Ester Transferred Across the Liquid Interface as a Function of Contact Time). Thus enhancement factors are obtained which are then compared with those theoretically predicted based on transfer with chemical reaction[B16][B14].

Sample calculations of the reaction zone thickness based on the experimental eddy diffusivities and transfer rates are also made.

X.1 Calculation of the Experimental Mass Transfer Rates as well as the Mass Transfer Coefficients

X.1.1. Averaged Mass Transfer Rate and Mass Transfer Coefficient

Data for these sample calculations are taken from Run #4 (ethyl acetate - 1.0 N sodium hydroxide) 50 minutes after initial phase contact. The total ester transferred across the interface up to 50 minutes of contact time is (refer to Figure 20) 0.341_{989} moles. Therefore, the mass transfer rate averaged over the period of 50 minutes is $(0.341_{989}/(50X60X353)) = 3.22_{936}X10^{-7}$ moles/sec.-cm.^{2} The respective mass transfer coefficient can then be obtained by the following equation:

$$\frac{N_i}{A} = D \left.\frac{\partial C_i}{\partial x}\right|_{x=0} = k_L(C_i^* - C_\infty) = k_L C_i^* \qquad (X.1)$$

where,

N_i = ester transfer rate, moles/sec.

A = interfacial area, $cm.^2$

k_L = mass transfer coefficient with chemical reaction, cm/sec.

C_i^* = equilibrium solubility of the ester in the aqueous salt solution, moles/c.c.

Based on the experimental data (Figure 18), the salt concentration at the interface is 0.850 N and the corresponding C_i^* is 0.560 moles/litre (Appendix XIII).

$$\therefore k_L = \frac{N}{A}\frac{1}{C_i^*} \qquad (X.2)$$

$$\frac{3.22936 \times 10^{-7}}{0.560 \times 10^{-3}} = 5.76_{671} \times 10^{-4} \text{ cm/sec.}$$

X.1.2 Instantaneous Mass Transfer Rates and Mass Transfer Coefficient

Based on the experimental data of Run #4, (ethyl acetate - 1.0 N sodium hydroxide), the total ester transferred across the interface at any contact time is given by the regression equation (Table 5).

$$N = 1.00_{589} \times 10^{-2}(T) - 7.11_{946} \times 10^{-5}(T^2) + 1.36_{246} \times 10^{-7}(T^3) \qquad (X.3)$$

where

N = total transfer of ester, moles

T = contact times, minutes

The instantaneous ester transfer rate at 50 minutes is obtained

by the differentiation of equation (X.3) with respect to T, and found to be 1.87_{030} X 10^{-7} moles/cm^2-sec. The corresponding mass transfer coefficient can again be obtained from equation (X.2) and found to be 3.33_{982} X 10^{-4} cm/sec.

X.2 Calculation of the Enhancement Factors based on the Unsteady State Transfer Model (B16)

X.2.1 Enhancement Factor Calculation based on the Averaged Ester Transfer Rate

From X.1.1 the mass transfer rate averaged over the period of 50 minutes for Run #4 (ethyl acetate - 1.0 N sodium hydroxide) is 3.22_{936} X 10^{-7} moles/cm^2-sec. The physical mass transfer rate averaged over the same period of time is 5.0_{7047} X 10^{-8} moles/cm^2-sec. (Table 5). Substituting these values into equation X.2 with the appropriate interfacial ester concentrations,

$$\phi = \frac{k_L}{k_L^*} = 9.66_{716}$$

The ϕ values for all the other runs and at the other contact time levels were calculated in a similar way. The results are shown in Table 10.

X.2.2 Enhancement Factor Calculation based on the Instantaneous Ester Transfer

From Section X.1.2, the instantaneous mass transfer rate at 50 minutes of contact time for Run #4 (ethyl acetate - 1.0 N sodium hydroxide) is 1.87_{030} X 10^{-7} moles/cm^2-sec. Similarly, the instantaneous physical ester transfer rate is calculated to be 2.1_{4681} X 10^{-8} moles/cm^2-sec. (Table 5). Substituting these values into equation (X.2) with the

appropriate interfacial ester concentrations

$$\phi = \frac{k_{L(inst.)}}{k^{*}_{L(inst.)}} = 13.22_{36}$$

Similar calculations were performed for all the other runs and at the other contact time levels. The results are shown in Table X.1.

X.2.3 Theoretical Calculation of the Enhancement Factor

The method proposed by Brian et al. as described in the Theoretical Section (Chapter 3:3.1.2) is used. The diffusivities of ethyl acetate and sodium hydroxide in water, taking into account of their concentration dependencies, are estimated to be 0.80×10^{-5} (4.4 - PART D), and 1.91×10^{-5} $cm^2/sec.$ respectively. Thus for the ethyl acetate - 1.0 N sodium hydroxide system,

$$r = \frac{1.910 \times 10^{-5}}{0.8 \times 10^{-5}} = 2.39$$

(Assuming that the ratio of diffusivities is not affected by the presence of multi-ions)

$$q = \frac{1.0}{0.56} = 1.786$$

$$\therefore q\sqrt{r} = 2.760$$

From equation (12) or Figure (1) of Reference (B16),

$$\phi a \cong 3.55$$

Also, for 50 minutes after the phase contact,

$$\sqrt{M} = \left(\frac{\pi}{4} 0.1 \times 1000 \times \frac{1.0}{1000} \times 50 \times 60\right)^{\frac{1}{2}} = 15.35_0$$

From equation 17 of Reference (B16); by trial and error method,

$$\phi' = 3.42_4, \quad \text{and} \quad \frac{\phi' - 1}{\phi_a - 1} = \frac{2.42_4}{2.55} = 0.95_{06}$$

TABLE X.1

INSTANTANEOUS ESTER MASS TRANSFER RATES AND ENHANCEMENT FACTORS IN THE ETHYL ACETATE-SODIUM HYDROXIDE AND THE METHYL PROPIONATE-SODIUM HYDROXIDE SYSTEMS

Run #	Ester transfer rates (moles/sec.-cm^2) X 10^7			Enhancement factors ϕ		
	25 minutes	50 minutes	75 minutes	25 minutes	50 minutes	75 minutes
EtAc - water	$.47_{073}$	$.21_{468}$	$.17_{653}$			
EtAc - 0.2 N NaOH	1.76_{298}	$.60_{529}$	$.55_{727}$	4.12_{360}	3.10_{436}	3.47_{572}
EtAc - 0.4 N NaOH	2.70_{057}	1.42_{917}	$.60_{996}$	6.96_{633}	8.03_{777}	4.16_{588}
EtAc - 0.6 N NaOH	3.10_{895}	1.65_{633}	$.46_{947}$	8.54_{467}	10.02_{75}	3.46_{175}
EtAc - 1.0 N NaOH	3.18_{916}	1.87_{030}	$.79_{266}$	10.47_{03}	13.22_{36}	6.69_{588}
EtAc - 1.4 N NaOH	3.49_{597}	2.25_{546}	1.09_{986}	12.93_{58}	18.44_{91}	10.63_{41}
MePr - water	1.80_{648}	1.41_{983}	1.13_{816}			
MePr - 0.4 N NaOH	1.46_{198}	1.14_{078}	1.05_{262}	$.92_{7577}$	$.92_{0894}$	1.06_{002}
MePr - 0.6 N NaOH	1.46_{198}	1.14_{078}	1.05_{262}	$.99_{9878}$	$.99_{7635}$	1.14_{835}
MePr - 1.0 N NaOH	1.62_{222}	1.18_{625}	$.92_{630}$	1.27_{188}	1.19_{241}	1.14_{401}

At this point a calibration curve is drawn from the data of Figures 6 to 8 of Reference (B16), with $100(\frac{\phi}{\phi'}-1)$ vs. ϕ_a at $\frac{\phi'-1}{\phi_a-1} = 0.95_{06}$ and r = 2.39. The calibration curve for this particular calculation is shown in Figure (X.1).

From the calibration curve,

$100(\frac{\phi}{\phi'} - 1)$ can be read off, at $\phi_a = 3.55$, to be 1.31.

$\therefore \phi = 3.46_9$

Similar calculations were performed for the 1.0 N run at 25 minutes and 75 minutes contact time, and also for the 1.4 N run, as well as the methyl propionate - 1.0 N sodium hydroxide system. The results are shown in Table (X.2).

X.3 Calculation of the Reaction Zone Thicknesses based on the Pseudo-Steady State Model.

As described in CHAPTER 3:3.1.1, under the steady state mass transfer conditions, the reaction zone thickness is given by equation;

$$x = 4.41 = 4.4 \left[\left(\frac{D_A D_B}{k\ N}\right)\right]^{1/3} \qquad (X.4)$$

where,

D_i = Diffusion coefficient of specis i, $cm^2/sec.$

k = reaction rate constant, $cm^3/mole\text{-}sec.$

N = molal flux, $moles/cm^2\text{-}sec.$

Data for these sample calculations are taken from Run #4, (ethyl acetate - 1.0 N sodium hydroxide), 50 minutes after initial phase contact.

FIGURE X.1

$100(\frac{\phi}{\phi'} - 1)$ VS. ϕ_a at $\frac{\phi'-1}{\phi_a-1} = 0.95$

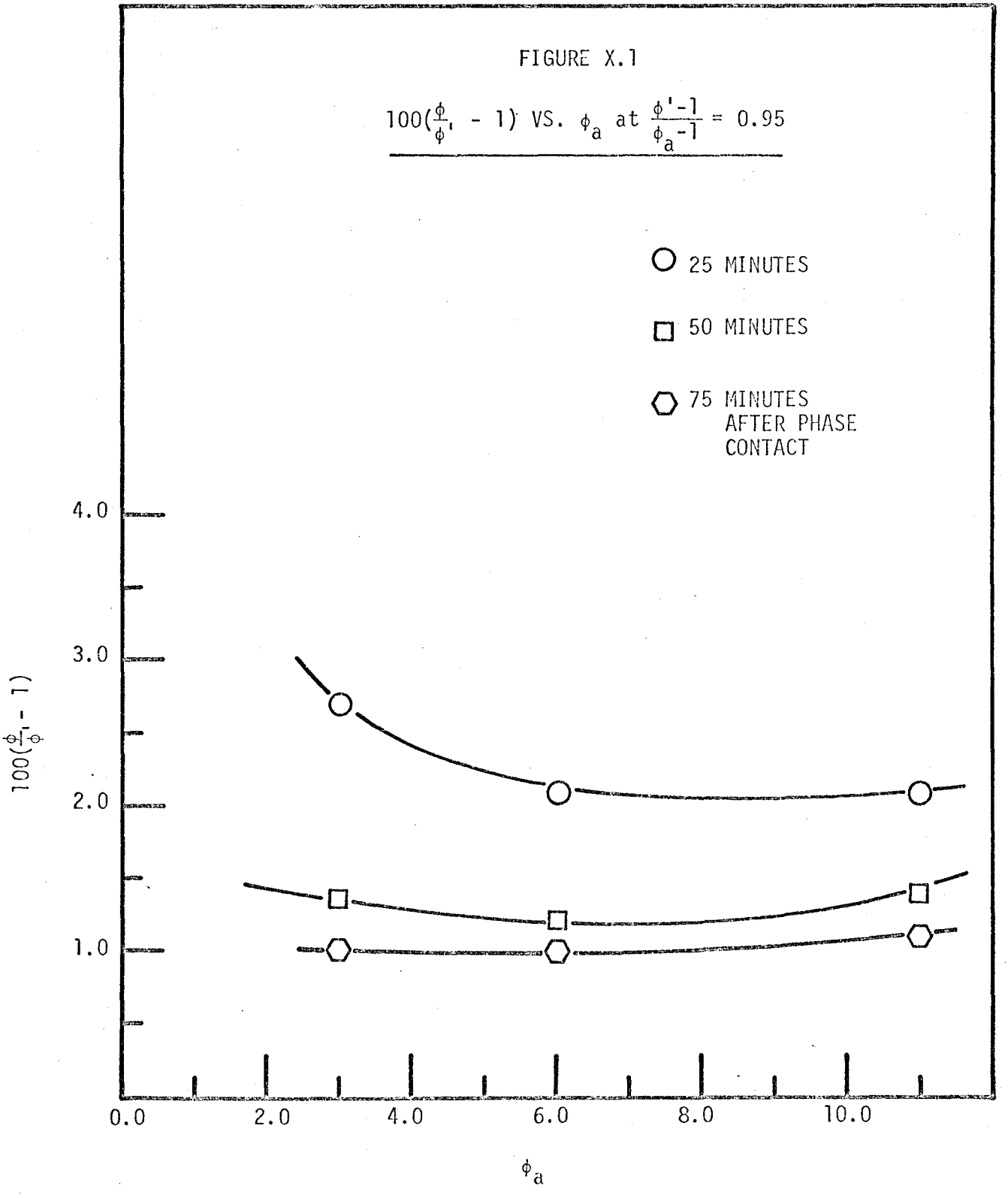

TABLE X.2

COMPARISON OF ENHANCEMENT FACTORS AS MEASURED FROM EXPERIMENTS AND AS PREDICTED FROM THE PENETRATION THEORY

Run No.	ϕ_a	$\sqrt{M} = (\pi k C_{Bo} t/4)^{\frac{1}{2}}$	ϕ'	ϕ
EtAc-1.0 N NaOH				
25 minutes	3.55	10.85_4	3.31_3	3.39_7
50 minutes	3.55	15.35_0	3.42_4	3.46_9
75 minutes	3.55	18.80_0	3.46_4	3.49_9
EtAc-1.4 N NaOH				
25 minutes	5.4	12.84_3	4.78_9	4.94_2
50 minutes	5.4	18.16_2	5.05_9	5.15_3
75 minutes	5.4	22.24_4	5.16_3	5.22_0
MePr-1.0 N NaOH				
25 minutes	3.8	10.85_4	3.50_9	3.60_0
50 minutes	3.8	15.35_0	3.64_3	3.68_9
75 minutes	3.8	18.80_0	3.69_2	3.72_7

X.3.1 Reaction Zone Thickness, calculated based on Experimentally Determined Eddy Diffusivities as well as the Time Averaged Ester Transfer Rate:

Since the systems under studied are turbulent, it is believed to be more realistic in these calculations to use the averaged experimental diffusion coefficient values of the four components rather than the individual diffusivities of the components involved.

$\therefore D_A = D_B = 0.000266_9$ cm^2/sec. (Refer to Table XVI.4)

The reaction rate constant is 100 cm^3/mole-sec. The mass transfer rate averaged over the period of 50 minutes is 3.22_{936} X 10^{-7} moles/cm^2-sec. (Refer to X.1.1)

$\therefore$ Substituting all these values into equation(X.4), l is calculated to be 0.57_{2769} cm.

The reaction zone thicknesses for Run #4, 25 minutes and 75 minutes, and for other runs were calculated in a similar way. The results are presented in Table 12.

X.3.2 Reaction Zone Thickness calculated based on the Experimentally Determined Eddy Diffusivities and the Instantaneous Ester Transfer Rate:

From Section X.1.2, the instantaneous ester transfer rate at 50 minutes is found to be 1.87_{030} X 10^{-7} moles/cm^2-sec. Substituting this transfer rate into equation X.4 together with the experimental eddy diffusivities values, l is calculated to be 0.68_{7145} cm.

The reaction zone thicknesses for all the other runs were calculated similarly. The results are presented in Table X.3.

TABLE X.3

COMPARISON OF THE REACTION ZONE THICKNESSES AS MEASURED EXPERIMENTALLY AND AS APPROXIMATED FROM THE PSEUDO-STEADY STATE MODEL (BASED ON INSTANTANEOUS ESTER TRANSFER RATES)

Run #	25 Minutes (cm.)		50 Minutes (cm.)		75 Minutes (cm.)	
	model	experimental	model	experimental	model	experimental
EtAc - 0.2 N NaOH	$.67_{1803}$	.57	$.67_{3694}$	.32	$.78_{7078}$	.47
EtAc - 0.4 N NaOH	$.75_{6939}$	.66	$.89_{0669}$	.52	1.27_{821}	.38
EtAc - 0.6 N NaOH	$.56_{3874}$	.62	$.83_{8384}$	.43	1.04_{254}	.38
EtAc - 1.0 N NaOH	$.24_{5219}$	.37	$.68_{7145}$	.36	$.80_{5919}$	.25
EtAc - 1.4 N NaOH	$.19_{9536}$	.38	$.36_{7849}$	.44	$.67_{4387}$	.32
MePr - 0.4 N NaOH	$.26_{3075}$	.46	$.38_{8455}$	.40	$.40_{8265}$	.26
MePr - 0.6 N NaOH	$.18_{5879}$	.29	$.27_{9587}$	.58	$.46_{8707}$	.34
MePr - 1.0 N NaOH	$.27_{7811}$	.34	$.26_{6016}$	.35	$.18_{0558}$	.36

X.3.3 Reaction Zone Thickness calculated based on Molecular Diffusivities and Theoretically Predicted Reaction Transfer Rate of the Ester

Theoretically, if the interfacial turbulence as well as the zone turbulence were neglected, then the average molecular diffusivities of the ethyl acetate and the sodium hydroxide, as estimated previously in X.2.3, would be 0.80×10^{-5} and 1.91×10^{-5} $cm^2/sec.$ respectively. The effect of multi-ion diffusion in the reaction system is neglected for these calculations. The reaction mass transfer rate would be $3.46_9 \times (0.560/0.850) \times$ physical transfer rate = 1.15883×10^{-7} $moles/cm^2/sec.$ for the ethyl acetate-1.0 N sodium hydroxide run at 50 minutes of contact time. Substituting all these values into equation(X.4), l is calculated to be 0.10_{195} cm.

Due to the limitations in obtaining the theoretical enhancement factors (X.2.3), the reaction zone thicknesses for only three runs were calculated (ethyl acetate-1.0 N and 1.4 N sodium hydroxide; methyl propionate-1.0 N sodium hydroxide). For the methyl propionate-sodium hydroxide system, the experimental physical transfer rates at different contact times were not used because of the so-called "density flow" observed in the methyl propionate-water system (Chapter 4: 4.2.3.3.3). Instead, the theoretical physical transfer rates (which were assumed to be the same as those of the ethyl acetate-water system due to their close similarities in properties; Table 1) based on the penetration model were

used (4.2.3.3.2). The theoretical results on the zone thicknesses are presented in Table 12.

Note X.1 .

Estimation of the enhancement factors based on the ionic penetration theory:

The "effective diffusivity ratio" method proposed by Brian et al. as described in Reference (B14) is used. The following calculations are based on the data from the ethyl acetate-1.0 N sodium hydroxide system.

Assumptions involved:

I No turbulent liquid motion in the aqueous phase;

II Concentration and viscosity dependencies of the diffusivities are neglected. Component diffusivities at infinite dilution are used.

$$r = \frac{D_B}{D_A} = \frac{2.14 \times 10^{-5}}{0.98 \times 10^{-5}} = 2.18$$

(c.f. the value of r = 2.39 calculated with the diffusivities averaged over their respective concentration ranges.)

$$r_{eff.} = \frac{2\,\frac{D_{OH^-}}{D_{EtAc}}}{1+\sqrt{\left(\frac{C_{OH^-}}{C_{Na^+}}\right)_o\left(\frac{D_{OH^-}}{D_{Ac^-}}-1\right)+1}}$$

(refer to equation (18) of Reference (B14))

Assuming no reaction or negligible acetate ions in the bulk aqueous phase,

$$\left(\frac{C_{OH^-}}{C_{Na^+}}\right)_o \cong 1$$

Substitution of the appropriate values into the equation gives

$$r_{eff.} = \frac{2\left(\frac{5.25 \times 10^{-5}}{0.98 \times 10^{-5}}\right)}{1+\sqrt{\frac{5.25 \times 10^{-5}}{1.09 \times 10^{-5}}}} = 3.36$$

$$q = \frac{1.0}{0.56} = 1.786$$

$$q\sqrt{r_{eff.}} = 3.28$$

From equation (12) or Figure 1 of Reference (B16),

$$\phi_a \cong 4.05$$

For 50 minutes after the phase contact,

$$\sqrt{M} = 15.35$$

$$\phi_{ionic} \cong 3.96$$

$$\phi_{mol.} = 3.47 \text{ (Section X.2.3)}$$

$$\therefore \text{ Increase of } \phi = \left(\frac{3.96 - 3.47}{3.47}\right) \times 100 = 14.1\%$$

If the amount of the NaOH reacted in the bulk aqueous phase is taken into consideration (the amount of the NaOH reacted inside the reaction layer is averaged over the entire aqueous phase; refer to Figure 28),

$$\left(\frac{C_{OH^-}}{C_{Na^+}}\right)_o \cong 0.855$$

$$r_{eff.} = \frac{2 \times \frac{5.25 \times 10^{-5}}{0.98 \times 10^{-5}}}{1 + \sqrt{0.855\left(\frac{5.25 \times 10^{-5}}{1.09 \times 10^{-5}} - 1\right) + 1}} = 3.51$$

$$q\sqrt{r_{eff.}} = 3.35$$

$$\phi_a \cong 4.12$$

$$\phi_{ionic} \cong 4.02$$

$$\therefore \text{ Increase of } \phi = \frac{4.02 - 3.47}{3.47} \times 100 = 15.9\%$$

For the case of ethyl acetate-1.4 N NaOH: 50 minutes after phase contact,

$$\phi_{ionic} \cong 6.30 \quad \text{for} \left(\frac{C_{OH^-}}{C_{Na^+}}\right)_o \cong 1$$

and the increase of $\phi \cong 22.4\%$.

Note X.2

Calculation to check the validity of the assumption (quasi-steady state) involved in the estimation of reaction zone thickness:

The following calculation is based on the data from ethyl acetate-1.0 N sodium hydroxide system: 50 minutes after phase contact.

Measured reaction zone thickness (X) = 0.36 cm.

Derived eddy diffusivity of ethyl acetate =

$$2.66_9 \times 10^{-4} \text{ cm}^2/\text{sec.}$$

$$\therefore \frac{l^2}{D_A t} = \frac{(\frac{0.36}{4.4})^2}{2.66_9 \times 10^{-4} \times 50 \times 60} = 0.008_{36}$$

The following table shows the calculated ($l^2/D_A t$) values for all the cases under study:

NaOH conc. \ phase contact time ($\frac{l^2}{D_A t}$)	25 Minutes	50 Minutes	75 Minutes
Ethyl acetate-sodium hydroxide system			
0.2 N	.045	.012	.014
0.4 N	.040	.014	.004
0.6 N	.052	.009	.007
1.0 N	.060	.008	.003
1.4 N	.087	.029	.006
Methyl propionate-sodium hydroxide system			
0.4 N	.130	.031	.008
0.6 N	.087	.100	.012
1.0 N	.062	.041	.059

APPENDIX XI

PRELIMINARY EXPERIMENTS IN THE ETHYL ACETATE-WATER SYSTEM

XI.1 Experimental Details

(Numbers in the following brief description refer to Figure XI.1)

The apparatus was assembled as shown schematically in Figure XI.1, the test cell (1) was made of pyrex glass, having an I.D. of 21.2 cm., and measured 7.5 cm. from bottom to top. The brass plate (2) holding the 15 sampling needles together with the point gauge was the same one as described previously (Chapter 4; 4.2 - PART B). A circular segment of 1.0 cm. in diameter was cut off from the edge of the brass plate to allow the aqueous phase feed tube to go through the plate and into the cell.

To start a run, the phase contactor (3) was lowered into the bottom of the cell. It was important, at this stage, to ensure that the feeding system (from the reservoir (6) to the pores of the sintered glass disc) should be free of air. Then 500 ml. of water-saturated ester was gently poured into the cell. The brass plate holding the needles was put on top horizontally and covered up the cell quite tightly. (The sampling needle inlets positions relative to the point gauge were already accurately measured.) B-D stopcocks (4), fitted on top of the needles chosen for sampling in the particular run, were closed. Stopcock (5) of the

FIGURE XI.1

APPARATUS FOR THE PRELIMINARY EXPERIMENTS
IN THE ETHYL ACETATE-WATER SYSTEM

1. Pyrex Glass Cell (21.2 cm. Diameter)
2. Brass Plate with 15 Needles plus Point Gauge
3. Phase Contactor
4. B-D Spring Loaded Stopcock (MS09)
5. Teflon Stopcock
6. Reservoir

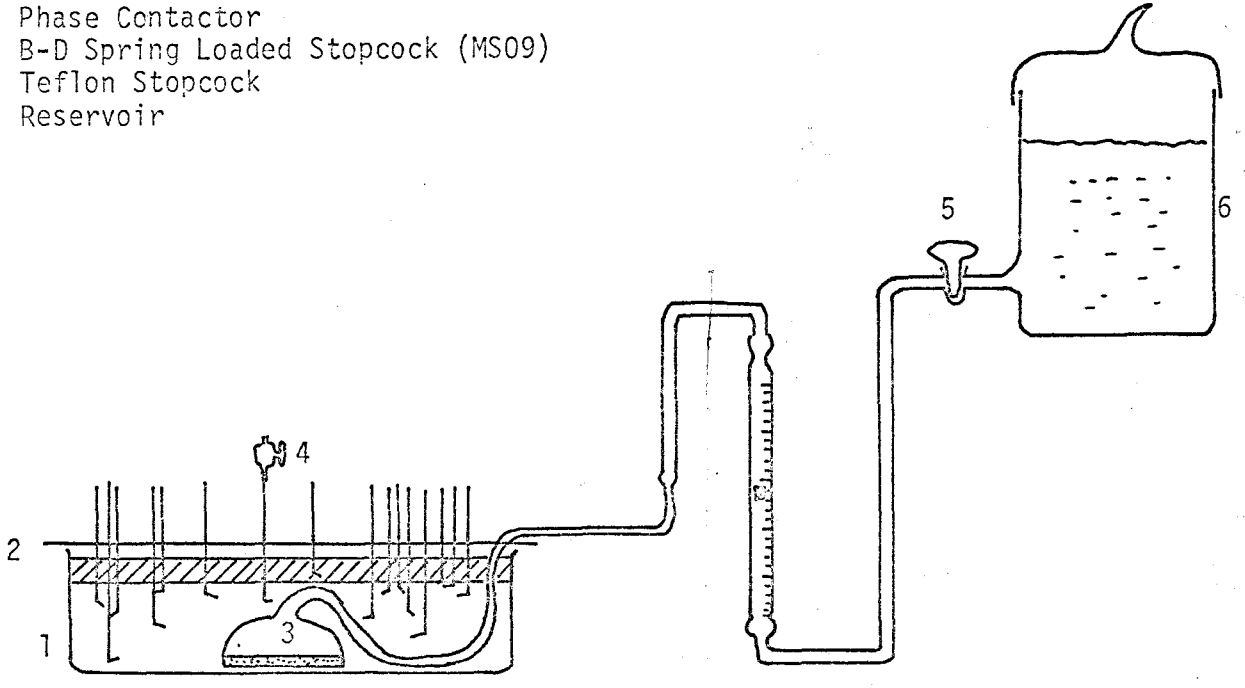

reservoir was opened and the timer was started. The aqueous solution was fed into the cell at the controlled flowrate of 0.28 litres/minute until the ester-water interface just touched the tip of the gauge needle. During the experimental run, small samples were taken at intervals from each of the set of needles chosen for sampling.

XI.2 Analysis of the Samples

The volume of each sample drawn into the syringe was read accurately. It was then transferred into the sampling tube and diluted with distilled water. The ethyl acetate concentration in the solution was analysed by means of a Burell (Khromotog model K-D) chromatograph.

XI.3 Results and Discussions

The analysis of the data is similar to that described in Chapter 4: 4.2.1. The concentration profiles obtained were plotted as shown in Figure XI.2. The total ethyl acetate transferred across the liquid interface at different contact times was calculated and plotted in Figure XI.3 (The extra amount of the ester transfer due to initial phase contact mixing was already accounted for)

Comparison of the ester transfer rate (Figure XI.3) obtained in the preliminary run with those obtained from the main run as described in 4.2.2.2 (Figure 20) indicates that the ester transfer is slightly higher in the preliminary run. This is probably due to the faster sampling rate used and some mechanical vibration induced during sampling. In the

FIGURE XI.2

CONCENTRATION PROFILES OF ETHYL ACETATE-WATER SYSTEM
PRELIMINARY EXPERIMENTS; RUN #2

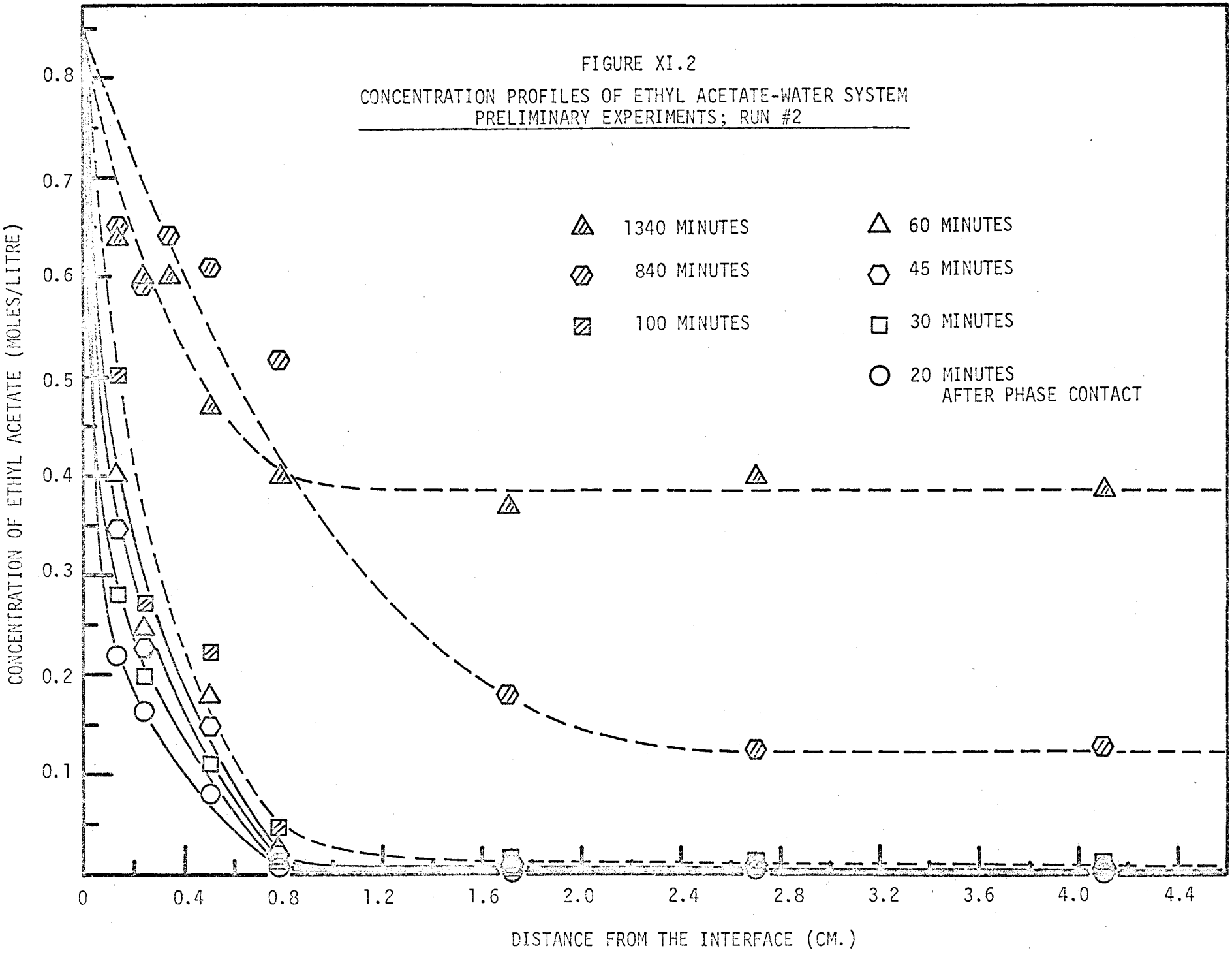

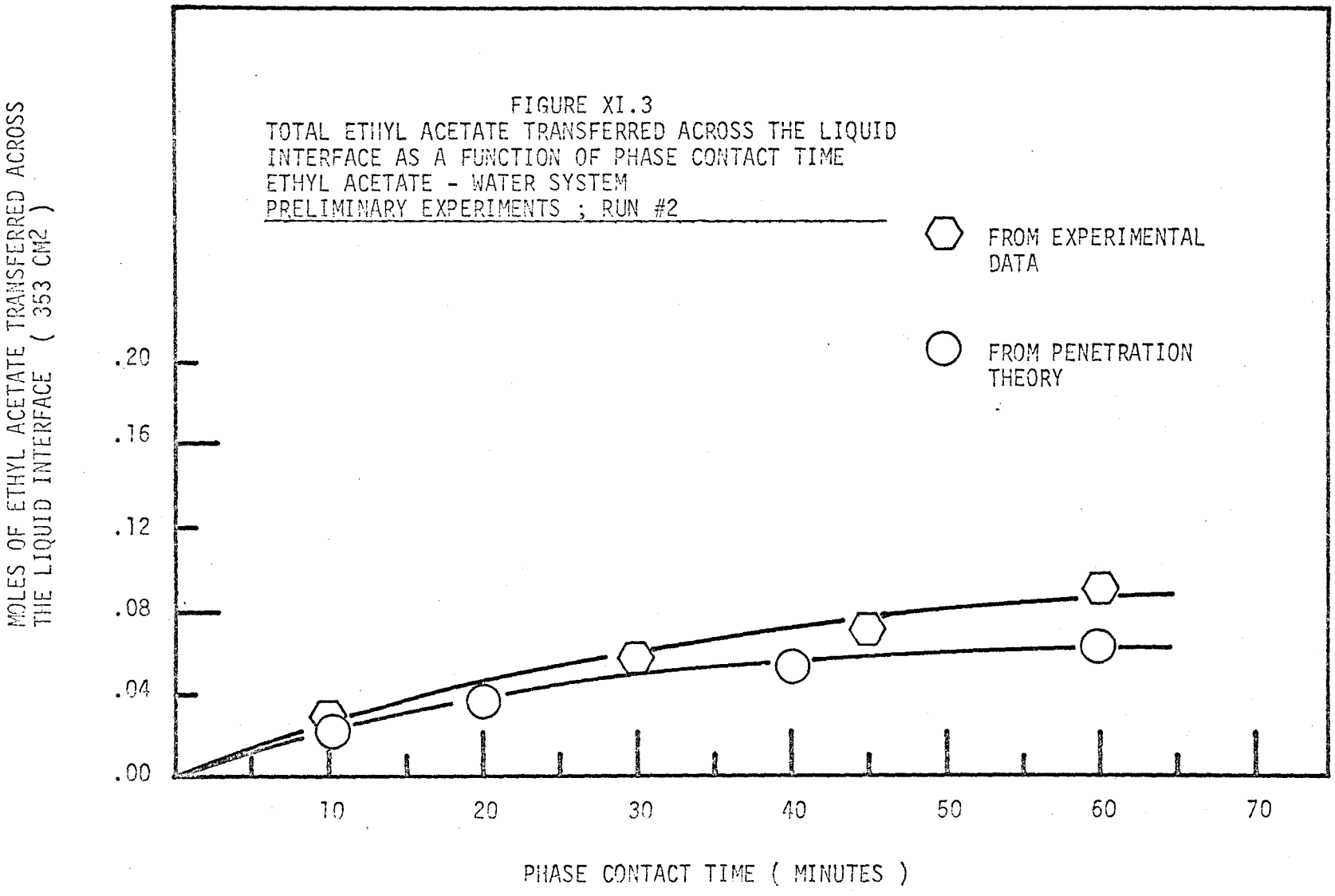
FIGURE XI.3
TOTAL ETHYL ACETATE TRANSFERRED ACROSS THE LIQUID INTERFACE AS A FUNCTION OF PHASE CONTACT TIME
ETHYL ACETATE - WATER SYSTEM
PRELIMINARY EXPERIMENTS ; RUN #2
FROM EXPERIMENTAL DATA
FROM PENETRATION THEORY
MOLES OF ETHYL ACETATE TRANSFERRED ACROSS THE LIQUID INTERFACE (353 CM2)
.20
.16
.12
.08
.04
.00
10
20
30
40
50
60
70
PHASE CONTACT TIME (MINUTES)

later apparatus an attempt was made to reduce such vibration, as described in Section 4.2.1.

APPENDIX XII

PRELIMINARY EXPERIMENTS ON THE MEASUREMENT OF CONCENTRATION DISTRIBUTION OF COMPONENTS IN THE ETHYL ACETATE-SODIUM HYDROXIDE SYSTEM

XII.1 Experimental procedure

(Numbers in the following brief description refer to Figure XII.1)

Preliminary experiments at 24 ± 1°C were performed in the same apparatus as described previously(S8) and as shown in Figure XII.1.

Four long stainless steel sampling needles (five needles in the ethyl acetate - 1.5 N sodium hydroxide run) were spaced within the test cell (1), which was 15.5 cm. in diameter and 12 cm. high. The needles (3) were bent at one end and the vertical distances of the sampling needle inlets with respect to each other were measured using a cathetometer. Ethyl acetate pre-saturated with water was poured into the test cell, filling one-eighth of its volume. Then the phase contactor (2) containing approximately 1½ litres of sodium hydroxide solution at the desired concentration level was lowered into the cell until the fritted glass disc just touched the bottom of the cell. After the cell top was tightly covered with clean aluminum foil to avoid evaporation of the upper phase, the sodium hydroxide solution was let out slowly through the sintered glass disc and under the ethyl acetate phase. The flowrate of approximately 0.4 litres/minute was controlled by the pipette filler. In this way, a smooth and

FIGURE XII.1

APPARATUS FOR THE PRELIMINARY EXPERIMENTS IN THE ETHYL ACETATE-SODIUM HYDROXIDE SYSTEM

1. Test Cell
2. Caustic Delivery Tube
3. Sampling Needles

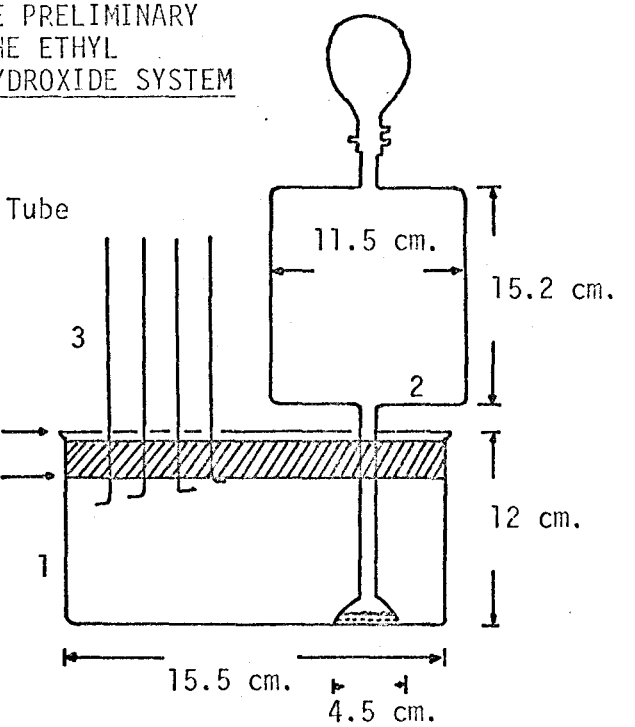

FIGURE XII.2

DISTILLATION APPARATUS

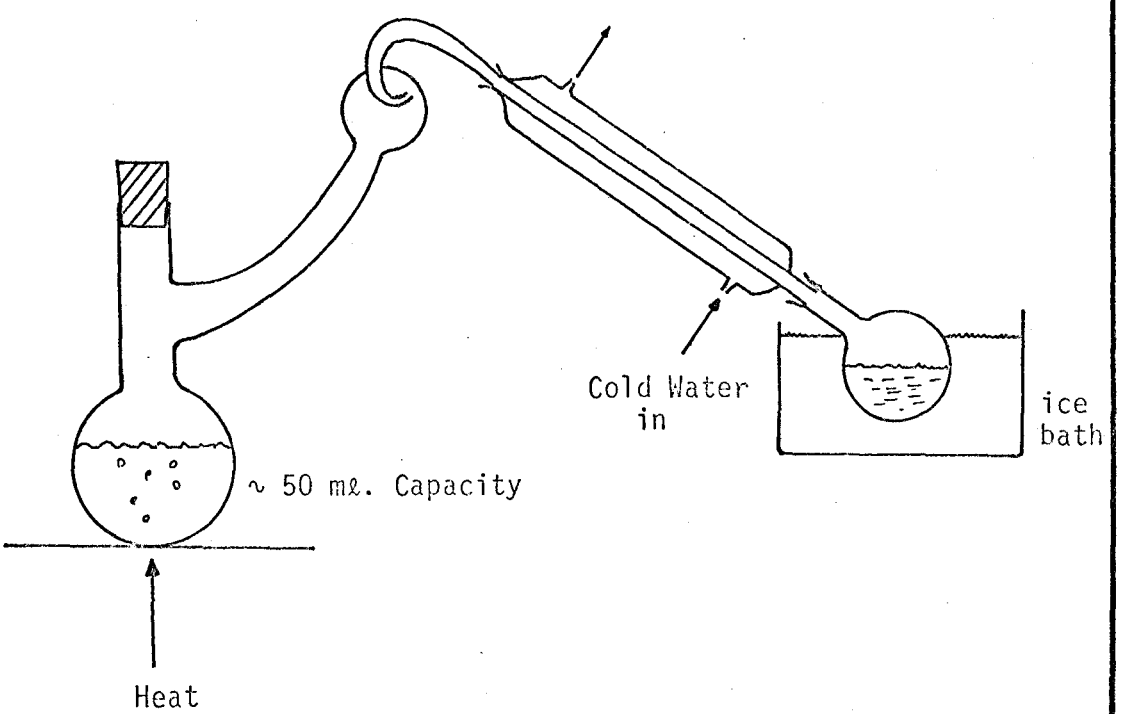

rather undisturbed interface between the ester phase and the caustic phase was formed. As more of the sodium hydroxide solution was introduced into the cell, the interface moved up gradually to a pre-determined level which was 1 mm. above the sampling inlet of the highest needle. Zero time for the experiment began as soon as the flow of sodium hydroxide was started. Duration of the experiment was 90 minutes. During the experimental run, three or four samples were taken at intervals from each sampling needle, and 2.5 ml. of the solution was drawn for each sample. The "phase contactor" was left inside the cell throughout the experiment.

After the experiment, both the test cell and the phase contactor were cleaned thoroughly with concentrated chromic acid and rinsed with a large amount of double distilled water.

XII.2 Analysis of Samples

XII.2.1 Sodium Hydroxide

Each sample freshly drawn from the cell was quickly put into a tube containing 5 ml. of ice-cold distilled water. The solution was titrated immediately with standard hydrochloric acid solution using a controlled volume of phenolphthalein solution as indicator.

XII.2.2 Ester and Alcohol

The sample, after being neutralized with standard hydrochloric acid solution, was diluted further with 15 - 20 ml. of ice-cold distilled water. The total volume of the sample was noted accurately. The sample, containing ester,

sodium chloride, sodium acetate and ethanol with a large amount of water, was charged into a small distillation unit (Figure XII.2) to separate the salts. The distillate was analysed for ester and ethanol in the way described in Chapter 4: 4.2.1.

A Burell (Khromotog model K-D) chromatograph with a column of 5% Carbowax 1500 on Fluoropak 80, 2½ meters long and ¼-inch O.D. was used for the analyses.

XII.2.3 Salt

The residue from the distillation flask was dissolved in approximately 350 ml. of distilled water. The sodium acetate concentration was analysed by conductometric titration in the same way as described in Chapter 4: 4.2.1 and in Appendix IV.

XII.3 Number of Experiments Performed

(The ethyl acetate phase was pre-saturated with water)

Three runs were performed at the controlled room temperature of 24 ± 1°C and at three sodium hydroxide concentration levels.

XII.4 Methods of Calculation

The methods of calculation were similar to those described in Chapter 4: 4.2.1.

XII.5 Results

The measured concentration profiles of the reactants and products for the three runs at 30 minutes, 45 minutes and 60 minutes of contact time were drawn. Typical profiles are shown in Figure XII.3.

FIGURE XII.3

CONCENTRATION PROFILES OF COMPONENTS
IN THE AQUEOUS PHASE
ETHYL ACETATE - 1.0N NaOH; 60 MINUTES
AFTER PHASE CONTACT

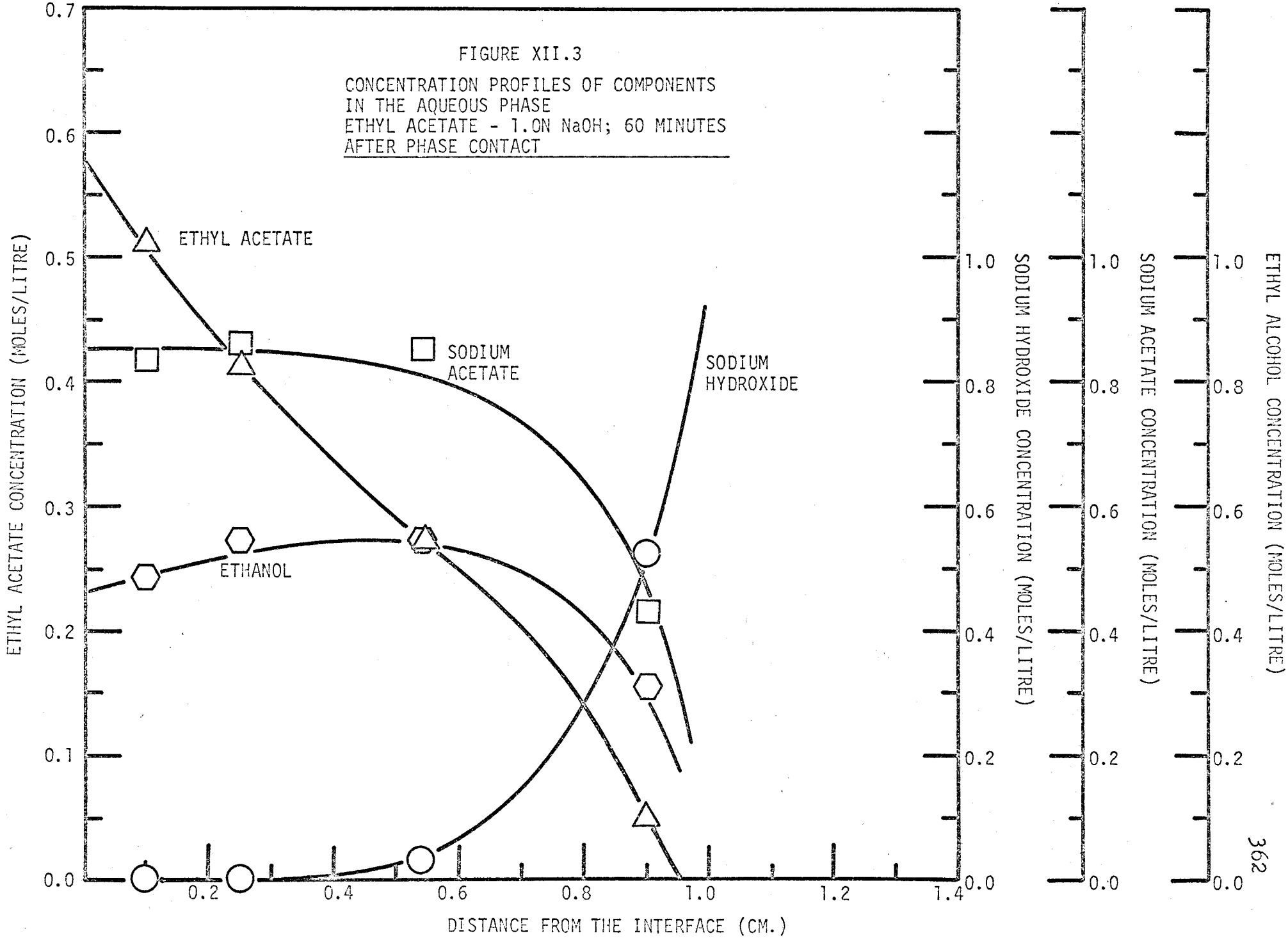

Due to the fairly large volume of liquid taken in each sample (2.5 ml.), the net volume of liquid transferred from the upper phase during the run was not enough to compensate for the volume of liquid taken out of the aqueous phase as samples. The result was a drop in the level of the interface with respect to the fixed inlet positions of the sampling needles. Furthermore, in some samples where the concentrations of both reactants were substantial, a significant amount of reactants would be consumed in the syringe before the sample could be transferred into the sampling tube and diluted with ice-cold distilled water. The titration of the sample with standard hydrochloric acid solution was performed immediately by an assistant. The drop of interface level as well as the reaction in the syringe had been accounted for when drawing the concentration profiles.

In general, the shape of the profiles was similar to the corresponding profiles obtained in Chapter 4, 4.2 - PART B (Figure 18). The total ester transferred across the liquid-liquid interface at various contact times as derived from the concentration profiles is given in Figure XII.4.

XII.6 Discussion of Results

XII.6.1 Comparison of the preliminary profiles with those obtained from the main experiments

Since the two sets of profiles were obtained at different contact times and at different caustic concentration levels, direct comparison becomes difficult. However, a close study

FIGURE XII.4

TOTAL ETHYL ESTER TRANSFERRED ACROSS THE LIQUID INTERFACE AS A FUNCTION OF PHASE CONTACT TIME
ETHYL ACETATE - NaOH SYSTEM
PRELIMINARY EXPERIMENTS

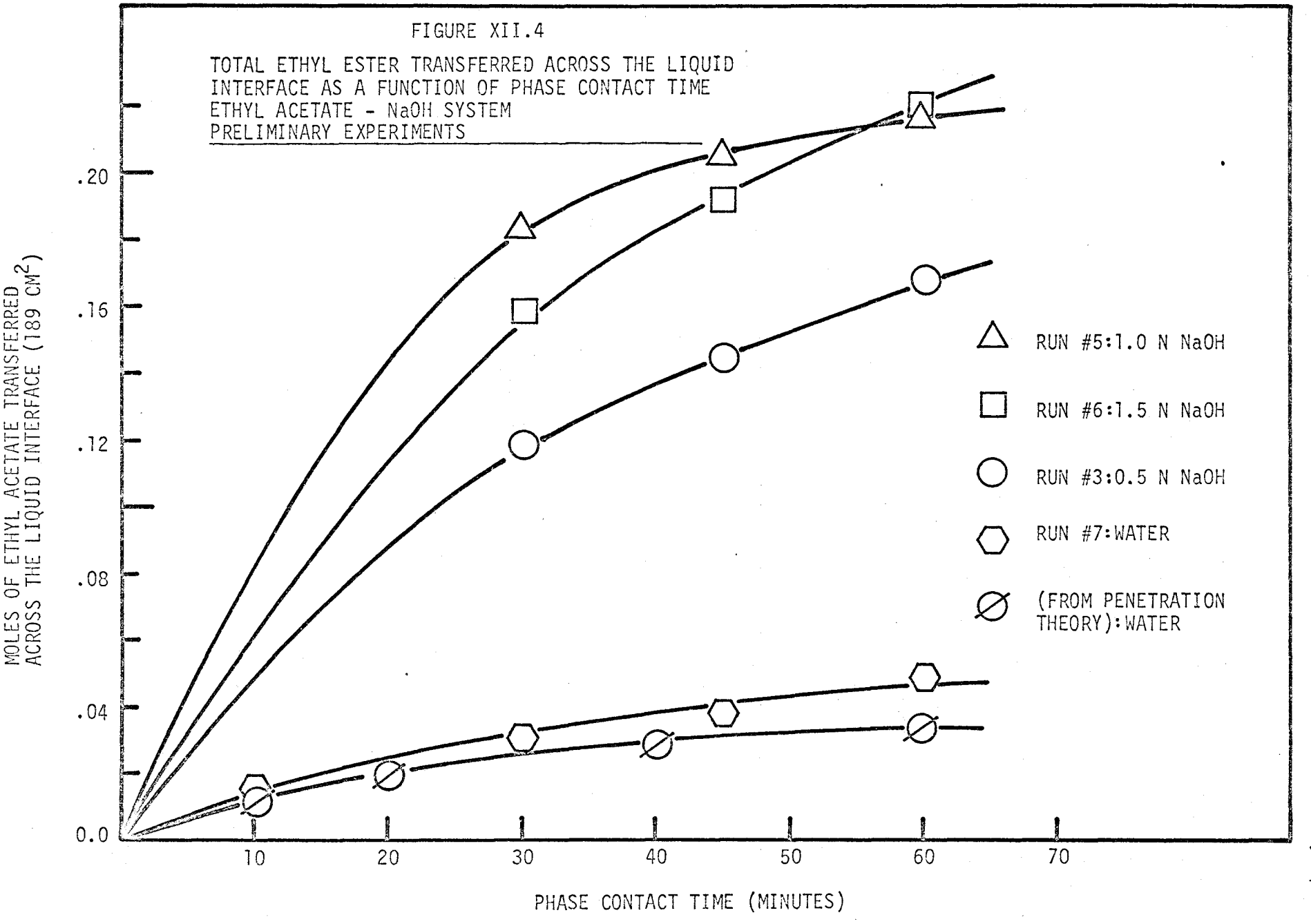

of all the available concentration profiles indicates that the ethyl acetate profile as well as the total ester transfer per unit interfacial area are higher in the preliminary runs, particularly at the earlier stage of the experiment (25 minutes to 50 minutes). This is probably because of the high filling rate of the lower phase used in the preliminary experiments as well as the mechanical vibration while sampling.

Considering the very limited amount of experimental data available in these preliminary runs, it is surprising to note that the two sets of total mass transfer data are, at least qualitatively, reproducible (Figure XII.5).

XII.6.2 Derivation of Eddy Diffusion Coefficients

Analog simulation of the experimental concentration profiles as described in Chapter 4: 4.2 - PART B: 4.2.3.4.4.3. and in Appendix IX was also carried out.

A typical set of simulated concentration profiles of the components in the reaction system is shown in Figure XII.6. The eddy diffusivities derived from the simulation are tabulated in Table XII.1. In general, the eddy diffusivities of ethyl acetate in the aqueous phase in these preliminary experiments are higher than those obtained from the profiles of the main sets of experiments (Chapter 4: 4.2.2). On the other hand, the values of the eddy diffusivities of the rest of the three components in the preliminary runs are comparable in the order of magnitude to those in the main experiments. Moreover, the values of sodium hydroxide, ethanol and sodium acetate

FIGURE XII.5

TOTAL ETHYL ESTER TRANSFERRED ACROSS 1 CM^2 OF THE LIQUID INTERFACE AS A FUNCTION OF PHASE CONTACT TIME

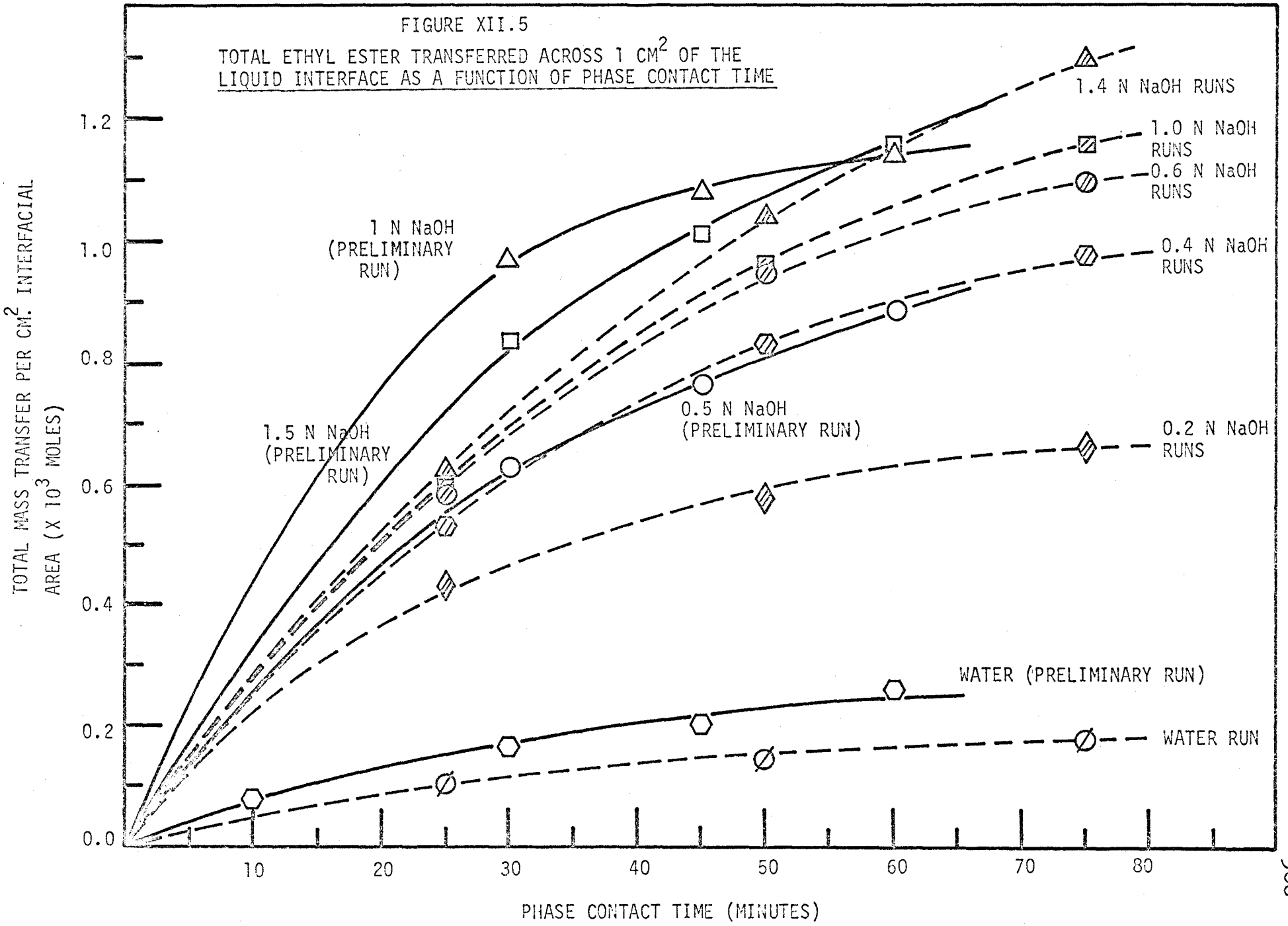

FIGURE XII.6 SIMULATION OF THE PROFILES IN FIGURE XII.3

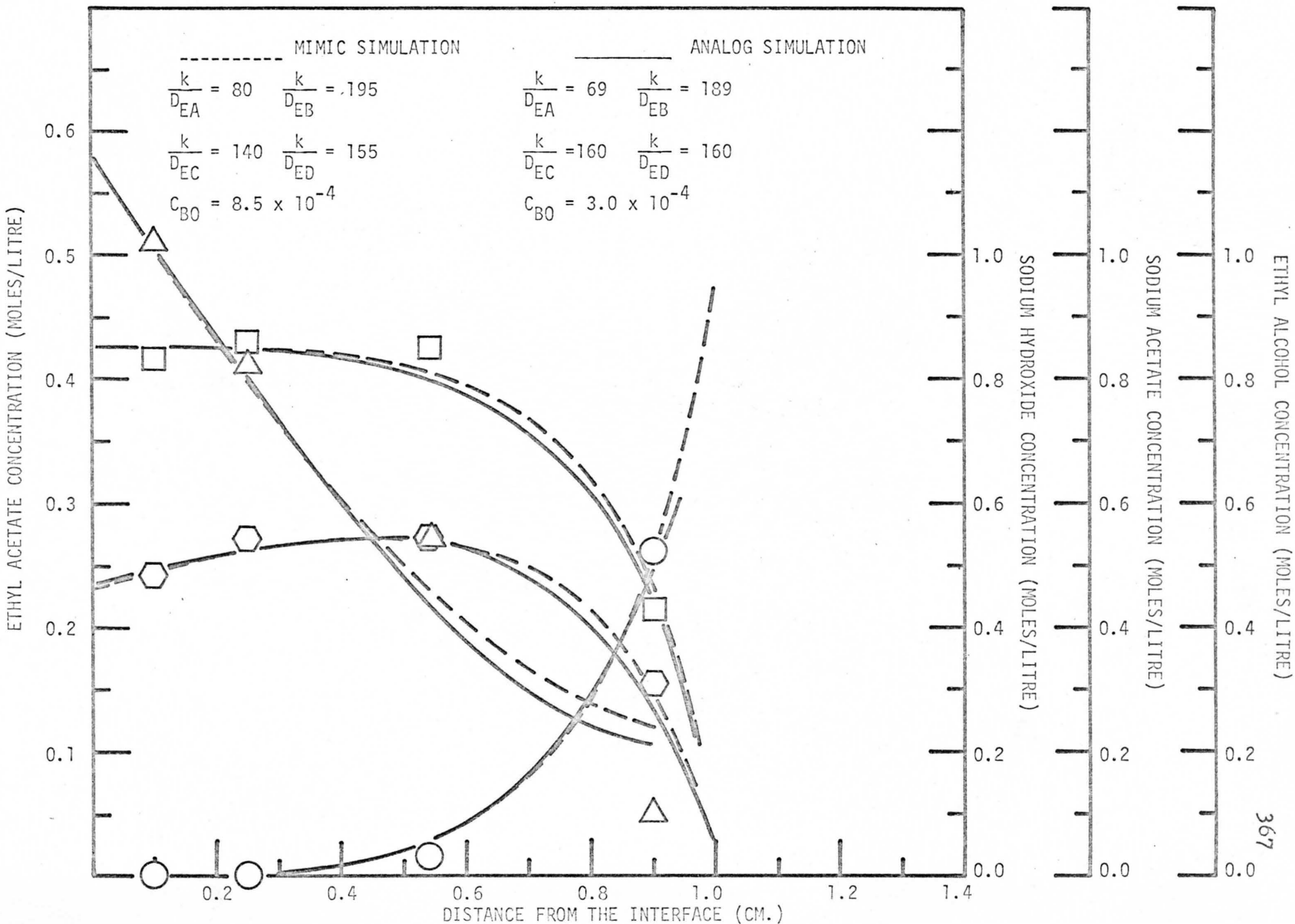

TABLE XII.1

ETHYL ACETATE - 0.5 N SODIUM HYDROXIDE
(Preliminary Experiments)

Contact time (Minutes)	Components	Diffusivities (cm^2/sec) X 10^6	Average Diffusivities (cm^2/sec) X 10^6
30	ester	1238	
	caustic	228	
	alcohol	189	
	salt	369	
	Sum	2024	506
45	ester	4000	
	caustic	128	
	alcohol	104	
	salt	329	
	Sum	4561	1140
60	ester	2000	
	caustic	935	
	alcohol	405	
	salt	300	
	Sum	3640	910
Total Sum & Average Diffusivities (cm^2/sec)X10^6		10225	852

TABLE XII.2

ETHYL ACETATE - 1.0 N SODIUM HYDROXIDE
(Preliminary Experiments)

Contact time (Minutes)	Components	Diffusivities (cm^2/sec) X 10^6	Average Diffusivities (cm^2/sec) X 10^6
30	ester	524	
	caustic	147	
	alcohol	183	
	salt	181	
	Sum	1035	259
45	ester	1040	
	caustic	180	
	alcohol	235	
	salt	198	
	Sum	1653	413
60	ester	1451	
	caustic	625	
	alcohol	572	
	salt	530	
	Sum	3178	795
Total Sum & Average Diffusivities (cm^2/sec)X10^6		5866	489

TABLE XII.3

ETHYL ACETATE - 1.5 N SODIUM HYDROXIDE
(Preliminary Experiments)

Contact time (Minutes)	Components	Diffusivities (cm^2/sec) X 10^6	Average Diffusivities (cm^2/sec) X 10^6
30	ester	474	
	caustic	73	
	alcohol	99	
	salt	86	
	Sum	732	183
45	ester	309	
	caustic	77	
	alcohol	116	
	salt	89	
	Sum	591	148
60	ester	1460	
	caustic	840	
	alcohol	840	
	salt	570	
	Sum	3710	928
Total Sum & Average Diffusivities (cm^2/sec)X10^6		5033	420

diffusivities from the same set of profiles are quite close to each other.

These results are in agreement with those mass transfer data discussed in the preceding section (higher ethyl acetate values are due to phase contact turbulence and the mechanical vibration while sampling).

MIMIC PROGRAMMING[C5] on IBM 7040 computer was also used to simulate some of the concentration profiles sets obtained in the preliminary experiments in order to cross check the results from the TR-10 analog computer. The execution program listings are shown in Figure XII.7. A typical comparison of the simulated profiles between the MIMIC and the TR-10 is shown in Figure XII.6. It is evident that similar results can be obtained from either the analog studies or the digital computer studies. The two-fold difference in the values of C_{B_o} obtained from the two simulations (3.0×10^{-4} moles/litre and 8.5×10^{-4} moles/litre), is probably due to the inaccuracy in reading too small a value on the voltmeter of the Analog Computer.

FIGURE XII.7

MIMIC PROGRAM LISTINGS

```
$EXECUTE        MIMIC
USING MIMIC TO SOLVE THE RATIO OF RATE CONSTANT AND DIFFUSIVITY
                CON(DT,DTMIN,DTMAX,TSTOP)
                CON(CAO,CCO,CBO,DCBO,DCDO)
                PAR(RA,RB,RC,RD)
                PAR(CBO,DCAO,DCCO)
        DCA     INT(RA*CA*CB,DCAO)
        CA      INT(DCA,CAO)
        DCB     INT(RB*CA*CB,DCBO)
        CB      INT(DCB,CBO)
        DCC     INT(-RC*CA*CB,DCCO)
        CC      INT(DCC,CCO)
        DCD     INT(-RD*CA*CB,DCDO)
        CD      INT(DCD,CDO)
                FIN(T,TSTOP)
                HDR(T,CA,CB,CC,CD)
                HDR
                OUT(T,CA,CB,CC,CD)
                END

                                CD TOT    0019
```

APPENDIX XIII

MEASUREMENT OF THE SOLUBILITIES OF ESTERS IN AQUEOUS SALT SOLUTIONS

When a water soluble salt is added into an ester-saturated aqueous system, the equilibrium condition in the aqueous phase is disturbed and droplets of ester are salted out. The salt effect of sodium acetate in aqueous ethyl acetate solution, the effect of sodium propionate in aqueous methyl propionate solution, the effect of sodium formate in aqueous ethyl formate solution as well as in aqueous methyl formate solution were determined experimentally.

In a typical measurement, a known amount of the salt was weighed and put into a one-litre standard volumetric flask. The flask with its contents was then filled to the mark with aqueous solution saturated with the ester at 24°C. The volume of the input ester solution was accurately recorded. The resulting salt solution was thermostated at 24°C and well shaken at intervals. After several hours, the flask was taken out and both the total volume of the final solution and the amount of the excess ester phase salted out were measured. The decrease in solubility of the ester in the aqueous salt solution was thus calculated. The experiment was repeated at other salt concentration levels and also with other aqueous ester-salt systems. The solubilities of the ester as a function of the salt concentration were plotted for different systems as shown in the following figures.

FIGURE XIII.1

SOLUBILITY OF ETHYL ACETATE IN AQUEOUS SODIUM ACETATE SOLUTIONS AT 24±1°C

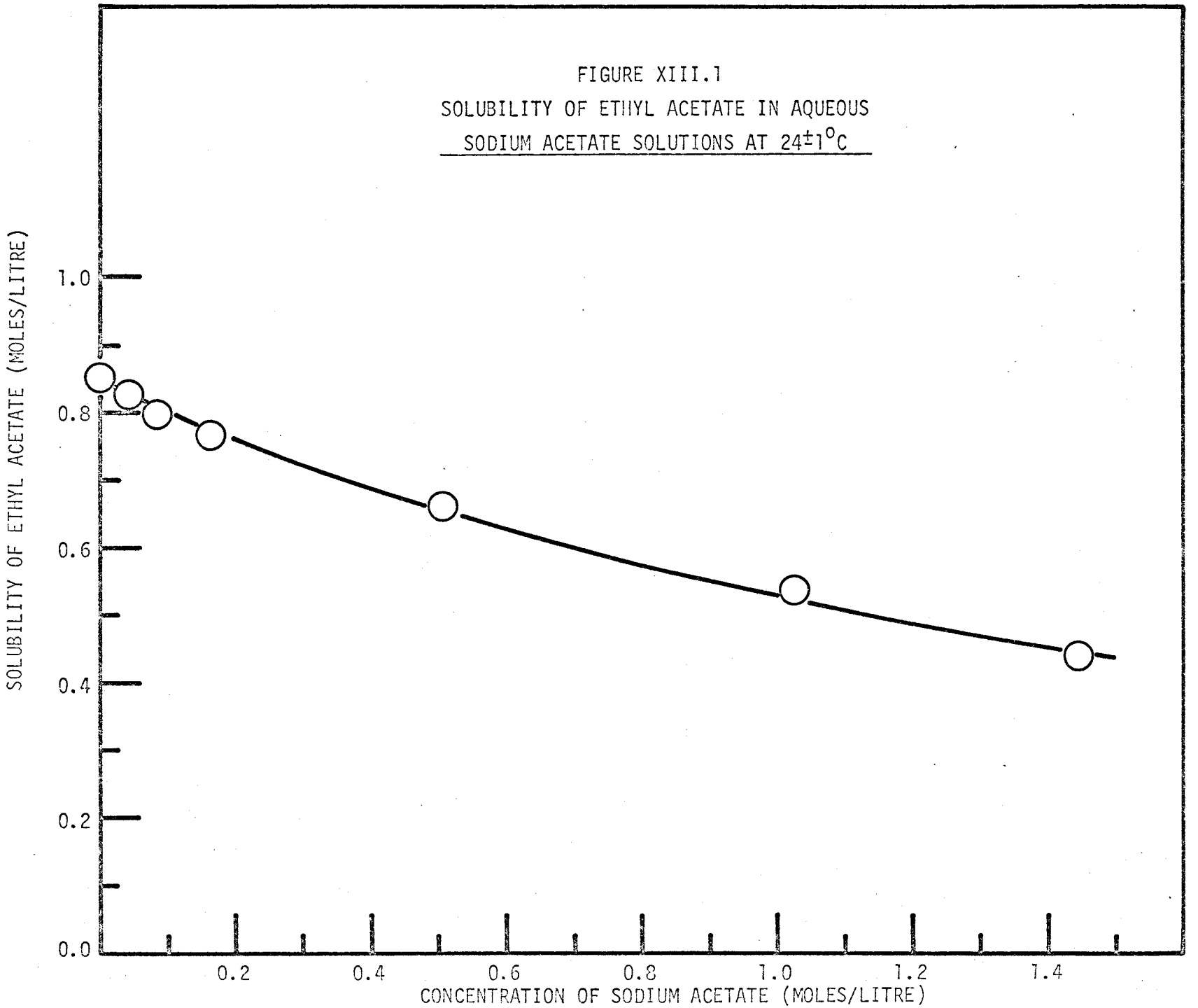

FIGURE XIII.2
SOLUBILITY OF METHYL PROPIONATE IN
AQUEOUS SODIUM PROPIONATE SOLUTIONS AT 24±1°C

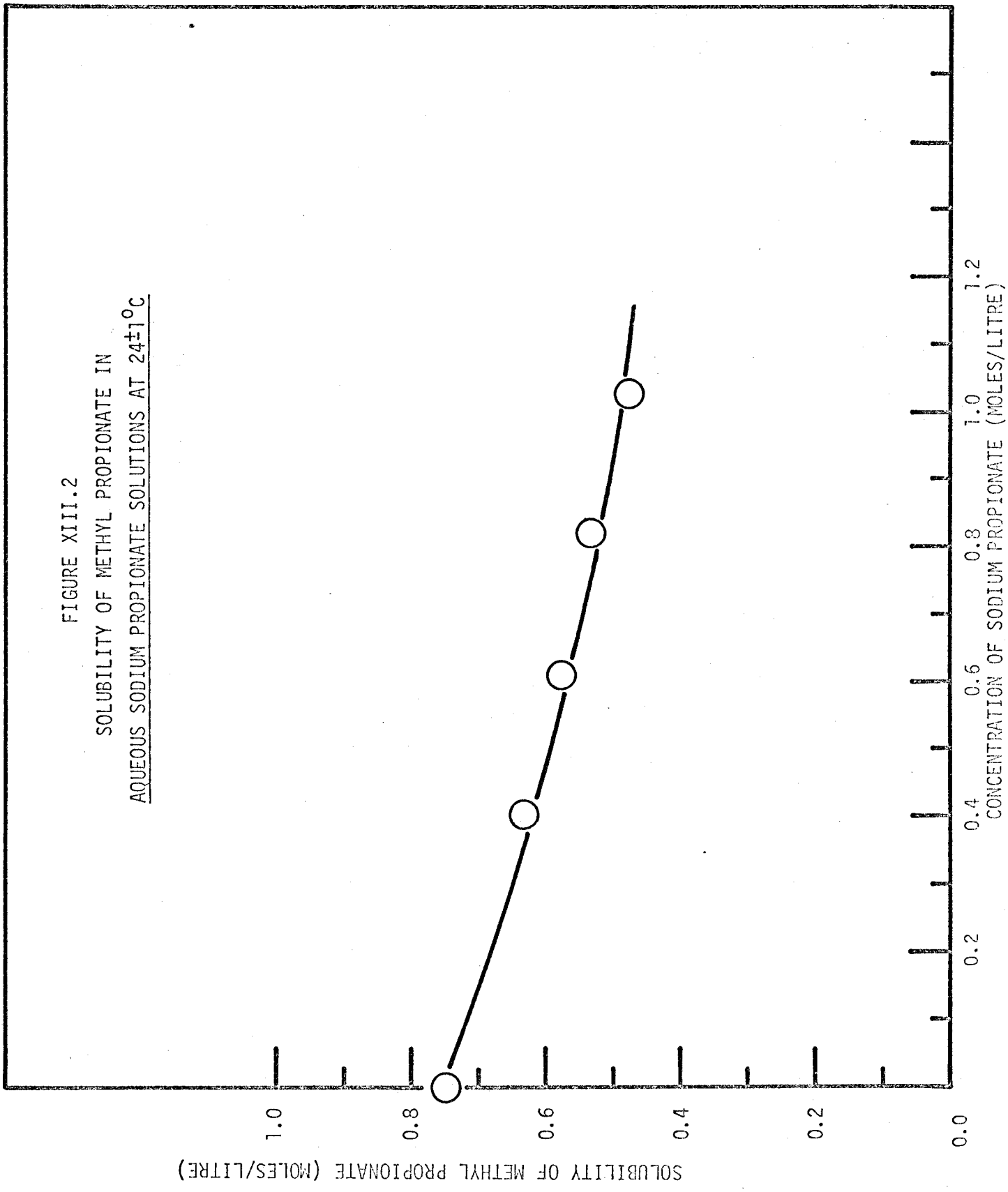

FIGURE XIII.3

SOLUBILITY OF METHYL FORMATE IN

AQUEOUS SODIUM FORMATE SOLUTIONS AT 24±1°C

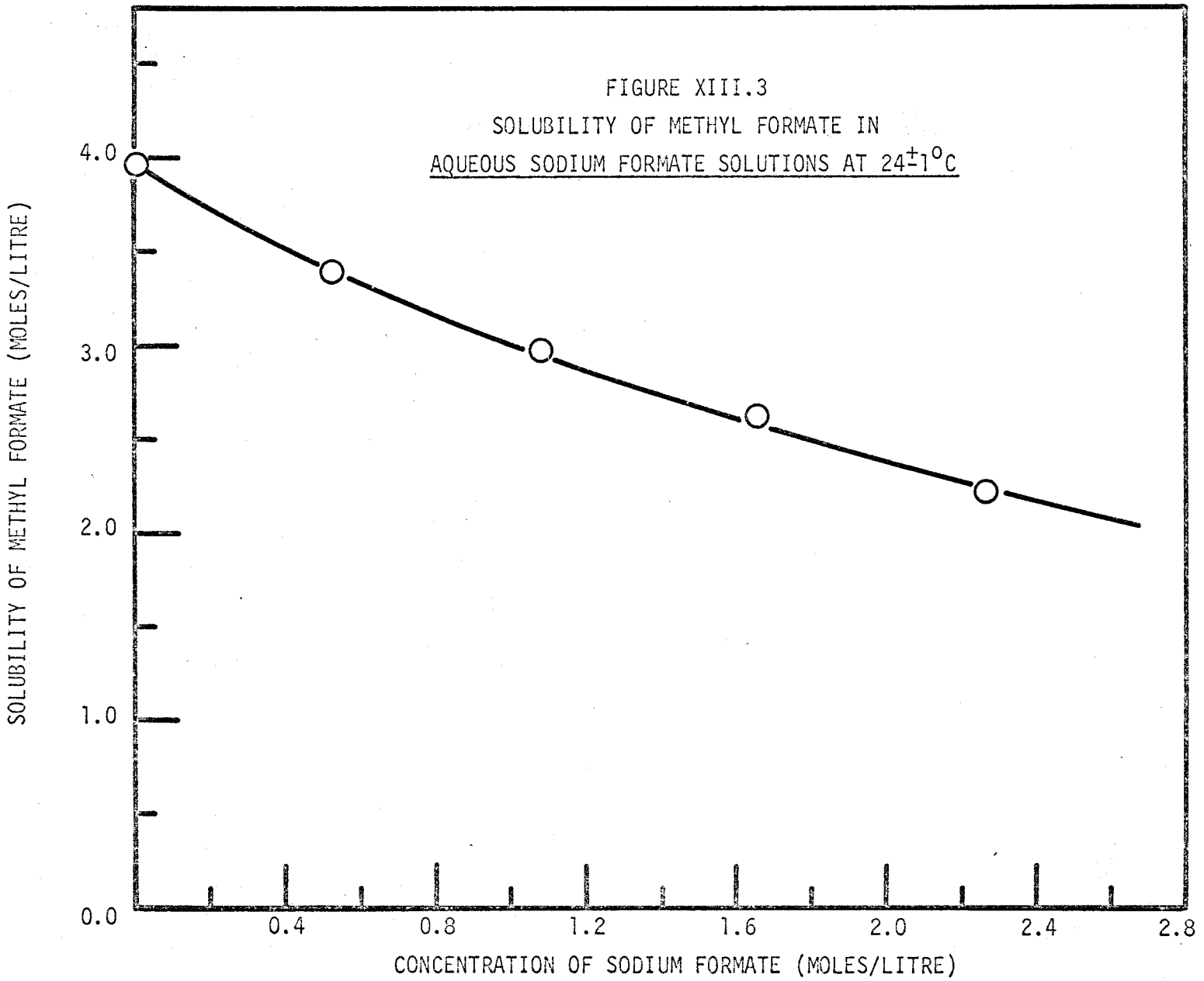

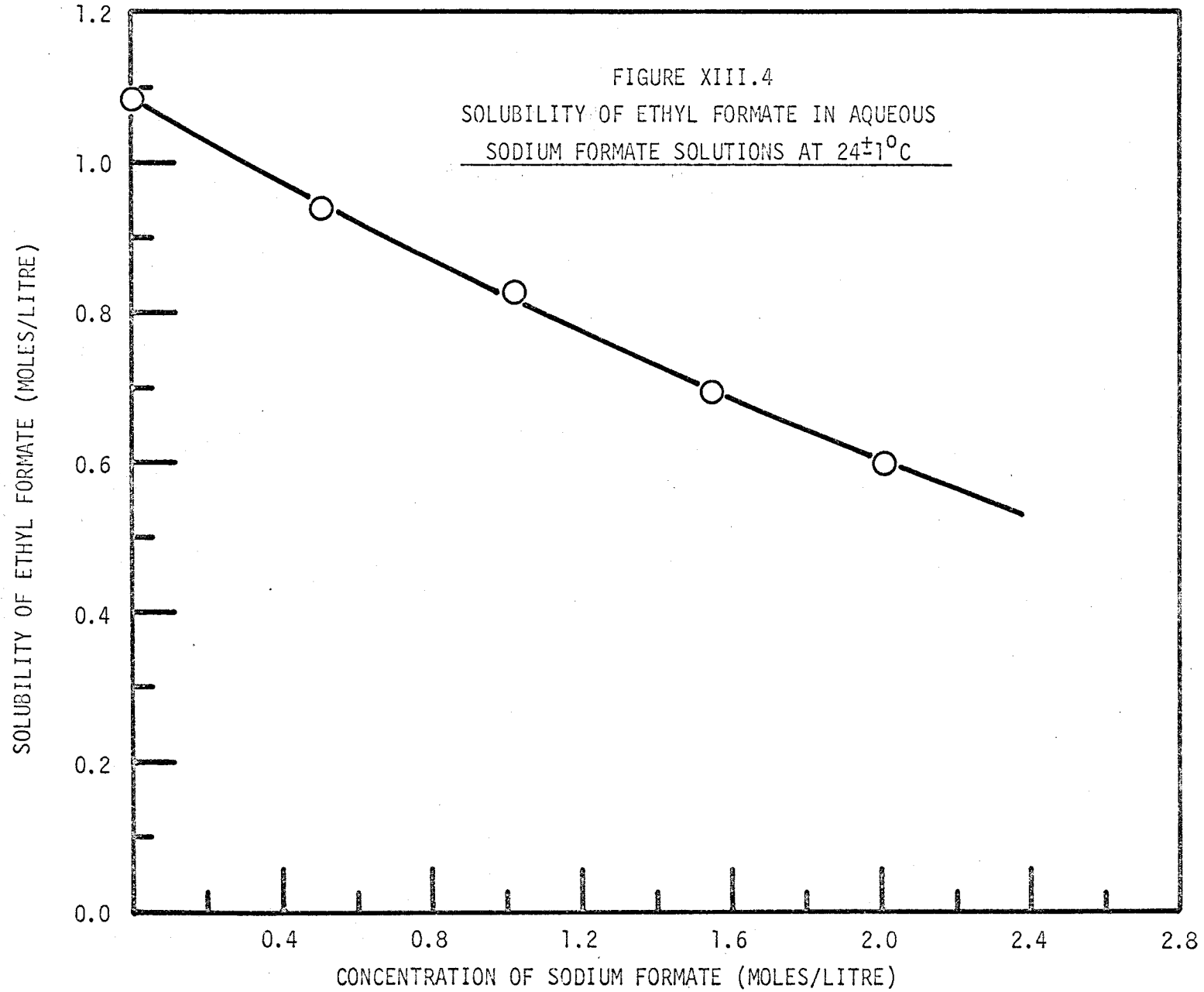
FIGURE XIII.4
SOLUBILITY OF ETHYL FORMATE IN AQUEOUS
SODIUM FORMATE SOLUTIONS AT 24±1°C
SOLUBILITY OF ETHYL FORMATE (MOLES/LITRE)
1.2
1.0
0.8
0.6
0.4
0.2
0.0
0.4
0.8
1.2
1.6
2.0
2.4
2.8
CONCENTRATION OF SODIUM FORMATE (MOLES/LITRE)

APPENDIX XIV

COMPARISON OF THE EXPERIMENTAL AND THE THEORETICAL CONCENTRATION PROFILES FOR THE N-BUTANOL-WATER AND THE ETHYL ACETATE-WATER SYSTEMS

The one-dimensional diffusion equation with variable diffusion coefficient for a binary liquid system at dilute concentration range can be expressed as the following:

$$\frac{\partial X_A}{\partial t} = D_{AB}\frac{\partial^2 X_A}{\partial z^2} + \frac{\partial D_{AB}}{\partial z} \cdot \frac{\partial X_A}{\partial z} \qquad \text{(XIV.1)}$$

where X_A = mole fraction

z = distance from the interface, cm.

t = time of diffusion, sec.

Transforming

$$C_A = \frac{X_A - X_{A_o}}{X_{A_s} - X_{A_o}} \; ; \quad y = \frac{z}{\sqrt{4\, D_{AB_o} t}}$$

where X_{A_o} = original uniform mole fraction of species A

X_{A_s} = equilibrium saturation mole fraction of species A at the interface.

D_{AB_o} = Diffusion coefficient of species A (at infinite dilution) in solution B, cm^2/sec.

Equation XIV.1 becomes

$$-\frac{\frac{1}{2}z}{\sqrt{4\, D_{AB_o}}}\frac{1}{t^{3/2}}\left(\frac{\partial C_A}{\partial y}\right) = \frac{D_{AB}}{D_{AB_o}}\left[\left(\frac{\partial^2 C_A}{\partial y^2}\right)\left(\frac{1}{4t}\right)\right] + \frac{1}{D_{AB_o}}\left(\frac{\partial D_{AB}}{\partial y}\right)\left(\frac{\partial C_A}{\partial y}\right)\left(\frac{1}{4t}\right) \qquad \text{(XIV.2)}$$

Multiply XIV.2 by $4t$;

$$-2y\frac{dC_A}{dy} = \frac{D_{AB}}{D_{AB_o}}\frac{d^2 C_A}{dy^2} + \frac{1}{D_{AB_o}}\frac{dD_{AB}}{dy}\frac{dC_A}{dy} \qquad \text{(XIV.3)}$$

Denoting $\frac{D_{AB}}{D_{AB_o}} = \overline{D_{AB}} = A_o + A_1 C_A + A_2 C_A^2 + A_3 C_A^3$

Equation XIV.3 becomes

$$-2y\frac{dC_A}{dy} = \frac{d^2C_A}{dy^2}(A_0 + A_1C_A + A_2C_A^2 + A_3C_A^3)$$

$$+ \left(\frac{dC_A}{dy}\right)^2(A_1 + 2A_2C_A + 3A_3C_A^2) \qquad \text{(XIV.4)}$$

At $y = 0$; $C_A = 1.0$

$y = \infty$; $C_A = 0.0$

Let $P = \frac{dC_A}{dy}$ (XIV.5)

Substituting XIV.5 into XIV.4

$$\frac{dP}{dy} = -2yP\left(\frac{1}{(A_0 + A_1C_A + A_2C_A^2 + A_3C_A^3)}\right)$$

$$-P^2\left(\frac{A_1 + 2A_2C_A + 3A_3C_A^2}{(A_0 + A_1C_A + A_2C_A^2 + A_3C_A^3)}\right) \qquad \text{(XIV.6)}$$

Equations XIV.5 and XIV.6 were solved numerically by the Fourth order Runge-Kutta method(H13). The solution was programmed on an IBM 7040 computer. The programme listings are shown in Figure XIV.1.

In these calculations, the initial value of the slope was required. With the diffusion coefficient set constant to be at infinite dilution of the solution, i.e. $\overline{D_{AB}} = 1.0$, an initial value of -1.13_{368} was obtained in order for the dimensionless mole fraction, C_A, to decrease to 0 at $y = 2.0$. Such result was in agreement with theoretical prediction for system with constant diffusion coefficient(B8).

With the variable diffusion coefficient (taken from the literature(J4) and as shown in Figure XIV.2) incorporated into

FIGURE XIV.1

FORTRAN LISTINGS FOR THE SOLUTION OF DIFFUSION EQUATION WITH VARIABLE DIFFUSION COEFFICIENT

```
C       DIFFUSION EQUATION WITH VARIABLE COEFFICIENT
C       NN IS NO OF PRINTOUTS
C       N IS NO OF CALC PER PRINTOUT
C       NOPROB IS NO SYSTEMS STUDIED
        DIMENSION P(8),PP(8),PPP(8)
        READ(5,3000) NOPROB
 3000   FORMAT (I5)
        NOGO=1
 3001   FORMAT(4F15.8)
        READ(5, 2000) NN
        READ(5,2500) (PP(I),I=1,8)
  501   READ(5,3001) A0,A1,A2,A3
        DO 8888 I=1,8
 8888   P(I)=PP(I)
        H=0.0001
        N=20
        II=0
        DO 100 I=1,8
C       INITIAL CONDITIONS (AT Y=0.0) ARE
        Y=0.
        CA=1.0
        WRITE(6, 1000) Y, CA, P(I)
  102   CONTINUE
        DO 101 J=1,N
        PPP(I)=P(I)
        CAA=CA
        YK01=P(I)*H
        YK02=H*(-2.*Y*P(I)/(A0+A1*CA+A2*CA**2+A3*CA**3)
       1-P(I)*P(I)*(A1+2.*A2*CA+3.*A3*CA**2)/(A0+A1*CA+A2*CA**2+A3*CA**3))
        Y=Y+0.5*H
        CA=CA+0.5*YK01
        P(I)=P(I)+0.5*YK02
        YK11=P(I)*H
        YK12=H*(-2.*Y*P(I)/(A0+A1*CA+A2*CA**2+A3*CA**3)
       1-P(I)*P(I)*(A1+2.*A2*CA+3.*A3*CA**2)/(A0+A1*CA+A2*CA**2+A3*CA**3))
        CA=CA+0.25*H*YK02
        P(I)=P(I)-0.5*YK02+0.5*YK12
        YK21=P(I)*H
        YK22=H*(-2.*Y*P(I)/(A0+A1*CA+A2*CA**2+A3*CA**3)
       1-P(I)*P(I)*(A1+2.*A2*CA+3.*A3*CA**2)/(A0+A1*CA+A2*CA**2+A3*CA**3))
        Y=Y+0.5*H
        CA=CA-0.25*H*YK02+0.5*YK01+0.5*H*YK12
        P(I)=P(I)-0.5*YK12+YK22
        YK31=P(I)*H
        YK32=H*(-2.*Y*P(I)/(A0+A1*CA+A2*CA**2+A3*CA**3)
       1-P(I)*P(I)*(A1+2.*A2*CA+3.*A3*CA**2)/(A0+A1*CA+A2*CA**2+A3*CA**3))
        CA=CAA+(YK01+2.*YK11+2.*YK21+YK31)/6.
        P(I)=PPP(I)+(YK02+2.*YK12+2.*YK22+YK32)/6.
```

```
  101 CONTINUE
      WRITE(6, 1000) Y, CA, P(I)
      II=II+1
      IF(II.EQ.NN) GO TO 103
      GO TO 102
  103 WRITE(6, 1001)
      II=0
  100 CONTINUE
      NOGO=NOGO+1
      IF(NOGO.GT.NOPROB) GO TO 500
      GO TO 501
 1000 FORMAT (1X,3F15.8)
 1001 FORMAT(//)
 2000 FORMAT (I5)
 2500 FORMAT (4F15.8)
  500 STOP
      END
$ENTRY
$IBSYS
```

CD TOT 0069

FIGURE XIV.2

EFFECT OF CONCENTRATION ON DIFFUSION COEFFICIENT
n-BUTANOL - WATER SYSTEM
(DATA FROM JOHNSON AND BABB)

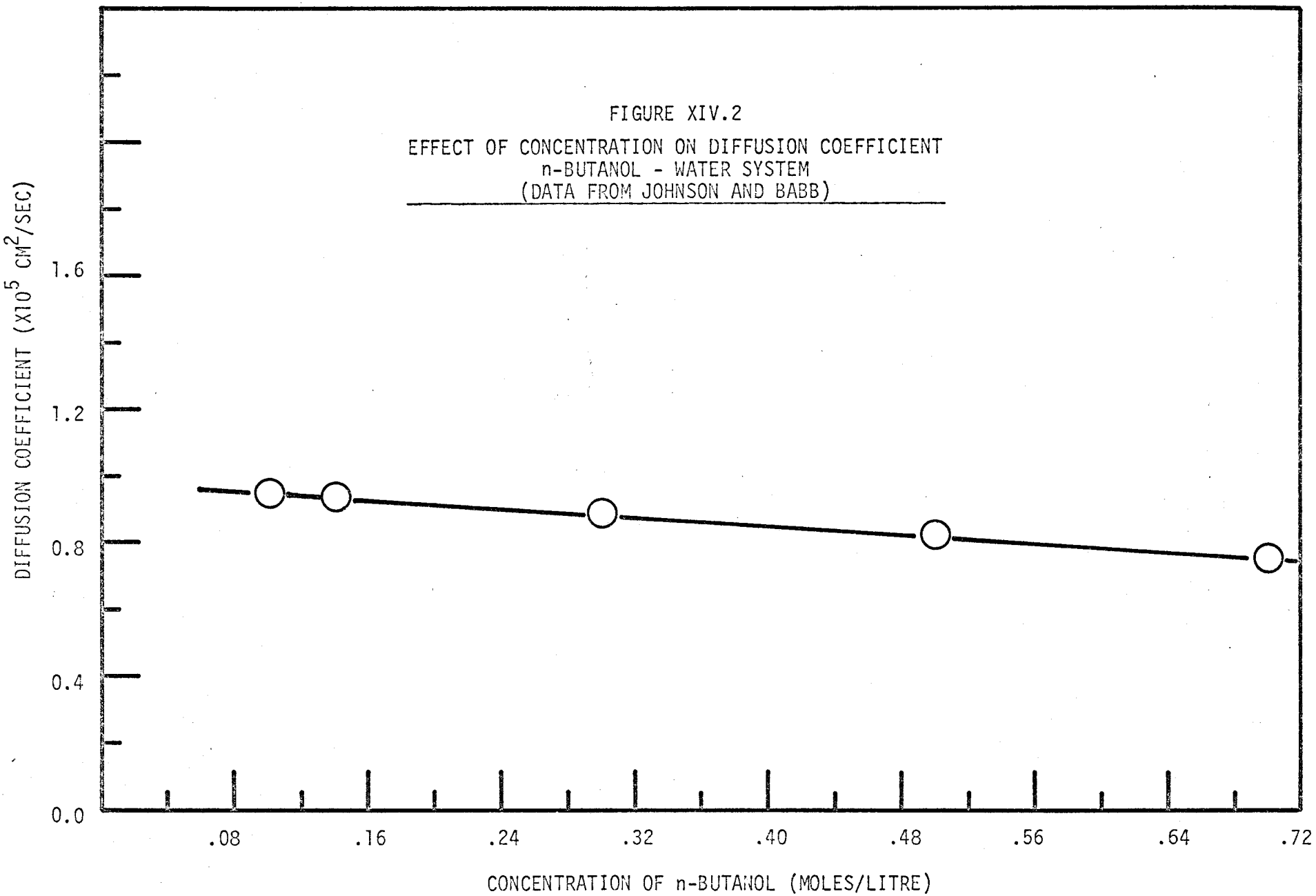

the diffusion equation, the dimensionless concentration profile for the n-butanol in water was calculated. Initial slope values were varied, one at a time; and the respective calculated concentration profiles were plotted. The process of trial and error was continued until a profile decreasing to zero at y = 2.0 was obtained. The initial slope for that particular profile was found to be -1.50_3. The profile of variable diffusion coefficient was compared with the experimentally determined concentration profiles from Run #3, 4 and 5 respectively (Figure 13). The results of the comparisons are shown in Figures XIV.3, XIV.4 and XIV.5.

Similarly, the dimensionless concentration profile for the ethyl acetate-water system was also calculated. The variable diffusion coefficient of ethyl acetate in water as a function of the ester concentration was experimentally determined as shown in Figure 39 (Chapter 4.4-PART D). The calculated profile was compared with the experimental profile (Figure 15). The comparison is best illustrated in Figure XIV.6.

FIGURE XIV.3

COMPARISON OF THEORETICAL AND EXPERIMENTAL DIMENSIONLESS CONCENTRATION PROFILES (n-BUTANOL - WATER SYSTEM RUN #3)

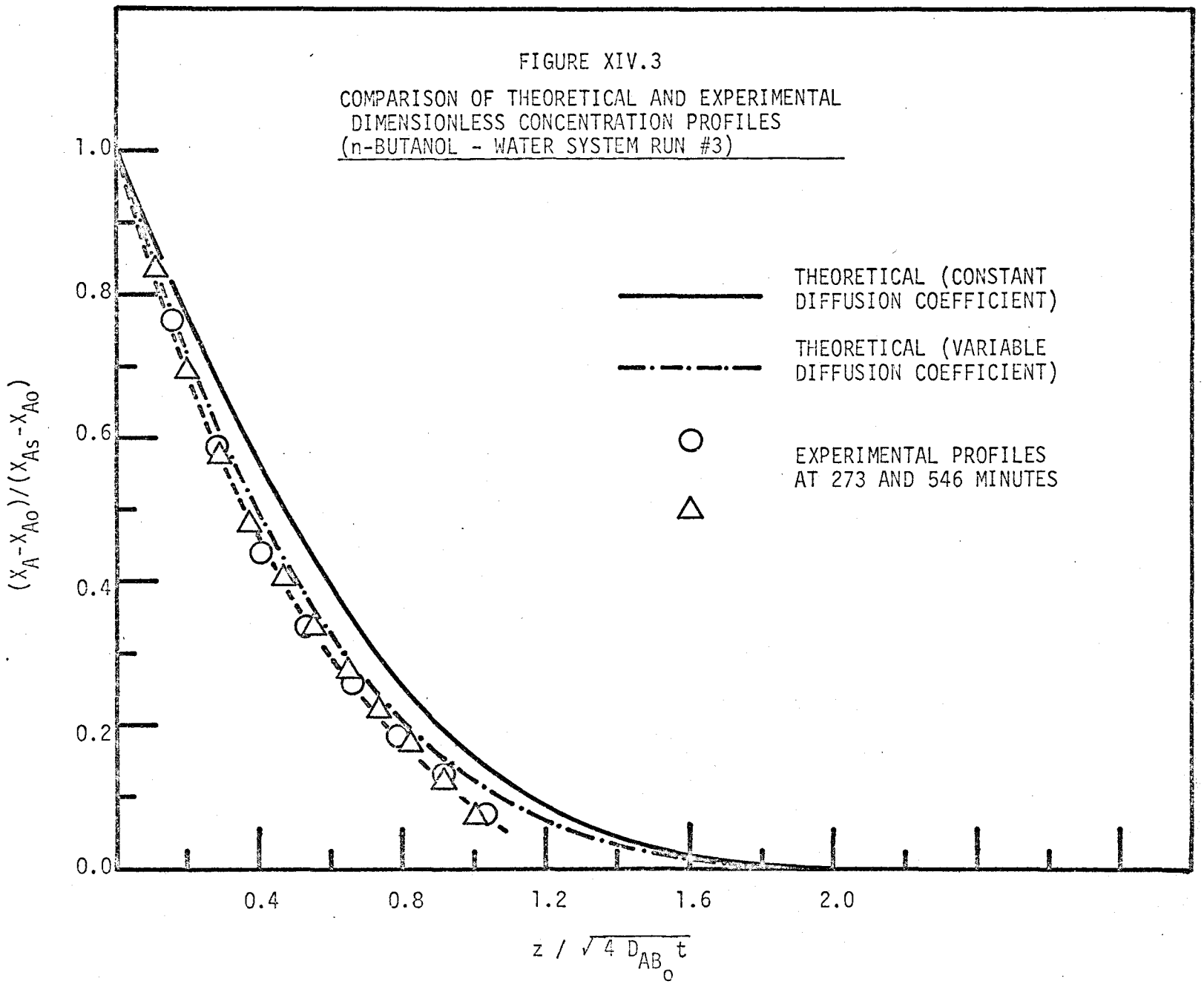

FIGURE XIV.4

COMPARISON OF THEORETICAL AND EXPERIMENTAL DIMENSIONLESS CONCENTRATION PROFILES (n-BUTANOL - WATER SYSTEM RUN #4)

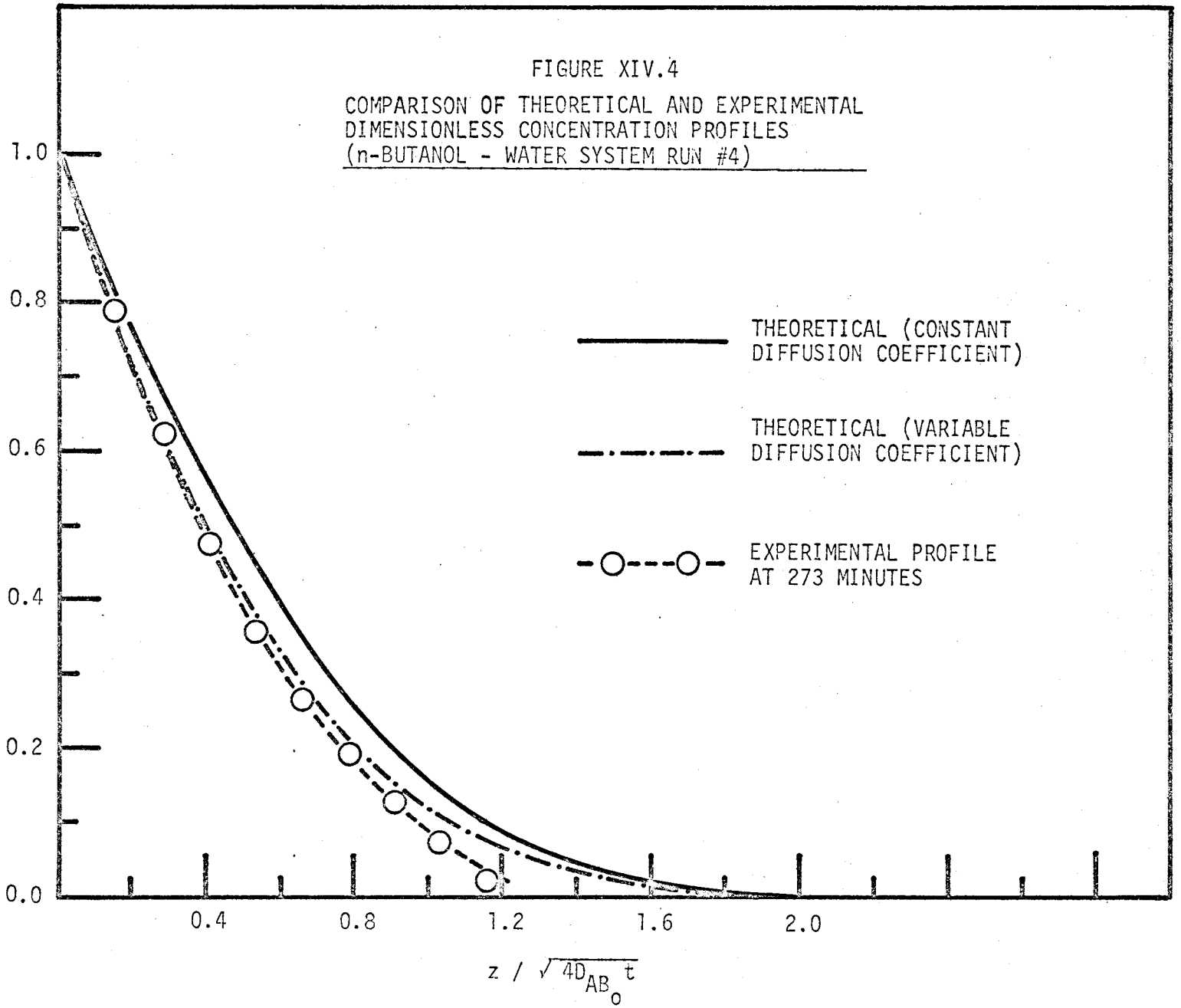

FIGURE XIV.5

COMPARISON OF THEORETICAL AND EXPERIMENTAL DIMENSIONLESS CONCENTRATION PROFILES (n-BUTANOL - WATER SYSTEM RUN #5)

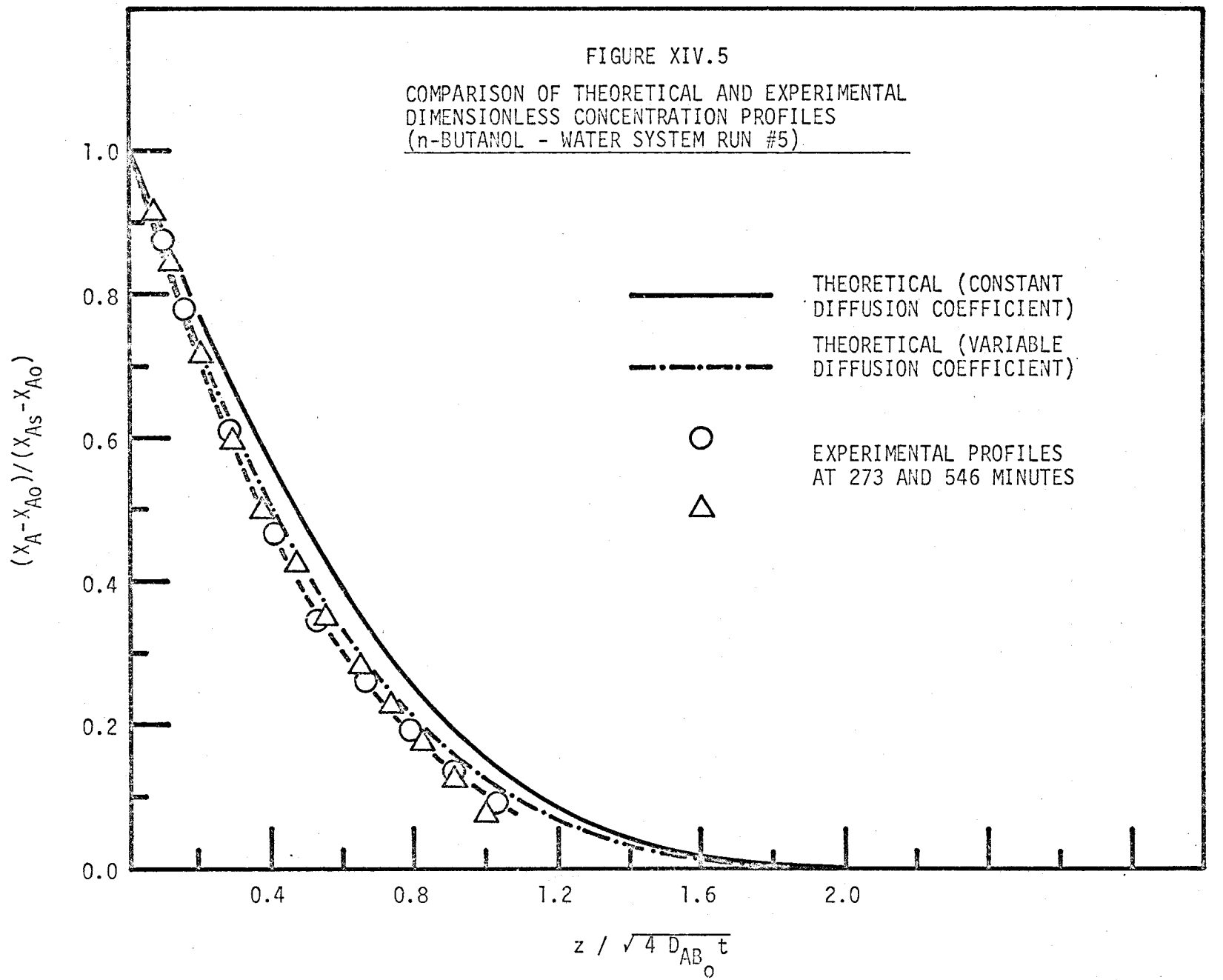

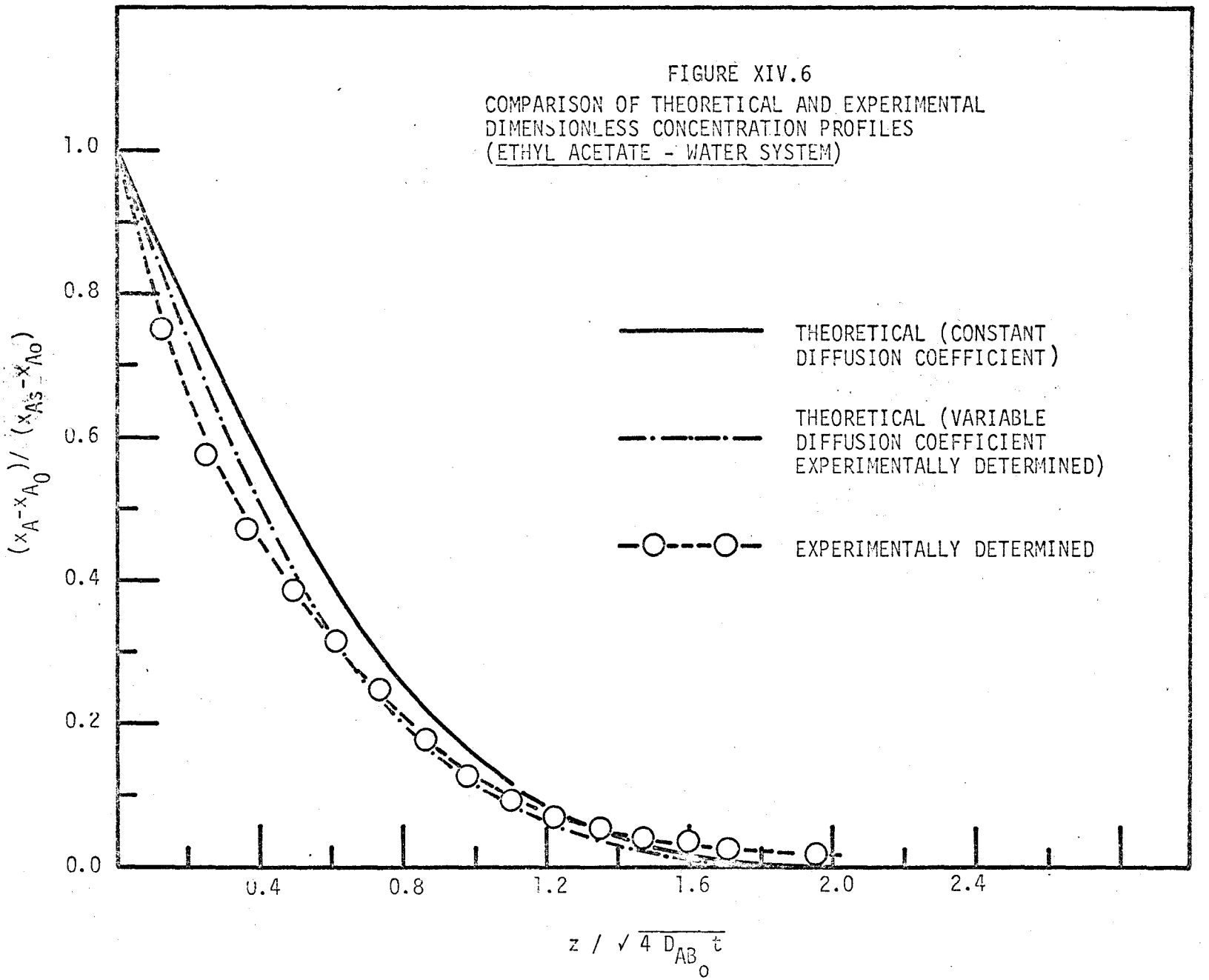
FIGURE XIV.6
COMPARISON OF THEORETICAL AND EXPERIMENTAL DIMENSIONLESS CONCENTRATION PROFILES
(ETHYL ACETATE - WATER SYSTEM)
THEORETICAL (CONSTANT DIFFUSION COEFFICIENT)
THEORETICAL (VARIABLE DIFFUSION COEFFICIENT EXPERIMENTALLY DETERMINED)
EXPERIMENTALLY DETERMINED
$(x_A - x_{A_0}) / (x_{A_S} - x_{A_0})$
$z / \sqrt{4 D_{AB_o} t}$
1.0
0.8
0.6
0.4
0.2
0.0
0.4
0.8
1.2
1.6
2.0
2.4

APPENDIX XV

EXPERIMENTAL CONCENTRATION DATA OF ETHYL ACETATE-AQUEOUS CAUSTIC SYSTEMS AND ETHYL ACETATE-WATER SYSTEM

TABLE XV.1

CONCENTRATION DATA OF ETHYL ACETATE-WATER SYSTEM

Sampling needle #	Dist. from interface (cm.)						
2	.094	Time (mins.)	14.5	47.8	77	178.7	297.6
		Concentration (moles/litre)	.236	.320	.408	.500	.590
3	.289	Time (mins.)	18.2	51.6	81.3		301.5
		Concentration (moles/litre)	.1185	.178	.224		.432
4	.359	Time (mins.)	23	56	85.4	182.8	305.5
		Concentration (moles/litre)	.085	.148	.210	.315	.410
12	.543	Time (mins.)	27		90.3		309.4
		Concentration (moles/litre)	.047		.115		.290
6	.604	Time (mins.)	31.2	60.2	94.4	187.2	314
		Concentration (moles/litre)	.026	.050	.074	.146	.240
7	.809	Time (mins.)	35.7	64.2	98.3	191.5	317.6
		Concentration (moles/litre)	.009	.016	.030	.071	.120
9	1.295	Time (mins.)	39.8		103.7		321
		Concentration (moles/litre)	.005		.0115		.039
15	3.897	Time (mins.)	44		107.9		324
		Concentration (moles/litre)	0.0		0.0		.001

TABLE XV.2

CONCENTRATION DATA OF ETHYL ACETATE -1.0 N SODIUM HYDROXIDE SYSTEM (RUN #4-1)

Sampling needle #	Dist. from interface (cm.)						
2	.094	Time (mins.)	14.1	22.0	37.0	51.2	69.8
		NaOH	.125	.000	.000	.000	.000
		NaAc	.743	.899	.845	.836	.821
		EtAc	.163	.400	.325	.406	.443
		EtOH	.394	-	.483	.470	.533
		(moles/litre)					
4	.361	Time (mins.)	18.2	25.6	41.5	54.9	74.2
		NaOH	.322	.181	.0175	.000	.000
		NaAc	.580	.715	.802	.863	.829
		EtAc	.0823	.034	.315	.347	.267
		EtOH	.295	.384	.496	.501	.574
		(moles/litre)					
6	.620	Time (mins.)		29.5	45.1	60.5	80
		NaOH		.746	.300	.140	.041
		NaAc		.172	.612	.750	.821
		EtAc		.000	.0173	.068	.196
		EtOH		.104	.408	.513	.541
		(moles/litre)					
8	1.016	Time (mins.)		32.8		64.4	84.9
		NaOH		.948		.787	.566
		NaAc		.000		.213	.384
		EtAc		.000		.000	.000
		EtOH		.0003		.194	.272
		(moles/litre)					

TABLE XV.3

CONCENTRATION DATA OF ETHYL ACETATE
-1.0 N SODIUM HYDROXIDE SYSTEM (RUN #4-2)

Sampling needle #	Dist. from interface (cm.)						
3	.262	Time (mins.)	14.0	24.1	34.4	53.5	71.1
		NaOH	.371	.121	.064	.000	.000
		NaAc	.488	.741	.791	.823	.82
		EtAc	.000	.152	.0824	.430	.406
		EtOH	.278	.456	.563	.508	.534
		(moles/litre)					
12	.524	Time (mins.)	19.9	27.2	37.5	57.8	74.8
		NaOH	.848	.626	.280	.045	.000
		NaAc	.112	.408	.666	.838	.843
		EtAc	.000	.003	.000	.283	.335
		EtOH	.038	.303	.450	.499	.536
		(moles/litre)					
7	.793	Time (mins.)		30.2	43.6	64.1	78.8
		NaOH		.908	.879	.640	.404
		NaAc		.000	.126	.375	.527
		EtAc		.000	.000	.000	.000
		EtOH		.000	.082	.282	.351
		(moles/litre)					
9	1.270	Time (mins.)				66.8	83.4
		NaOH				.946	.861
		NaAc				.000	.100
		EtAc				.000	.000
		EtOH				.065	.075
		(moles/litre)					

FIGURE XV.1

VARIATION OF THE ESTER CONCENTRATIONS WITH PHASE CONTACT TIME

○ NEEDLE #2 ; 0.094 CM
△ NEEDLE #3 ; 0.262 CM
⬡ NEEDLE #4 ; 0.361 CM
□ NEEDLE #12; 0.524 CM
◭ NEEDLE #6 ; 0.620 CM
◍ NEEDLE #7 ; 0.793 CM
◍ NEEDLE #8 ; 1.016 CM
▨ NEEDLE #9 ; 1.270 CM

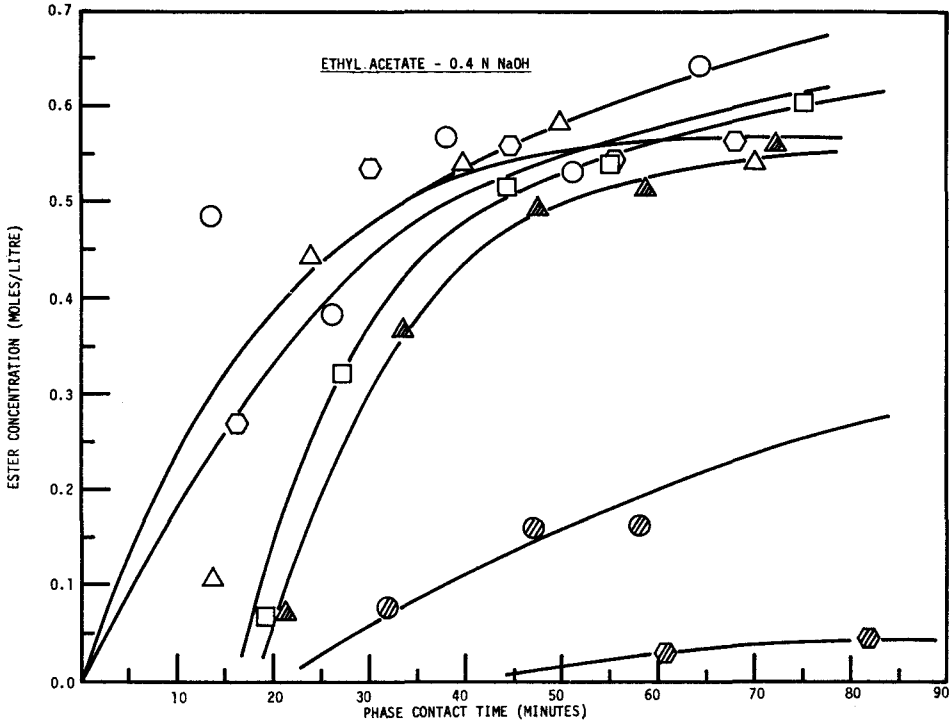

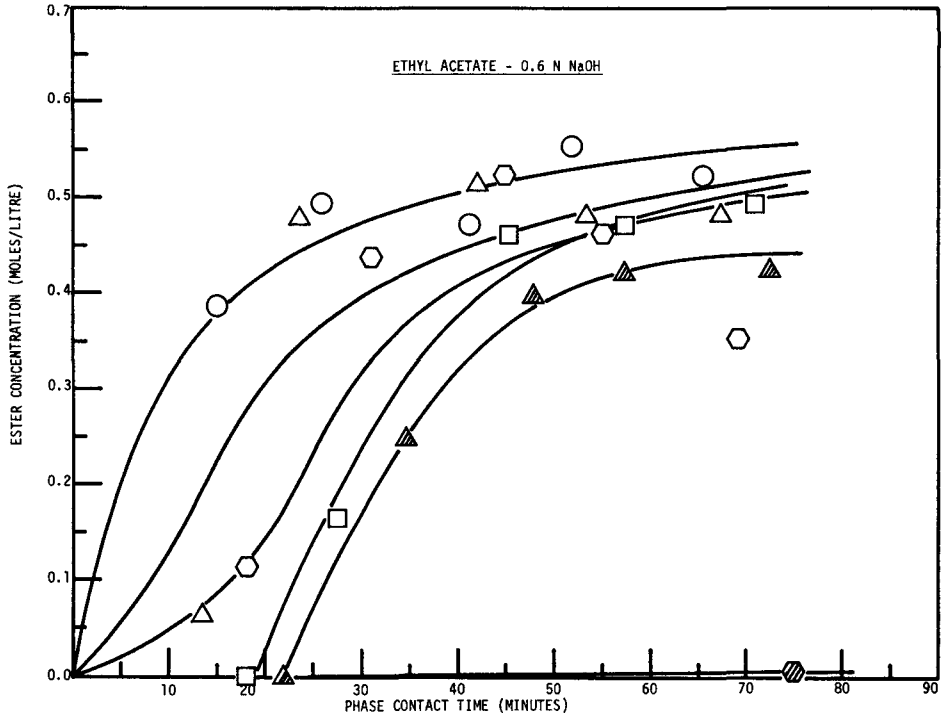

APPENDIX XVI

EDDY DIFFUSIVITIES OF VARIOUS COMPONENTS AS DERIVED FROM THE SIMULATION OF THE EXPERIMENTAL CONCENTRATION PROFILES

The experimental concentration profiles of the reactants and the products in the aqueous phase for each run in the ester-caustic systems were obtained (4.2 - PART B, Figures 18-19 and Appendix XVII).

The profiles were simulated on a TR-10 computer (Appendix IX) and on an IBM 7040 computer using MIMIC PROGRAMMING (Appendix XII). Quasi-steady state mass transfer situation was assumed.

The eddy diffusivities obtained from the simulation studies were tabulated separately for each run.

TABLE XVI.1

Ethyl Acetate - 0.2 N NaOH (Run #1)

Contact time (minutes)	Components	Diffusivities (cm^2/sec) X 10^6	Average Diffusivities (cm^2/sec) X 10^6
25	ester	200	
	caustic	265	
	alcohol	286	
	salt	251	
	Sum	1002	251
50	ester	172	
	caustic	154	
	alcohol	101	
	salt	164	
	Sum	591	148
75	ester	143	
	caustic	333	
	alcohol	71	
	salt	167	
	Sum	714	179
Total Sum & Average diffusivities (cm^2/sec)X10^6		2307	193

TABLE XVI.2

Ethyl Acetate - 0.4 N NaOH (Run #2)

Contact time (minutes)	Components	Diffusivities (cm^2/sec) X 10^6	Average Diffusivities (cm^2/sec) X 10^6
25	ester	456	
	caustic	258	
	alcohol	543	
	salt	226	
	Sum	1483	371
50	ester	426	
	caustic	277	
	alcohol	348	
	salt	327	
	Sum	1378	345
75	ester	467	
	caustic	496	
	alcohol	256	
	salt	327	
	Sum	1546	387
Total Sum & Average Diffusivities (cm^2/sec)X10^6		4407	368

TABLE XVI.3

Ethyl Acetate - 0.6 N NaOH (Run #3)

Contact time (minutes)	Components	Diffusivities (cm^2/sec) X 10^6	Average Diffusivities (cm^2/sec) X 10^6
25	ester	460	
	caustic	207	
	alcohol	147	
	salt	210	
	Sum	1024	256
50	ester	332	
	caustic	250	
	alcohol	413	
	salt	359	
	Sum	1354	339
75	ester	191	
	caustic	242	
	alcohol	302	
	salt	265	
	Sum	1000	250
Total Sum & Average Diffusivities (cm^2/sec)X10^6		3378	282

TABLE XVI.4

Ethyl Acetate - 1.0 N NaOH (Run #4)

Contact time (minutes)	Components	Diffusivities (cm^2/sec) X 10^6	Average Diffusivities (cm^2/sec) X 10^6
25	ester	118	
	caustic	58	
	alcohol	74	
	salt	48	
	Sum	298	75
50	ester	357	
	caustic	217	
	alcohol	249	
	salt	244	
	Sum	1067	267
75	ester	313	
	caustic	184	
	alcohol	184	
	salt	203	
	Sum	884	221
Total Sum & Average Diffusivities (cm^2/sec)X10^6		2249	188

TABLE XVI.5

Ethyl Acetate - 1.4 N NaOH (Run #5)

Contact time (minutes)	Components	Diffusivities (cm^2/sec) X 10^6	Average Diffusivities (cm^2/sec) X 10^6
25	ester	78	
	caustic	56	
	alcohol	55	
	salt	40	
	Sum	229	57
50	ester	177	
	caustic	103	
	alcohol	96	
	salt	83	
	Sum	459	115
75	ester	442	
	caustic	125	
	alcohol	96	
	salt	133	
	Sum	796	199
Total Sum & Average Diffusivities (cm^2/sec)X10^6		1484	124

TABLE XVI.6

Methyl Propionate - 0.4 N NaOH (Run #6)

Contact time (minutes)	Components	Diffusivities (cm^2/sec) X 10^6	Average Diffusivities (cm^2/sec) X 10^6
25	ester	53	
	caustic	51	
	alcohol	51	
	salt	69	
	Sum	224	56
50	ester	47	
	caustic	93	
	alcohol	88	
	salt	127	
	Sum	355	89
75	ester	67	
	caustic	80	
	alcohol	108	
	salt	112	
	Sum	367	92
Total Sum & Average Diffusivities (cm^2/sec)X10^6		946	79

TABLE XVI.7

Methyl Propionate - 0.6 N NaOH (Run #8)

Contact time (minutes)	Components	Diffusivities (cm^2/sec) X 10^6	Average Diffusivities (cm^2/sec) X 10^6
25	ester	30	
	caustic	29	
	alcohol	34	
	salt	39	
	Sum	132	33
50	ester	58	
	caustic	54	
	alcohol	50	
	salt	54	
	Sum	216	54
75	ester	125	
	caustic	109	
	alcohol	99	
	salt	119	
	Sum	452	113
Total Sum & Average Diffusivities (cm^2/sec)X10^6		800	67

TABLE XVI.8

Methyl Propionate - 1.0 N NaOH (Run #7)

Contact time (minutes)	Components	Diffusivities (cm^2/sec) X 10^6	Average Diffusivities (cm^2/sec) X 10^6
25	ester	69	
	caustic	57	
	alcohol	63	
	salt	67	
	Sum	256	64
50	ester	50	
	caustic	45	
	alcohol	40	
	salt	69	
	Sum	204	51
75	ester	26	
	caustic	24	
	alcohol	22	
	salt	29	
	Sum	101	25
Total Sum & Average Diffusivities (cm^2/sec)X10^6		561	47

APPENDIX XVII

CONCENTRATION PROFILE DATA OF ESTER-AQUEOUS CAUSTIC SYSTEMS

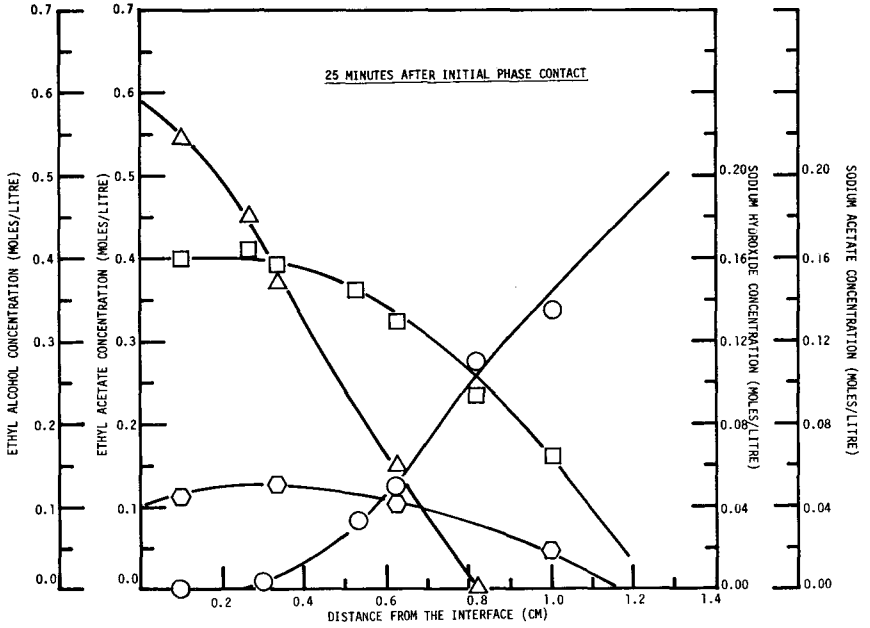

FIGURE XVII.1
CONCENTRATION PROFILES OF REACTANTS AND PRODUCTS
IN THE AQUEOUS PHASE
(ETHYL ACETATE - 0.2N NaOH; 24±1°C)

△ △ ETHYL ACETATE
○ ○ SODIUM HYDROXIDE
⬡ ⬡ ETHYL ALCOHOL
□ □ SODIUM ACETATE

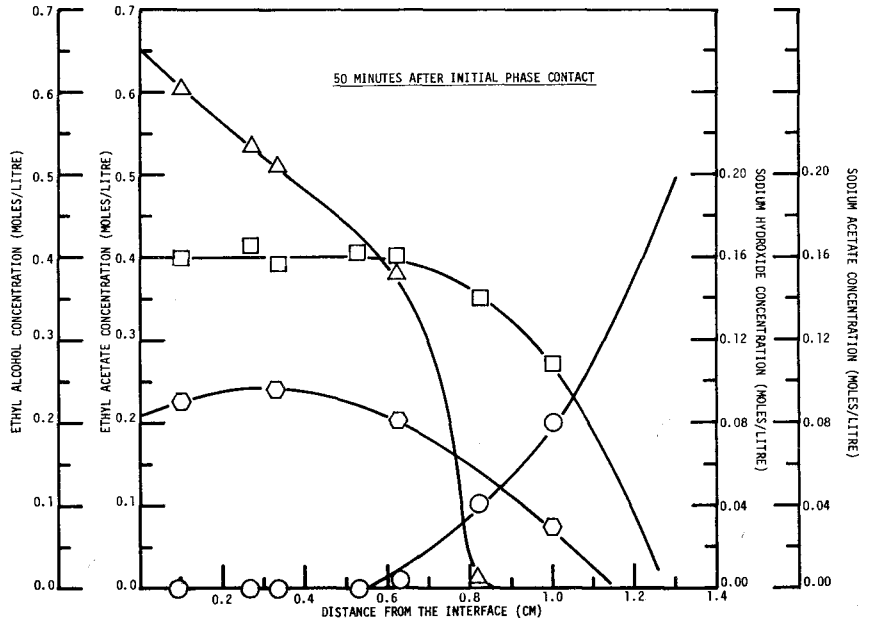

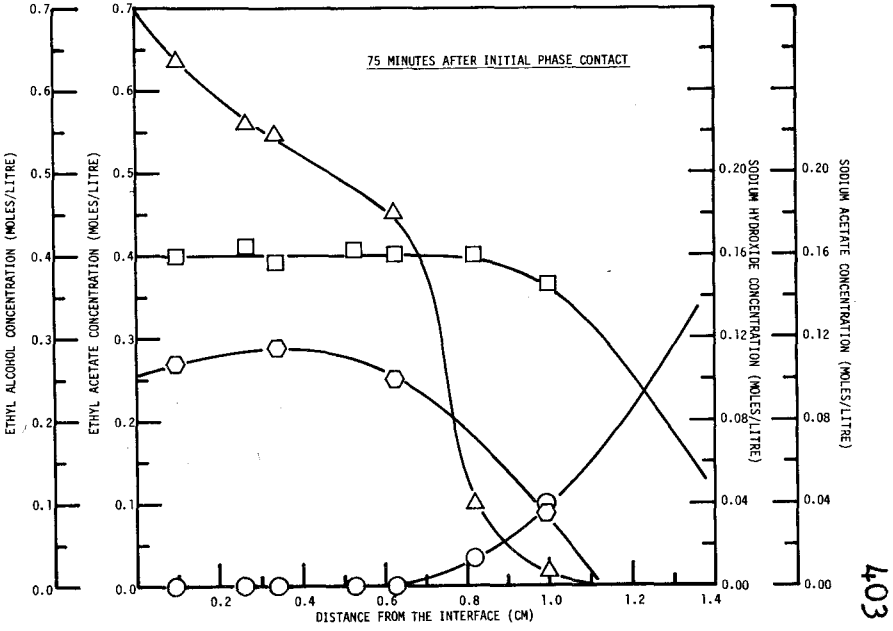

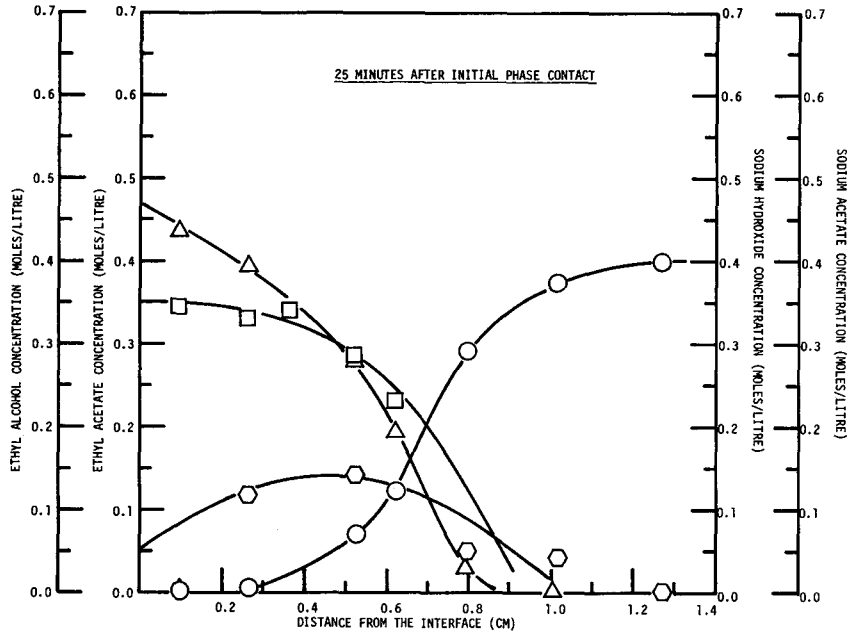

FIGURE XVII.2
CONCENTRATION PROFILES OF REACTANTS AND PRODUCTS
IN THE AQUEOUS PHASE
(ETHYL ACETATE - 0.4N NaOH; 24±1°C)

△ △ ETHYL ACETATE
○ ○ SODIUM HYDROXIDE
⬡ ⬡ ETHYL ALCOHOL
□ □ SODIUM ACETATE

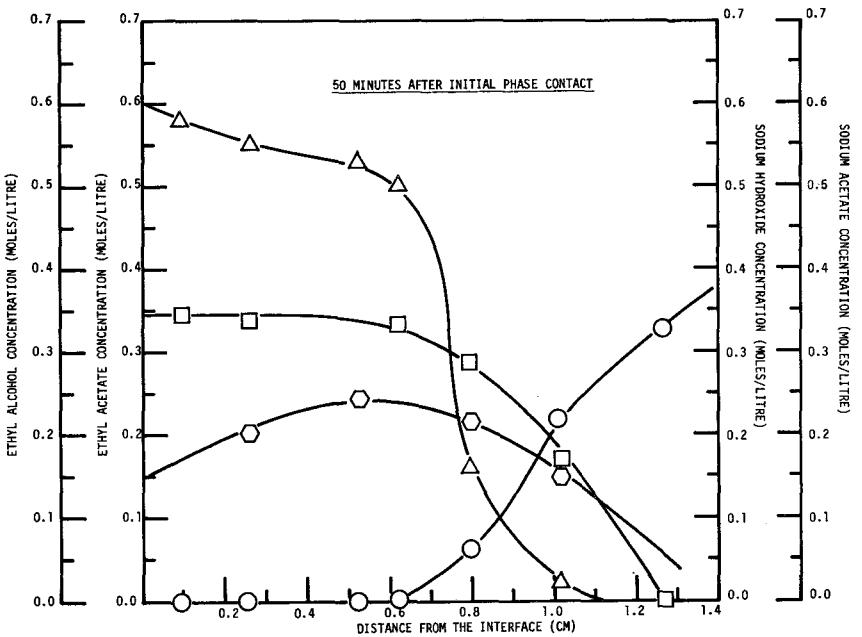

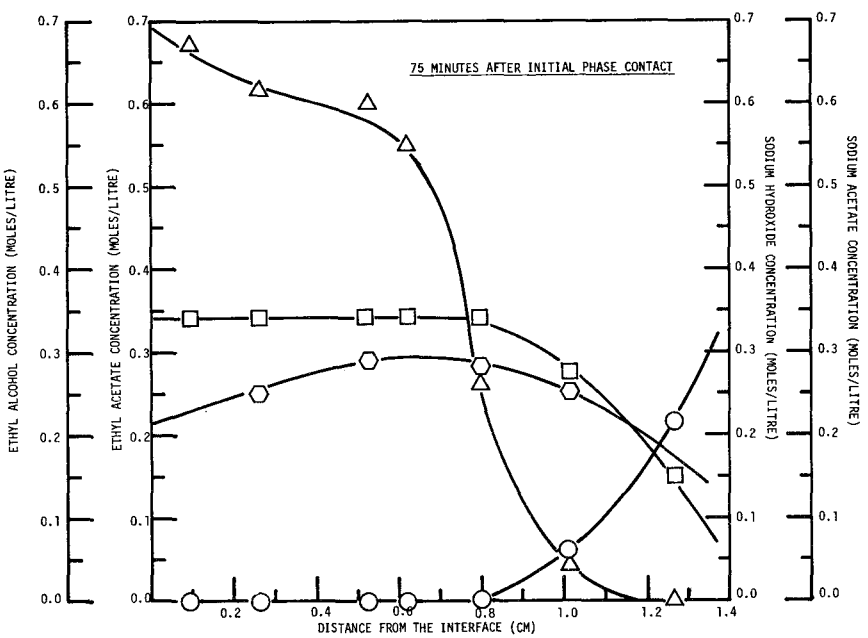

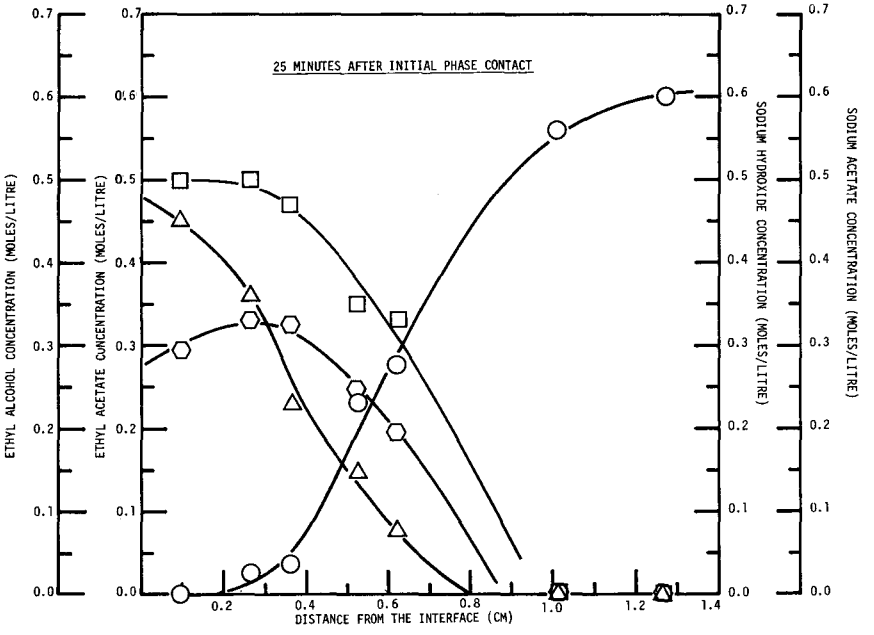

FIGURE XVII.3
CONCENTRATION PROFILES OF REACTANTS AND PRODUCTS
IN THE AQUEOUS PHASE
(ETHYL ACETATE - 0.6N NaOH; 24±1°C)

△ △ ETHYL ACETATE
○ ○ SODIUM HYDROXIDE
⬡ ⬡ ETHYL ALCOHOL
□ □ SODIUM ACETATE

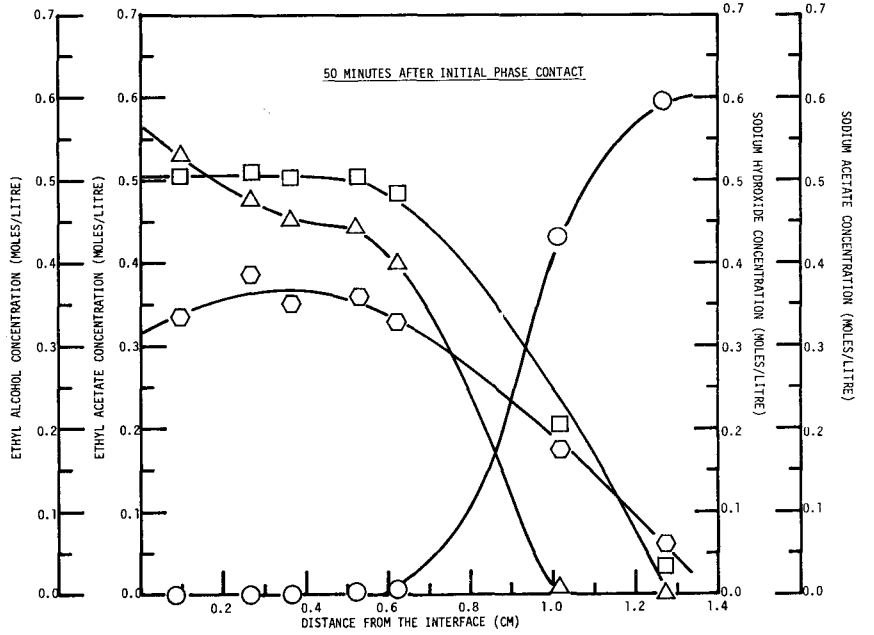

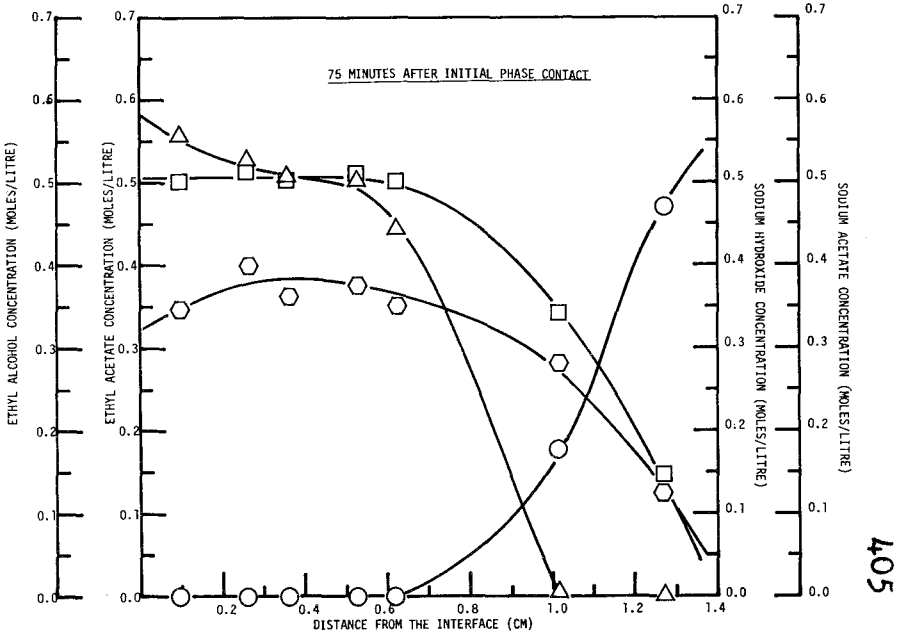

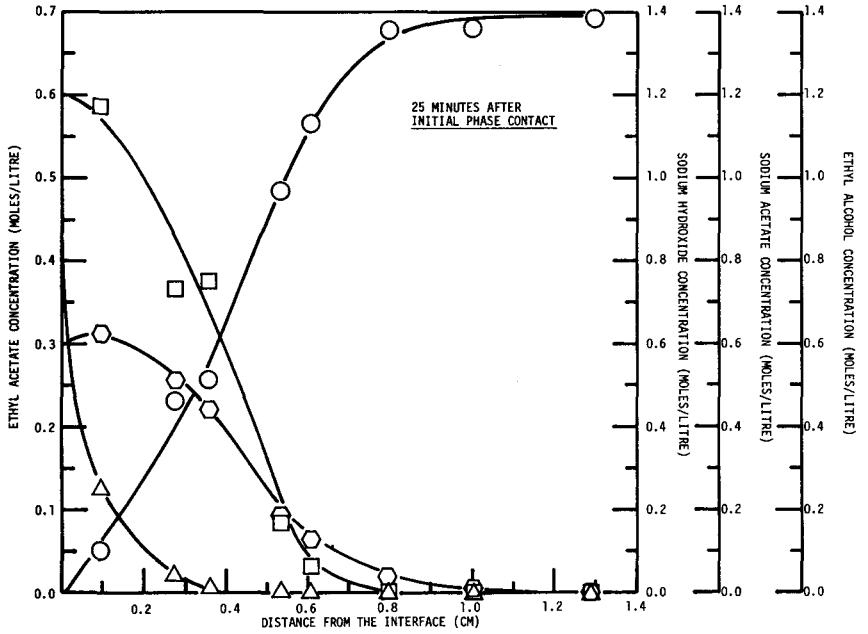

FIGURE XVII.4
CONCENTRATION PROFILES OF REACTANTS AND PRODUCTS
IN THE AQUEOUS PHASE
(ETHYL ACETATE - 1.4 N NaOH; 24±1°C)

△ △ ETHYL ACETATE
○ ○ SODIUM HYDROXIDE
⬡ ⬡ ETHYL ALCOHOL
□ □ SODIUM ACETATE

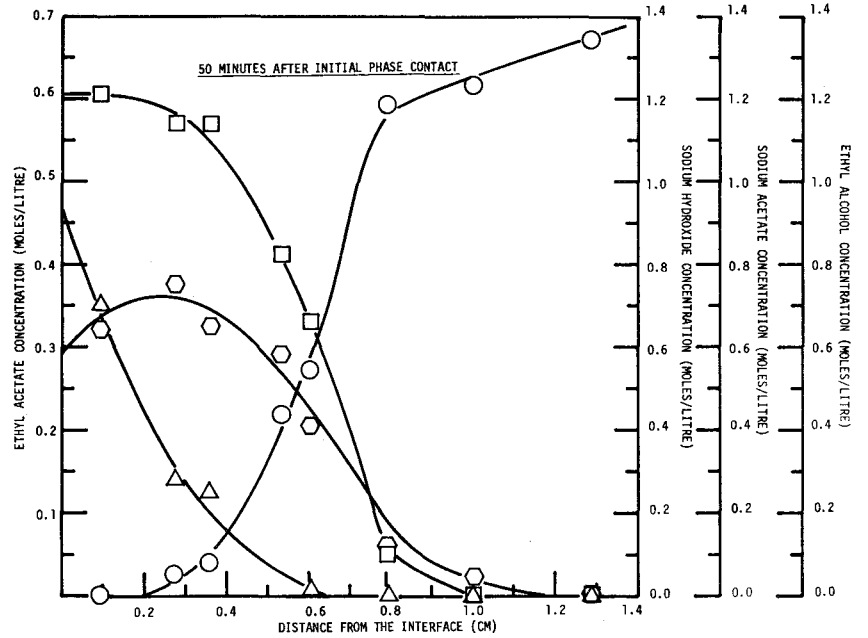

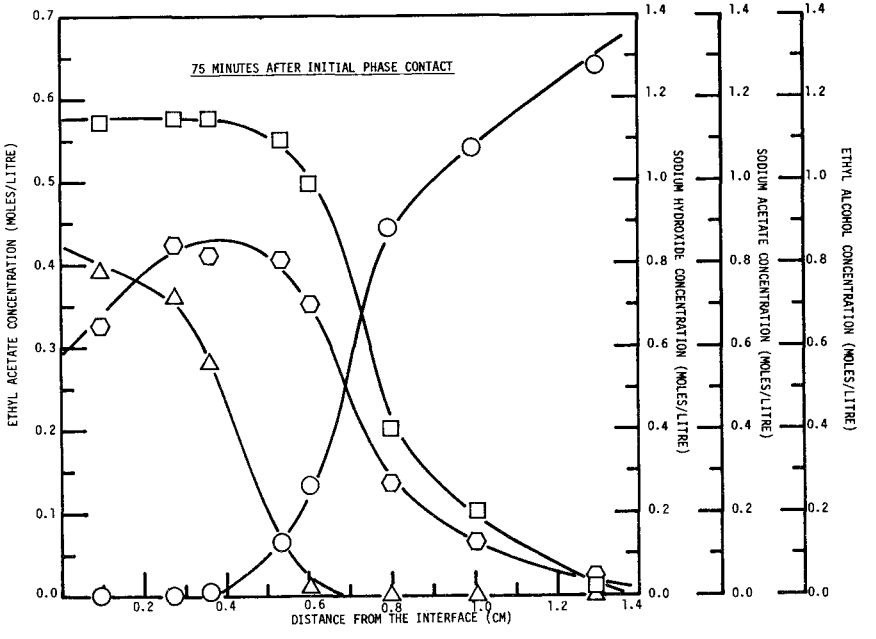

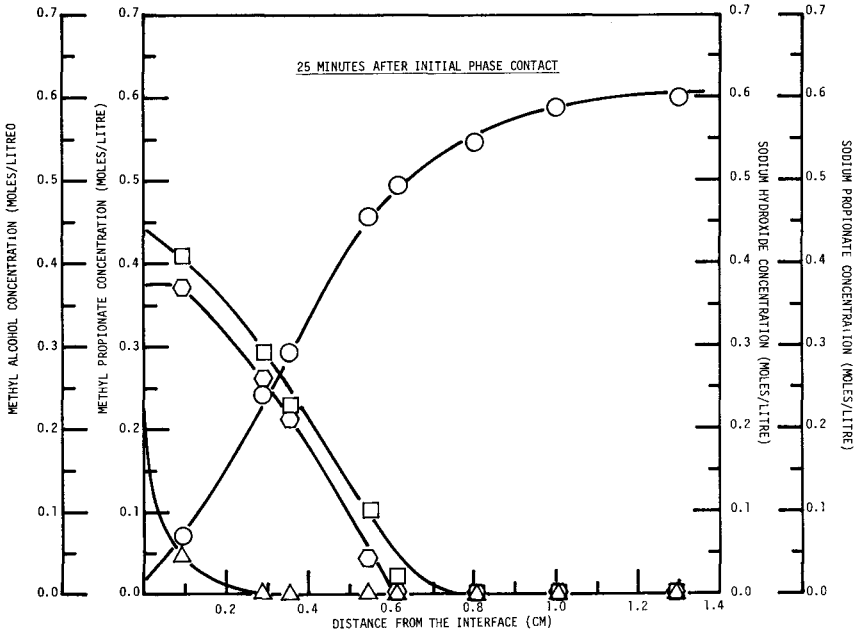

FIGURE XVII.5
CONCENTRATION PROFILES OF REACTANTS AND PRODUCTS
IN THE AQUEOUS PHASE
(METHYL PROPIONATE - 0.6N NaOH; 24±1°C)

△ △ METHYL PROPIONATE
○ ○ SODIUM HYDROXIDE
⬡ ⬡ METHYL ALCOHOL
□ □ SODIUM PROPIONATE

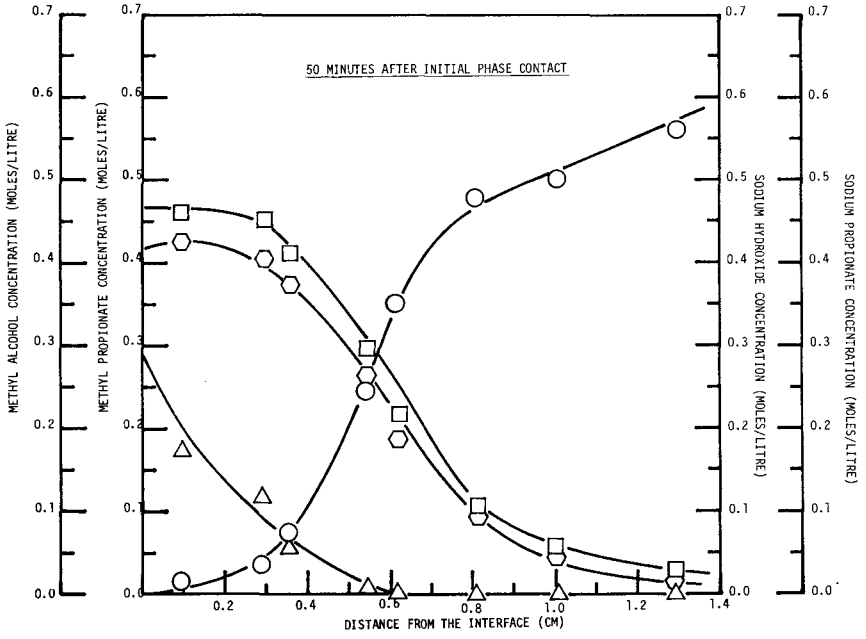

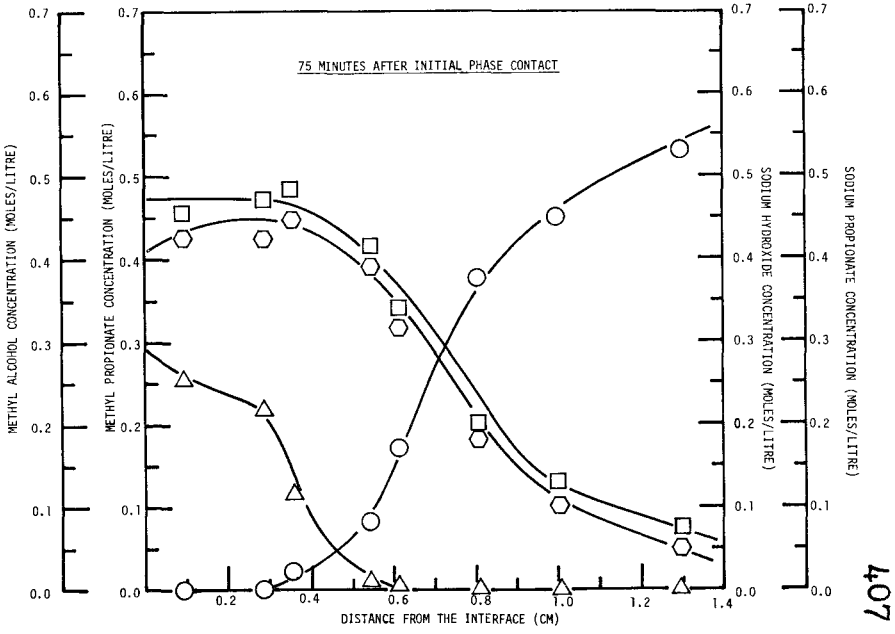

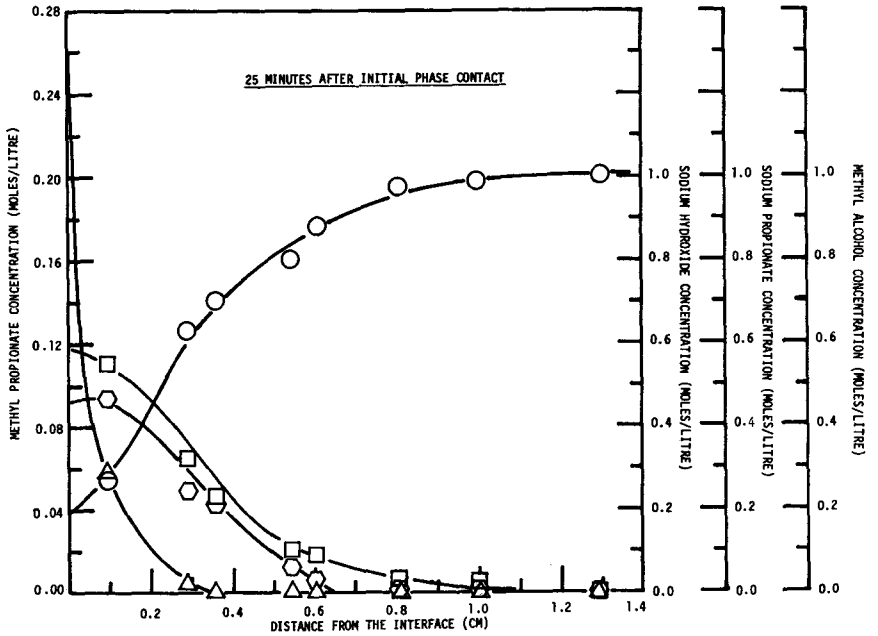

FIGURE XVII.6
CONCENTRATION PROFILES OF REACTANTS AND PRODUCTS
IN THE AQUEOUS PHASE
(METHYL PROPIONATE - 1.0N NaOH; 24±1°C)

△ △ METHYL PROPIONATE
○ ○ SODIUM HYDROXIDE
⬡ ⬡ METHYL ALCOHOL
□ □ SODIUM PROPIONATE

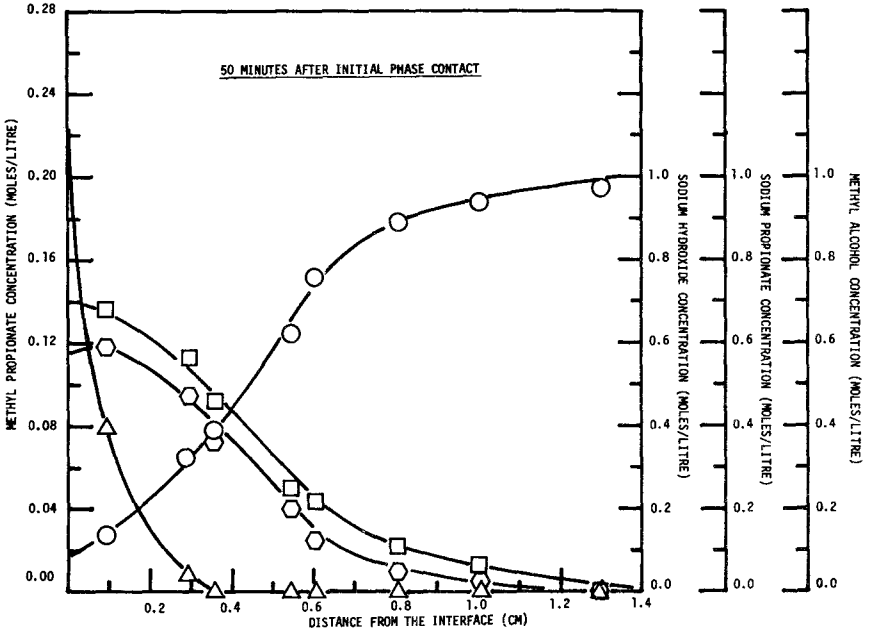

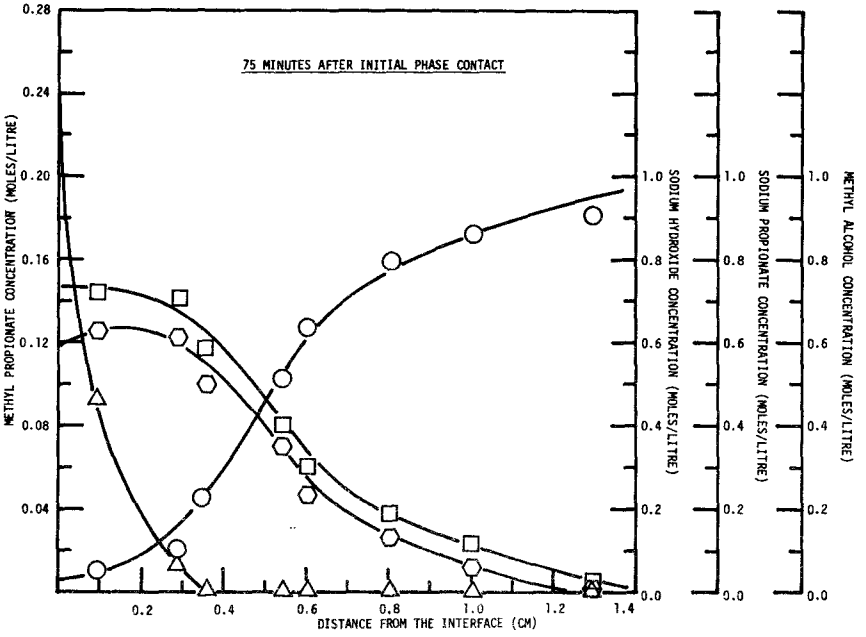

APPENDIX XVIII

TURBULENT REACTION LAYER PROPAGATION RATE DATA OF ESTER-AQUEOUS CAUSTIC SYSTEMS

FIGURE XVIII.1
(TURBULENT LAYER THICKNESS)^2 VS. PHASE CONTACT TIME
METHYL ACETATE - KOH SYSTEM

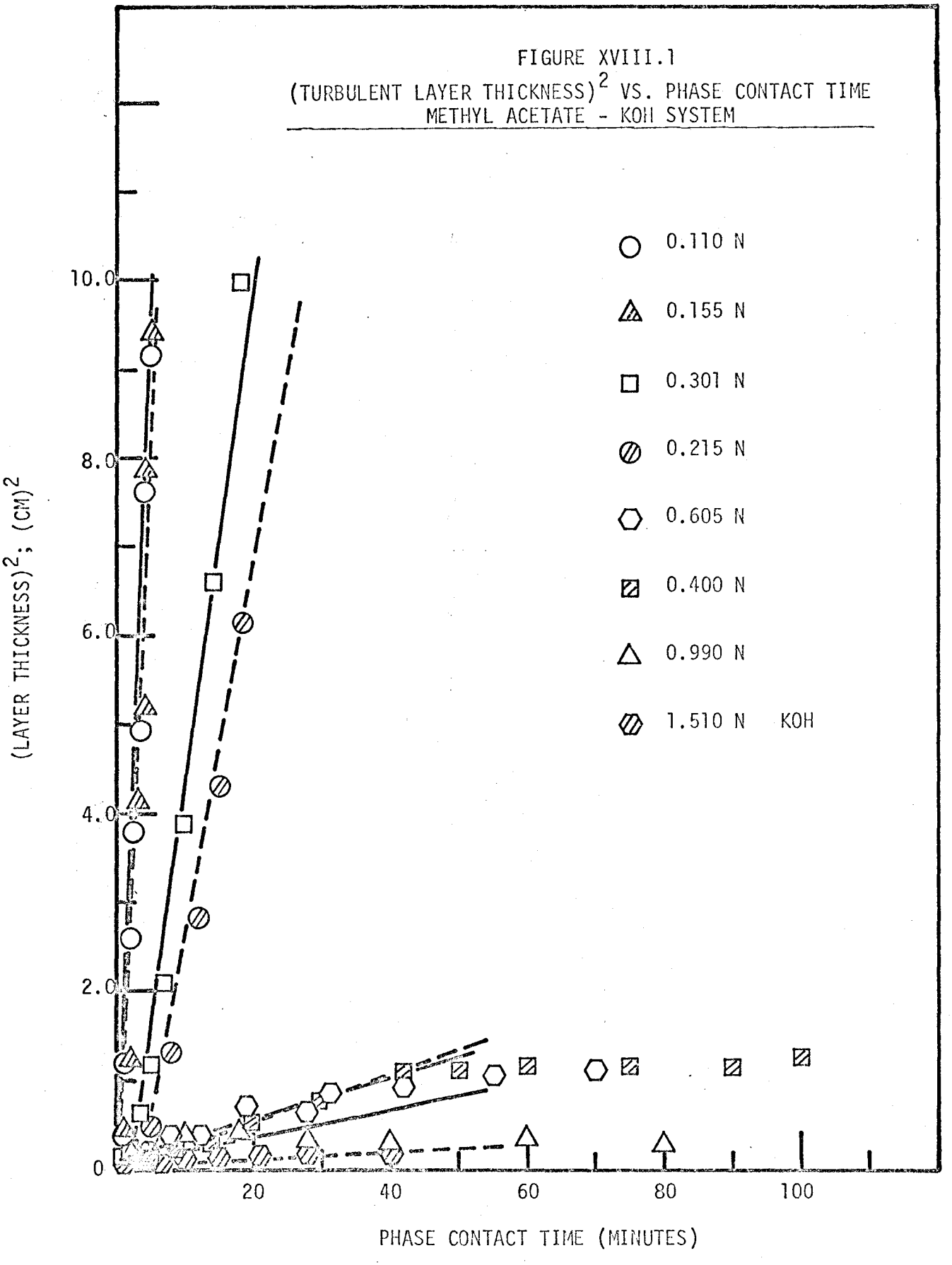

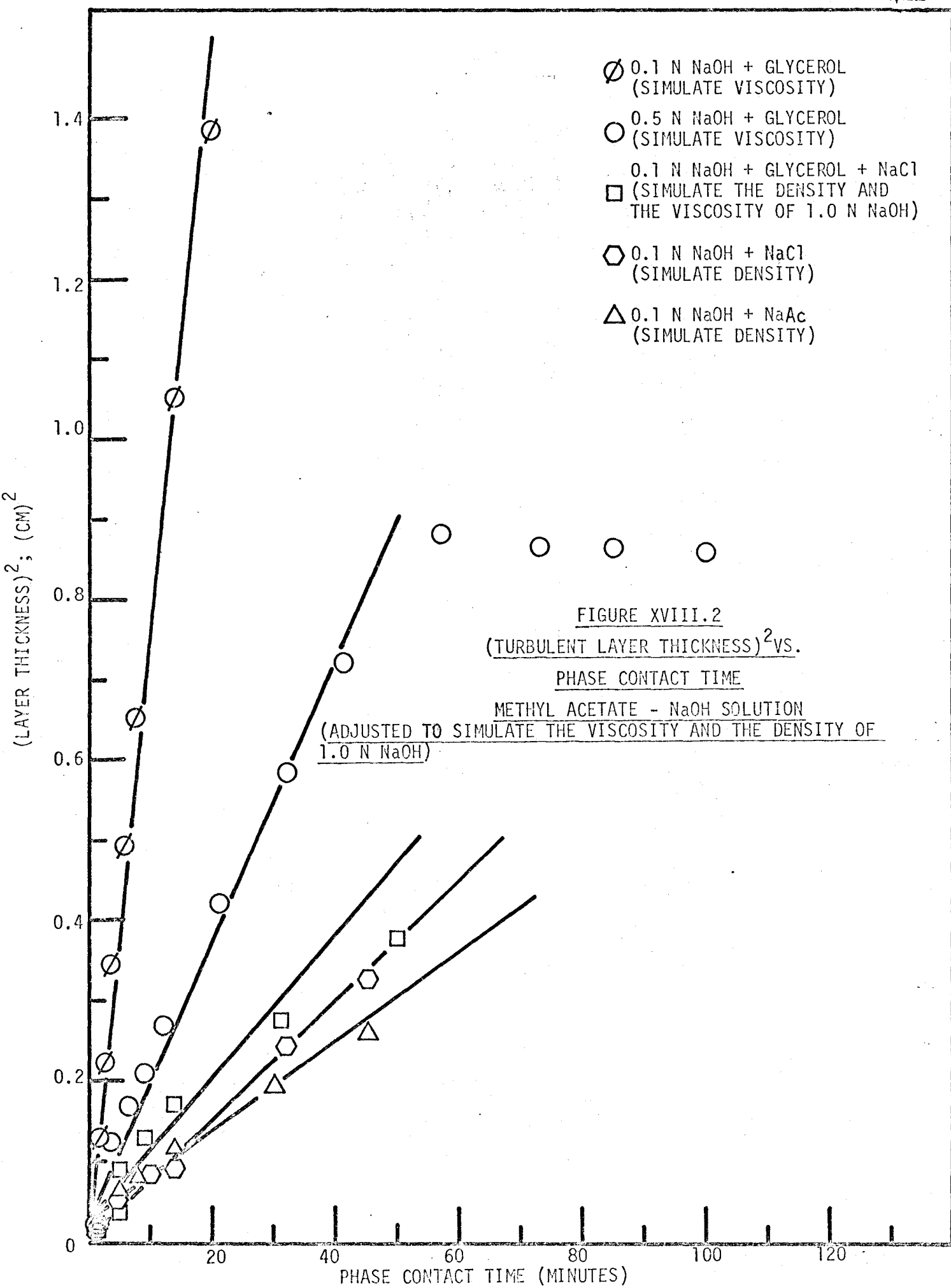

FIGURE XVIII.2

(TURBULENT LAYER THICKNESS)^2 VS.

PHASE CONTACT TIME

METHYL ACETATE - NaOH SOLUTION

(ADJUSTED TO SIMULATE THE VISCOSITY AND THE DENSITY OF 1.0 N NaOH)

FIGURE XVIII.3

(TURBULENT LAYER THICKNESS)^2 VS. PHASE CONTACT TIME
METHYL PROPIONATE - KOH SYSTEM

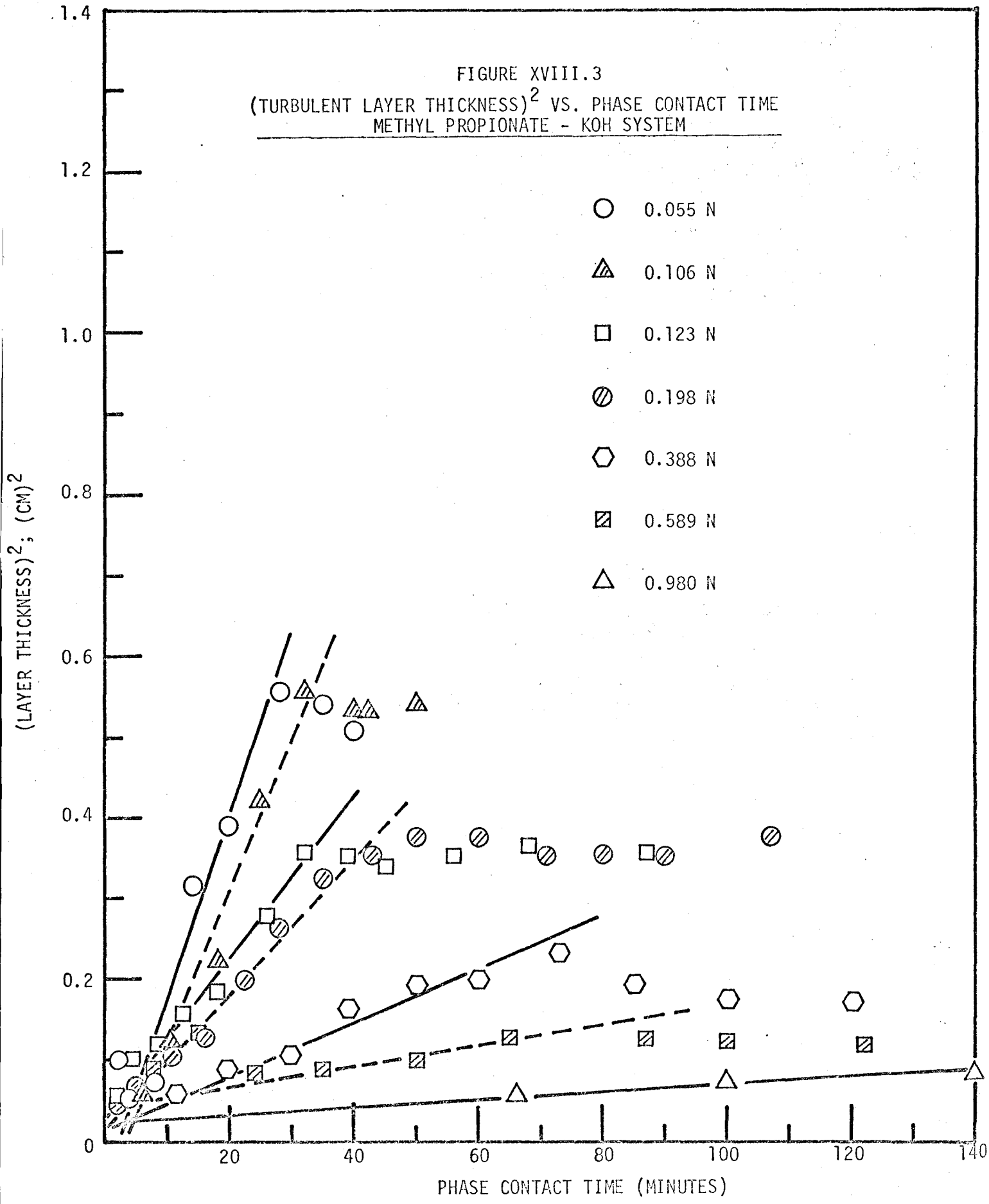

FIGURE XVIII.4
(TURBULENT LAYER THICKNESS)^2 VS. PHASE CONTACT TIME
ETHYL ACETATE - NaOH SYSTEM

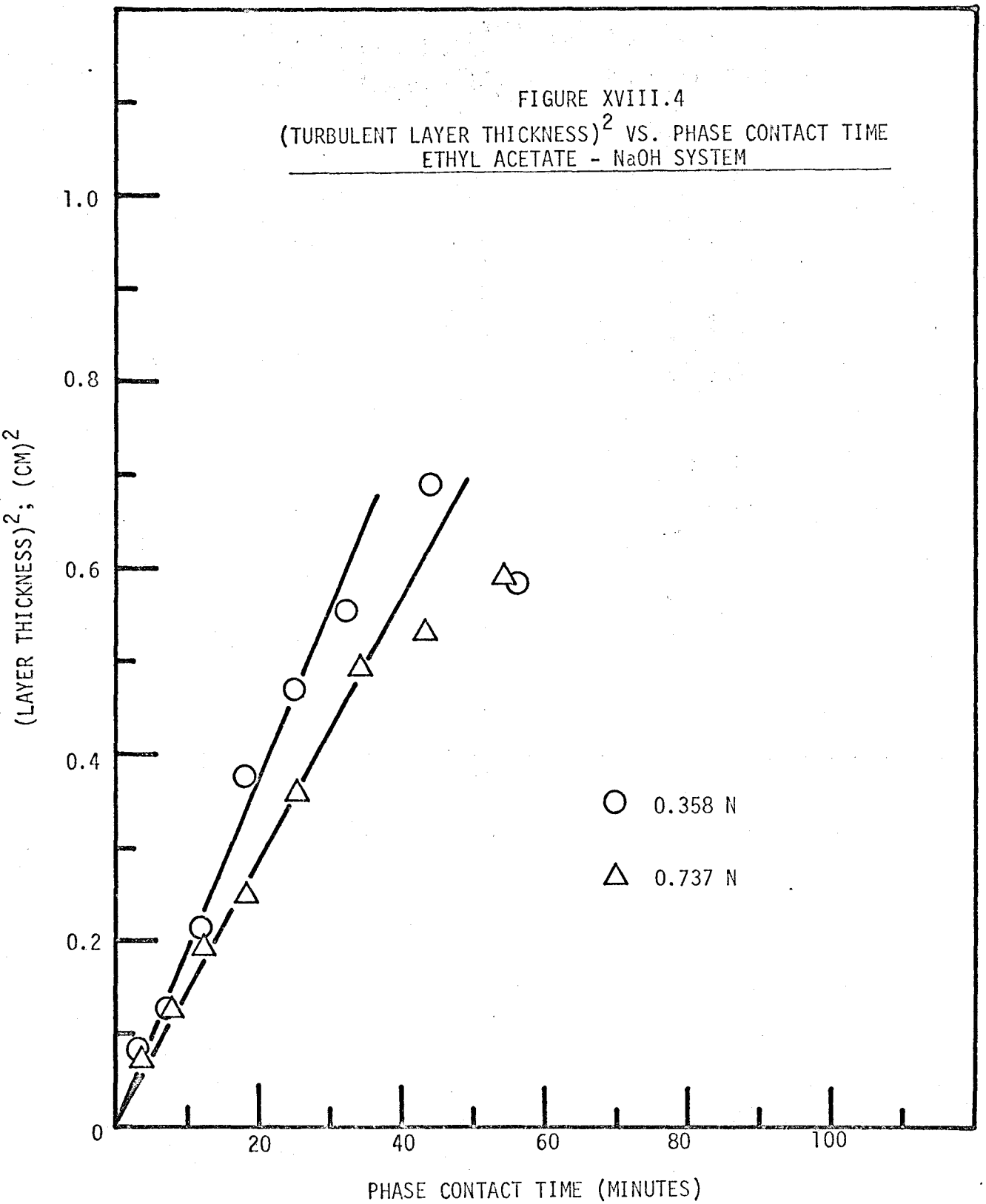

FIGURE XVIII.5

(TURBULENT LAYER THICKNESS)^2 VS. PHASE CONTACT TIME
ETHYL ACETATE - KOH SYSTEM

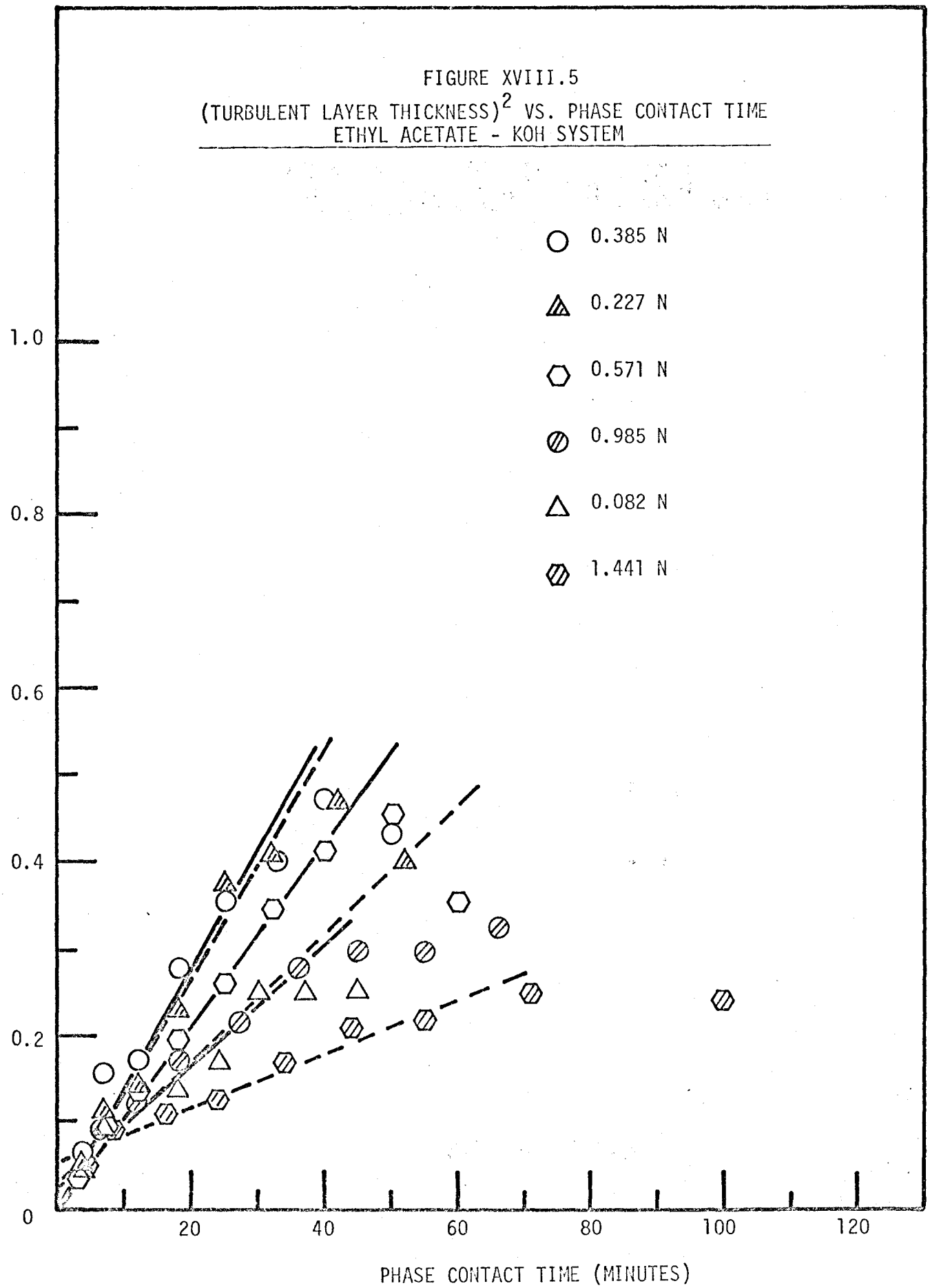

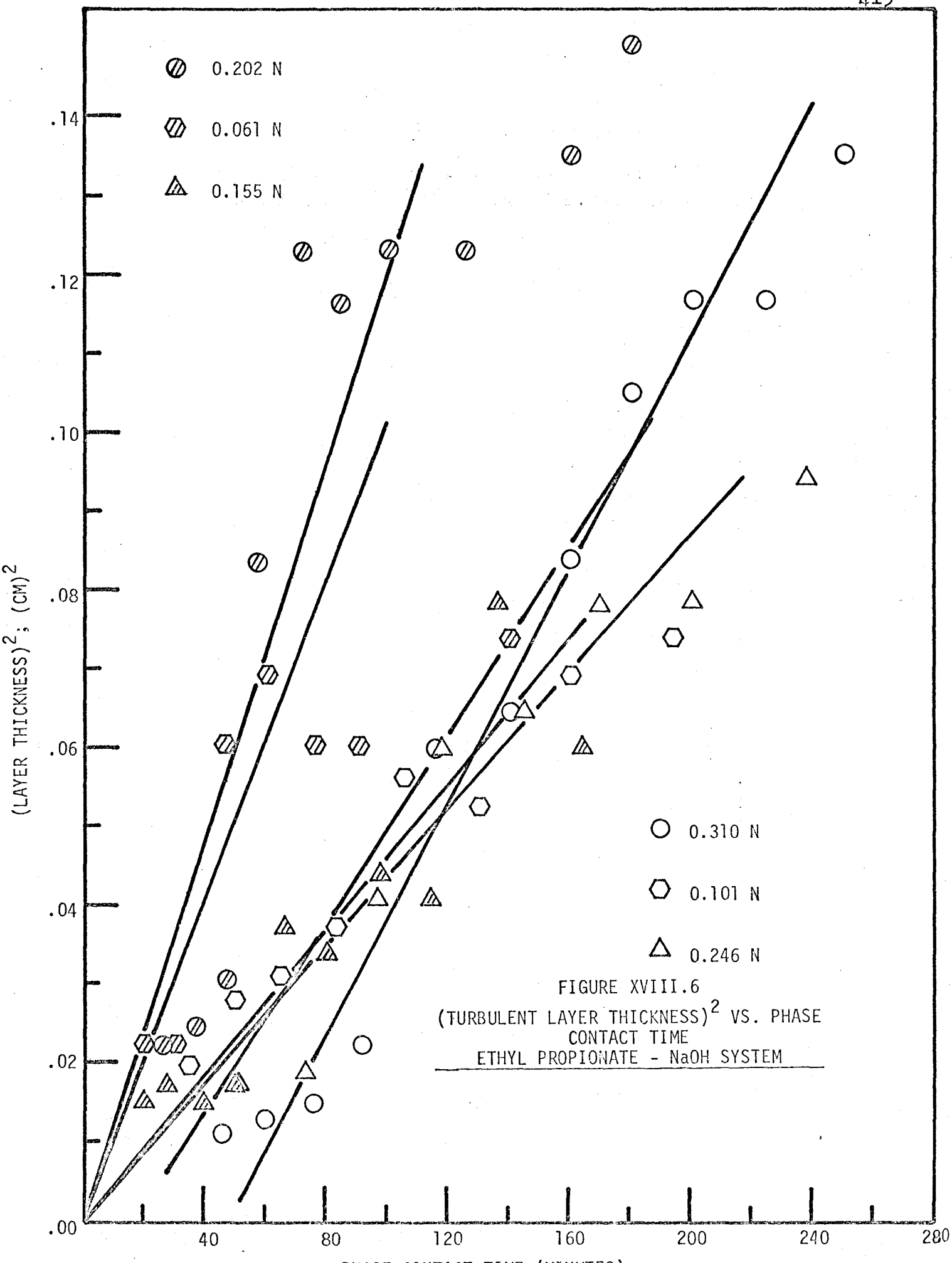

FIGURE XVIII.6
(TURBULENT LAYER THICKNESS)^2 VS. PHASE CONTACT TIME
ETHYL PROPIONATE - NaOH SYSTEM

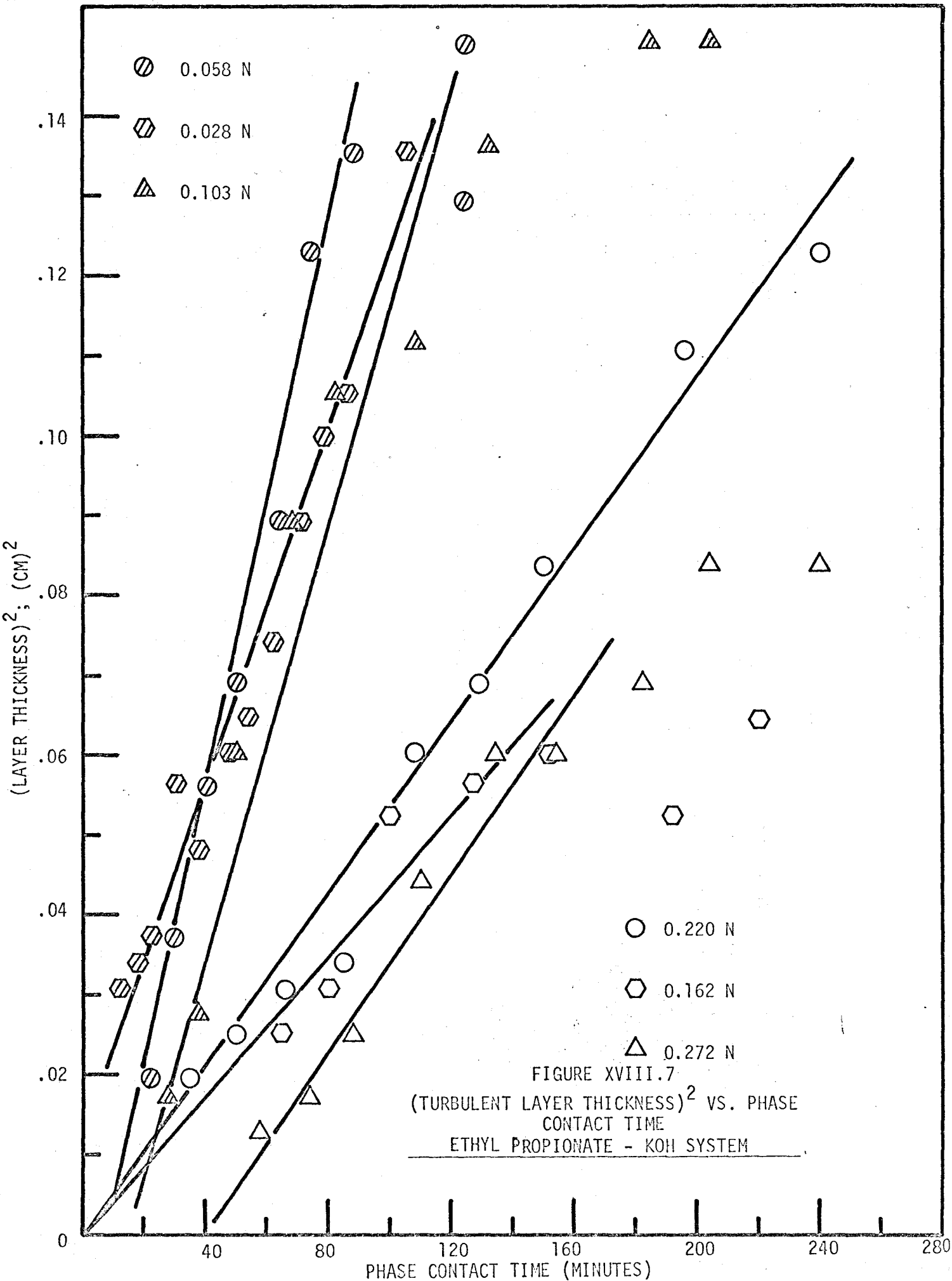

FIGURE XVIII.7
(TURBULENT LAYER THICKNESS)^2 VS. PHASE CONTACT TIME
ETHYL PROPIONATE - KOH SYSTEM

FIGURE XVIII.8

(TURBULENT LAYER THICKNESS)^2 VS. PHASE CONTACT TIME
PROPYL FORMATE - NaOH SYSTEM

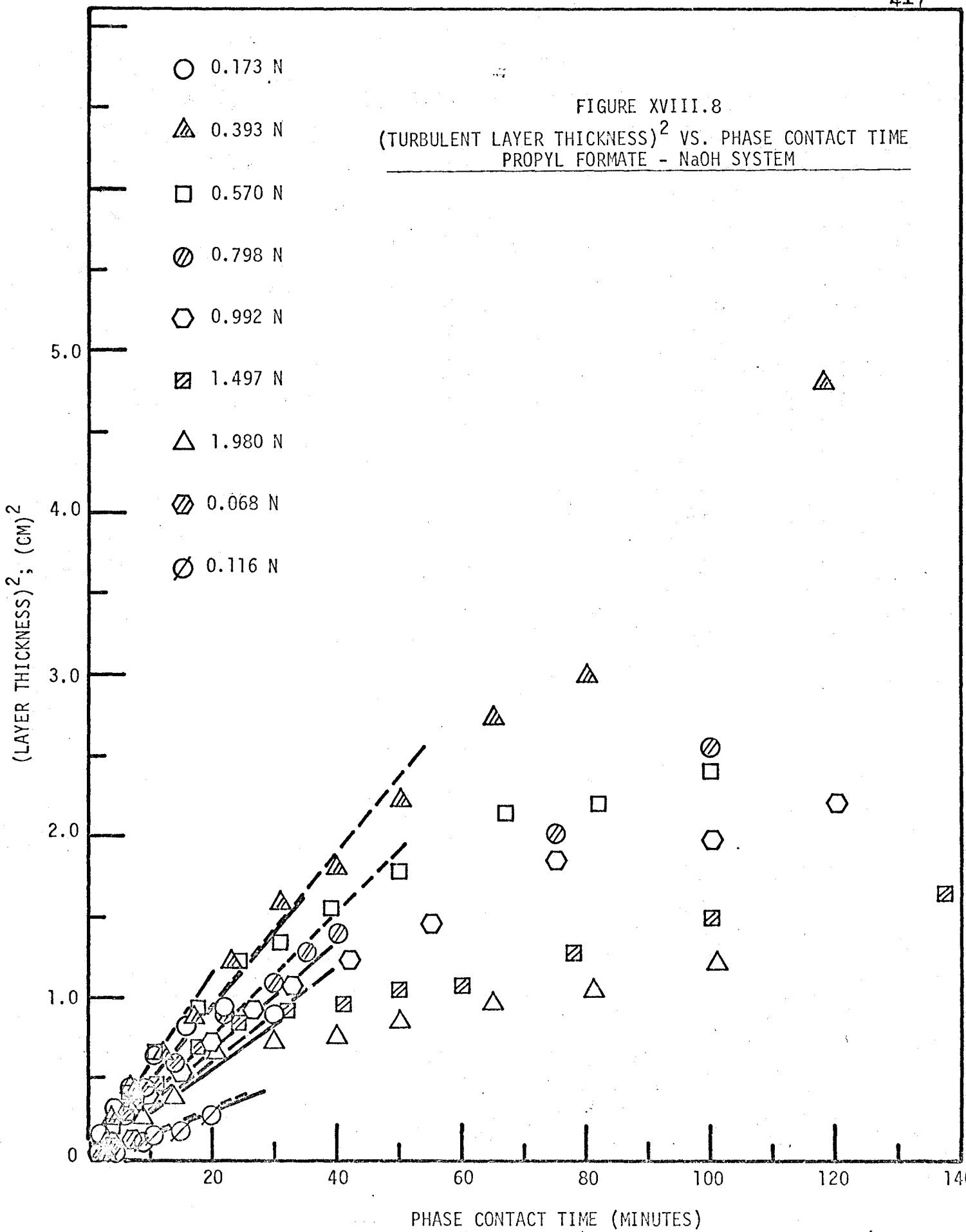

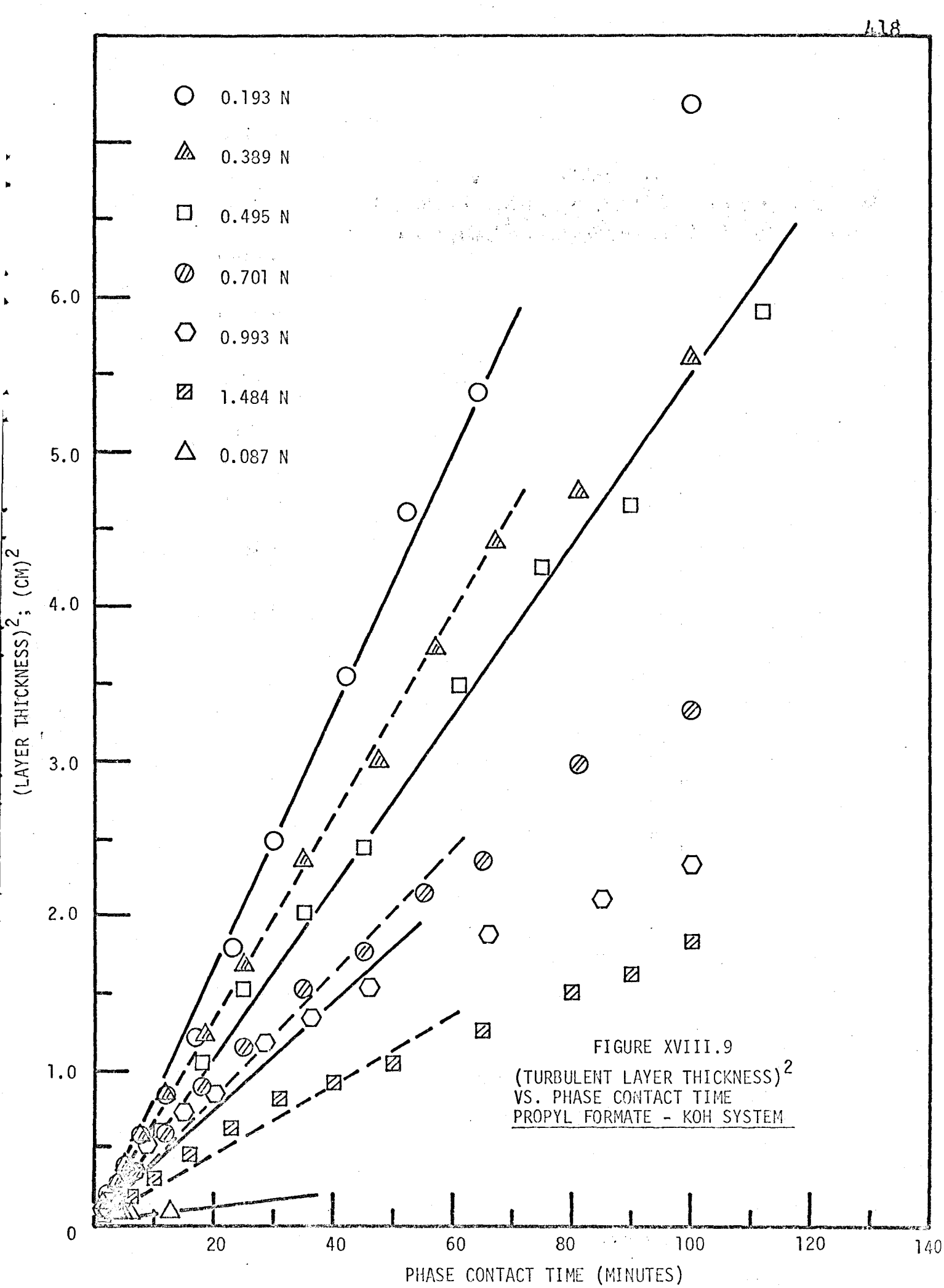

FIGURE XVIII.9
(TURBULENT LAYER THICKNESS)^2
VS. PHASE CONTACT TIME
PROPYL FORMATE - KOH SYSTEM

FIGURE XVIII.10

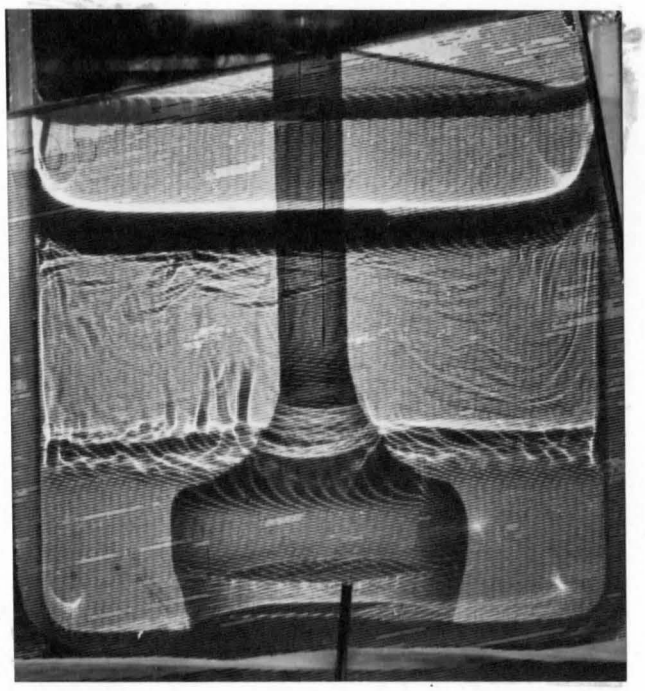

PROPYL FORMATE - 0.4 N NaOH SYSTEM :
80 MINUTES AFTER INITIAL PHASE CONTACT

FIGURE XVIII.11
(TURBULENT LAYER THICKNESS)^2 VS. PHASE CONTACT TIME; ETHYL FORMATE - NaOH SOLUTION (ADJUSTED TO SIMULATE THE VISCOSITY AND THE DENSITY OF 1.0 N NaOH)

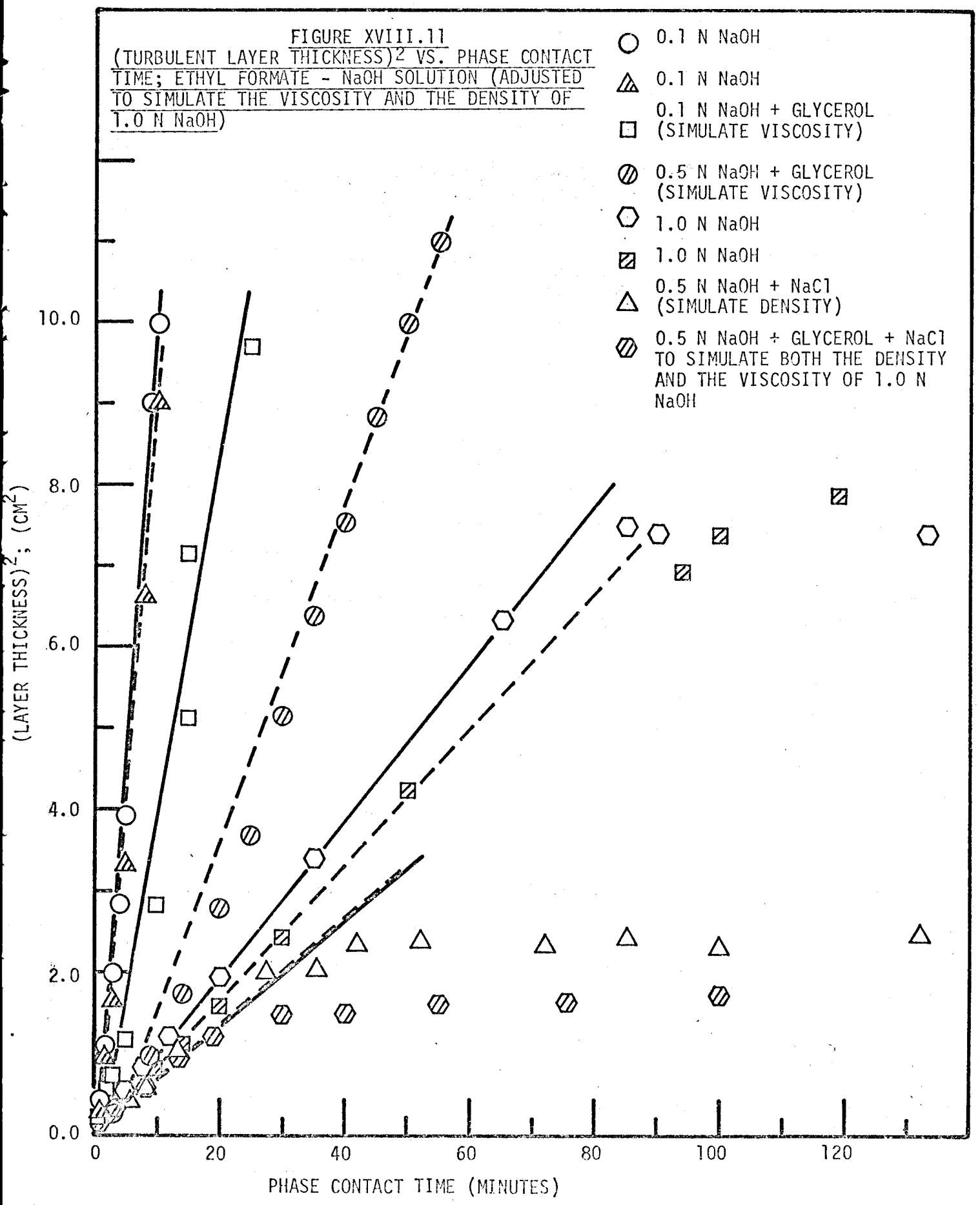

FIGURE XVIII.12

(TURBULENT LAYER THICKNESS)^2 VS. PHASE CONTACT TIME

ETHYL FORMATE - 0.1 N NaOH SOLUTION (ADJUSTED TO SIMULATE THE VISCOSITY AND THE DENSITY OF 1.0 N NaOH)

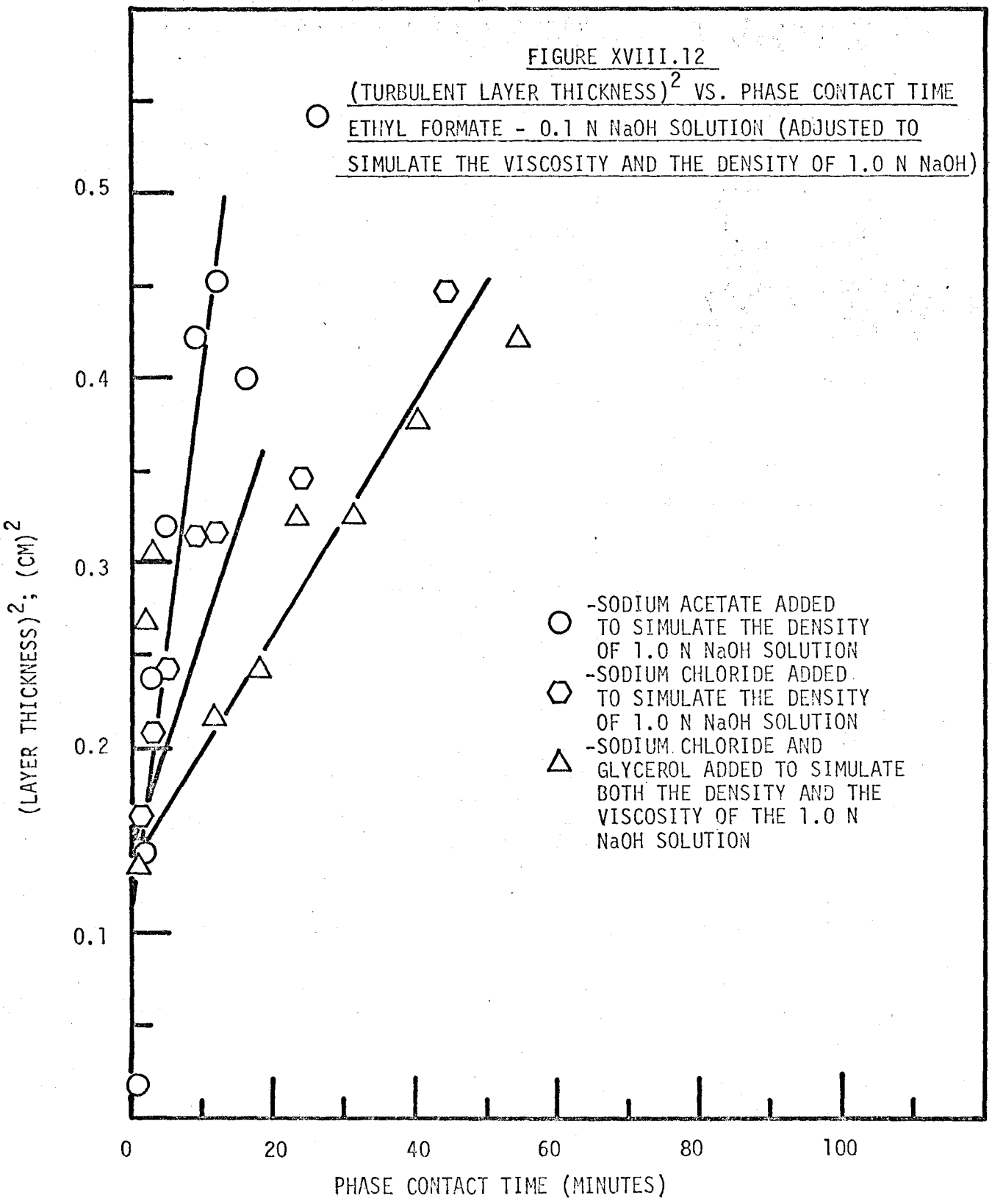

FIGURE XVIII.13

(TURBULENT LAYER THICKNESS)^2 VS. PHASE CONTACT TIME

ETHYL ACETATE - NaOH SOLUTION (ADJUSTED TO SIMULATE THE VISCOSITY OF THE 1.0 N NaOH)

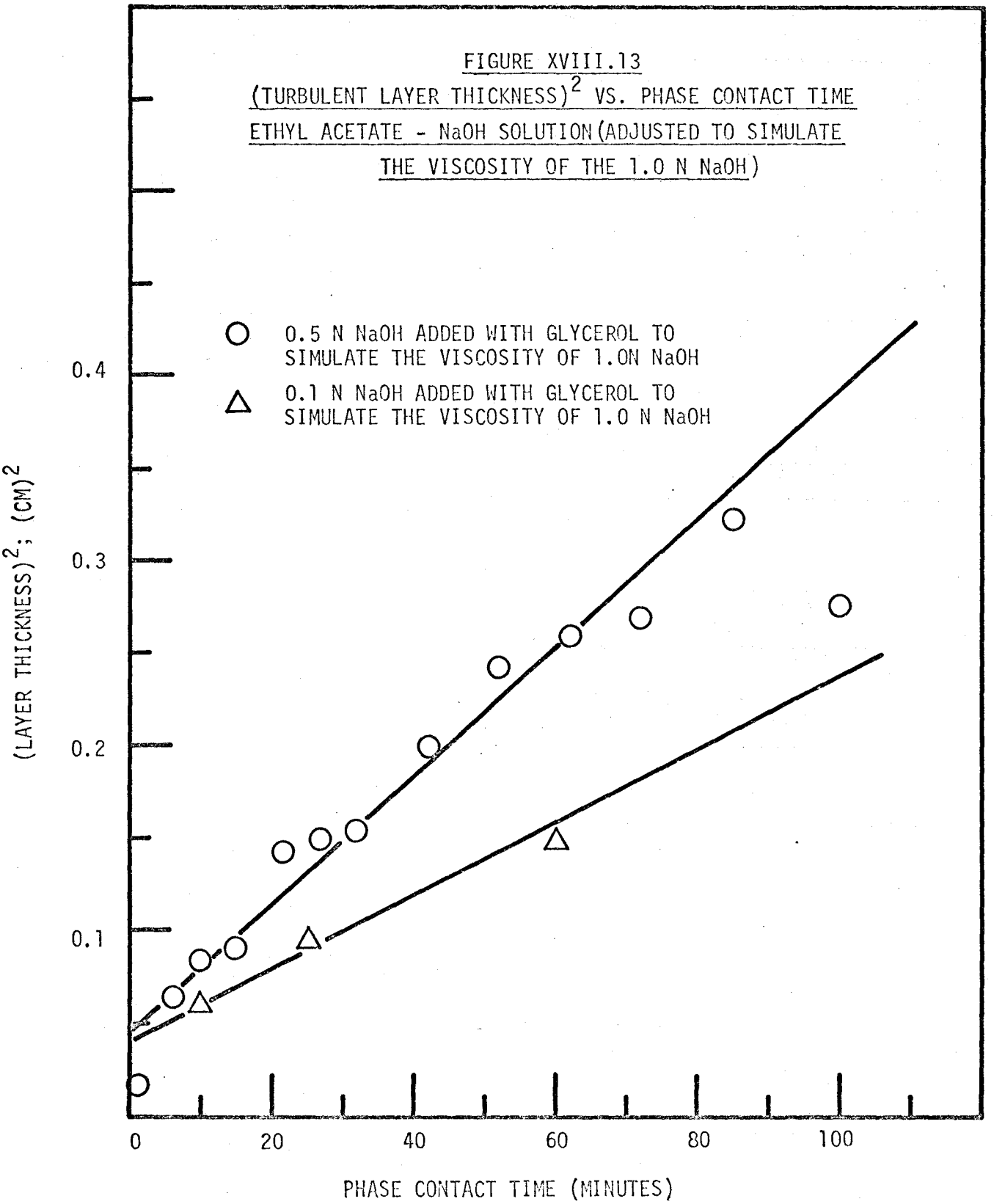

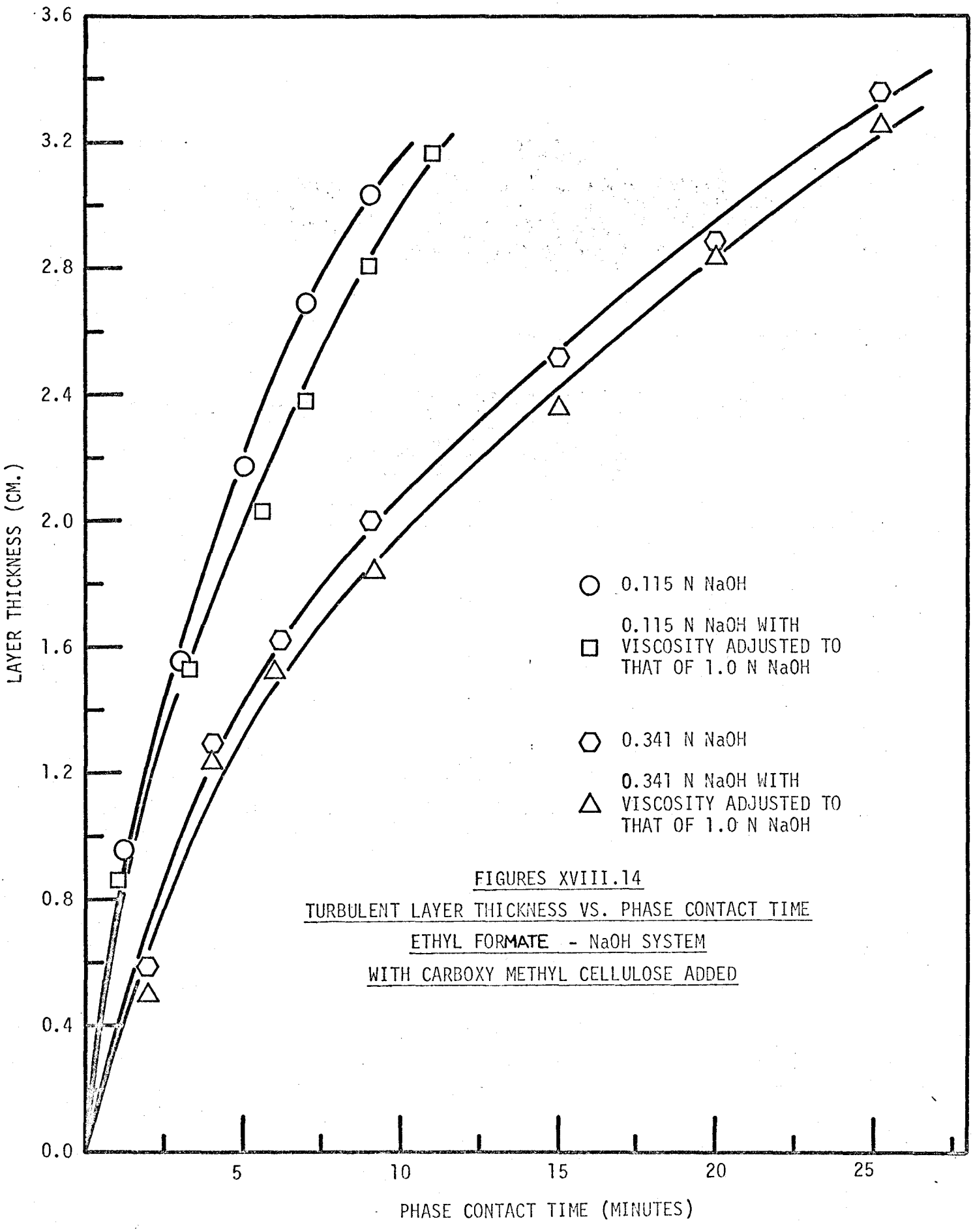

FIGURES XVIII.14

TURBULENT LAYER THICKNESS VS. PHASE CONTACT TIME

ETHYL FORMATE - NaOH SYSTEM

WITH CARBOXY METHYL CELLULOSE ADDED

APPENDIX XIX

COMPARISON OF THE CALCULATED AND THE EXPERIMENTALLY MEASURED REACTANT CONCENTRATIONS IN THE LOWER PHASE OF THE STEADY FLOW REACTOR

In the steady state transfer experiments, the concentration of the reactants in the lower phase may be approximated by assuming that the lower phase is well-mixed and the components reacted homogeneously (Section 4.3.1.4). On the other hand, the concentration of the caustic in the lower phase was measured for five runs in the ethyl formate-sodium hydroxide system using a conductivity cell located immediately at the outlet of the flow reactor. The conductivities (or the resistivities) measured were converted back to the sodium hydroxide concentrations through calibration curves.

One calibration curve was prepared for each input sodium hydroxide concentration. The same experimental apparatus and the procedure for the transfer runs applied to the calibration runs as well. In the preparation of a calibration curve, solutions of various combinations of the salt and the caustic concentrations were flowed into the stirred reactor and the conductivity (or the resistivity) of each of the combined solution was recorded respectively. Each combined solution of the caustic and the salt should have the total concentration value equal to that of the input sodium hydroxide concentration. A sample calibration curve is presented in Figure XIX.1. In such calibrations, the effect of the small amount of ethyl formate on the conductivity (or the resistivity) of the out-

FIGURE XIX.1

RESISTANCE VS. CONCENTRATION OF NaOH :
CALIBRATION CURVE FOR RUN #7 ETHYL FORMATE - NaOH SYSTEM
(CONSTANT TOTAL CONCENTRATION OF NaOH + HCOONa = 0.5N)

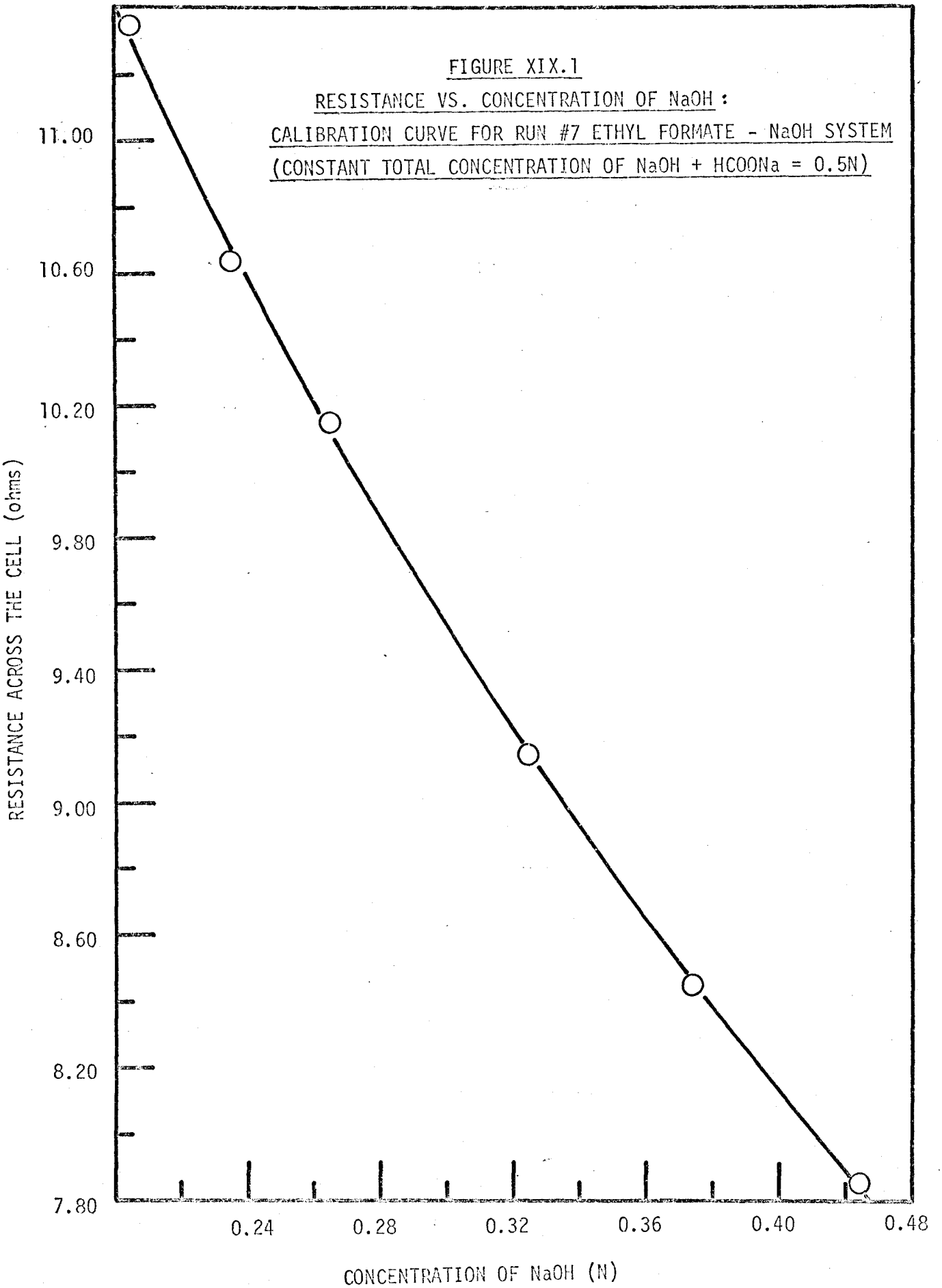

flowing solution during the actual transfer runs was assumed to be negligible.

A detailed sample comparison of the calculated and the measured reactant concentrations is presented in the following: Data are taken from Run #7; Group I of the ethyl formate-sodium hydroxide system,

Original input sodium hydroxide concentration (C_{B_o}), 0.5 N.

Transfer rate of the ethyl formate phase (N_A), 23.7 ml./hr. or $.291_{959}$ moles/hr.

Volume of the lower phase compartment (V), 0.098 litres

Reaction rate constant at 25°C (k), 74400 litre/mole-hr.

Flowrate of the lower phase (F), 1.5 litres/hr.

Substituting these values into Equations (23)and (24),

Calculated sodium hydroxide concentration at steady state, 0.305_{492} moles/litre.

Calculated ethyl formate concentration at steady state, 0.000_{131} moles/litre

The resistance (considered as resistivity in this case since the same conductivity cell was used for all the runs) of the lower phase solution at steady state was measured to be 10.19 ohms. From the calibration curve (Figure XIX.1), the lower phase sodium hydroxide concentration is 0.301 N.

$\therefore$ percentage of deviation between the measured and the calculated sodium hydroxide concentrations is 1.5

Results of all five check runs show that the maximum deviation between the measured and calculated values is no more than 3.5%.

REFERENCES

A1 Akehata, T. and Johnson, A. I., Can.J.Chem.Eng., 43, 262 (1965).

A2 Arnold, J. H., J.Am.Chem.Soc., 52, 3937 (1930).

A3 Astarita, G., Chem.Eng.Sci., 16, 202 (1961).

A4 Astarita, G., "Mass Transfer with Chemical Reaction," Elsevier Publishing Co., Amsterdam (1967).

A5 Austin, L. J., Ying, W. E. and Sawistowski, H., Chem.Eng.Sci., 21, 1109 (1966).

B1 Bakker, C. A. P., van Buytenen, P. M. and Beek, W. J., Chem.Eng.Sci., 21, 1039 (1966).

B2 Bakker, C. A. P., van Vlissingen, F. H. F. and Beek, W. J., Chem.Eng.Sci., 22, 1349 (1967).

B3 Banerjee, S., Rhodes, E. and Scott, D. S., Chem.Eng.Sci., 22, 43 (1967).

B4 Banerjee, S., Scott, D. S. and Rhodes, E., I. & E. C. Fundamentals, 7, 22 (1968).

B5 Becker, F., and Spalink, F., Z.Physik.Chem., 26, 1 (1960).

*B6 Bénard, H., J. de Phys., 9, 513 (1900).

B7 Bikerman, J. J., "Surface Chemistry," 2nd ed. Academic Press, New York (1958).

B8 Bird, R. B., Steward, W. E. and Lightfoot, E. N., "Transport Phenomena," John Wiley and Sons Inc., New York (1960).

B9 Block, M. J., Nature, 78, 650 (1956).

B10 Blokker, P. C., Proc. 2nd Intern. Congr. Surface Activity, London Vol. 1, p. 503 (1957).

*B11 Boltzmann, L., Ann. Physik., 53, 959 (1894).

B12 Boyd, D. P. and Marchello, J. M., Chem.Eng.Sci., 21, 769 (1966).

* References not studied in the original form

B13 Brian, P. L. T., A.I.Ch.E.J., 10, 5 (1964).

B14 Brian, P. L. T., Baddour, R. F. and Matiatos, D. C., A.I.Ch.E.J., 10, 727 (1964)

B15 Brian, P. L. T. and Beaverstock, M. C., Chem.Eng.Sci., 20, 47 (1965)

B16 Brian, P. L. T., Hurley, J. F. and Hasseltine, E. H., A.I.Ch.E.J., 7, 226 (1961).

B17 Brian, P. L. T., Vivian, J. E. and Habib, A. G., A.I.Ch.E.J. 8, 205 (1962).

B18 Brian, P. L. T., Vivian, J. E. and Matiatos, D. C., A.I.Ch.E.J., 13, 28 (1967).

*B19 Brücke, Akad. Wiss. Wien., 79, 267 (1879).

*B20 Brückner, R., Naturwissenschaften, 47, 372 (1960).

C1 Cho, D. H. and Ranz, W. E., Chem.Eng.Progr. Symposium, Ser. No. 72, 63, 37 (1966).

C1a Cho, D. H., Ph.D. Thesis, Dept. Chem. Eng., Univ. of Minnesota (1966).

C1b Claesson, S., Nature, 158, 824 (1946).

C2 Clarke, J. K. A., I.& E.C. Fundamentals, 3, 239 (1964).

C3 Colello, R. G. and Springer, G. S., Intern. J. Heat Mass Transfer, 9, 1391 (1966).

C4 Crank, J., "Mathematics of Diffusion," Oxford Press, London (1955).

C4a Crank, J., and Nicholson, P., Proc. Cambridge Phil. Soc., 43, 50 (1947).

C4b Creeth, J. M., J.Am.Chem.Soc., 77, 6428 (1955).

C5 Cress, P., "MIMIC - A Digital-Analogue Simulator," Computing Centre, University of Waterloo, Waterloo, Ontario (1966).

C6 Cullinan, H. T., I. & E.C. Fundamentals, 5, 281 (1966).

C7 Curtiss, C. F. and Hirschfelder, J. O., J.Chem.Phys., 17, 550 (1949).

D1 Danckwerts, P. V., Trans. Faraday Soc., 46, 300 (1950).

D2 Danckwerts, P. V., Trans. Faraday Soc., 46, 701 (1950).

D3 Danckwerts, P. V., Ind. Eng. Chem., 43, 1460 (1951).

D4 Danckwerts, P. V., Chem. Eng. Sci., 23, 1045 (1968).

D5 Danckwerts, P. V. and Da Silva, A. T., Chem. Eng. Sci., 22, 1513 (1967).

D6 Danckwerts, P. V. and Kennedy, A. M., Trans. Inst. Chem. Engrs., 32, S49 and S53 (1954).

D7 Danckwerts, P. V. and Kennedy, A. M., Chem. Eng. Sci., 8, 201 (1958).

D8 Daniels, F. et al., "Experimental Physical Chemistry," McGraw-Hill Pub. Co., New York (1949).

D9 Davies, J. T., "Advances in Chemical Engineering," Vol. 4, Academic Press, New York (1963).

D10 Davies, J. T. and Haydon, D. A., Proc. 2nd Intern. Congr. Surface Activity, (London) Vol. 1, 417 (1957).

D11 Davies, T. V. and Haydon, D. A., Proc. Roy. Soc., A243, 492 (1958).

D12 Davies, J. T. and Rideal, E. K., "Interfacial Phenomena," Academic Press, New York, 2nd ed., (1963).

D13 Davies, J. T. and Ting, S. T., Chem. Eng. Sci., 22, 1539 (1967).

D14 Deybe, P., Z. Physik. Chem., 130, 55 (1927).

D15 Dinsmore, D. G., B.Eng. Thesis, Dept. Chem. Eng., Royal Military College (1964).

D16 Dobbins, W. E., J. San. Eng. Div., Proc. A.S.C.E., 53 (1964).

D17 Duda, J. L. and Vrentas, J. S., I. & E. C. Fundamentals, 5, 434 (1966).

E1 Ellis, S. R. M. and Biddulph, M., Chem. Eng. Sci., 21, 1107 (1966).

E2 Emmert, R. E. and Pigford, R. L., A. I. Ch. E. J., 8, 171, 702 (1962).

E3 Eriksen, T., Chem. Eng. Sci., 22, 727 (1967).

F1 Fortescue, G. E. and Pearson, J. R. A., Chem. Eng. Sci., 22, 1163 (1967).

F2 Friedlander, S. K. and Keller, K. H., Chem. Eng. Sci., 18, 365 (1963).

F3 Friedlander, S. K. and Litt, M., Chem. Eng. Sci., 7, 229 (1958).

F4 Fujinawa, K. and Maruyama, T., Kagaku Kogaku, 21, 75 (1957).

F5 Fujinawa, K. and Nakaike, Y., Kagaku Kogaku, 25, 280 (1961).

F6 Fujinawa, K., Maruyama, T. and Nakaike, Y., Kagaku Kogaku, 22, 96 (1958).

*F7 Fürth, R., Physik. Z., 26, 719 (1925).

G1 Gabor, J. D., Mecham, W. J., Jonke, A. A. and Rodgers, W. A., USAEC Rept. ANL 6131 (1959).

*G2 Gad, Arch. Anat. Physiol. Lpz. p. 181 (1878).

G3 Garner, F. H., Nutt, C. W. and Mohtadi, M. F., Nature, 175, 603 (1955).

G4 Gaven, J. V., S.M. Thesis in Chem. Eng. M.I.T., (1953).

G5 Gehlawat, J. K. and Sharma, M. M., Chem. Eng. Sci., 23, 1173 (1968).

G6 Gilliland, E. R., Ind. Eng. Chem., 26, 681 (1932).

G7 Gilliland, E. R., Baddour, R. F. and Brian, P. L. T., A. I. Ch. E. J., 4, 223 (1958).

G8 Glueck, A. R. and Kenney, C. N., Chem. Eng. Sci., 23, 1257 (1968).

G9 Goltz, G. E., J. Imp. Coll. Chem. Eng. Soc., 13, 40 (1958).

G10 Gore, M.Sc. Thesis, Dept. of Chem. Eng., University of Minnesota (1960).

G11 Goren, S. L. and Mani, R. V. S., A. I. Ch. E. J., 14, 57 (1968).

G11a Gosting, L. J., Measurement and Interpretation of Diffusion, "Advances in Protein Chem." XI, Academic Press, New York (1956).

G12 Groothuis, H. and Kramers, H., Chem. Eng. Sci., 4, 17 (1955).

G13 Guild, J., "Theory of Moiré Fringes," Oxford University Press, (1956).

*H1 Hahn, H. T., Report HW-32626, U.S. Atomic Energy Commission, as quoted in Reference (D9).

H2 Hanratty, T. J., A. I. Ch. E. J., 2, 359 (1956).

H3 Hansen, C. M., I. & E. C. Fundamentals, 6, 609 (1967).

H4 Hansford, G. S. and Litt, M., Chem. Eng. Sci., 23, 849 (1968).

H5 Harned, H. S. and Owen, B. P., "Physical Chemistry of Electrolytic Solutions, Monograph Series #137", p. 736, Reinhold Pub. Co. (1958).

H6 Harriott, P., Chem. Eng. Sci., 17, 149 (1962).

*H7 Hatta, S., Technical Reports, Tohoku Imp. Univ., 8, 1 (1928-29) and 10, 119 (1932).

H8 Haydon, D. A., Nature, 176, 839 (1955).

H9 Haydon, D. A., Proc. Roy. Soc., A243, 483 (1958).

H10 Hays, D. F. and Curd, H. N., J. Franklin Inst. 283, 300 (1967).

H10a Hiby, J. W., Braun, D., Eickel, K. H., Chem. Ing. Tech., 39, 297 (1967).

H11 Higbie, R., Trans. Am. Inst. Chem. Engrs., 35, 365 (1935).

H12 Hikita, H. and Asai, S., International Chemical Engineering, 4, 332 (1964).

H13 Hildebrand, F. B., "Introduction to Numerical Analysis," McGraw-Hill Inc., New York (1956).

H14 Hirschfelder, J. O., Bird, R. B. and Spotz, E. L., Trans. A.S.M.E., 71, 921 (1949).

H15 Hoshino, S. and Sato, K., Kagaku Kogaku (English Edition), 4, 307 (1966).

H16 Houghton, W. T., Ph.D. Thesis, McMaster University (1966).

H17 Howard, D. W. and Lightfoot, E. N., A. I. Ch. E. J., 14, 458 (1968).

H18 Hsu, H. W. and Bird, R. B., A. I. Ch. E. J., 6, 517 (1960).

H19 Huang, C. J. and Kuo, C. H., A. I. Ch. E. J., 9, 161 (1963).

I1 Inoue, Y., Osugi, A. and Inoue, T., Kagaku Kogaku (English Edition), 4, 66 (1966).

I2 "International Critical Tables," McGraw-Hill Pub. Co., New York (1926).

J1 Jeffreys, H., Quart. J. Mech. Appl. Math., 4, 283 (1951)

J2 Jhaveri, A. S. and Sharma, M. M., Chem. Eng. Sci., 22, 1 (1967).

J3 Jhaveri, A. S. and Sharma, M. M., Chem. Eng. Sci., 23, 1 (1968).

J4 Johnson, P. A. and Babb, A. L., Chem. Reviews, 56, 387 (1956).

J5 Jost, W., "Diffusion in Solids, Liquids and Gases," Academic Press (1952).

K1 Kaminski and McBain, Proc. Roy. Soc., A198, 447 (1949).

K2 Kass, W. and O'Keefee, M., J. Appl. Phys., 37, 2377 (1966).

K3 Kataoka, H. and Miyauchi, T., Kagaku Kogaku (English Edition), 4, 335 (1966).

*K3a Kindsvater, H. M., Thesis, State Univ. of Iowa (1938).

K4 Kintner, R. C., "Advances in Chemical Engineering," Vol. 4, Academic Press, New York (1963).

K5 Kirkwood, J. G., Chem. Revs., 24, 233 (1939).

*K6 Kishinevskii, M. K., J. Appl. Chem. U.S.S.R., 28, 881 (1955).

*K7 Kishinevskii, M. K. and Serebryanskii, V. T., J. Appl. Chem. U.S.S.R., 29, 29 (1956).

K8 Kobayashi, T. and Saito, Hirotaro, Kagaku Kogaku (English Edition), 4, 11 (1966).

K9 Kobayashi, T., Inoue, H. and Yagi, S., Kagaku Kogaku (English Edition), 5, 211 (1967).

*K10 Kroepelin H., Abhandl. Braunschweig. Wiss. Ges., 9, 135 (1957).

*K11 Kroepelin, H. and Neumann, H. J., Naturwissenschaften, 43, 347 (1956).

*K12 Kroepelin, H. and Neumann, H. J., Naturwissenschaften, 44, 304 (1957).

*K13 Kroepelin, H. and Prott, E., Naturwissenschaften, 45, 333 (1958).

L1 Langmuir, I. and Langmuir, D. B., J. Phys. Chem., 31, 1719 (1927).

L1a Lamm, O., Kolloid. Z., 98, 45 (1942).

L2 Le, C. D., M. Eng. Thesis, McMaster University (1968).

L3 Lewis, J. B., Trans. Inst. Chem. Engrs. (London), 31, 323, 325 (1953).

L4 Lewis, J. B., Chem. Eng. Sci., 3, 248 (1954).

L5 Lewis, J. B. and Pratt, H. R. C., Nature, 171, 1155 (1953).

L6 Lewis, W. K. and Whitman, W. G., Ind. Eng. Chem., 16, 1215 (1924).

L7 Lightfoot, E. N. and Cussler, E. L. Jr., Chem. Eng. Progr. Symposium Ser. 58, 61, 66 (1965).

L8 Lin, C. S., Moulton, R. W. and Putnam, C. L., Ind. Eng. Chem., 45, 636 (1953); Ind. Eng. Chem., 45, 640 (1953).

L9 Linde, H., Fette, Seifen. Anstrichmittal, 60, 1053 (1958).

L10 Linde, H., Monatsber. Deut. Akad. Wiss., 1, 699 (1959).

L11 Linde, H., Zeit. für Physik. Chemie, 225, 72 (1964).

L12 Linde, H., Pfaff, S. and Zirkel, C., Z. Physik. Chem., 225, 72 (1964).

L13 Linde, H., Schwarz, E. and Gröger, K., Chem. Eng. Sci., 22, 823 (1967).

L14 Long, F. A. and McDevit, W. F., Chem. Revs., 158, 119 (1946).

L15 Low, A. R. and Brunt, D., Nature, 115, 299 (1925).

M1 Marangozis, J., Ph.D. Thesis, Chemical Engineering Department, University of Toronto, (1960).

M2 Marchello, J. M. and Toor, H. L., I. & E. C. Fundamentals, 2, 8 (1963).

M3 Maroudas, N. G., and Sawistowski, H., Nature, 188, 1186 (1960).

M4 McBain and Woo, Proc. Roy. Soc., A163, 182 (1937).

M5 Merson, R. L. and Quinn, J. A., A. I. Ch. E. J., 10, 804 (1964).

M6 Mickley, H. S., Sherwood, T. K. and Reid, C. E., "Applied Mathematics in Chemical Engineering," 2nd ed. McGraw-Hill, New York (1957).

M7 Mijnlieff, P. F. and Vreedenberg, H. A., J. Phys. Chem., 70, 2158 (1966).

M7a Mills, R. and Adamson, A. W., J. Am. Chem. Soc., 77, 3454 (1955).

M8 Mills, R., Woolf, L. A. and Watts, R. O., A. I. Ch. E. J., 14, 671 (1968).

M9 Mitchell, W. J. and Quinn, J. A., Chem. Eng. Sci., 23, 503 (1968).

M10 Mutriskov, A. Y. and Maminov, O. V., International Chemical Engineering, 8, 410 (1968).

N1 Nanda, A. K. and Sharma, M. M., Chem. Eng. Sci., 22, 769 (1967).

N2 Nernst, W., Z. Physik. Chem., 47, 52 (1904).

N3 Nernst, W., "Theoretical Chemistry," English translation by L. W. Codd, MacMillan & Co. Ltd., London (1923).

N4 Nijsing, R. A. T. O., Hendriksz, R. H. and Kramers, H., Chem. Eng. Sci., 10, 88 (1959).

N5 Noordsij, P. and Rotte, J. W., Chem. Eng. Sci., 22, 1475 (1967).

O1 Olander, D. R., A. I. Ch. E. J., 13, 191 (1967).

O2 Olander, D. R. and Camahort, J. L., A. I. Ch. E. J., 12, 693 (1966).

O3 Olander, D. R. and Reddy, L. B., Chem. Eng. Sci., 19, 67 (1964).

O4 Oliver, D. R. and Atherinos, T. E., Chem. Eng. Sci., 23, 525 (1968).

O5 Orell, A. and Westwater, J. W., A. I. Ch. E. J., 8, 350 (1962).

*O6 Osborne, R. J., S.M. Thesis, Dept. of Chem. Eng. M.I.T. (1952) as quoted in Reference (S15).

O7 Oster, G. and Nishijima, Y., Sci. Am., 208, 54 (1963).

P1 Pang, K. H., M. Eng. Thesis, McMaster University (1965).

P2 Pao, Y. H., Chem. Eng. Sci., 19, 694 (1964)

P3 Peaceman, D. W., Sc.D. Thesis, Dept. Chem. Eng. M.I.T. (1951).

P4 Pearson, T. R. A., J. Fluid Mech., 4, 489 (1958).

P5 Pellew, A. and Southwell, R. V., Proc. Roy. Soc., A176, 312 (1940).

P6 Perlmutter, D. D., Chem. Eng. Sci., 16, 287 (1961).

P7 Perry, R. H. and Pigford, R. L., Ind. Eng. Chem., 45, 1247 (1953).

P7a Philpot, J. St. L. and Cook, G. H., Research, 1, 234 (1948).

P7b Polson, A. and Kahn, D. S. J., Phys. Chem., 51, 816 (1947).

P8 Potts, J. E. and Amis, E. S., J. Am. Chem. Soc., 71, 2112 (1949).

P9 Powell, R. E., Roseveare, W. E. and Eyring, H., Ind. Eng. Chem., 33, 430 (1941).

*P10 Prandtl, L., Physik. Z., 29, 487 (1928).

R1 Raal, J. D., Ph.D. Thesis, Dept. Chem. Eng., University of Toronto (1960).

R2 Raal, J. D. and Johnson, A. I., Can. J. Chem. Eng., 37, 218 (1959).

R3 Ramshaw, C. and Thornton, J. D., Nature, 184, 719 (1959).

R4 Rayleigh, L., The London, Edinburgh and Dublin Philosophical Magazine and Journal of Science, Series 4, Vol. 47, No. 310, 81-93 (1874).

R5 Rayleigh, L., Phil. Mag., 32, 529 (1916).

R6 Reid, S. J., B.Eng. Thesis, Dept. Chem. Eng., Royal Military College (1965).

R7 Roberts, D. and Danckwerts, P. V., Chem. Eng. Sci., 17, 961 (1962).

R8 Roper, G. H., Hatch, T. F. Jr., and Pigford, R. L., I. & E. C. Fundamentals, 1, 144 (1962).

R9 Ruckenstein, E., Chem. Eng. Sci., 18, 233 (1963).

R10 Ruckenstein, E., Chem. Eng. Sci., 19, 505 (1964).

R11 Ruckenstein, E., Chem. Eng. Sci., 23, 363 (1968).

R12 Ruckenstein, E. and Berbente, C., Chem. Eng. Sci., 19, 329 (1964).

R13 Ruthven, D. M. and Kenney, C. N., Chem. Eng. Sci., 22, 1561 (1967).

R14 Ruthven, D. M. and Kenney, C. N., Chem. Eng. Sci., 23, 981 (1968).

S1 Sani, R. L., A.I.Ch.E.J., 11, 971 (1965).

S2 Sato, K., Hoshino, S. and Miyamoto, K., Kagaku Kogaku (English Edition), 2, 242 (1964).

S3 Schmidt, R. J. and Milverton, S. W., Proc. Roy. Soc., A152, 586 (1935).

S4 Scriven, L. E., A. I. Ch. E. J., 7, 524 (1961).

S5 Scriven, L. E. and Sternling, C. V., J. Fluid Mech., 19, 321 (1964).

S6 Searle, R. and Gordon, K. F., A. I. Ch. E. J., 3, 490 (1957).

S7 Secor, R. M., A. I. Ch. E. J., 11, 452 (1965).

S8 Seto, P., M.Eng. Thesis, McMaster University (1963).

S9 Seto, P., Furter, W. F. and Johnson, A. I., Can. J. Chem. Eng., 43, 292 (1965).

S10 Seto, P., "Summer Report" Dept. Chem. Eng., McMaster University (1966)

S11 Sharma, M. M. and Danckwerts, P. V., Chem. Eng. Sci., 18, 729 (1963).

S12 Sherwood, T. K. and Pigford, R. L., "Absorption and Extraction," McGraw-Hill Pub. Co. (1952).

S13 Sherwood, T. K. and Ryan, J. M., Chem. Eng. Sci., 11, 81 (1959).

S14 Sherwood, T. K. and Wei, J. C., A. I. Ch. E. J., 1, 522 (1955).

S15 Sherwood, T. K. and Wei, J. C., Ind. Eng. Chem., 49, 1030 (1957).

S16 Shrier, A. L., Chem. Eng. Sci., 22, 1391 (1967).

S17 Seidell, "Solubilities of Organic Compounds," D. Van Nostrand Co. Inc. (1941).

*S18 Sigwart, K., Ver Deut. Ing. Zeit., 98 453 (1956).

*S19 Sigwart, K. and Nassenstein, H., Naturwissenschaften, 42, 458 (1955).

S20 Slattery, J. C. and Bird, R. B., A. I. Ch. E. J., 4, 137 (1958).

S21 Smith, K. A., J. Fluid Mech., 24, 401 (1966).

S22 Sternling, C. V. and Scriven, L. E., A. I. Ch. E. J., 5, 514 (1959).

S23 Stewart, W. E., "Transport Phenomena," P. 571, John Wiley & Sons, Inc. (1962).

S24 Stewart, W. E. and Prober, R., I. & E. C. Fundamentals, 3, 224 (1964).

S25 Stokes, R. H., J. Am. Chem. Soc., 72, 763 (1950).

S26 Stokes, R. H., J. Am. Chem. Soc., 72, 2243 (1950).

S27 Sugano, Y. and Ratkowsky, D. A., Chem. Eng. Sci., 23, 707 (1968).

S28 Szekely, J., Chem. Eng. Sci., 22, 777 (1967).

S29 Szekely, J., Todd, M. R. and Martins, G. P., Chem. Eng. Sci., 22, 81 (1967).

T1 Takamatsu, T., Hiraoka, M., Tanaka, K., Inoue, Y. and Osugi, A., Kagaku Kogaku (English Edition), 2, 246 (1964).

T2 Takamatsu, T., Hiraoka, M., Tanaka, K., Inoue, Y. and Osugi, A., Kagaku Kogaku (English Edition), 3, 65 (1965).

T3 Tham, M. J., Bhatia, K. K. and Gubbins, K. E., Chem. Eng. Sci., 22, 309 (1967).

T4 Thomas, W. J. and McK.Nicholl, E., Chem. Eng. Sci., 22, 1877 (1967).

T5 Toor, H. L. and Sebulsky, R. T., A. I. Ch. E. J., 7, 558 (1961).

T6 Toor, H. L., A. I. Ch. E. J., 10, 448, 460 (1964).

T7 Toor, H. L., I. & E. C. Fundamentals, 6, 152 (1967).

T8 Toor, H. L. and Marchello, J. M., A. I. Ch. E. J., 4, 97 (1958).

*T9 Topp, W. M., Mutech. Chem. Eng. J., 2, 19 (1959).

V1 Van Krevelen, D. W. and Hoftijzer, P. J., Rec. Trav. Chim., 67, 563 (1948).

V2 Vassilatos, G., M.A.Sc. Thesis, Dept. Chem. Eng., University of Toronto (1960).

V3 Vidal, A. and Acrivos, A., I. & E. C. Fundamentals, 7, 53 (1968).

V4 Vinograd, J. R. and McBain, J. W., J. Am. Chem. Soc., 63, 2008 (1941).

V5 Volk, W., "Applied Statistics for Engineers," McGraw-Hill Inc., New York (1958).

V6 Von Karman, T., Trans. Am. Soc. Mech. Engrs., 61, 705 (1939).

W1 Ward, A. F. H. and Brooks, L. H., Trans. Faraday Soc., 48, 1124 (1952).

W2 Watada, D., Ph.D. Thesis, McMaster University (1968).

W3 Wiggill, J. B., Ph.D. Thesis, University of Cambridge, England (1958).

W4 Wilke, C. R., Chem. Eng. Progr. 45, 218 (1949).

W5 Wilke, C. R., Chem. Eng. Progr. 46, 95 (1950).

W6 Wilke, C. R. and Chang, P., A. I. Ch. E. J., 1, 270 (1955).

*Z1 Zierep, J., Beitr. Phys. Atmos., 30, 215 (1958) as quoted from Reference (M9).